UNIVERSIDADE FEDERAL DO RIO GRANDE DO SUL
INSTITUTO DE GEOCIÊNCIAS
PROGRAMA DE PÓS-GRADUAÇÃO EM GEOCIÊNCIAS

TERMOTECTÔNICA FANEROZOICA DA PROVÍNCIA MANTIQUEIRA E CRÁTONS ADJACENTES E SUA RELAÇÃO COM A EVOLUÇÃO DE ZONAS TRANSICIONAIS NA MARGEM CONTINENTAL BRASILEIRA

EDGAR DO AMARAL SANTOS

ORIENTADORA – Profa Dra. Andréa Ritter Jelinek

Porto Alegre, 2023

UNIVERSIDADE FEDERAL DO RIO GRANDE DO SUL
INSTITUTO DE GEOCIÊNCIAS
PROGRAMA DE PÓS-GRADUAÇÃO EM GEOCIÊNCIAS

TERMOTECTÔNICA FANEROZOICA DA PROVÍNCIA MANTIQUEIRA E CRÁTONS ADJACENTES E SUA RELAÇÃO COM A EVOLUÇÃO DE ZONAS TRANSICIONAIS NA MARGEM CONTINENTAL BRASILEIRA

EDGAR DO AMARAL SANTOS

ORIENTADORA – Profa. Dra. Andréa Ritter Jelinek

BANCA EXAMINADORA

Profa. Dra. Ana Maria Pimentel Mizusaki – Universidade Federal do Rio Grande do Sul

Prof. Dr. Mauricio Parra Amézquita - Universidade de São Paulo

Prof. Dr. Miguel Tupinambá - Universidade do Estado do Rio de Janeiro

Tese de Doutorado apresentada como requisito parcial para a obtenção do Título Doutor em Ciências.

Porto Alegre, 2023

CIP - Catalogação na Publicação

Santos, Edgar do Amaral
TERMOTECTÔNICA FANEROZOICA DA PROVÍNCIA MANTIQUEIRA E CRÁTONS ADJACENTES E SUA RELAÇÃO COM A EVOLUÇÃO DE ZONAS TRANSICIONAIS NA MARGEM CONTINENTAL BRASILEIRA / Edgar do Amaral Santos. -- 2023.
197 f.
Orientadora: Andréa Ritter Jelinek.

Tese (Doutorado) -- Universidade Federal do Rio Grande do Sul, Instituto de Geociências, Programa de Pós-Graduação em Geociências, Porto Alegre, BR-RS, 2023.

1. Termocronologia. 2. Cráton São Francisco. 3. Faixa Araçuaí. 4. Cinturão Dom Feliciano. 5. Traços de Fissão em Apatita e (U-Th)/He em Apatita e Zircão. I. Jelinek, Andréa Ritter, orient. II. Título.

Elaborada pelo Sistema de Geração Automática de Ficha Catalográfica da UFRGS com os dados fornecidos pelo(a) autor(a).

Aos meus pais, Maria Enedina e Domício (*in memoriam)*

AGRADECIMENTOS

Este trabalho é fruto do meu empenho, dedicação e perseverança. Ele foi desenvolvido durante alguns dos anos mais sombrios que o Brasil viveu e, portanto, representa não somente a minha vitória, mas a vitória do povo unido em defesa da democracia que ainda existe, das instituições de ensino públicas, gratuitas e de qualidade, de pessoas de origem humilde e, no meu caso particular, de um homem gay. Este trabalho é uma vitória política, individual e coletiva, e retrato de sobrevivência.

Agradeço imensamente e eternamente aos meus pais, Maria Enedina e Domício (*in memoriam*) que sempre me incentivaram e deram o seu suor para me impulsionar e conquistar os meus sonhos. Essa conquista é para vocês dois, a quem amo e sempre amarei. A vocês devo tudo o que tenho e tudo que eu sou. Obrigado!

Agradeço aos meus irmãos, Isaura e Eduardo, que também me apoiaram e compartilharam junto a mim e minha família muitas dificuldades para permitir que hoje eu chegasse a esse momento. Sou muito grato a vocês por tudo tudo.

Agradeço ao Raphael Amaral, Edilene Amaral e Giovane Santos que primeiramente me deram a oportunidade de estudar e entrar no mundo da geologia. Obrigado por acreditar em mim.

Agradeço ao Jeferson Dutra, meu amor, meu companheiro de vida, que esteve comigo nesses últimos quase seis anos, sempre me apoiando, incentivando e sendo porto seguro. Eu amo você e é uma alegria enorme poder dividir a vida contigo. Agradeço a todos os seus familiares por me acolher junto a vocês, que agora são também minha família.

Agradeço à Profa. Dra. Andréa Ritter Jelinek, que me deu a oportunidade de trabalhar com termocronologia e me recebeu de braços abertos em seu laboratório. Obrigado por confiar em mim e me ajudar a desenvolver meu potencial. Obrigado pela orientação, pelas portas abertas e incentivo.

Aos meus amigos, de perto e de longe, das geociências ou não, que tornaram essa caminhada mais fácil: Carol Ruela, Thiago, Flávia, Carolzinha, Larissa, Fran, Talita, Edvaldo, Igor, Pedro, Diego, Ricardo, Josi, João Pacífico, Maris, Bruno e Denise. Obrigado!

Agradeço às queridas psicólogas Morgana Zanini e Nicole Nemetz que me auxiliaram profundamente a trabalhar questões profissionais e pessoais e a avançar no

entendimento sobre o mais importante conhecimento que eu poderia adquirir durante o doutorado: eu mesmo e minhas raízes, meus desejos, medos, fortalezas. O apoio incondicional e generosidade de vocês transformou minha vida e quem eu sou. Obrigado!

Ao CNPq, pela concessão da bolsa de doutorado, e à UFRGS e PPGGEO pela infraestrutura e corpo docente sempre compartilhando conhecimentos, orientação e oportunidades, obrigado.

RESUMO

A Província Mantiqueira é o sistema orogênico resultado do amalgamento de blocos cratônicos pré-Neoproterozoicos que formaram o supercontinente Gondwana durante eventos colisionais do Neoproterozoico ao Ordoviciano. Os crátons são nomeados Crátons São Francisco, Rio de la Plata e Luís Alves, enquanto os cinturões orogênicos são, de sul para norte, o Cinturão Dom Feliciano, Faixa Ribeira e Faixa Araçuaí. Além desses domínios essencialmente pré-cambrianos, encontram-se bacias sedimentares Paleozoicas a Cenozoicas sobre a Plataforma Sulamericana e as que compõem a margem continental, datadas do Meso ao Cenozoico. Algumas regiões desses cinturões próximos à margem continental comportam-se como regiões transicionais de diversas naturezas, como reológica, topográfica e termocronológica. Este trabalho tem como objetivo compreender a evolução tectonotermal de duas dessas regiões transicionais entre Província Mantiqueira e crátons adjacentes durante o Fanerozoico, utilizando para isso três termocronômetros de baixa temperatura: traços de fissão em apatita (TFA), (U-Th)/He em apatita (AHe) e zircão (ZHe). O uso combinado desses métodos permite obter dados térmicos dos quilômetros superiores da crosta e estimar idades de resfriamento. As idades das amostras deste trabalho para o método de ZHe são datadas do Paleozoico, enquanto as idades de TFA e AHe são Mesozoicas e Cenozoicas. Além disso, a partir das idades e dados térmicos, com a construção de modelos inversos em softwares especializados, foi possível determinar diversos episódios de resfriamento e reaquecimento, determinar taxas de denudação e espessuras de seções denudadas e construir modelos geodinâmicos para cada uma dessas regiões. A região composta pela litosfera do Cráton São Francisco apresentou as idades mais antigas e registrou dados térmicos do Paleozoico, enquanto a Faixa Araçuaí iniciou esse registro apenas no Mesozoico, evidenciando um forte controle reológico entre esses domínios. A erosão das ombreiras do rifte durante o Mesozoico também foi registrado nas Faixas Araçuaí e Ribeira norte e praticamente ausente no Cráton São Francisco. Ainda, observou-se que a presença de intrusões ígneas, diques alimentadores e a reativação de falhas, zonas de cisalhamento e zonas de fraturas de direção NW-SE e E-W auxiliaram na manutenção de temperaturas elevadas, gerando as idades mais jovens obtidas, o que torna a análise das regiões transicionais importantes na compreensão da evolução Fanerozoica da Província Mantiqueira.

Palavras-chave: *Província Mantiqueira; Cráton São Francisco; Faixa Araçuaí; Cinturão Dom Feliciano; Termocronologia; Traços de Fissão em Apatita; (U-Th)/He em Apatita e Zircão*

ABSTRACT

The Mantiqueira Province is the orogenic system resulting from the amalgamation of pre-Neoproterozoic cratonic blocks that formed the Gondwana supercontinent during collisional events from the Neoproterozoic to the Ordovician. The cratons are named São Francisco, Rio de la Plata and Luís Alves Cratons, while the orogenic belts are, from south to north, the Dom Feliciano Belt, Ribeira Belt and Araçuaí Belt. In addition to these essentially Precambrian domains, there are Paleozoic to Cenozoic sedimentary basins on the South American Platform and those that make up the continental margin, dating from the Meso to the Cenozoic. Some regions of the belts close to the continental margin behave as transitional regions of different natures, such as rheological, topographic and thermochronological. This work aims to understand the tectonothermal evolution of two of these transitional regions between Mantiqueira Province and adjacent cratons during the Phanerozoic, using three low-temperature thermochronometers: apatite fission track, (U-Th)/He in both apatite and zircon. The combined use of these methods makes it possible to obtain thermal data from the upper kilometers of the crust and estimate cooling ages. The ages of the samples in this work for the ZHe method are dated to the Paleozoic, while the ages of TFA and AHe are Mesozoic and Cenozoic. Furthermore, based on the ages and thermal data, with the construction of inverse models in specialized software, it was possible to determine several episodes of cooling and reheating, determine denudation rates and thicknesses of denuded sections and build geodynamic models for each of these regions. The region composed of the lithosphere of the São Francisco Craton presented the oldest ages and recorded thermal data from the Paleozoic, while the Araçuaí Belt began this record only in the Mesozoic, showing a strong rheological control between these domains. The erosion of rift shoulders during the Mesozoic was also recorded in the northern Araçuaí and Ribeira Belts and practically absent in the São Francisco Craton. Furthermore, it was observed that the presence of igneous intrusions, feeding dikes and the reactivation of faults, shear zones and fracture zones of NW-SE and E-W directions helped to maintain high temperatures, generating the youngest ages obtained, which makes the analysis of transitional regions important in understanding the Phanerozoic evolution of the Mantiqueira Province.

Keywords: *Mantiqueira Province; São Francisco Craton; Araçuaí Belt; Dom Feliciano Belt; Thermochronology; Apatite Fission Track; Apatite and Zircon (U-Th)/He*

LISTA DE FIGURAS

Figura 1. 1: Mapa esquemático da continente Sulamericano evidenciando os blocos cratônicos, províncias Neoproterozoicas e coberturas sedimentares. A Província Mantiqueira e crátons adjacentes estão circulados em vermelho (modificado de Basei et al., 2010).....16

Figura 1. 2: Modelo digital de terreno da América do Sul gerado a partir de dados da Shuttle Radar Topographic Mission (SRTM), NASA/JPL/NIMA delimitando a Província Mantiqueira e o Cráton São Francisco (CSF). Fundo oceânico gerado a partir de dados gravimétricos evidenciando zonas de fraturas (extraído de Sandwell et al., 2014).....18

Figura 1. 3: Distribuição das idades centrais de Traços de Fissão em Apatita ao longo da Província Mantiqueira e crátons adjacentes (modificado de Engelmann de Oliveira and Jelinek, 2017; Hueck et al., 2019; Novo et al., 2021).....20

Figura 2. 1: Mapa geológico do sudeste a nordeste brasileiro evidenciando os pontos amostrais e os terrenos arqueanos e proterozoicos do Cráton São Francisco (CSF), Faixa Araçuaí (AB), Faixa Ribeira (RB), Faixa Brasília (BB) e Província Borborema (BP), além da cobertura vulcanossedimentar das Bacias do Paraná (PaB), Sanfranciscana e Parnaíba, e as bacias da margem continental. Também estão presentes as zonas de fraturas, os principais plútons kimberlíticos, alcalino-carbonatíticos da região e a Província Magmática de Abrolhos (AMP) e a Cadeia Vitória-Trindade (VTSC) (modificado de Dalton de Souza et al., 2003; Perrota et al., 2005; Heilbron et al., 2016; Silva et al., 2020).....26

Figura 2. 2: Mapa geológico da área de estudo com a localização das amostras coletadas compreendendo o Escudo Catarinense e seus principais terrenos e zonas de cisalhamento (modificado de Wildner et al., 2014).....29

Figura 1. 4: Temperatura de fechamento (Zona de Retenção/Apagamento Parcial) dos principais geocronômetros e termocronômetros. O quadro em destaque circunda os três métodos utilizados neste trabalho (modificado de Evans et al., 2003).....34

Figura 3. 1: a) Figura esquemática ilustrando um cristal de apatita e os traços de fissão confinados e semiconfinados. TINT são traços de fissão confinados interceptados por um traço de fissão que intercepta a superfície revelado pelo ataque químico. b) Fotomicrografia de um cristal de apatita evidenciando os traços de fissão (extraído de Hurford, 2019).....38

Figure 5. 1: a) West Gondwana map evidencing the cratonic nuclei, the Brasiliano/Pan-African belts, and the recent orogenic belts (after Oriolo et al., 2017). The red rectangle indicates the study area. Abbreviations are: SFC: S˜ao Francisco Craton; CC: Congo Craton; PP: Paranapanema Block; NP: Nico Perez Terrane; RPC: Rio de la Plata Craton; AmC: Amazon Craton; WAC: West Africa Craton; LMC: Latea Metacraton; SMC: Sahara Metacraton; KC: Kalahari Craton; ANS: Arabian-Nubian Shield. b) Geologic map of the São Francisco Craton (SFC) and the Araçuaí Orogen (ArO) displaying the most important units in the selected area (after Almeida, 1981; De Alkmim, 2015; Alkmim et al., 2016) and the basins of the continental margin; R-Tb: Recôncavo-Tucano basins Volcanosed.: Volcanosedimentary; Pass.: passive; Ophiol.: ophiolite; Coll.: collisional. (For interpretation of the references to colour in this figure legend, the reader is referred to the web version of this article.) 64

Figure 5. 2: Geologic map of the study area with sampling sites along the border of the São Francisco Craton (SFC) and the Araçuaí Orogen (ArO); Abbreviations are: Mba: Mucuri basin; Cba: Cumuruxatiba basin; Jba: Jequitinhonha basin.....66

Figure 5. 3: a) Geomorphological 3d map of the study area displaying both land and undersea topography. The red dots indicate sampling sites and blue lines are the drainage network. b) Lineament map plotted over a hillshade of the study area, showing topography in 2d. Abbreviations are: SFC: São Francisco Craton; ArO:

Araçuaí Orogen; CC: sedimentary Cenozoic cover; thin grey lines: lineaments. c) Rosace diagrams for the cratonic, orogenic, and Cenozoic cover domains evidencing the orientation of the manually traced lineaments and their frequency. (For interpretation of the references to colour in this figure legend, the reader is referred to the web version of this article.)....69
Figure 5. 4: Hillshade map displaying AFT central ages and AHe average ages available in the literature and ZHe and AHe average ages reported in this study. Data displayed in the figure indicate results from Amaral et al. (1997), Japsen et al. (2012), Jelinek et al. (2014), Amaral-Santos et al. (2019), Van Ranst et al. (2020), and Fonseca et al. (2021). Abbreviations are: SFC: São Francisco Craton; ArO: Araçuaí Orogen. 71
Figure 5. 5: ZHe corrected ages plotted against a) eU concentration and b) Equivalent Spherical Radius (ESR). The grey shading in both charts indicates the correlation between the parameters analyzed. Error bars (2σ) for each sample are displayed in the charts.....80
Figure 5. 6: AHe corrected ages plotted against a) eU concentration and b) Equivalent Spherical Radius (ESR). The grey shading in both charts indicates the correlation between the parameters analyzed. Error bars (2σ) for each sample are displayed in the charts. 81
Figure 5. 7: Results of MCMC inverse modeling in QTQt (Gallagher, 2012) for samples BHS-02, BHS-06, BHS-10, BHS-12, BHS-13, BHS-15, and BHS-17. The expected model is defined by the range between both black curves (95% credible interval). The magenta curve represents the weighted mean path of the expected model. The dashed lines making a rectangle at the bottom and at the top of the time-temperature chart are the ZHePRZ and AHePRZ, respectively. The relative probability of time-temperature paths increases from blue to red, according to the scale bar next to the thermal history chart. Observed age versus Predicted age charts are shown on the right of the respective thermal history. ZHe single-crystal ages are plotted as upside down red triangles whereas upside pointing blue triangles are AHe single crystal ages. (For interpretation of the references to colour in this figure legend, the reader is referred to the web version of this article.).....83
Figure 5. 7: (continued). 84
Figure 5. 8: a) Combined ZHe and AHe thermal model from samples BHS-02, BHS-06, BHS-13, and BHS-15. The dark blue curve is the weighted mean path of the BHS-02 sample; The yellow curve is the weighted mean path of the BHS-13 sample; The green and purple curves are the mean paths of the BHS-06 and BHS-15 samples, respectively. Light blue curves are the 95% confidence interval of the BHS-02 sample whereas magenta curves are the 95% credible interval of the BHS-15 sample (lower in the profile). b) Observed versus Predicted Age chart. Upside pointing triangles are AHe single-crystal ages and upsidedown triangles are ZHe single-crystal ages. Blue triangles represent BHS-02 ages, green triangles indicate BHS-06 ages, yellow triangles represent BHS-13 ages, and BHS-15 ages are indicated by purple triangles. (For interpretation of the references to colour in this figure legend, the reader is referred to the web version of this article.) 85
Figure 5. 9: ZHe Average Age plotted against a) Distance to the coast; b) Altitude (meters above sea level); c) Distance to the craton border. The grey shading refers to the trend observed on the charts. Error bars (2σ) for each sample are displayed in the charts. 87
Figure 5. 10: AHe Average Age plotted against a) Distance to the coast; b) Altitude (meters above sea level); c) Distance to the craton border. These charts contain data from this study as well as apatite (U–Th)/He data from Van Ranst et al. (2020). The grey shading refers to the trend observed on the samples of this study whereas green shading encompasses the trend generated from this study and Van Ranst et al. (2020). Error bars (2σ) for each sample are displayed in the charts. (For interpretation of the references to colour in this figure legend, the reader is referred to the web version of this article.)....88
Figure 5. 11: Schematic chart evidencing thermal histories of this study, cooling phases, sedimentation in the

surrounding basin depocenters, and major tectonic events associated with the chronostratigraphic chart. Continuous lines represent fast exhumation (>15 m.Ma^{-1}) and dashed lines slow exhumation (≤ 15 m.Ma^{-1}), steadystate, or reheating. Sample ID is placed on the mean corrected ZHe age. Abbreviations are: Parn.: Parnaíba basin; San.: Sanfranciscana basin; E. Margin: continental margin basins formed coevally to South Atlantic opening. v: intraplate magmatism (Parnaíba and Sanfranciscana basins); Andean Orog.: Andean orogeny.....90

Figure 6. 1: a) West Gondwana map showing the cratonic nuclei, the belts formed in the Brasiliano/Pan-African event, and the recent orogenic belts (after Oriolo et al., 2017). Abbreviations are RDLP: Rio de La Plata Craton; NP: Nico Pérez Terrane; PP: Paranapanema Block; SFC: São Francisco Craton; AmC: Amazon Craton; KC: Kalahari Craton; CC: Congo Craton; LMC: Latea Metacraton; WAC: West Africa Craton; SMC: Sahara Metacraton; ANS: Arabian-Nubian Shield. b) The Dom Feliciano Belt and adjacent cratons along the continental margin of southern Brazil and Uruguay. After CPRM (2008) and Philipp et al. (2016).....109

Figure 6. 2: The study area of this work comprises the Catarinense Shield and its main terranes. Sampling sites are shown in the figure and were restricted to the Florianópolis Batholith. Shear Zones: a: Itajaí-Perimbó Shear Zone; b: Major-Gercino Shear Zone. After CPRM (2014).....113

Figure 6. 3: Compilation of Apatite Fission Track and Apatite (U–Th)/He ages available for the Catarinense Shield and surrounding sediments. Results presented in this study are shown in bold. After CPRM (2014) and (Jelinek et al., 2021).....121

Figure 6. 4: Compiled Apatite Fission Track (AFT) ages of this study and from the literature plotted against a) Mean Track Length (MTL) and b) Standard Deviation (Std. Dev). c) Mean Track Lengths versus Standard Deviation. The AFT ages of the Uruguayan and Sul-Rio-Grandense shield are somewhat similar and grouped into the "Southern Dom Feliciano Belt" data set. AFT ages for the northern and southern Dom Feliciano Belt are shown as diamonds and X shapes, respectively. Error bars (1σ) are shown in the charts. Abbreviation is Orig. age: original age.....122

Figure 6. 5: Compiled central Apatite Fission Track ages (AFT) of this study and available in the literature plotted against a) Elevation; b) Distance to the coastline. Error bars (1σ) are shown in the charts. Abbreviation is: m.a.s.l.: meters above sea level.....123

Figure 6. 6: Apatite (U–Th)/He ages for all crystals analyzed in this study and available in the literature plotted against a) Effective uranium concentration (eU), b) Equivalent Spherical Radius (ESR). Mean Apatite (U–Th)/He ages in each sample of this study and in the literature plotted against c) Elevation and d) Distance to the coastline. Error bars (2σ) are shown for each sample.....126

Figure 6. 7: Inverse modeling results generated in QTQt (Gallagher, 2012) for samples SC-34, SC-35, SC-36, SC-37, SC-38, SC-41, SC-42, SC-44, SC-46 and SC-48. The 95% credible interval defines the expected model (black curves). The weighted mean path is represented by the magenta curve. The range of the AFTPAZ and AHePRZ is defined by the dashed lines. The relative probability scale increases from blue to red. On the right of the thermal histories are shown observed versus predicted ages charts. Upside-down red triangles indicate AFT ages whereas AHe single-crystal ages are displayed in upside-pointing blue triangles. The Mean Track Length (MTL) distribution of AFT data is represented as bars, with the red line indicating track lengths modeled. (For interpretation of the references to colour in this figure legend, the reader is referred to the web version of this article.).....127

Figure 6. 7: (continued). 129

Figure 6. 8: Basement temperatures across the Dom Feliciano Belt and surrounding cratons from 360 to 30 Ma assessed by the Inverse Distance Weighted (IDW) interpolation technique. The time-temperature points were obtained from inverse models from this work and de Borba et al. (2002, 2003), Jelinek et al. (2003), Gomes

(2011), Kollenz (2015), de Oliveira et al. (2016) Gomes and Almeida (2019), Krob et al. (2019), Machado et al. (2019, 2020) Red stars indicate the country or state capital city. Abbreviations are: SC: Santa Catarina State; RS: Rio Grande do Sul State; UY: Uruguay; FLN: Florianópolis; POA: Porto Alegre; MVD: Montevideo. (For interpretation of the references to colour in this figure legend, the reader is referred to the web version of this article.) 130

Figure 7. 1: a) West Gondwana map depicting the cratons, some orogenic belts formed during the West Gondwana amalgamation, and the recent orogenic belts (after Oriolo et al., 2017). SFC: São Francisco Craton; CC: Congo Craton. b) Geologic map of the study area in southeastern to northeastern Brazil (after Leite et al., 2004), evidencing the limits of the São Francisco Craton and the adjacent Araçuaí Belt (AB), Ribeira Belt (RB), Brasília Belt (BB), the Borborema Province (BP), and the intracratonic Paraná (PaB), Parnaíba, Sanfranciscana, Recôncavo-Tucano-Jatobá Basins, as well as the Continental Rift of Southeastern Brazil (CRSB) (Riccomini et al., 2004) and the Cretaceous/Paleogene kimberlites and alkaline-carbonatitic rocks. The offshore region displays the gravity anomaly map of the South Atlantic Ocean seafloor (Sandwell et al., 2014) eastward of the study area, evidencing the Abrolhos Magmatic Province (AMP), the Vitória-Trindade seamount chain (VTSC), and the Cretaceous/Cenozoic marginal basins (Mohriak and Fainstein, 2012). 154

Figure 7. 2: Distribution of the new AFT ages of this data set along with AFT, AHe, and ZHe ages available in the literature from the northern Araçuaí Belt (AB) and the São Francisco Craton (SFC) (Amaral et al., 1997; Harman et al., 1998; Cupertino, 2000; Turner et al., 2008; Japsen et al., 2012; Jelinek et al., 2014, 2020; do Amaral Santos et al., 2022; Fonseca et al., 2022, 2023). Results of this study are displayed in bold and is the only work to incorporate both ZHe and AHe data in the area. 160

Figure 7. 3: a) Inverse distance weighted (IDW) map displaying the spatial distribution of Apatite Fission Track central ages in southeastern to northeastern Brazil. The interpolation process considered samples from Gallagher et al. (1994), Amaral et al. (1997), Harman et al. (1998), Cupertino (2000), Oliveira et al. (2000), Hadler et al. (2001), Tello Saenz et al. (2003), Carmo (2005), Franco et al. (2005), Ribeiro et al. (2005, 2011), Silva (2006), Hackspacher et al. (2007), Genaro (2008), Turner et al., (2008), Franco-Magalhaes et al. (2010, 2014), Hiruma et al. (2010), Gomes (2011), Cogné et al. (2012), Japsen et al. (2012), Doranti-Tiritan (2013), Karl et al. (2013), Jelinek et al. (2014, 2020), Souza et al. (2014), Engelmann de Oliveira et al. (2016), Soares et al. (2016), Amaral-Santos et al. (2019), Krob et al. (2019), Van Ranst et al. (2020), Fonseca et al. (2020, 2021, 2022, 2023), Gezatt et al. (2021), and Costa, (2022). Samples from the Phanerozoic cover were not considered for interpolation. Abbreviations are: SFC: São Francisco Craton; AB: Araçuaí Belt; RB: Ribeira Belt; BB: Brasília Belt; BP: Borborema Province; PaB: Paraná Basin; RJ: Rio de Janeiro City; SA: Salvador City; BH: Belo Horizonte City. After Engelmann de Oliveira and Jelinek (2017), Hueck et al. (2019), and Novo et al. (2021). 161

Figure 7. 4: Chronological chart evidencing the expected model's weighted mean trajectories of the new thermal histories provided in this study, along with the leading local and regional events (sedimentary deposition, tectonism, mantle dynamics, and magmatism). 163

Figure 7. 5: Inverse distance weighted maps created through the interpolation of data collected from thermal models of basement samples across the São Francisco Craton (SFC), Araçuaí Belt (AB), and Ribeira Belt (RB) from 360 to 270 Ma. The time-temperature points collected from this work and samples available in the literature are displayed in Supplementary Data S3. Pink stars refer to the state capital city. Abbreviations are: RJ: Rio de Janeiro City; SA: Salvador City; BH: Belo Horizonte City. 166

Figure 7. 6: Inverse distance weighted maps created through the interpolation of data collected from thermal models of basement samples across the São Francisco Craton (SFC), Araçuaí Belt (AB), and Ribeira Belt

(RB) from 240 to 150 Ma. The time-temperature points collected from this work and samples available in the literature are displayed in Supplementary Data S3. Pink stars refer to the state capital city. Abbreviations are: RJ: Rio de Janeiro City; SA: Salvador City; BH: Belo Horizonte City. 167

Figure 7. 7: Inverse distance weighted maps created through the interpolation of data collected from thermal models of basement samples across the São Francisco Craton (SFC), Araçuaí Belt (AB), and Ribeira Belt (RB) from 120 to 30 Ma. The time-temperature points collected from this work and samples available in the literature are displayed in Supplementary Data S3. Pink stars refer to the state capital city. Abbreviations are: RJ: Rio de Janeiro City; SA: Salvador City; BH: Belo Horizonte City. 168

LISTA DE TABELAS

TABLE 5. 1: DETAILS FROM SAMPLES ANALYZED IN THIS STUDY. N: NORTHING; E: EASTING, COORDINATES IN UTM ZONE 24 K, DATUM WGS84; M.A.S.L.: METERS ABOVE SEA LEVEL; DIST. COAST: THE SHORTEST DISTANCE TO THE ATLANTIC OCEAN; DIST. CRATON: THE SHORTEST DISTANCE TO THE SÃO FRANCISCO CRATON. ZHE: ZIRCON (U–TH)/HE DATING; AHE: APATITE (U–TH)/HE DATING. 72

TABLE 5. 2: SUMMARY OF ZIRCON (U–TH)/HE AGES AND PARAMETERS; ABBREVIATIONS ARE: EU: EFFECTIVE URANIUM, CALCULATED AS EUMG/G = [UMG/G + (0.235*THMG/G) + (0.00463*SMMG/G)]; ESR: EQUIVALENT SPHERICAL RADIUS; FT: CORRECTION FACTOR AFTER (FARLEY ET AL., 1996); CORR.: CORRECTED; AVER.: AVERAGE; SD: STANDARD DEVIATION. ITALIC AND UNDERSCORE DATA REFER TO SAMPLES INFORMATION THAT WERE NOT CONSIDERED FROM DISCUSSION. 77

TABLE 5. 3: SUMMARY OF APATITE (U–TH)/HE AGES AND PARAMETERS; ABBREVIATIONS ARE EU: EFFECTIVE URANIUM, CALCULATED AS EUMG/G = [UMG/G + (0.235*THMG/G) +0.00463*SMMG/G); ESR: EQUIVALENT SPHERICAL RADIUS; FT: CORRECTION FACTOR AFTER (FARLEY ET AL., 1996); CORR.: CORRECTED; AVER.: AVERAGE; SD: STANDARD DEVIATION. ITALIC AND UNDERSCORE DATA REFER TO SAMPLES INFORMATION THAT WERE NOT CONSIDERED FROM DISCUSSION. 79

TABLE 6. 1: DETAILS FROM SAMPLES ANALYZED IN THIS STUDY. COORDINATES WERE ACQUIRED IN UTM ZONE 22 J, DATUM WGS84; DIST. COAST: THE DISTANCE TO THE ATLANTIC OCEAN; M.A.S.L.: METERS ABOVE SEA LEVEL; AFT: APATITE FISSION TRACK DATING; AHE: APATITE (U–TH)/HE DATING. 114

TABLE 6. 2: NEW APATITE FISSION TRACK DATA FROM THE CATARINENSE SHIELD, IN THE NORTHERN DOM FELICIANO BELT, SOUTHERN BRAZIL. UNDERSCORE ITALIC DATA ARE OUTLIERS, WHICH WERE DISCARDED FROM INVERSION. 120

TABLE 6. 3: SUMMARY OF APATITE (U–TH)/HE AGES AND PARAMETERS; THE ABBREVIATIONS REPORTED IN TABLE ARE: EU: EFFECTIVE URANIUM, CALCULATED AS EUMG/G = [UMG/G + (0.235*THMG/ G) + 0.00463*SMMG/G)]; FT: CORRECTION FACTOR AFTER (FARLEY ET AL., 1996); ESR: EQUIVALENT SPHERICAL RADIUS; CORR.: CORRECTED; SD: STANDARD DEVIATION; AVER.: AVERAGE. ITALIC AND UNDERSCORED DATA POINT TO OUTLIER SAMPLES (OUTLIERS) AND DISCARDED FROM INVERSION. 124

TABLE 7. 1: DETAILS FROM SAMPLES ANALYZED IN THIS STUDY. COORDINATES IN DECIMAL DEGREE; AHE AND ZHE DATA PUBLISHED IN DO AMARAL SANTOS ET AL. (2022) AND AVAILABLE IN SUPPLEMENTARY DATA S1. AFT: APATITE FISSION TRACK; AHE: APATITE (U-TH)-HE DATING; ZHE: ZIRCON (U-TH)/HE DATING. 156

TABLE 7. 2: NEW APATITE FISSION TRACK DATA FROM THE ARAÇUAÍ BELT AND THE SÃO FRANCISCO CRATON, IN SOUTHEASTERN TO NORTHEASTERN BRAZIL. 159

SUMÁRIO

RESUMO 1

ABSTRACT 3

LISTA DE FIGURAS 4

LISTA DE TABELAS 9

ESTRUTURA DA TESE 15

CAPÍTULO 1 - INTRODUÇÃO 16

1.1 INTRODUÇÃO 16

1.2 OBJETIVOS 20

1.2.1 OBJETIVO GERAL 20

1.2.2 OBJETIVOS ESPECÍFICOS 21

CAPÍTULO 2 – CONTEXTO GEOLÓGICO 23

2.1 O CRÁTON SÃO FRANCISCO E AS FAIXAS ARAÇUAÍ E RIBEIRA 23

2.2 OS CRÁTONS RIO DE LA PLATA E LUÍS ALVES E O CINTURÃO DOM FELICIANO 26

2.3 REGISTRO GEOLÓGICO DURANTE O FANEROZOICO: BACIA SEDIMENTARES INTRACONTINENTAIS, MARGEM CONTINENTAL BRASILEIRA E COBERTURAS VULCANOSSEDIMENTARES 30

CAPÍTULO 3 – MÉTODOS 33

3.1 TERMOCRONOLOGIA DE BAIXA TEMPERATURA 33

3.2 TRAÇOS DE FISSÃO EM APATITA 35

3.3 (U-TH)/HE EM ZIRCÃO E APATITA 38

3.4 MODELAGEM TÉRMICA INVERSA 40

CAPÍTULO 4 – SÍNTESE INTEGRADORA 42

4.1 INTRODUÇÃO 42
4.2 TERMOCRONOLOGIA DA FAIXA ARAÇUAÍ E CRÁTON SÃO FRANCISCO 42
4.3 TERMOCRONOLOGIA DO ESCUDO CATARINENSE E CINTURÃO DOM FELICIANO 47
4.4 INTEGRAÇÃO, CONCLUSÕES E PROPOSIÇÕES FUTURAS 48

REFERÊNCIAS BIBLIOGRÁFICAS 51

CAPÍTULO 5 – THERMAL HISTORY ALONG THE ARAÇUAÍ OROGEN AND SÃO FRANCISCO CRATON BORDER, EASTERN BRAZILIAN CONTINENTAL MARGIN, BASED ON LOW-TEMPERATURE THERMOCHRONOLOGIC DATA 62

NOTA EXPLICATIVA 62
ABSTRACT 62
5.1 INTRODUCTION 63
5.2 GEOLOGICAL AND GEOMORPHOLOGICAL BACKGROUND 65
5.2.1 GEOLOGIC SETTING 65
5.2.2 TECTONISM AND PHYSIOGRAPHY 68
5.2.3 EXISTING THERMOCHRONOLOGY DATA 69
5.3 SAMPLING AND ANALYTICAL METHODS 71
5.3.1 SAMPLING STRATEGY 71
5.3.2 STRUCTURAL INHERITANCE 72
5.3.3 APATITE AND ZIRCON (U-TH)/HE ANALYSIS 72
5.3.4 THERMAL HISTORY MODELING 74
5.4 RESULTS 75
5.4.1 LINEAMENT DIRECTIONS 75
5.4.2 RESULTS FROM ZHE AND AHE DATA 75
5.4.3 THERMAL INVERSION 81
5.5 DISCUSSION 85
5.5.1 INTRA- AND INTERSAMPLE VARIATIONS 85
5.5.1.1 Zircon 86
5.5.1.2 Apatite 87
5.5.2 COOLING PHASES, GEODYNAMIC FORCES AND DENUDATION RATES 88

5.5.2.1 End of the Brasiliano event (Early Paleozoic) to Pangea breakup 88
(Early Cretaceous)....88
5.5.2.2 Pangea breakup (Early Cretaceous) to present day 92
5.5.3 STRUCTURAL AND RHEOLOGICAL INHERITANCE 94
5.6 CONCLUSION 95
5.7 ACKNOWLEDGMENTS 97
REFERENCES 97
5.8 EMAIL DE ACEITE 106

CAPÍTULO 6 – CONTRASTING THERMAL HISTORIES IN THE DOM FELICIANO BELT TRIGGERED BY MAGMATISM RELATED TO THE PARANÁ-ETENDEKA LIP AND FRACTURE ZONE PROXIMITY 107

NOTA EXPLICATIVA....107
ABSTRACT....107
6.1 INTRODUCTION....108
6.2 GEOLOGICAL BACKGROUND 109
6.3 SAMPLING AND ANALYTICAL METHODS 113
6.3.1 SAMPLING APPROACH 114
6.3.2 LOW-TEMPERATURE THERMOCHRONOMETRY 114
6.3.2.1 Apatite Fission-Track 115
6.3.2.2 Apatite (U-Th)/He 116
6.3.2.3 Thermal history inversion....117
6.3.2.4 Previous thermochronology studies and data integration 118
6.4 RESULTS....119
6.4.1 APATITE FISSION-TRACK....119
6.4.2 APATITE (U-TH)/HE 123
6.4.3 THERMAL HISTORY MODELING....126
6.4.4 BASEMENT TEMPERATURES ASSESSMENT 129
6.5 DISCUSSION 132
6.5.1 DISTRIBUTION OF APATITE FISSION TRACK AGES IN THE NORTHERN AND SOUTHERN DOM FELICIANO BELT 132
6.5.2 APATITE (U-TH)/HE INTRA AND INTERSAMPLE AGE VARIATIONS....133
6.5.3 TIMING AND SPATIAL PATTERNS INFERRED FROM THERMOCHRONOLOGY AND DATA INTERPOLATION....134
6.6. CONCLUSION....138
6.7 ACKNOWLEDGMENTS....139

REFERENCES **139**

6.8 EMAIL DE ACEITE **149**

CAPÍTULO 7 – CONTRASTING BEHAVIOR AND DYNAMICS OF LITHOSPHERIC PROCESSES IN SÃO FRANCISCO CRATON AND ADJACENT BELTS: INSIGHTS FROM THERMOCHRONOLOGICAL ANALYSIS **150**

NOTA EXPLICATIVA **150**

ABSTRACT **150**

7.1 INTRODUCTION **151**

7.2 GEOLOGIC FRAMEWORK **152**

7.3 METHODS **155**

7.4 RESULTS **158**

7.4.1 SPATIAL DISTRIBUTION OF AFT AGES AND MTL 158

7.4.2 THERMAL HISTORY PATTERNS AND TEMPERATURE VARIATIONS: INSIGHTS FROM THERMAL MODELS AND DATA KRIGING 162

7.5 THERMOTECTONIC ASSESSMENT OF THE SÃO FRANCISCO CRATON AND SURROUNDING OROGENS **164**

7.5.1 THE NORTHERN ARAÇUAÍ BELT AND SÃO FRANCISCO CRATON: THE NEW AFT DATA SET 164

7.5.2 THE SÃO FRANCISCO CRATON AND SURROUNDING BELTS: REGIONAL ASSESSMENT 165

7.5.2.1 Carboniferous to Triassic 165

7.5.2.2 Triassic to Jurassic 170

7.5.2.3 Late Jurassic-Early Cretaceous and Cenozoic 171

7.6 CONCLUSION **174**

7.7 ACKNOWLEDGMENTS **176**

REFERENCES **176**

7.8 EMAIL DE CONFIRMAÇÃO DE SUBMISSÃO **183**

APÊNDICES **184**

A.1 – XII SOUTH AMERICAN SYMPOSIUM ON ISOTOPE GEOLOGY – 2022 ..... **184**

A.2 – XII SOUTH AMERICAN SYMPOSIUM ON ISOTOPE GEOLOGY – 2022 ..... **185**

A.3 – IV SEMANA ACADÊMICA DOS PÓS-GRADUANDOS DO INSTITUTO DE GEOCIÊNCIAS – SAPIGEO – 2022 ..... **186**

A.4 – 50º CONGRESSO BRASILEIRO DE GEOLOGIA – 2021 ..... **187**

A.5 – 50º CONGRESSO BRASILEIRO DE GEOLOGIA – 2021 ..... **188**

A.6 – CAPÍTULO DO LIVRO "CONTRIBUIÇÕES À GEOLOGIA DO RIO GRANDE DO SUL E DE SANTA CATARINA – 2021

(DISPONÍVEL EM: HTTPS://LUME.UFRGS.BR/HANDLE/10183/221989) 189

A.7 – ORGANIZAÇÃO DE EVENTOS – 2022 190

A.7 – ORGANIZAÇÃO DE EVENTOS – 2019 191

ESTRUTURA DA TESE

Esta tese de doutorado está estruturada em três artigos científicos: dois deles publicados no periódico *Tectonophysics*, classificado no estrato Qualis-CAPES A1 – quadrênio 2017-2020, e um artigo submetido e em processo avançado de revisão no periódico *Gondwana Research*, classificado no estrato Qualis-CAPES A1 – quadriênio 2017-2020. A organização da tese compreende as seguintes partes:

- Texto Integrador composto por: Capítulo 1) Introdução, com a formulação do problema de investigação, hipóteses e objetivos da pesquisa; Capítulo 2) Contexto geológico da área de estudo; Capítulo 3) Métodos utilizados; Capítulo 4) Síntese integradora, com os principais resultados obtidos, interpretações e conclusões; Referências bibliográficas.
- Artigos: corpo principal da tese, constituído dos artigos desenvolvidos durante o doutorado. O Capítulo 5) corresponde ao artigo publicado no ano de 2022 no periódico *Tectonophysics*; o Capítulo 6) corresponde ao artigo publicado no ano de 2023 no periódico *Tectonophysics*; e o capítulo 7) corresponde ao artigo submetido em 2023 ao periódico *Gondwana Research*.
- Apêndices: compreendem trabalhos acadêmicos publicados durante o doutoramento 1) resumos em congressos, 2) capítulos de livros; 3) organização de eventos.

CAPÍTULO 1 - INTRODUÇÃO

1.1 Introdução

A Província Mantiqueira (Fig. 1.1) é um sistema orogênico com cerca de 3.000 km de extensão que cobre a porção sudeste e sul do território brasileiro e se estende até o Uruguai. Seus limites são a margem continental brasileira a leste, o Cráton São Francisco a norte e noroeste, a Província Tocantins a oeste e a Bacia do Paraná como seu limite na parte sudoeste a sul (de Almeida et al., 1981). A Província Mantiqueira é composta por três cinturões orogênicos nomeados Cinturão Dom Feliciano (porção meridional), Faixa Ribeira (porção central) e Faixa Araçuaí (porção setentrional).

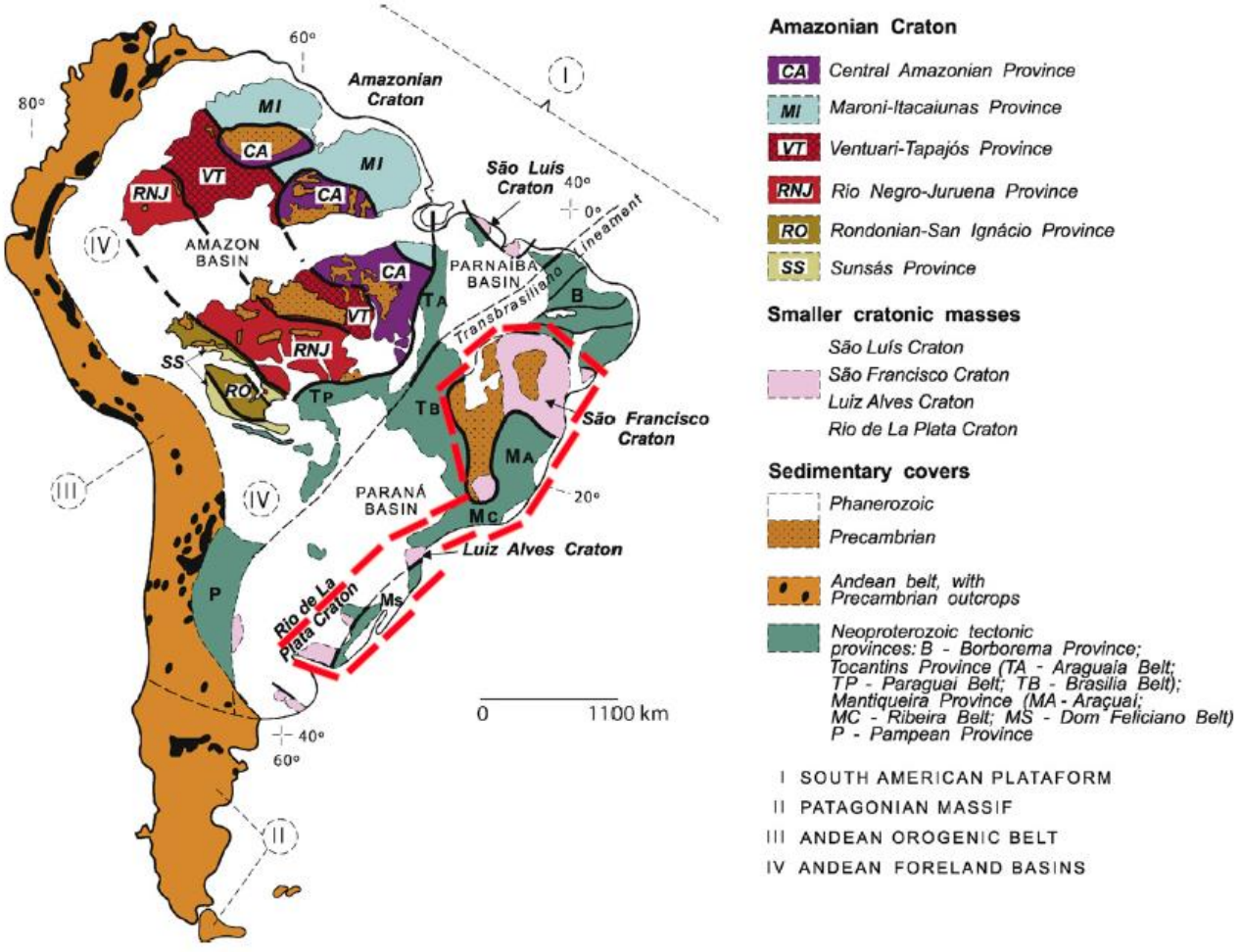

Figura 1. 1: Mapa esquemático da continente Sulamericano evidenciando os blocos cratônicos, províncias Neoproterozoicas e coberturas sedimentares. A Província Mantiqueira e crátons adjacentes estão circulados em vermelho (modificado de Basei et al., 2010).

Disposta sobre o embasamento constituído pelas rochas da Província Mantiqueira, a margem continental Atlântica da América do Sul é caracterizada por uma grande

variação em topografia, geologia e estruturação do embasamento cristalino. Essa margem é segmentada por diversas zonas de fraturas (Fig. 1.2), desde a Zona de Fraturas Cadeia, localizada na porção equatorial brasileira, até a Zona de Fraturas Agulhas-Malvinas, a sul, limítrofe com a Placa de Scotia. Pode-se dividir a margem continental Atlântica em quatro setores:

- A norte, o embasamento da margem Atlântica forma um mosaico composto por terrenos da Província Borborema, de idade pré-Cambriana, justapostos por grandes zonas de cisalhamento, sendo sua estruturação perpendicular à atual linha de costa.
- A nordeste, a margem Atlântica é composta por rochas Arqueanas e Proterozoicas do Cráton São Francisco e da porção setentrional da Província Mantiqueira que recebe o nome de Faixa Araçuaí, a qual exibe topografia elevada e estruturação paralela a subparalela à linha de costa.
- A porção leste e sudeste é constituída por rochas Arqueanas do Cráton Luís Alves e Neoproterozoicas do Cinturão Ribeira e trecho norte do Cinturão Dom Feliciano. A topografia neste setor é acidentada e paralela à linha de costa, com picos que atingem altitudes até cerca 2900 m. A estruturação do embasamento também é predominantemente paralela à linha de costa, porém foi herdada dos domínios Neoproterozoicos. Essa porção da margem possui escarpas que a separam do interior continental, que é, geralmente, elevado, tal qual a margem sudoeste da África (Gilchrist and Summerfield, 1990). Além disso, existe a presença de importantes zonas de fraturas de direção NW-SE que se formaram a partir da abertura do Oceano Atlântico Sul devido a rotação da Placa Sulamericana (Szatmari and Milani, 2016; Salomon et al., 2017).
- A sul, nas imediações do Escudo Catarinense até a região da Bahía Blanca, na Argentina, a margem torna-se progressivamente mais baixa, sendo que a sul do Rio de la Plata inexiste o embasamento pré-Cambriano aflorante. A Província Mantiqueira meridional, bem como o Cráton Rio de la Plata e o Terreno Patagônia, se inserem neste domínio.

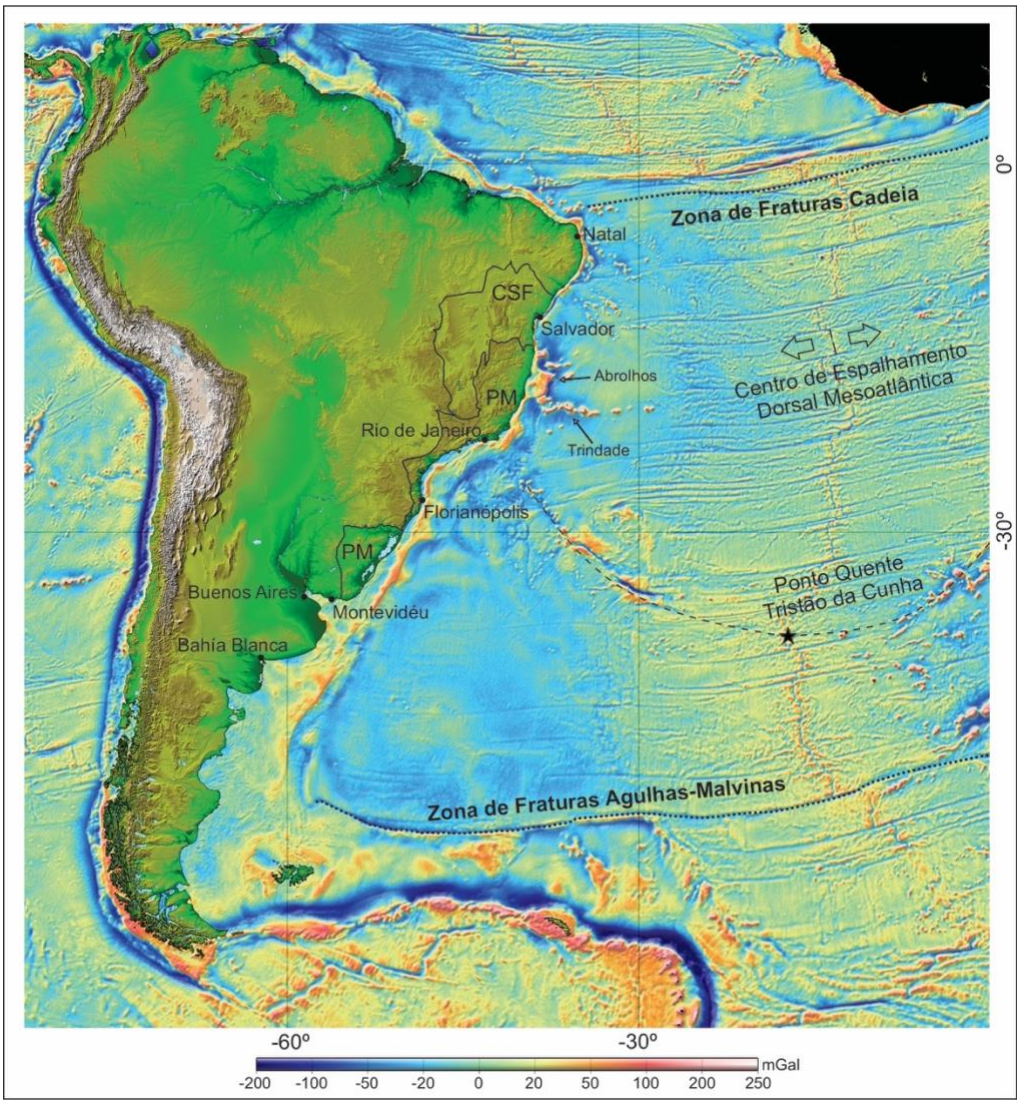

Figura 1. 2: Modelo digital de terreno da América do Sul gerado a partir de dados da Shuttle Radar Topographic Mission (SRTM), NASA/JPL/NIMA delimitando a Província Mantiqueira e o Cráton São Francisco (CSF). Fundo oceânico gerado a partir de dados gravimétricos evidenciando zonas de fraturas (extraído de Sandwell et al., 2014).

A transição entre os setores nordeste/leste e sudeste/sul da margem continental na Província Mantiqueira não é gradual, o que reflete a influência da natureza da margem no desenvolvimento das bacias sedimentares adjacentes, assim como sugere a influência de processos mantélicos na estruturação da margem continental (Cogné et al., 2011; Hueck et al., 2019). Na margem brasileira encontram-se duas das principais zonas de transição observadas na margem continental do Atlântico Sul que carecem de dados termocronológicos até o presente momento ou que necessitam melhor entendimento de alguns de seus processos evolutivos. São elas:

O Escudo Catarinense, pertencente ao segmento norte do Cinturão Dom Feliciano, marca uma forte transição topográfica, estrutural e termocronológica entre terrenos

elevados a norte, com picos acima de 1200 m, e menos elevados, de média não superior a poucas centenas de metros, a sul. Nas proximidades de Florianópolis, essa transição é bastante evidente. A região também se situa adjacente à divisa entre a Bacia de Santos, que possui elevado potencial prospectivo para hidrocarbonetos, e a Bacia de Pelotas, de baixo potencial. Hueck et al. (2019) mencionam em seu trabalho essa diferença marcante de transição topográfica, ao passo que Karl et al. (2013), Hueck et al. (2018a), Krob et al. (2019) e do Amaral Santos et al. (2023) sugerem o apagamento parcial ou total de termocronômetros como Traços de Fissão em Apatita (TFA) e Zircão (TFZ) e (U-Th)/He em Apatita (AHe) e Zircão (ZHe), na região sul do Estado de Santa Catarina.

A porção sul do Estado da Bahia marca uma forte transição reológica entre a litosfera cratônica, composta por rochas do Cráton São Francisco, e a litosfera orogênica, composta por rochas da Faixa Araçuaí, exibindo topografia elevada próxima à linha de costa e paralela a ela. Além disso, um traço marcante particular a esta zona transicional é que as bacias marginais Mesozoicas a norte exibem caráter não-magmático ao passo que a sul dessa transição o comportamento é de extensão/ruptura essencialmente magmática, até o limite com a Bacia de Pelotas. Existe também um forte controle térmico observado nas idades de TFA que marca a transição entre estes terrenos, sendo que a Província Mantiqueira abriga idades mais jovens, essencialmente relacionadas às fases de ruptura continental, enquanto o Cráton São Francisco registra idades Paleo- e Mesozoicas (Engelmann de Oliveira and Jelinek, 2017; Fonseca et al., 2021).

Tendo isto em consideração, e constatando que até o momento estas zonas não foram trabalhadas em detalhe, conforme pode ser visto no levantamento dos dados até então publicados, sintetizados na Fig. 1.3, este trabalho tem como objetivo estudar os efeitos destas zonas de transição da margem continental na evolução termotectônica Fanerozoica na Província Mantiqueira e dos crátons adjacentes a ela. A principal abordagem metodológica a ser aplicada neste estudo é a termocronologia de baixa temperatura, por TFA e AHe e ZHe. O uso destes termocronômetros combinados é justificado por serem imprescindíveis na construção de um modelo térmico que apresente a trajetória térmica da amostra analisada em uma variada faixa de temperaturas. Isso permite evidenciar os episódios de resfriamento e aquecimento que as amostras foram submetidas nos quilômetros superficiais da crosta, assim como permite correlacionar tais episódios a eventos geológicos locais e regionais que darão bases para a construção de modelos geodinâmicos destas regiões.

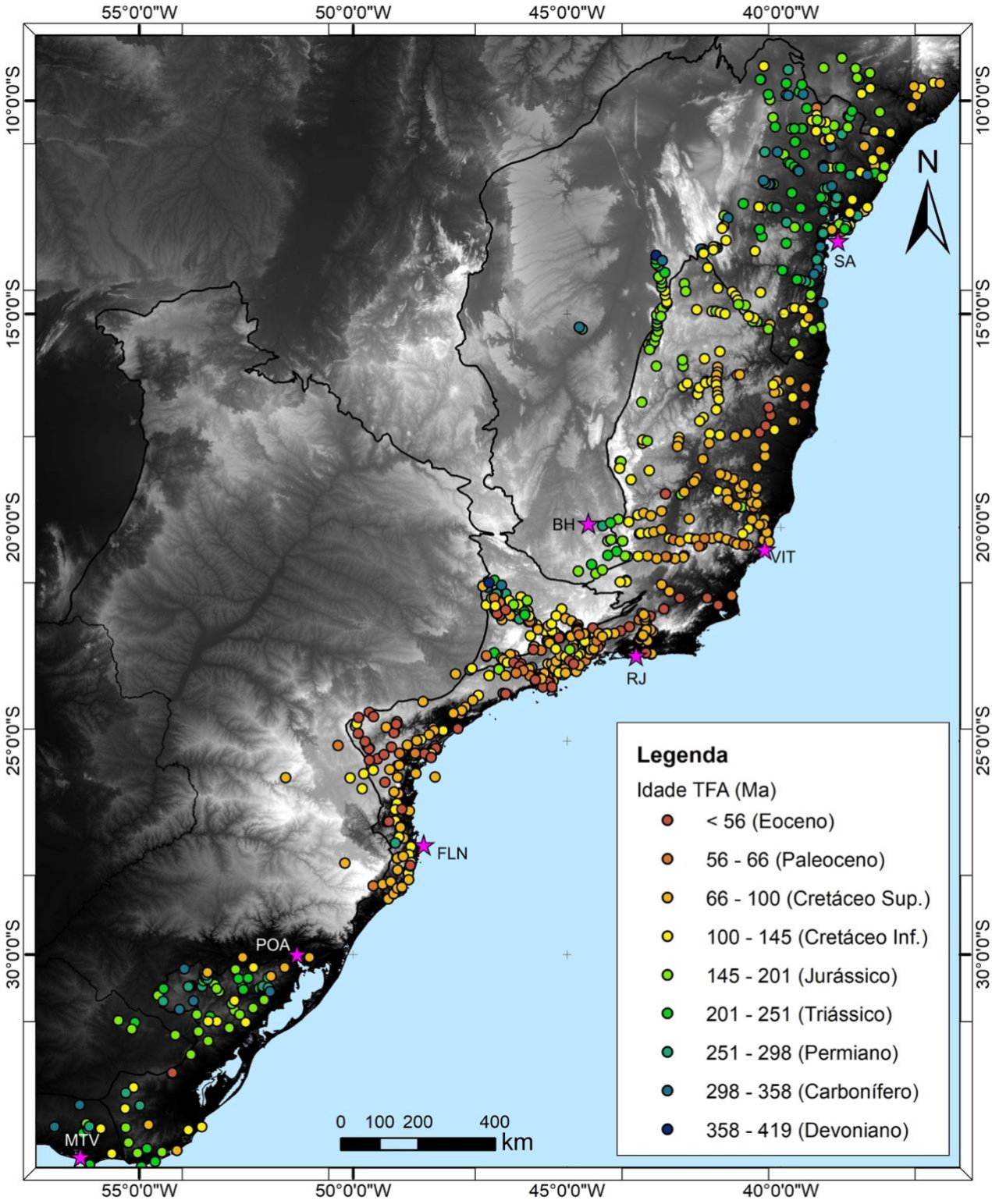

Figura 1. 3: Distribuição das idades centrais de Traços de Fissão em Apatita ao longo da Província Mantiqueira e crátons adjacentes (modificado de Engelmann de Oliveira and Jelinek, 2017; Hueck et al., 2019; Novo et al., 2021).

1.2 Objetivos

1.2.1 Objetivo Geral

Este trabalho tem como objetivo principal compreender a evolução tectonotermal Fanerozoica de zonas transicionais da margem continental que tem como embasamento a Província Mantiqueira e crátons adjacentes. No entanto, a Província Mantiqueira apresenta algumas regiões menos estudadas que são extremamente importantes para reconstruir por completo a evolução Fanerozoica da margem continental na área da Província Mantiqueira, que se refere às zonas transicionais, e que, portanto, serão detalhadas neste estudo. Utilizando-se da termocronologia de baixa temperatura nessas áreas, será possível aperfeiçoar o entendimento da evolução termotectônica Fanerozoica da Província Mantiqueira e correlacionar com o contexto tectônico do Gondwana Ocidental e formação da margem passiva brasileira.

A hipótese central deste trabalho é que o registro termocronológico das regiões estudadas permite obter dados que caracterizem os eventos de resfriamento e reaquecimento da porção superior da crosta, tanto de áreas cratônicas e de escudos, quanto de regiões orogênicas e da margem continental. Além disso, a análise desses dados permite estimar espessuras denudadas da porção continental que podem ser correlacionadas à registros em bacias sedimentares da margem e do próprio continente.

1.2.2 Objetivos Específicos

- Obter dados termocronológicos por TFA, AHe e ZHe das mesmas amostras, quando possível, nas duas áreas-alvo deste estudo: região norte do Cinturão Dom Feliciano (TFA e AHe) e porção extremo-norte da Faixa Araçuaí e do Cráton São Francisco (TFA, ZHe e AHe).

- Determinar os eventos de resfriamento e aquecimento que possam ter contribuído para acelerar ou retardar a exumação das rochas amostradas para ambas as regiões estudadas.

- Estimar possíveis taxas de resfriamento e erosão durante o Fanerozoico.

- Compreender os efeitos da abertura do Oceano Atlântico Sul no registro termocronológico.

- Investigar a magnitude e a abrangência espacial do apagamento parcial ou total dos TFA, AHe e ZHe.

- Investigar a influência das zonas de transição topográfica, geológica e estrutural

no registro termocronológico.

- Investigar a influência dos magmatismos da Bacia do Paraná, da anomalia térmica de Trindade, da Província Magmática de Abrolhos, bem como a presença de diques alimentadores da Bacia do Paraná no registro termocronológico.

- Elaborar um modelo geodinâmico de cada região estudada incorporando os dados existentes para a margem continental brasileira.

CAPÍTULO 2 – CONTEXTO GEOLÓGICO

A pesquisa aqui apresentada focou em dois segmentos da margem continental brasileira que tem como embasamento a Província Mantiqueira e que representam zonas transicionais sob diversos aspectos como mencionado no Cap. 1. Este capítulo apresenta uma breve revisão sobre o contexto geológico de cada uma dessas áreas, desde a formação do embasamento cristalino aos registros geológicos Cenozoicos.

A primeira parte deste capítulo será referente à área de estudo setentrional, logo referente à Faixa Araçuaí e o Cráton São Francisco, além de uma breve descrição da porção central da Província Mantiqueira – Faixa Ribeira, visto que foi analisada em um dos artigos aqui apresentados. A segunda parte se refere ao Cinturão Dom Feliciano e crátons Luís Alves e Rio de la Plata, que é o cinturão que caracteriza a porção meridional da Província Mantiqueira.

A Província Mantiqueira é o resultado do amalgamento de blocos cratônicos pré-Neoproterozoicos que formaram o supercontinente Gondwana durante eventos colisionais do Neoproterozoico ao Ordoviciano (de Almeida et al., 1981; Hasui, 2010; Bento dos Santos et al., 2015) conhecidos como Orogenia Brasiliana/Pan-Africana (Basei et al., 2010) ou Ciclo Brasiliano. Os núcleos cratônicos e microplacas envolvidos nesses eventos foram os crátons São Francisco, Paranapanema, Rio de la Plata e Luís Alves na porção Sulamericana e os crátons Congo e Kalahari na contraparte africana (Cordani et al., 1973; Porada, 1989). Desta forma, esta província corresponde ao cinturão orogênico formado entre estes fragmentos cratônicos, subdividida nos Cinturões Dom Feliciano a sul, Ribeira na porção central e Araçuaí a norte (Fig. 1.1).

2.1 O Cráton São Francisco e as Faixas Araçuaí e Ribeira

O Cráton São Francisco (CSF) é um fragmento cratônico que compõe a Placa Sulamericana e que já foi parte do Cráton do Congo. Estes dois crátons eram conectados por uma ponte crustal localizada entre o sistema Sergipano-Oubanguides ao norte e Orógeno Araçuaí-Congo Ocidental a sul (Porada, 1989). Esses crátons permaneceram juntos até a completa dispersão do paleocontinente Gondwana Ocidental durante o Cretáceo Inferior, dando origem ao Oceano Atlântico (Heilbron et al., 2017a). A história evolutiva do embasamento CSF é mais antiga que 1,8 Ga, enquanto a cobertura do cráton é mais jovem. O embasamento é caracterizado por rochas tonalíticas-

trondhjemíticas-granodioríticas e gnaisses arqueanos, granitoides, *greenstone belts*, além de plútons e sucessões supracrustais Paleoproterozoicos (Almeida, 1977; Heilbron et al., 2017a). Esse conjunto de rochas afloram na porção sul e nordeste do CSF, que possui a forma de uma península (Alkmim and Martins-Neto, 2012), sendo que ele forma um bloco estável de orientação NS ligado a dois segmentos de orógenos Paleoproterozoicos (Barbosa and Sabaté, 2004).

A cobertura do CSF, por outro lado, é caracterizada por rochas Proterozoicas e Fanerozoicas que se agrupam em três domínios no interior do cráton: a Bacia do São Francisco (Reis et al., 2017), o aulacógeno Paramirim (Cruz and Alkmim, 2017) e o rifte Recôncavo-Tucano-Jatobá (Milani et al., 1988), sendo que a Bacia do São Francisco será melhor caracterizada adiante. O entorno do CSF é dominado por cinturões orogênicos formados durante o Neoproterozoico, exceto a leste na qual o oceano Atlântico o bordeja. Os cinturões orogênicos compõem diversos sistemas orogênicos, como a Província Mantiqueira, e se formaram durante a consolidação do paleocontinente Gondwana Ocidental, que era composto por diversos núcleos cratônicos dos atuais continentes Sulamericano e Africano. Neste subitem, o enfoque será nos cinturões que se localizam a sudeste e sul do CSF, que recebem o nome de Faixa Araçuaí e Faixa Ribeira, respectivamente (Almeida, 1977).

A Faixa Araçuaí, um cinturão orogênico de idade Neoproterozoica a Cambriana, é interpretada como o domínio externo do Orógeno Araçuaí-Congo Ocidental (Pedrosa-Soares and Wiedemann-Leonardos, 2000) e caracterizado pela presença de deformação envolvendo o embasamento (*thick-skinned deformation)*. Esse cinturão se formou a partir da interação dos crátons São Francisco e Congo em um ambiente confinado semelhante a uma baía (Alkmim et al., 2006, 2017; Pedrosa-Soares et al., 2008; Pedrosa-Soares and Alkmim, 2011). O embasamento cristalino do segmento localizado em território brasileiro é mais antigo que 1,8 Ga. Este segmento herdou lascas ofiolíticas (Queiroga et al., 2007), zonas de sutura e o arco magmático (Tedeschi et al., 2016) e registrou magmatismo sin a pós-colisional (Pedrosa-Soares et al., 2008). Também compõem a Faixa Araçuaí sucessões sedimentares do tipo rifte-sag de idade Paleo a Mesoproterozoica representadas pelo Supergrupo Espinhaço, unidades de margem passiva do Grupo Macaúbas (Souza et al., 2019) e sequências sin-orogênicas. O lapso temporal entre o clímax sin-metamórfico ao plúton granítico mais velho, de aproximadamente entre 590 e 530 Ma, marca o desenvolvimento desse orógeno (Alkmim

et al., 2017). Também estão presentes diversas estruturas extensionais que registram o colapso orogênico entre 530 e 480 Ma (Pedrosa-Soares and Alkmim, 2011).

A Faixa Ribeira, localizada a sul do CSF, se formou a partir de múltiplos episódios colisionais e acrescionários durante o Neoproterozoico ao Cambriano (Heilbron and Machado, 2003; Heilbron et al., 2017b), com registro metamórfico entre 630 a 510 Ma (Heilbron et al., 2017b). Esse cinturão orogênico é composto por quatro terrenos tectono-estratigráficos, com a presença de embasamento retrabalhado no setor externo. Diversos tipos de bacia compõem esse cinturão, como o desenvolvimento de unidades típicas de margem passiva e de margem ativa, além de arcos magmáticos continentais, da intrusão de plútons graníticos no embasamento cristalino e de unidades supracrustais (Heilbron et al., 2020). A Faixa Ribeira também é caracterizada pela ancoragem de terrenos (*terrane docking*) e retrabalhamento, ocasionado pela ancoragem do Terreno Cabo Frio e consequente geração de dobras regionais e instalação de zonas de cisalhamento transpressionais dextrais (Schmitt et al., 2016, 2018).

Para este trabalho, foram coletadas 23 amostras de rochas de composição predominantemente graníticas do CSF e da Faixa Araçuaí (Fig. 2.1), que são tipos de rochas geralmente ricas em apatita e zircão. Todas as 23 amostras foram analisadas para a técnica de TFA, enquanto sete delas foram analisadas para ZHe e AHe.

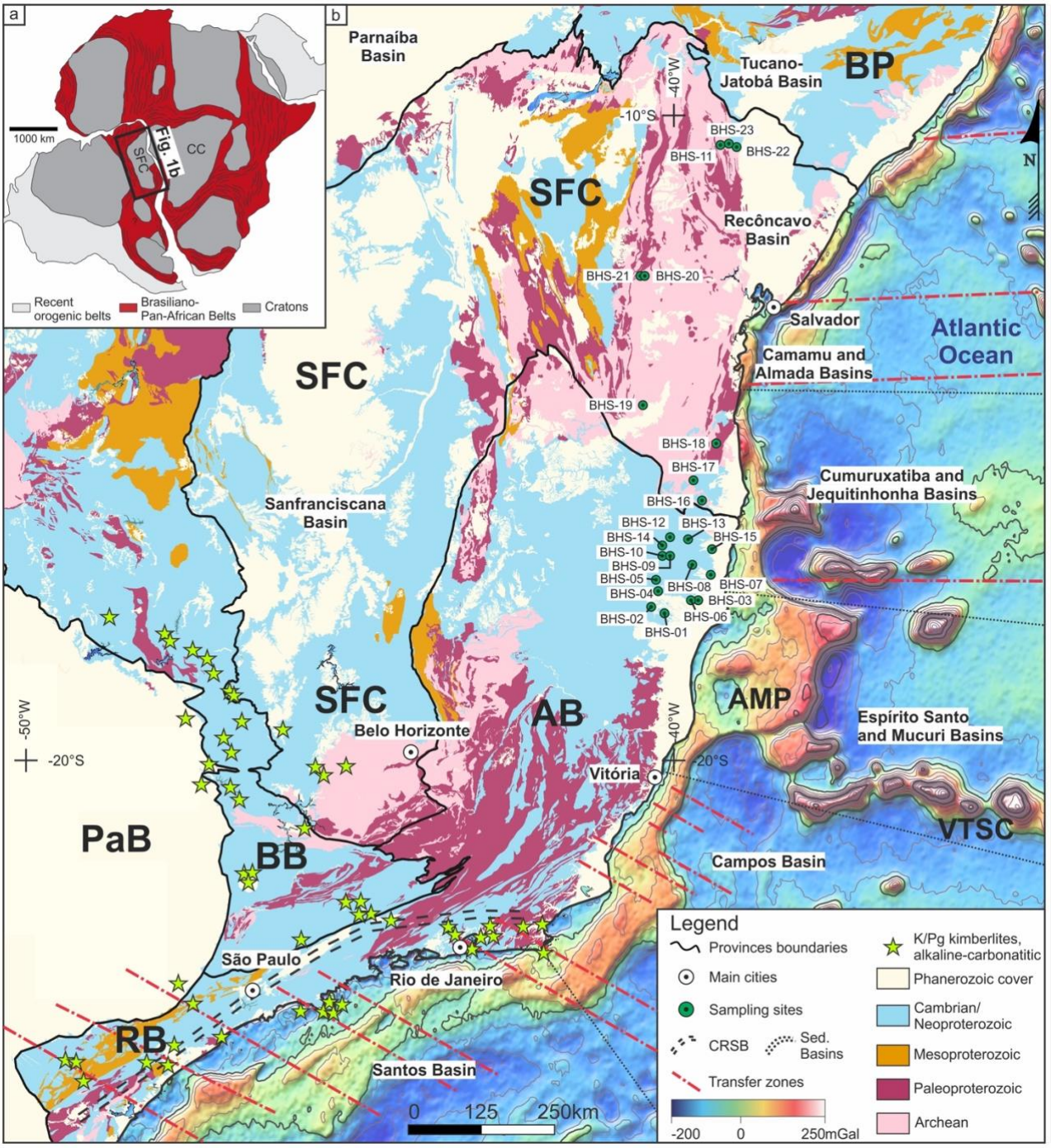

Figura 2. 1: Mapa geológico do sudeste a nordeste brasileiro evidenciando os pontos amostrais e os terrenos arqueanos e proterozoicos do Cráton São Francisco (CSF), Faixa Araçuaí (AB), Faixa Ribeira (RB), Faixa Brasília (BB) e Província Borborema (BP), além da cobertura vulcanossedimentar das Bacias do Paraná (PaB), Sanfranciscana e Parnaíba, e as bacias da margem continental. Também estão presentes as zonas de fraturas, os principais plútons kimberlíticos, alcalino-carbonatíticos da região e a Província Magmática de Abrolhos (AMP) e a Cadeia Vitória-Trindade (VTSC) (modificado de Dalton de Souza et al., 2003; Perrota et al., 2005; Heilbron et al., 2016; Silva et al., 2020)

2.2 Os Crátons Rio de la Plata e Luís Alves e o Cinturão Dom Feliciano

O Cráton Rio de la Plata é composto de diversos terrenos graníticos e gnáissicos

Paleoproterozoicos (2,2 a 2,1 Ga) que representam magmatismo acrescionário. Também estão presentes relictos de rochas supracrustais Paleoproterozoicas, sendo que todas essas rochas sofreram metamorfismo de fácies xisto verde. Dois terrenos compõem as principais exposições do Cráton Rio de la Plata: o terreno Piedra Alta e o terreno Tandilla (Oyhantçabal et al., 2018a). Estes terrenos são compostos por rochas de natureza granítica e gnáissica separadas por cinturões metamórficos de rochas supracrustais (Bossi and Cingolani, 2009). Já o terreno Nico Perez, que aflora tanto no Brasil quanto no Uruguai, encontra-se exposto em três blocos distintos, sendo que as unidades que os compõem são caracterizadas como ortognaisses, anfibolitos, migmatitos, rochas ígneas de natureza máfica a ultramáfica e metassedimentos (Oriolo et al., 2016; Philipp et al., 2016; Oyhantçabal et al., 2018b).

Já o Cráton Luís Alves, localizado entre os Estados de Santa Catarina e Paraná, representa fragmentos continentais pré-existentes ou microplacas envolvidos no fechamento do oceano Adamastor durante a formação do paleocontinente Gondwana Ocidental (Passarelli et al., 2018). Esse cráton é caracterizado por rochas tonalíticas-trondhjemíticas-granodioríticas, corpos máficos a ultramáficos e blocos crustais de composição paragnáissica. A fácies metamórfica que caracteriza essas rochas é de granulito de médio a alto grau (Basei et al., 1992). Intrudindo estas rochas, encontram-se também granitoides Neoproterozoicos, além de unidades supracrustais de mesma idade (Passarelli et al., 2018).

Por fim, o Cinturão Dom Feliciano, que representa o setor meridional da Província Mantiqueira e aflorante nos Estados de Santa Catarina e Rio Grande do Sul, além do Uruguai, se formou a partir da acresção de diversos terrenos durante o Neoproterozoico (Philipp et al., 2016). Diversos terrenos compõem o Cinturão Dom Feliciano caracterizados como migmatitos e granulitos de alto grau, arcos juvenis de idade 890 a 860 Ma e 770 e 720 Ma e bacias colisionais tardias (Hueck et al., 2018b). Além desses registros, encontram-se *inliers* de embasamento de idade Paleoproterozoica, granitos metamorfizados, anfibolitos e complexos metamulcanossedimentares. Também existem batólitos gerados durante e após a orogenia Dom Feliciano e que aproveitou a presença de zonas de cisalhamento de alto ângulo para se alojarem na crosta (Philipp and Machado, 2005). Esses grandes corpos ígneos recebem o nome de Aiguá (Uruguai), Pelotas (Rio Grande do Sul) e Florianópolis (Santa Catarina). Bacias pós-colisionais Neoproterozoicas compostas por sucessões vulcanossedimentares também estão

presentes junto ao Cinturão Dom Feliciano e crátons adjacentes (Guadagnin et al., 2010).

Para este trabalho, foram coletadas 13 amostras de rochas de composição predominantemente graníticas do Batólito Florianópolis (Fig. 2.2). Todas as 13 amostras foram analisadas para a técnica de TFA, enquanto seis delas foram analisadas para AHe.

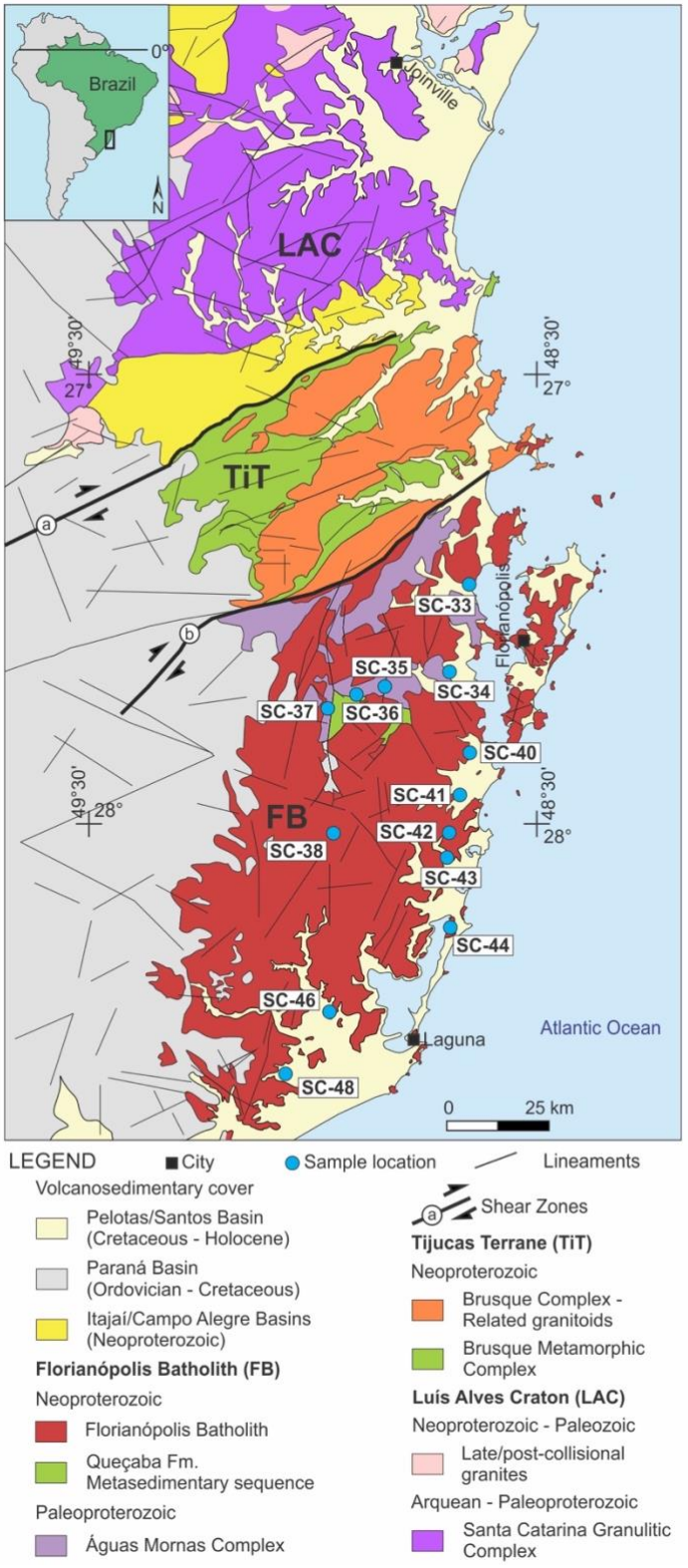

Figura 2. 2: Mapa geológico da área de estudo com a localização das amostras coletadas compreendendo o Escudo Catarinense e seus principais terrenos e zonas de cisalhamento (modificado de Wildner et al., 2014).

2.3 Registro geológico durante o Fanerozoico: Bacia sedimentares intracontinentais, margem continental brasileira e coberturas vulcanossedimentares

Após o final da orogenia Brasiliana/Pan-Africana no Ordoviciano, o paleocontinente Gondwana Ocidental iniciou um estágio de estabilidade durante o qual diversos depocentros se formaram e permitiram o acúmulo de sedimentos erodidos e transportados dos cinturões brasilianos (Carneiro et al., 2012). As Bacias do Paraná, Parnaíba e Sanfranciscana são algumas dessas depressões (Fig. 2.1), hoje situadas sobre a Plataforma Sulamericana, que registram a exumação dos orógenos Neoproterozoicos (Linol et al., 2015) e serão pontuadas a seguir de forma breve.

Os registros iniciais da Bacia do Paraná datam do Ordoviciano. Esta bacia sedimentar é caracterizada por ciclos transgressivos-regressivos e constituída por seis supersequências que são separadas por inconformidades regionais. As três primeiras supersequências abrangem o intervalo temporal entre o Ordoviciano e o Permiano/Triássico, que registram ambientes essencialmente marinhos, glacial e costeiro. Por outro lado, as três supersequências superiores, de idade Triássica a Cretácica, tem registros que apontam para o caráter continental da bacia, com unidades vulcanossedimentares (Scherer et al., 2023). Destacam-se nesse conjunto estratigráfico as unidades vulcânicas do Grupo São Bento, Formação Serra Geral, datadas do Cretáceo Inferior, que compõem essa bacia, com magmatismo básico a ácido que cobre cerca de $1{,}2 \times 10^6$ km^2 entre o Brasil, Paraguai, Argentina e Uruguai (Milani et al., 1998, 2007a).

A Bacia do Parnaíba iniciou seu desenvolvimento durante o Siluriano, possivelmente decorrente da instalação de estruturas na forma de grabéns e formando seu depocentro inicial (de Oliveira and Mohriak, 2003). Essa bacia é constituída por cinco supersequências que registram a flutuação eustática de mares epicontinentais. As duas supersequências basais, datadas do Siluriano e Devoniano/Carbonífero (Mississipiano), são caracterizadas por unidades marinhas e glaciais. As três unidades superiores, que abrangem do Carbonífero (Pennsylvaniano) ao Cretáceo Superior registram unidades que migram do ambiente marinho raso ao continental (Vaz et al., 2007). A Bacia do Parnaíba também guarda registros magmáticos denominados Formação Mosquito e Formação Sardinha, que registram o refiteamento do Atlântico Sul e Central, e são caracterizadas como rochas ígneas intrusivas e extrusivas de composição básica

(Macêdo Filho et al., 2023; Vaz et al., 2007).

A Bacia Sanfranciscana é caracterizada como pertencente à Bacia do São Francisco, porém registra apenas a porção de idade Fanerozoica, entre o Carbonífero/Permiano ao Cretáceo. Essa bacia se localiza integralmente dentro do CSF e possui registros de unidades formadas em ambientes glácio-marinhos e desértico continentais, além de magmatismo extrusivo (Sgarbi et al., 2001; Zalán and Silva, 2007; Reis et al., 2017).

A formação das bacias da margem continental brasileira se iniciou durante o Cretáceo Inferior contemporaneamente ao rifteamento que culminou com a dispersão do paleocontinente Gondwana Ocidental (Nürnberg and Müller, 1991; Chang et al., 1992). De sul para norte, as Bacia de Pelotas, Santos, Campos, Espírito Santo e Mucuri, se assentam sobre rochas que compõem a Província Mantiqueira, enquanto as bacias Cumuruxatiba, Jequitinhonha, Almada, Camamu e Jacuípe tem como embasamento o CSF. Cada uma dessas bacias possui suas particularidades, como a bacia de Pelotas que apresenta uma margem essencialmente vulcânica com a presença de refletores mergulhantes para o mar (*seaward-dipping reflectors*) (Bueno et al., 2007) e as bacias de Santos, Campos e Espírito Santo que possuem uma espessa camada de evaporitos (Moreira et al., 2007; Milani et al., 2007b; Mohriak et al., 2008). Além do registro sedimentar, a instalação do rifte à leste da Província Mantiqueira levou à formação de diversas zonas de fraturas de direção EW e NW-SE, muitas delas reativadas durante o Cretáceo e o Cenozoico, promovendo exumação e entalhamento da rede de drenagem (Van Ranst et al., 2020; Brandão et al., 2022; dos Santos et al., 2023).

Também durante a transição do Cretáceo para o Cenozoico se formou o rifte continental do sudeste brasileiro, que é essencialmente paralelo à linha de costa e às zonas de cisalhamento da Faixa Ribeira (Riccomini et al., 2004; Zalán and De Oliveira, 2005). O rifte cenozoico promoveu exumação de rochas da Faixa Ribeira e levou à formação de diversas bacias sedimentares no sudeste brasileiro, como as bacias de Taubaté, Volta Redonda, São Paulo, entre outras (Riccomini, 1990). Por fim, durante esse período, a região próxima à margem continental e algumas porções do interior da plataforma Sulamericana registraram vulcanismo kimberlítico e alcalino-carbonatítico (Ferreira et al., 2022), como é o caso dos corpos alojados nas proximidades do rifte Cenozoico mencionando anteriormente (Zalán and De Oliveira, 2005), o Maciço Alcalino de Poços de Caldas e kimberlitos do CSF e Faixa Brasília (Takenaka et al., 2023), a

Província Magmática de Abrolhos (Stanton et al., 2021) e a cadeia Vitória-Trindade (Cordani, 1970; Thompson et al., 1998).

CAPÍTULO 3 – MÉTODOS

A pesquisa aqui apresentada utilizou dois métodos de datação radiométrica: a técnica de traços de fissão e de (U-Th)/He. Esses métodos são amplamente utilizados em pesquisas envolvendo as geociências, de modo que este capítulo não busca apresentar um referencial teórico detalhado, mas apenas os conceitos teóricos básicos dos métodos, as faixas de temperatura que eles operam e a complementariedade entre eles. Além disso, será apresentada neste capítulo a técnica de modelagem térmica inversa, largamente utilizada para a obtenção de histórias térmicas.

Os métodos supracitados são conhecidos como termocronômetros de baixa temperatura, visto que são técnicas sensíveis a temperaturas abaixo de 300 °C, registrando, portanto, eventos térmicos nas porções mais rasas da crosta. De posse das idades termocronológicas, de parâmetros físicos dos minerais analisados e de modelos cinéticos, foi possível reconstruir a história térmica de cada amostra por meio da modelagem inversa. A partir desses dados, interpretados em conjunto com estudos geológicos de natureza complementar, como geomorfologia, sedimentologia, geologia estrutural e estratigrafia, foi possível inferir eventos de resfriamento e aquecimento, além de exumação de rochas dos domínios orogênicos e cratônico estudados.

3.1 Termocronologia de baixa temperatura

A termocronologia é a prática de se obter histórias térmicas de minerais e rochas a partir de seu conteúdo químico, isotópico ou de propriedades físicas de minerais que são sensíveis à temperatura e ao tempo (Reiners, 2021). Os termocronômetros são o conjunto de decaimento radioativo pai-filho específico para cada mineral que é determinado a partir de modelos cinéticos. O átomo filho, que é o produto do decaimento radioativo, pode ser um átomo radiogênico ou um dano físico induzido pela radiação que se acumula somente em condições de temperatura abaixo da temperatura de fechamento do mineral que o hospeda e para o sistema isotópico considerado (Fig. 3.1). A temperatura de fechamento não é um valor de temperatura específico, mas uma faixa de temperaturas, de modo que essa faixa é definida como Zona de Retenção Parcial (ZRP – *Partial Retention Zone*) ou Zona de Apagamento Parcial (ZAP – *Partial Annealing Zone)* a depender de qual termocronômetro se aborda.

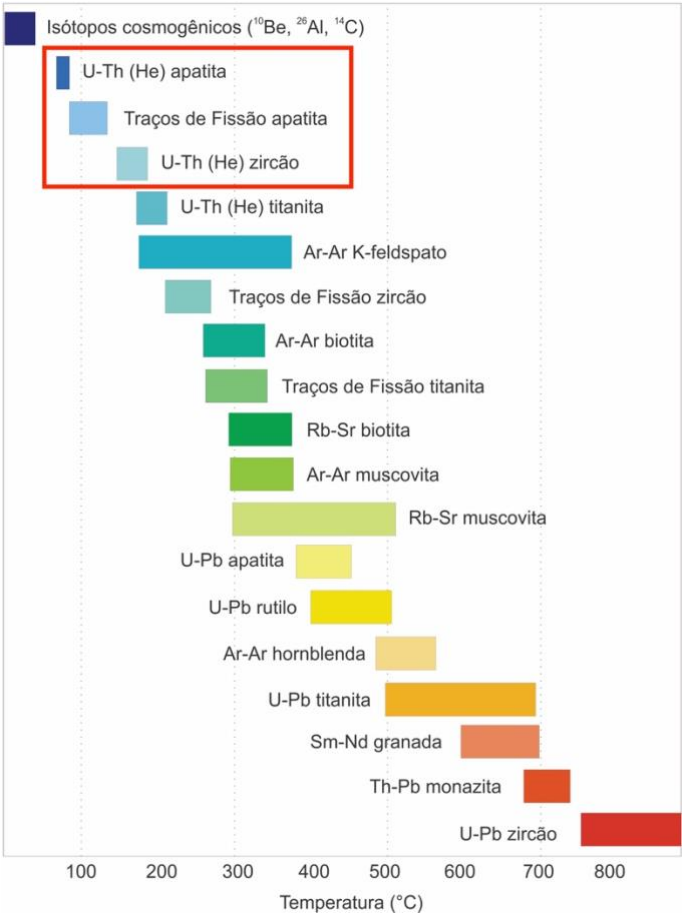

Figura 1. 4: Temperatura de fechamento (Zona de Retenção/Apagamento Parcial) dos principais geocronômetros e termocronômetros. O quadro em destaque circunda os três métodos utilizados neste trabalho (modificado de Evans et al., 2003).

Neste trabalho foram utilizados três termocronômetros de baixa temperatura: TFA, AHe e ZHe. Cada um desses termocronômetros possui uma temperatura de fechamento (Fig. 3.1), sendo que em conjunto eles cobrem uma faixa de temperaturas que varia de aproximadamente 40 a 200 ºC, o que corresponde a profundidades de cerca de 1,0 a 7,0 km, demonstrando a complementariedade entre esses métodos e a importância de utilizá-los conjuntamente quando oportuno. Quando a temperatura da rocha/mineral é semelhante à temperatura de fechamento do sistema isotópico, a acumulação e a perda de produtos do decaimento radioativo/fissão espontânea são simultâneas, ao passo que em temperaturas inferiores a ZRP ou ZAP ocorre a completa retenção dos produtos. Por outro lado, quando a temperatura é superior a ZRP ou ZAP, todo produto radiogênico gerado é perdido. Entretanto, alguns fatores podem alterar os limites da faixa de temperatura de cada um desses métodos, como a quantidade acumulada de dano causado pela radiação (Shuster et al., 2006; Flowers et al., 2009; Guenthner et al., 2013) e a taxa de resfriamento (Ault and Flowers, 2012; Reiners et al., 2017), entre outros, o

que também ocasiona uma alteração na idade produzida.

Por meio da termocronologia é possível obter idades de resfriamento, chamadas assim uma vez que elas geralmente não registram um evento geológico específico, mas um ponto de tempo-temperatura que se situa dentro da ZRP o ZAP (Reiners et al., 2017). Em termo gerais, a idade termocronológica é dependente da concentração dos isótopos pai e filho e da constante de decaimento radioativo específica do sistema isotópico analisado de acordo com a equação:

$$t = \frac{1}{l}\, ln\left(\frac{N_d}{N_p} + 1\right)$$

onde *t* é a idade da amostra, λ é a constante de decaimento radioativo do sistema isotópico analisado, *ln* é o logaritmo neperiano, N_d é a concentração de elementos radiogênicos (produtos do decaimento) e N_p é a concentração de elementos radioativos-pai. Essa equação será retomada nos tópicos seguintes, de modo que cada sistema isotópico terá sua própria equação.

3.2 Traços de Fissão em Apatita

A técnica de TFA diz respeito ao acúmulo de traços de fissão produzidos ao longo do tempo a partir da fissão natural e espontânea de átomos de ^{238}U localizados no retículo cristalino da apatita (Price and Walker, 1963; Fleischer and Price, 1964). Cada traço de fissão é produzido a partir de um átomo, de modo que o evento de fissão do núcleo atômico cria um par de fragmentos que se repele do local da reação em direções opostas, produzindo uma trilha linear de comprimento 16,3 μm. Diferentemente das técnicas de datação radiométrica, a técnica de traços de fissão tem como “isótopo-filho” não um átomo, mas um defeito cristalino que é o próprio traço. Isso faz com que o procedimento de datação seja conduzido por meio de equipamentos óticos, normalmente sob aumentos de 1.000x ou mais.

A densidade de traços de fissão espontâneos presente em uma amostra é largamente dependente da quantidade (concentração) de ^{238}U, que é determinado a partir da irradiação desta amostra com nêutrons de baixa energia. Esse processo de irradiação induz a fissão de uma proporção de ^{235}U, um isótopo de urânio menos abundante, produzindo uma segunda geração de traços de fissão que geralmente são contados com o uso de um detetor acoplado a amostra. A razão entre os traços de fissão espontâneos e induzidos se relaciona com a medida de átomos de urânio que se

fissionaram e que restaram no cristal, de modo que se utilizar a taxa da constante de decaimento da fissão espontânea do ^{238}U, será possível obter o tempo em que esses traços se acumularam na amostra. Logo, equivale a dizer que esta é a idade aparente da amostra (Hurford, 2019). Para este método, a equação que permite calcular o tempo (idade) é:

$$t = \frac{1}{l} ln \left[1 + lz \frac{r_S}{r_I} r_D\right]$$

onde l é a constante de decaimento por fissão espontânea do ^{238}U, *ln* é o logaritmo neperiano, ζ é um parâmetro para calibração do método de traços de fissão, ρ_S é a densidade de traços de fissão espontâneos na amostra, ρ_I é a densidade de traços de fissão induzidos no detetor externo e ρ_D é a densidade de traços de fissão medidas em um detetor acoplado a um vidro dopado com urânio.

Como a técnica de TFA é um termocronômetro, ela está intimamente relacionada à temperatura e ao tempo. Neste caso, os traços de fissão espontâneos tendem a se apagar (*annealing)* ao longo do tempo geológico quando as condições de temperatura são mais altas que as condições ambientes. Se a temperatura se situar entre 60 e 120 ºC (Green et al., 1989), a produção de novos traços de fissão será concomitante ao contínuo apagamento e encurtamento dos traços produzidos, definindo a ZAP da apatita. Isso leva a uma consequência: cada traço de fissão é formado em um momento diferente da história da amostra e esse traço estará exposto a uma parte da história térmica desse cristal. Dessa forma, ao se analisar o conjunto da distribuição dos traços de fissão medidos, sendo que cada traço possuirá um tamanho distinto, é possível reconstruir a história térmica dessa amostra. Importante ressaltar que a temperatura é o principal fator a ser considerado no apagamento dos traços. Porém, os limites de temperatura inferior e superior ZAP da apatita podem sofrer alteração a depender, por exemplo, da composição química da apatita e da quantidade de dano radioativo acumulado no cristal (Gleadow et al., 1986; Donelick et al., 2005; Tagami and O'Sullivan, 2005).

Este estudo utilizou a técnica do detetor externo (Hurford, 1990a) e as amostras foram irradiadas no reator do CNEM-IPEN em São Paulo, Brasil. Para cada amostra, mais de 300 cristais de apatitas foram selecionados à mão sob lupa binocular com aumento de 50 x. Esses cristais foram montados em pastilhas de resina epóxi, polidos até aproximadamente a porção central e atacados com uma solução de HNO_3 5.5 M a 21 ºC por 20 s (Carlson et al., 1999; Donelick et al., 2005) para revelar os traços de fissão

espontâneos. Lâminas de mica de baixo concentração de urânio foram fixadas nas pastilhas contendo as apatitas, aos vidros dopados com concentrações conhecidas de urânio (CN-5 *glass*) e padrões de idade Durango. Para revelar os traços induzidos no detetor externo, uma solução de 48 % HF for 18 minutos foi utilizada.

As análises para a datação e medida de comprimento e ângulo dos traços de fissão foram conduzidas no Labmodel, na Universidade Federal do Rio Grande do Sul. As análises foram feitas utilizando-se um microscópio Leica CTR 6000 com um aumento de 1000x a seco. O cálculo da idade se baseou em, no mínimo, 20 cristais por amostra, que foram calibradas de acordo com o método ζ (Hurford and Green, 1983; Hurford, 1990b). A homogeneidade das idades foi avaliada utilizando-se o teste χ^2 (Galbraith, 1981) no RadialPlotter 9.4 (Vermeesch, 2009).

Para a modelagem inversa, em cada amostra coletou-se a medida dos comprimentos dos traços de fissão horizontais confinados e o ângulo destes com o eixo c da apatita (Fig. 3.2). Buscou-se medir 100 traços horizontais confinados do tipo TINT (Donelick et al., 2005). Além disso, o parâmetro cinético Dpar foi medido em todos os cristais contendo traços de fissão horizontais confinados. Esse parâmetro representa uma figura geométrica formada pela interseção de um traço de fissão e o eixo c da apatita após realizado o polimento e o ataque químico da superfície do cristal (Donelick et al., 2005).

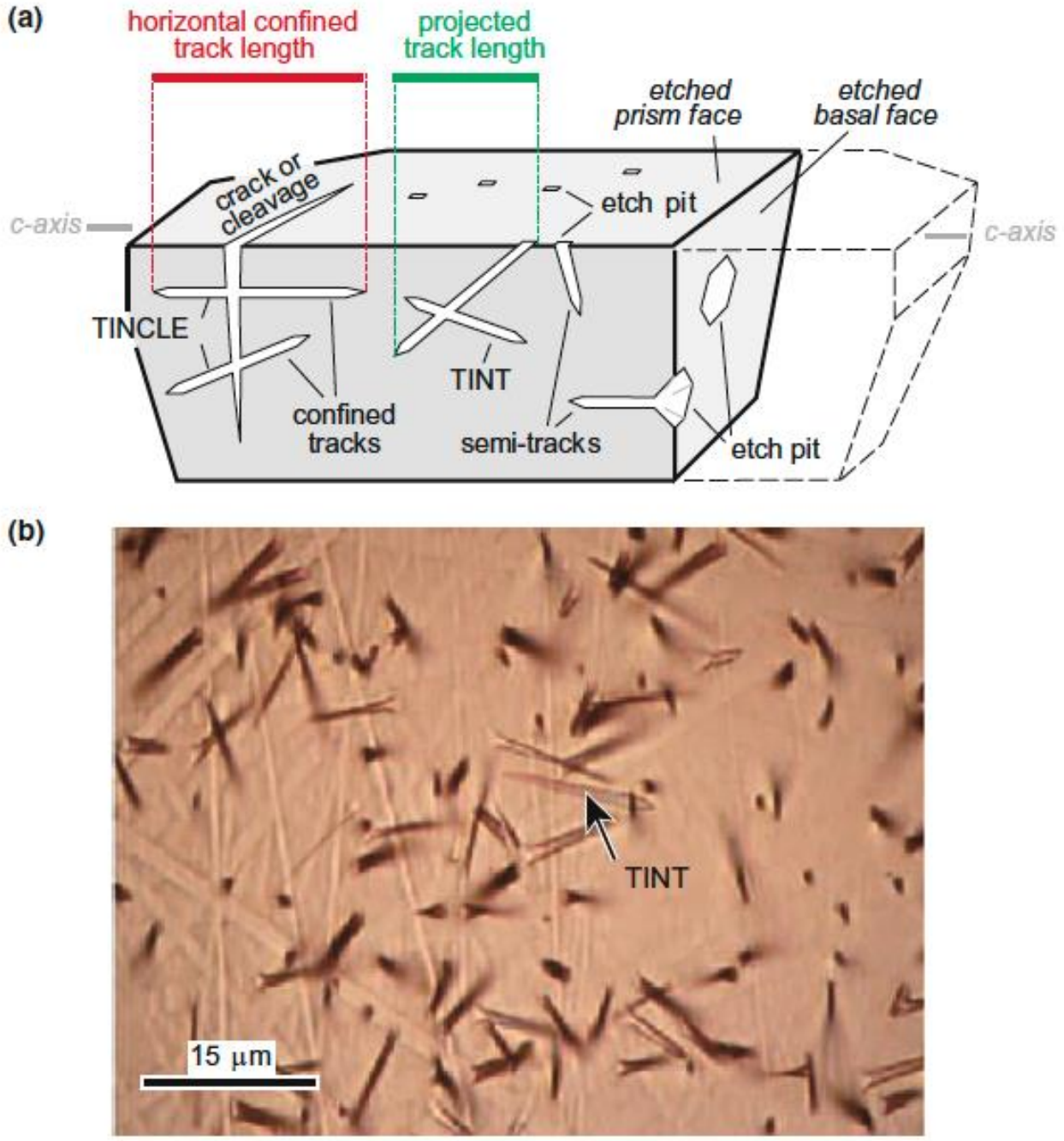

Figura 3. 1: a) Figura esquemática ilustrando um cristal de apatita e os traços de fissão confinados e semiconfinados. TINT são traços de fissão confinados interceptados por um traço de fissão que intercepta a superfície revelado pelo ataque químico. b) Fotomicrografia de um cristal de apatita evidenciando os traços de fissão (extraído de Hurford, 2019).

3.3 (U-Th)/He em zircão e apatita

O método (U-Th)/He se baseia no acúmulo de átomos de ^{4}He (ou partícula α) dentro do retículo cristalino de minerais. Esses átomos são um dos produtos radiogênicos do decaimento radioativo α em cadeia dos átomos ^{238}U, ^{235}U, ^{232}Th e ^{147}Sm, além dos

elementos radioativos intermediários dessa cadeia que leva a formação de ^{206}Pb, ^{207}Pb, ^{208}Pb e ^{143}Nd estáveis (Reiners et al., 2017). Tal qual o método de traços de fissão, o método (U-Th)/He também produz idades aparentes, de modo que a equação para obtenção do tempo é definida como:

$$^{4}He = 8.^{238}U\left(e^{\lambda_{238}t} - 1\right) + 7.^{235}U\left(e^{\lambda_{235}t} - 1\right) + 6.^{232}Th\left(e^{\lambda_{232}t} - 1\right) + ^{147}Sm\left(e^{\lambda_{147}t} - 1\right)$$

onde, os nuclídeos são expressos em átomos ou mols, λ é a constante de decaimento radioativo de cada nuclídeo e t é o tempo. Importante ressaltar que essa equação assume o equilíbrio secular dos átomos-filhos em todas as cadeias de decaimento, o que sugere ser apropriado para minerais e rochas mais velhos que aproximadamente 1 Ma (Flowers et al., 2022).

Quando a temperatura é suficientemente alta, o ^{4}He escapa do cristal por difusão térmica ativada (Zeitler et al., 1987; Wolf et al., 1998; Stockli et al., 2000; Farley, 2002), resultando em uma idade zero. Porém, quando a temperatura é semelhante a ZRP do termocronômetro analisado, a produção e retenção das partículas α se equivale. Para a apatita, a temperatura da ZRP varia, aproximadamente, entre 40 e 70 ºC (Wolf et al., 1996, 1998; Farley, 2002), enquanto que para o zircão a temperatura da ZRP varia de 140 a 200 ºC (Reiners, 2005; Reiners et al., 2005, 2017). Assim como na técnica de traços de fissão, os limites de temperatura superiores e inferiores da ZRP de ambos os termocronômetros, logo a perda difusiva de ^{4}He, são afetadas por diversos fatores, como o tamanho do cristal (Farley, 2000; Reiners et al., 2002; Flowers et al., 2022), o acúmulo de dano por radiação (Flowers et al., 2007; Shuster et al., 2006; Gautheron et al., 2009), imperfeições dos cristais (Flowers et al., 2022), e a concentração efetiva de urânio e química dos cristais – (eU = [U] + 0,234*[Th} + 0,00463*[Sm]; Flowers et al., 2009; Reiners et al., 2017). Além disso, existem diversas fontes de dispersão das idades obtidas dentro de uma amostra, além dos citados acima, como zoneamento dos isótopos radioativos (Reiners et al., 2017), fragmentação dos cristais (Beucher et al., 2013; Brown et al., 2013), implantação de ^{4}He a partir de cristais vizinhos ou inclusões ricos em U e Th (Lippolt et al., 1994; Farley, 2002; Fitzgerald et al., 2006; Murray et al., 2014), e a taxa de resfriamento (Spiegel et al., 2009; Ault and Flowers, 2012; Reiners et al., 2017). Esses efeitos podem ser amplificados caso a amostra experimente longa residência dentro da ZRP (Ault and Flowers, 2012; Green and Duddy, 2018).

Nota-se também que a produção de ^{4}He sempre gera um dano na estrutura cristalina, uma vez que a cada evento de decaimento o átomo-pai é deslocado uma curta

distância, da ordem de centenas de nanômetros se considerada toda a cadeia de decaimento radioativo, criando um dano devido ao recuo do átomo radioativo. Além disso, quando o átomo radiogênico é gerado, ele também se desloca dentro do retículo cristalino com alta energia cinética, produzindo colisões elásticas e deslocando átomos dentro da estrutura cristalina. Dessa forma, pode-se dizer que a cada evento de decaimento radioativo, o cristal que hospeda os elementos radioativos U, Th e Sm experimenta irradiação (Flowers et al., 2022), o que produz o dano por radiação mencionado anteriormente.

Neste trabalho, alíquotas de cerca de quatro a sete cristais, tanto apatitas quanto zircões, foram analisadas no laboratório UTChron – (U-Th)/He e U-Pb Geo-Thermochronometry, na University of Texas em Austin, TX. Utilizou-se um estereomicroscópio Nikon SMZ-U/100 acoplada a uma câmera Nikon para selecionar os cristais com base em sua forma, tamanho, ausência de inclusões visíveis e alterações. As dimensões dos cristais foram medidas para utilizar a correção de ejeção alfa (Ft; Farley et al., 1996) e os cristais foram fotografados. Buscou-se selecionar cristais que continham as duas terminações. Os cristais selecionados foram introduzidos em pequenos tubos de platina e submetidos à remoção de He em condições de aquecimento com o uso de lasers Nd-YAG. Um espectrômetro de massa quadrupolo mediu e quantificou o gás extraído. Então, esses cristais foram recuperados e dissolvidos com ácido nítrico (HNO_3) a 65 % para determinação isotópica (U, Th e Sm) em um espectrômetro de massa de alta resolução (HR-ICP-MS Element 2).

3.4 Modelagem térmica inversa

Após a obtenção dos dados termocronológicos de TFA, ZHe e AHe, utilizou-se o *software* QTQt versão 5.7.2 K (artigos publicados em 2022 e 2023 – Cap. 5 e 6) e a versão 5.8.0 (artigo que se encontra submetido – Cap. 7), para a modelagem das histórias térmicas (Gallagher et al., 2009; Gallagher, 2012). Esse *software* utiliza simulações matemáticas baseadas em inversões Bayesianas transdimensionais com aplicação de Markov Chain Monte Carlo (MCMC), produzindo uma aproximação com a história térmica.

Buscou-se não utilizar nenhuma restrição aos modelos a serem criados, de modo que o *software* pudesse criar livremente os caminhos de tempo-temperatura, exceto a restrição de que a temperatura atual da superfície terrestre em 20 ± 10 ºC. As condições

iniciais de tempo inseridas no programa eram correspondentes a duas vezes a idade mais antiga da amostra, independente se essa idade se referia a uma idade de TFA, ZHe ou AHe. Além disso, para modelos baseados apenas em TFA ou TFA e AHe, utilizou-se uma caixa com temperaturas variando 70 ± 70 ºC, o que possibilitaria a criação de um modelo abrangendo temperaturas superiores ao limite de temperatura mais alta da ZAP da apatita (cerca de 120 ºC) e de temperaturas semelhantes às condições superficiais atuais. Por outro lado, quando havia a disponibilidade de dados de ZHe para a amostra, a caixa de temperaturas foi expandida para 100 ± 100 ºC, possibilitando o registro térmico do termocronômetro com temperatura mais elevada utilizado. Também se considerou o gradiente geotérmico $\partial T/\partial t$ de 30 ºC/m.y., semelhante ao registrado em cinturões orogênicos e áreas cratônicas.

Os modelos cinéticos utilizados para modelagem inversa foram as medidas de Dpar e de projeção dos ângulos formados entre o traço de fissão e o eixo c da apatita para a técnica de TFA (Ketcham et al., 2007) e o os modelos de RDAAM (*Radiation Damage Accumulation and Annealing Model* para a apatita; Flowers et al., 2009) e ZRDAAM (*Zircon Radiation Damage Accumulation and Annealing Model* para o zircão; Guenthner et al., 2013). Valores apropriados para o algoritmo MCMC foram definidos após simulações iniciais de 30.000 iterações *post-burn-in*. Ajustados os parâmetros, foram consideradas 200.000 iterações *post-burn-in* para criação dos modelos finais. A interpretação dos modelos térmicos inversos produzidos considerou o caminho médio ponderado (*weighted mean path*) produzido e a probabilidade relativa dos modelos. Além disso, buscou-se a melhor concordância entre as idades observadas e preditas pelo *software* QTQt, apesar de nem sempre ter sido satisfatória essa concordância quando os três termocronômetros eram utilizados conjuntamente. Para os modelos baseados apenas em TFA, buscou-se a melhor concordância observando-se a distribuição média dos traços de fissão horizontais confinados.

CAPÍTULO 4 – SÍNTESE INTEGRADORA

4.1 Introdução

A margem continental Atlântica da América do Sul possui uma grande variação em termos topográficos, geológicos, estruturais e termocronológicos. Duas regiões que marcam fortes transições segundo esses aspectos mencionados se situam ao sul da cidade de Florianópolis, no Estado de Santa Catarina, e ao sul do Estado da Bahia. A região de Florianópolis é composta por rochas metamórficas pertencentes ao Batólito Florianópolis (Escudo Catarinense) e integrantes do Cinturão Dom Feliciano. Por outro lado, o segmento da margem continental ao sul da Bahia é composto por rochas metamórficas da Faixa Araçuaí e do CSF.

Analisando-se estas regiões, buscou-se aprimorar o entendimento sobre a dinâmica evolutiva Fanerozoica de regiões transicionais da margem continental brasileira que tem como embasamento a Província Mantiqueira e crátons adjacentes. Este trabalho não esgota o estudo sobre estas regiões, de modo que ainda serão necessários estudos que integrem outras áreas das geociências à termocronologia.

4.2 Termocronologia da Faixa Araçuaí e Cráton São Francisco

Os resultados termocronológicos obtidos a partir de rochas da Faixa Araçuaí e CSF alcançados com este trabalho apontam para maior cobertura espacial de dados de TFA da margem continental brasileira, adição de algumas idades de AHe para rochas da Faixa Araçuaí e CSF e as primeiras idades de ZHe da Faixa Araçuaí e CSF. As idades médias corrigidas de ZHe para ambos os domínios geológicos são Paleozoicas, variando entre 448,1 e 253,0 Ma, sendo que a idade obtida para o CSF é a mais antiga do conjunto de dados apresentado. As idades de ZHe não guardam relação direta com algum evento geológico específico, sendo caracterizadas como idades de resfriamento. Essas idades também podem ser interpretadas de acordo com a temperatura, o que sugere que os eventos tectônicos ocorridos nestes domínios geológicos durante o Fanerozoico não elevaram a temperatura acima de 200 ºC, o que seria suficiente para apagar este termocronômetro. As idades de ZHe e o eU possuem correlação positiva não-linear que é atribuída a danos causados por baixas doses de radiação α e resfriamento lento dentro da faixa de sensibilidade desse termocronômetro, o que pode ser também corroborado pelas idades de TFA.

Por outro lado, as idades médias corrigidas de AHe são Mesozoicas a Cenozoicas, variando entre 95,7 e 43,9 Ma. Essas idades são mais jovens que o evento de rifteamento que culminou com a abertura do Oceano Atlântico e algumas delas são compatíveis com a colocação de corpos ígneos da Província Magmática de Abrolhos. Dessa forma, infere-se que a temperatura à qual as rochas da região transicional entre a Faixa Araçuaí e o Cráton São Francisco estavam submetidas estavam acima de 120 ºC durante todo o Paleozoico até o Cretáceo, o que com o rifteamento e a presença de rochas vulcânicas, manteve a temperatura elevada ou que essas rochas já se encontravam próximas de condições superficiais e foram levemente reaquecidas, apagando este termocronômetro. A correlação entre as idades AHe e o eU, assim como para o zircão, é positiva e não-linear, sugerindo alta retenção de partículas α e as apatitas expostas a taxas de resfriamento lentas e/ou submetidas a longos períodos dentro da ZRP da apatita.

As idades centrais de TFA são Mesozoicas a Cenozoicas, variando entre 154,4 e 37,1 Ma, sendo que as idades obtidas nas amostras da Faixa Araçuaí são mais jovens que aquelas obtidas ns amostras do CSF. Este resultado indica que grande parte das amostras do CSF estavam em temperaturas abaixo de 120 ºC e que os eventos de rifteamento e intrusão ígneas da Província Magmática de Abrolhos não perturbaram excessivamente o termocronômetro de TFA. Entretanto, como as idades de TFA da Faixa Araçuaí são consideravelmente mais jovens, este termocronômetro possivelmente permaneceu aberto durante esses eventos, o que indica temperaturas semelhantes à da ZAP da apatita. As idades de TFA também apresentam correlação positiva em relação a linha de costa, o que sugere que o interior do continente registra idades mais antigas e amostras preservadas da exumação, enquanto a porção costeira experimenta maior exumação e idades mais jovens.

Em resumo, as idades de ZHe observadas são consideravelmente mais antigas que as idades de TFA, enquanto as idades de AHe são mais jovens ou semelhantes que as idades de TFA. Duas idades de AHe desse conjunto de dados são exceções a esse comportamento, visto serem mais antigas que as idades de TFA de uma mesma amostra. Esse efeito é causado pela longa permanência da amostra na porção rasa da crosta e por experimentar leve reaquecimento, o que torna as apatitas mais retentivas e as faz ter ZRP com temperaturas semelhantes à ZAP (Flowers et al., 2009; Flowers and Kelley, 2011).

Além das idades termocronológicas obtidas, este trabalho também contribuiu com histórias térmicas construídas a partir da modelagem inversa. Diversos foram os parâmetros utilizados na construção dessas histórias, como as idades de TFA, ZHe e AHe, modelos de acúmulo e apagamento dos danos causados pela radiação tanto para a apatita quanto para o zircão, Dpar, projeção dos ângulos dos traços de fissão horizontais confinados no eixo c dos cristais analisados, concentração de He, U, Th e Sm e as dimensões dos cristais datados por (U-Th)He. A interpretação das histórias térmicas levou à definição de eventos de resfriamento lento e acelerado e episódios de reaquecimento da porção superior da crosta, sendo que os modelos exibiam um ou mais desses eventos. Juntamente com a análise das histórias térmicas, este trabalho também permitiu obter dados que dimensionassem a taxa de denudação e a espessura erodida experimentada pelos domínios cratônicos e orogênicos, discutidos abaixo.

Algumas amostras registraram resfriamento acelerado durante o Paleozoico o qual foi interpretado como o resultado da propagação de estresses intraplaca advindos dos ciclos orogênicos Gondwanides e Famatiniano (Milani and Ramos, 1998). Além da região norte da Faixa Araçuaí e CSF, outras regiões do interior do continente Gondwana Ocidental também registraram esse evento de resfriamento, o que sugere ser um evento abrangente (Jelinek et al., 2014; Kasanzu et al., 2016; Amaral-Santos et al., 2019; Hueck et al., 2019; Machado et al., 2019; Martins-Ferreira et al., 2020; Fonseca et al., 2021). As rochas exumadas forneceram sedimentos para diversos depocentros atuantes durante o Paleozoico, como a Bacia Araripe, que possui registros de paleocorrentes que dão suporte a estas interpretações, além das bacias do Paraná, Parnaíba, Recôncavo-Tucano-Jatobá, entre outras. As taxas de denudação do evento de resfriamento durante o Paleozoico se situam entre 10 e 12 $m.Ma^{-1}$ e espessura denudada de 0,8 a 1,2 km, registros estes semelhantes a outras regiões da Faixa Araçuaí (Amaral-Santos et al., 2019). Entretanto, considerando-se dados termocronológicos de temperaturas mais elevadas (datação Ar/Ar; Vauchez et al., 2019), foram estimadas taxas de denudação mais aceleradas, variando entre 23 e 25 $m.Ma^{-1}$ e erosão aproximada de 6,0 km entre o Ordoviciano ao final do Permiano. Estes dados encontram suporte na literatura, visto estarem presentes na Faixa Araçuaí rochas metamórficas granulíticas aflorantes, o que aponta para regiões profundas da crosta trazidas à superfície decorrentes de acentuada erosão posterior ao ciclo brasiliano. Além disso, outras regiões elevadas de Gondwana Ocidental apresentam taxas semelhantes, como observado no Cráton da Tanzânia

(Kasanzu, 2017; Kasanzu et al., 2016), no Escudo Sul-Rio-Grandense (Machado et al., 2019) e na Faixa Brasília (Fonseca et al., 2020).

Durante a transição do Paleozoico para o Mesozoico, também foram observados registros térmicos que foram interpretados como estágios finais da orogenia Cabo de la Ventana (Milani and De Wit, 2014), também observados em amostras da Faixa Ribeira (Hiruma et al., 2010). Os sedimentos gerados pela erosão desses terrenos foram depositados nas bacias do Paraná, Sanfranciscana e nas seções pré-rifte das bacias marginais hoje localizadas no nordeste brasileiro.

A partir do Cretáceo, também foram registrados alguns eventos de resfriamento acelerado. O primeiro deles, de idade aproximada entre 120 e 110 Ma, foi interpretado como sendo compatível com o soerguimento e erosão das ombreiras do rifte que deu origem ao Oceano Atlântico. Isto pois durante o processo de ruptura da crosta, ocorre soerguimento normalmente associado à elevação da astenosfera, seguido por falhamento e erosão das bordas do rifte. Esse episódio é marcante na Faixa Araçuaí, enquanto é praticamente ausente em amostras do CSF. Para esse episódio de resfriamento acelerado, a espessura total denudada foi estimada em cerca de 2,0 a 4,0 km, estimativas compatíveis com dados presentes na literatura (Harman et al., 1998; Jelinek et al., 2014).

O último episódio de resfriamento registrado diz respeito ao período de transição entre o Cretáceo e o Paleoceno ao qual são atribuídas diversas causas que atuaram concomitantemente, como o enfraquecimento térmico da crosta superior devido a presença do vulcanismo da Província Magmática de Abrolhos e da instalação da Cadeia vulcânica Vitória-Trindade (Cogné et al., 2011), delaminação da crosta inferior induzindo soerguimento e erosão corroborados pela presença de anomalias de alta velocidade situadas embaixo da margem continental (Hu et al., 2018) e mudanças no regime compressivo da placa Sulamericana advindas do cinturão Andino e do espalhamento acelerado da dorsal mesoatlântica. A espessura denudada registrada nesse evento de resfriamento é próxima de 2,0 km, valor este compatível com o registro sedimentar das bacias da margem continental conexas à Faixa Araçuaí e Cráton São Francisco.

Um episódio de leve reaquecimento foi registrado em alguns modelos, que podem de fato serem interpretados como reaquecimento ou como estabilidade térmica (do Amaral Santos et al., 2022). A interpretação conduzida neste trabalho advoga a respeito de leve reaquecimento da crosta superior decorrente da colocação de corpos ígneos na

Província Magmática de Abrolhos, visto que algumas idades de TFA e AHe são semelhantes ao momento de intrusão dessas rochas entre, aproximadamente, 70 e 30 Ma (Stanton et al., 2021).

Outro dado importante avaliado na região de Transição da Faixa Araçuaí e CSF foi o papel da herança estrutural em relação aos termocronômetros. Este estudo demonstrou que pontos amostrais situados próximos a lineamentos de direção NW-SE apresentaram idades AHe e AFT mais jovens. Esses lineamentos possivelmente atuaram como condutos de calor, mantendo a temperatura elevada e permitindo a difusão de partículas α e o apagamento dos traços de fissão, de modo que os termocronômetros permaneceram dentro da ZRP ou ZAP da apatita.

Por fim, este estudo produziu também uma série de mapas que documentaram a evolução da temperatura do embasamento cristalino das Faixas Araçuaí e Ribeira e do Cráton São Francisco. Os dados apontaram para um forte controle reológico entre os domínios cratônico e orogênico demonstrado pela presença de histórias térmicas paleozoicas no CSF e da ausência de dados térmicos para um grande segmento da Faixa Araçuaí. O controle reológico também foi evidente observando-se a distribuição das idades centrais de TFA, uma vez que as idades de TFA no CSF são essencialmente mais antigas, variando entre o Permiano ao Jurássico, ao passo que as faixas Araçuaí e Ribeira apresentam idades que variam entre o Cretáceo Inferior ao Cenozoico. Além disso, os mapas documentaram a exposição do CSF a temperaturas semelhantes às condições superficiais durante o Carbonífero ao Triássico, o que sugere que esta região não experimentou exumação acelerada desde então. Também se caracterizou para ambos os cinturões mencionados acima o resfriamento atribuído a erosão das ombreiras do rifte, com a acumulação de sedimentos em um pilha sedimentar de cerca de 4.400 m nas bacias sedimentares adjacentes, como Campos, Espírito Santo e Mucuri.

Importante mencionar que a série de mapas também demonstrou que a formação do Rifte Continental do Sudeste Brasileiro promoveu reaquecimento das rochas do seu entorno na Faixa Ribeira, não somente pela reativação em si, mas também pela intrusão de corpos alcalinos próximos à borda do rifte. O reaquecimento se deu também em regiões que possuem feixe de lineamentos de direção NW-SE, tanto na Faixa Araçuaí quanto na Faixa Ribeira, que possivelmente se tornaram condutos para transporte de calor e de intrusão de corpos ígneos, além de promoverem mudanças nos cursos de drenagens que posteriormente levaram a exumação de rochas. Os dados térmicos

analisados também são embasados nas idades de TFA desta região, visto que eles são mais jovens que o entorno, o que indica manutenção das temperaturas relativamente altas dentro da ZAP da apatita, permitindo o encurtamento e a geração de novos traços concomitantemente.

4.3 Termocronologia do Escudo Catarinense e Cinturão Dom Feliciano

A partir da análise de apatitas coletadas em rochas do Escudo Catarinense, no Batólito Florianópolis, adensou-se a cobertura espacial dos dados de TFA e AHe desta região. As idades centrais de TFA são Mesozoicas e abrangem o Cretáceo Inferior e Superior, com a exceção de apenas uma amostra, datada do Paleoceno, sendo que elas variam entre 126,6 e 60,3 Ma. Essas idades são semelhantes ou mais jovens que o rifteamento que culminou com a abertura do Oceano Atlântico, sugerindo que a temperatura deste evento e das fases pós-rifte à qual a crosta estava submetida era alta o suficiente para apagar os traços de fissão presentes concomitantemente à geração de novos traços. A distância do ponto amostral à linha de costa e a elevação não aparentam exercer nenhum controle sobre a distribuição das idades neste conjunto de dados.

Todas as idades médias de AHe obtidas neste trabalho são Mesozoicas, situadas entre o Cretáceo Inferior e Superior, tal qual as idades centrais de TFA. Elas variam entre 117,5 e 71,8 Ma. Os parâmetros eU, distância à linha de costa, elevação e raio esférico equivalente não guardam nenhuma correlação evidente com as idades AHe obtidas. Algumas amostras apresentaram idades invertidas em relação ao termocronômetro TFA. Porém, as análises conduzidas neste estudo foram insuficientes para explicar a inversão das idades. Possivelmente, a inversão pode ser atribuída à elevação da temperatura à qual a ZRP da apatita opera, o que produz idades de TFA e AHe semelhantes ou invertidas. Ou ainda, pode-se atribuir a dificuldade do entendimento dos problemas que existem decorrentes da sistemática de difusão da apatita (Green and Duddy, 2018).

A ausência de histórias térmicas mais antigas que 150 Ma em conjunto com as idades jovens de TFA e AHe indicam que um evento de temperatura elevada obliterou os registros térmicos das apatitas. Este trabalho defende a hipótese que uma série de fatores moldaram a temperatura do Cinturão Catarinense nos últimos 150 Ma, como a intrusão e derrame de rochas vulcânicas da Província Magmática Paraná-Etendeka, a intrusão dos diques alimentadores desse magmatismo fissural recortando o Escudo Catarinense com o consequente aumento do gradiente geotérmico local, intrusão de

plútons alcalinos-carbonatíticos associados a presença da Zona de Fraturas Florianópolis, de direção E-W. Além disso, o lineamento Cruzeiro do Sul, de direção NW-SE, é relacionado a Zona de Fraturas Florianópolis e responsável por uma reorganização intraplaca durante o Cenozoico, o que levou à colocação de uma série de plútons na Bacia de Santos.

4.4 Integração, conclusões e proposições futuras

O presente estudo foi planejado para avaliar o registro termocronológico de regiões transicionais da Província Mantiqueira e crátons adjacentes. O primeiro ponto abordado aqui diz respeito as idades termocronológicas obtidas, em especial as idades centrais de TFA, uma vez que esse termocronômetro foi bastante utilizado em diversos estudos que detalharam a margem continental, os cinturões orogênicos Dom Feliciano, Ribeira e Araçuaí e os crátons São Francisco, Rio de la Plata e Luís Alves. As idades centrais de TFA são Mesozoicas a Cenozoicas, variando entre o Jurássico e o Eoceno, sendo que as idades mais antigas se concentram no Cráton São Francisco, as idades intermediárias se situam nos cinturões orogênicos e as idades mais jovens também se concentram nos cinturões orogênicos, porém sofreram apagamento devido a eventos de temperatura elevada que (1) resetaram os termocronômetros e obliteraram a história térmica prévia e (2) resetaram parcialmente os termocronômetros devido a manutenção de temperaturas elevadas por um longo período de tempo. Como mencionado nos tópicos anteriores deste capítulo e discutido em detalhe nos capítulos seguintes (artigos publicados e artigo submetido), as idades de TFA jovens da Faixa Araçuaí são decorrentes do magmatismo da Província Magmática de Abrolhos e as idades jovens do Cinturão Dom Feliciano no Escudo Catarinense são advindas do gradiente geotérmico elevado causado por diversas fontes de calor. O que essas áreas têm em comum é a presença de falhas, de direção NW-SE, E-W e NE-SW, que possivelmente atuaram como condutos para transporte de calor, mantendo a temperatura elevada e os termocronômetros TFA e AHe abertos e sujeitos à difusão/geração de partículas α e o apagamento/geração dos traços de fissão.

As histórias térmicas modeladas demonstram diversos episódios de resfriamento acelerado, especialmente quando se considera os dados termocronológicos existentes na literatura, o que permite ter uma abordagem regional da evolução da Província Mantiqueira e crátons adjacentes. Durante o Paleozoico, alguns segmentos da atual plataforma Sulamericana já se encontravam em condições de crosta rasa ou à superfície,

como é o caso do CSF e de segmentos do Cinturão Dom Feliciano, Cráton Rio de la Plata e Faixa Ribeira. A exumação de rochas dos cinturões orogênicos levou a deposição de sedimentos nos depocentros das bacias sedimentares do Paraná, Parnaíba, Sanfranciscana, entre outras. Trechos do Cinturão Dom Feliciano foram recobertos por sedimentos da Bacia do Paraná, enquanto a Bacia Sanfranciscana recobria o CSF, registrando paleocorrentes que indicam a direção de transporte sedimentar advindos da Faixa Araçuaí.

No início do Mesozoico, alguns pontos da Faixa Araçuaí e da Faixa Ribeira registram resfriamento acelerado que foi interpretado como decorrente de esforços intraplaca advindos de orogenias que ocorriam na margem sudoeste do continente Gondwana Ocidental, que também promovia soerguimento e exumação no Escudo Sul-Rio-Grandense. Durante o Cretáceo, o segmento a norte da cidade do Rio de Janeiro até o sul da Bahia indica resfriamento compatível com a erosão das ombreiras do rifte que culmina com a abertura do Oceano Atlântico.

Por fim, durante a transição do Cretáceo Superior para o Paleoceno, um episódio de resfriamento foi observado em toda a Província Mantiqueira, atestando o efeito generalizado deste episódio, que é decorrente da reorganização da Placa Sulamericana – compressão na margem Andina e espalhamento acelerado na dorsal mesoatlântica – e da propagação de estresses intraplaca associados a anomalias térmicas e de fraturas, lineamentos e zonas de cisalhamento, o que gera relevo disponível para ser erodido.

Episódios de reaquecimento durante o Cretáceo e Cenozoico apontam como causas principais a presença de diversas fontes de calor mencionadas anteriormente, mantendo a temperatura elevada e promovendo o apagamento parcial ou completo do registro termocronológico.

Em resumo, a história termotectônica Fanerozoica da Província Mantiqueira e crátons adjacentes – São Francisco, Rio de la Plata e Luís Alves – está relacionada com (1) eventos de resfriamento acelerado e exumação durante o Paleozoico advindos dos ciclos Gondwanides e Famatiniano, com deposição de sedimentos nas sinéclises Paleozoicas da Bacias do Paraná, Sanfranciscana, Parnaíba, entre outras de menor abrangência espacial; (2) resfriamento durante o Cretáceo Inferior compatível com a erosão das ombreiras do rifte no segmento entre o norte da Faixa Ribeira e a Faixa Araçuaí e ausência de resfriamento regional no Cráton São Francisco, evidenciando a denudação diferencial atribuída à reologia – diferenças entre a litosfera cratônica e

orogênica; (3) resfriamento acelerado entre o Cretáceo Superior e o Paleoceno causados pela geração de relevo e reorganização da Placa Sulamericana associada a fontes térmicas que enfraqueceram a crosta superior. Os episódios de reaquecimento estão relacionados à (1) intrusão e derrame das rochas da Província Magmática Paraná-Etendeka e instalação de seus diques alimentadores; (2) intrusão de corpos kimberlíticos e alcalinos-carbonatíticos no entorno do CSF, nas Faixas Ribeira e Brasilía e Cinturão Dom Feliciano; (3) intrusão das rochas pertencentes a Província Magmática de Abrolhos; e (4) reativação de falhas e zonas de cisalhamento do Rifte Continental do Sudeste Brasileiro, da Zona de Fratura de Florianópolis e de lineamentos próximos a transição da Faixa Araçuaí para o CSF.

As proposições futuras que este trabalho recomenda são:

- Adensamento da cobertura espacial de TFA no Cráton Luís Alves, segmento sul e norte da Faixa Ribeira, porção sul da Faixa Araçuaí, porção interior da Faixa Araçuaí distante da margem continental e do CSF e setor sul do CSF em direção à Faixa Brasília.
- Adensamento de TFA e AHe nas regiões onde há forte presença de falhas, zonas de cisalhamento e fraturas de direção NW-SE com objetivo de determinar a reativação dessas estruturas, a idade da reativação e o grau de reaquecimento das rochas que hospedam essas descontinuidades
- Utilização de traços de fissão em zircão para restringir as histórias térmicas que possam ter registrado o início do Paleozoico, após o final do ciclo brasiliano, gerando a história térmica completa dos cinturões do ciclo brasiliano.
- Integração e modelagem numérica dos dados termocronológicos de ZHe, TFA, AHe com termocronômetros de mais baixa temperatura, como isótopos cosmogênicos e traços de fissão em monazita.
- Por fim, iniciar a análise de TFA em rochas sedimentares das bacias do Paraná, Sanfranciscana, Parnaíba e da margem continental, associadas a análises geomorfológicas e estratigráficas, com o objetivo de construir o ciclo *source-to-sink* dos cinturões componentes da Província Mantiqueira.

REFERÊNCIAS BIBLIOGRÁFICAS

Alkmim, F.F., Kuchenbecker, M., Reis, H.L.S. (2017). The Araçuaí Belt, in: Heilbron, M., Cordani, U.G., Alkmim, F.F. (Eds.), *São Francisco Craton, Eastern Brazil.* Springer, Cham, pp. 255–276. https://doi.org/10.1007/978-3-319-01715-0

Alkmim, F.F., Marshak, S., Pedrosa-Soares, A.C., Peres, G.G., Cruz, S.C.P., Whittington, A. (2006). Kinematic evolution of the Araçuaí-West Congo orogen in Brazil and Africa: Nutcracker tectonics during the Neoproterozoic assembly of Gondwana. *Precambrian Res.* 149, 43–64. https://doi.org/10.1016/j.precamres.2006.06.007

Alkmim, F.F., Martins-Neto, M.A. (2012). Proterozoic first-order sedimentary sequences of the São Francisco craton, eastern Brazil. *Mar. Pet. Geol.* 33, 127–139. https://doi.org/10.1016/j.marpetgeo.2011.08.011

Almeida, F.F.M. de (1977). O Cráton do São Francisco. *Rev. Bras. Geociências* 7, 349–364.

Amaral-Santos, E., Jelinek, A.R., Almeida-Abreu, P.A., Genezine, F.A. (2019). Phanerozoic cooling history of Archean/Paleoproterozoic basement in the southern Espinhaço Range, southeastern Brazil, through apatite fission-track analysis. *J. South Am. Earth Sci.* 96, 102352. https://doi.org/10.1016/j.jsames.2019.102352

Ault, A.K., Flowers, R.M. (2012). Is apatite U-Th zonation information necessary for accurate interpretation of apatite (U-Th)/He thermochronometry data? *Geochim. Cosmochim. Acta* 79, 60–78. https://doi.org/10.1016/j.gca.2011.11.037

Barbosa, J.S.F., Sabaté, P. (2004). Archean and Paleoproterozoic crust of the São Francisco Craton, Bahia, Brazil: Geodynamic features. *Precambrian Res.* 133, 1–27. https://doi.org/10.1016/j.precamres.2004.03.001

Basei, M.A.S., Neves, B.B.B., Siga, O., Babinski, M., Pimentel, M.M., Gaeta Tassinari, C.C., Hollanda, M.H.B., Nutman, A., Cordani, U.G. (2010). Contribution of SHRIMP U-Pb zircon geochronology to unravelling the evolution of Brazilian Neoproterozoic fold belts. *Precambrian Res.* 183, 112–144. https://doi.org/10.1016/j.precamres.2010.07.015

Basei, M.A.S., Siga Jr., O., Machiavelli, A., Mancini, F. (1992). Evolução Tectônica Dos Terrenos Entre Os Cinturões Ribeira E Dom Feliciano (Pr-Sc). *Rev. Bras. Geociências* 22, 216–221. https://doi.org/10.25249/0375-7536.1992216221

Bento dos Santos, T.M., Tassinari, C.C.G., Fonseca, P.E. (2015). Diachronic collision, slab break-off and long-term high thermal flux in the Brasiliano-Pan-African orogeny: Implications for the geodynamic evolution of the Mantiqueira Province. *Precambrian Res.* 260, 1–22. https://doi.org/10.1016/j.precamres.2014.12.018

Beucher, R., Brown, R.W., Roper, S., Stuart, F., Persano, C. (2013). Natural age dispersion arising from the analysis of broken crystals: Part II. Practical application to apatite (U-Th)/He thermochronometry. *Geochim. Cosmochim. Acta* 120, 395–416. https://doi.org/10.1016/j.gca.2013.05.042

Bossi, J., Cingolani, C. (2009). Extension and General Evolution of the Río de la Plata Craton, in: Gaucher, C., Sial, A.N., Halverson, G.P., Frimmel, H.E. (Eds.), *Developments in Precambrian Geology*. Elsevier, pp. 73–85. https://doi.org/10.1016/S0166-2635(09)01604-1

Brandão, D.R., Ferraz, A., Ferrari, A.L., Gamboa, L.A.P. (2022). Tectonic reactivation along the Florianopolis Fracture Zone, Brazil. *Brazilian J. Geophys.* 40, 1–17. https://doi.org/10.22564/brjg.v40i2.2173

Brown, R.W., Beucher, R., Roper, S., Persano, C., Stuart, F., Fitzgerald, P. (2013). Natural age dispersion arising from the analysis of broken crystals. Part I: Theoretical basis and implications for the apatite (U-Th)/He thermochronometer. *Geochim. Cosmochim. Acta* 122, 478–497. https://doi.org/10.1016/j.gca.2013.05.041

Bueno, G.V., Zacharias, A.A., Oreiro, S.G., Cupertino, J.A., Falkenhein, F.U.H., Martins-Neto, M.A. (2007). Bacia de Pelotas. *Bol. Geociencias da Petrobras* 15, 551–559.

Carlson, W.D., Donelick, R.A., Ketcham, R.A. (1999). Variability of apatite fission-track annealing kinetics: I. Experimental results. *Am. Mineral.* 84, 1213–1223. https://doi.org/10.2138/am-1999-0901

Carneiro, C.D.R., Almeida, F.F.M. de, Hasui, Y., Zalán, P. V., Teixeira, J.B.G. (2012). Estágios evolutivos do Brasil no Fanerozoico, in: Hasui, Y., Carneiro, C.D.R., Almeida, F.F.M. de, Bartorelli, A. (Eds.), *Geologia Do Brasil.* Beca, São Paulo, pp. 131–137.

Chang, H.K., Kowsmann, R.O., Figueiredo, A.M.F., Bender, A.A. (1992). Tectonics and stratigraphy of the East Brazil Rift system: an overview. *Tectonophysics* 213, 97–138. https://doi.org/10.1016/0040-1951(92)90253-3

Cogné, N., Gallagher, K., Cobbold, P.R. (2011). Post-rift reactivation of the onshore margin of southeast Brazil: Evidence from apatite (U–Th)/He and fission-track data*. Earth Planet. Sci. Lett.* 309, 118–130. https://doi.org/10.1016/j.epsl.2011.06.025

Cordani, U.G. (1970). Idade do vulcanismo no Oceano Atlântico Sul. *Bol. IGA* 1, 9–75.

Cordani, U.G., Delhal, J., Ledent, D. (1973). Orogenèses superposées dans le Précambrien du Brésil Sud-oriental (États de Rio de Janeiro et de Minas Gerais). *Rev. Bras. Geociências* 3, 1–22.

Cruz, S.C.P., Alkmim, F.F. (2017). The Paramirim Aulacogen, in: Heilbron, M., Cordani, U.G., Alkmim, F.F. (Eds.), *São Francisco Craton, Eastern Brazil.* Springer, Cham, pp. 97–115. https://doi.org/10.1007/978-3-319-01715-0_6

Dalton de Souza, J., Kosin, M., Melo, R.C., Santos, R.A., Teixeira, L.R., Sampaio, A.R., Guimarães, J.T., Vieira Bento, R., Borges, V.P., Martins, A.A.M., Arcanjo, J.B., Loureiro, H.S.C., Angelim, L.A.A. (2003). Mapa Geológico do Estado da Bahia - Escala 1:1.000.000. *Programa Geol. do Bras.* CPRM.

de Almeida, F.F.M., Hasui, Y., de Brito Neves, B.B., Fuck, R.A. (1981). Brazilian structural provinces: An introduction. *Earth Sci. Rev.* 17, 1–29. https://doi.org/10.1016/0012-8252(81)90003-9

de Oliveira, D.C., Mohriak, W.U. (2003). Jaibaras trough: An important element in the early tectonic evolution of the Parnaíba interior sag basin, Northern Brazil. *Mar. Pet. Geol.* 20, 351–383. https://doi.org/10.1016/S0264-8172(03)00044-8

do Amaral Santos, E., Jelinek, A.R., Machado, J.P., Stockli, D. (2022). Thermal history along the Araçuaí Orogen and São Francisco Craton border, eastern Brazilian continental margin, based on low-temperature thermochronologic data. *Tectonophysics* 825, 229232. https://doi.org/10.1016/j.tecto.2022.229232

do Amaral Santos, E., Jelinek, A.R., Stockli, D., Genezine, F.A. (2023). Contrasting thermal histories in the Dom Feliciano Belt triggered by magmatism related to the Paraná-Etendeka LIP and fracture zone

proximity. *Tectonophysics* 857, 229841. https://doi.org/10.1016/j.tecto.2023.229841

Donelick, R.A., O'Sullivan, P.B., Ketcham, R.A. (2005). Apatite fission-track analysis, in: Reiners, P.W., Ehlers, T.A. (Eds.), *Reviews in Mineralogy and Geochemistry.* pp. 49–94. https://doi.org/10.2138/rmg.2005.58.3

dos Santos, J.M., Salamuni, E., Val, P., da Silva, C.L., Morales, N., de Souza, I.A., Sanches, E. (2023). Cenozoic tectonic reactivation and its implications for landscape transience in southeastern Brazil. *Earth Surf. Process. Landforms* 1–21. https://doi.org/10.1002/esp.5670

Engelmann de Oliveira, C.H., Jelinek, A.R. (2017). História termotectônica da margem continental Brasileira a partir de dados de traços de fissão em apatita. *Pesqui. em Geociências* 44, 387–400. https://doi.org/10.22456/1807-9806.83263

Evans, D., Gehrels, G., Karlstrom, K., Wernicke, B. (2003). Co-evolution of Earth and Life, in: Kronenberg, A., Brandon, M.T., Fletcher, R., Karlstrom, K., Rushmer, T., Simpson, C., Yin, A. (Eds.), *New Departures in Structural Geology and Tectonics.* Tectonics Program, Earth Sciences Division, and National Science Foundation (GEO/EAR), pp. 41–51.

Farley, K.., Wolf, R.., Silver, L.. (1996). The effects of long alpha-stopping distances on (U-Th)/He ages. *Geochim. Cosmochim. Acta* 60, 4223–4229. https://doi.org/https://doi.org/10.1016/S0016-7037(96)00193-7

Farley, K. (2000a). Helium diffusion from apatite, General behavior as illustrated by Durango fiuorapatite The implied He closure temperature for a grain. *J. Geophys. Res*. 105, 2903–2914.

Farley, K.A. (2002). (U-Th)/He dating: Techniques, calibrations, and applications. *Rev. Mineral. Geochemistry* 47, 819–844. https://doi.org/10.2138/rmg.2002.47.18

Ferreira, A.C.D., Conceição, R.V., Mizusaki, A.M.P. (2022). Mesozoic to Cenozoic alkaline and tholeiitic magmatism related to West Gondwana break-up and dispersal. *Gondwana Res.* 106, 15–33. https://doi.org/10.1016/j.gr.2022.01.005

Fitzgerald, P.G., Baldwin, S.L., Webb, L.E., O'Sullivan, P.B. (2006). Interpretation of (U-Th)/He single grain ages from slowly cooled crustal terranes: A case study from the Transantarctic Mountains of southern Victoria Land. *Chem. Geol.* 225, 91–120. https://doi.org/10.1016/j.chemgeo.2005.09.001

Fleischer, R.L., Price, P.B. (1964). Techniques for geological dating of minerals by chemical etching of fission fragment tracks. *Geochim. Cosmochim. Acta* 28, 1705–1714. https://doi.org/10.1016/0016-7037(64)90017-1

Flowers, R.M., Kelley, S.A. (2011). Interpreting data dispersion and "inverted" dates in apatite (U-Th)/He and fission-track data sets. *Geochim. Cosmochim. Acta* 75, 5169–5186. https://doi.org/10.1016/j.gca.2011.06.016

Flowers, R.M., Ketcham, R.A., Shuster, D.L., Farley, K.A. (2009). Apatite (U-Th)/He thermochronometry using a radiation damage accumulation and annealing model. *Geochim. Cosmochim. Acta* 73, 2347–2365. https://doi.org/10.1016/j.gca.2009.01.015

Flowers, R.M., Shuster, D.L., Wernicke, B.P., Farley, K.A. (2007). Radiation damage control on apatite (U-Th)/He dates from the Grand Canyon region, Colorado Plateau. *Geology* 35, 447–450. https://doi.org/10.1130/G23471A.1

Flowers, R.M., Zeitler, P.K., Danišík, M., Reiners, P.W., Gautheron, C., Ketcham, R.A., Metcalf, J.R.,

Stockli, D.F., Enkelmann, E., Brown, R.W. (2022). (U-Th)/He chronology: Part 1. Data, uncertainty, and reporting. *Bull. Geol. Soc. Am.* 135, 104–136. https://doi.org/10.1130/B36266.1

Fonseca, A.C., Piffer, G.V., Nachtergaele, S., Van Ranst, G., De Grave, J., Novo, T.A. (2020). Devonian to Permian post-orogenic denudation of the Brasília Belt of West Gondwana: insights from apatite fission track thermochronology. *J. Geodyn.* 137, 101733. https://doi.org/10.1016/j.jog.2020.101733

Fonseca, A.C.L., Novo, T.A., Nachtergaele, S., Fonte-Boa, T.M.R., Van Ranst, G., De Grave, J. (2021). Differential Phanerozoic evolution of cratonic and non-cratonic lithosphere from a thermochronological perspective: São Francisco Craton and marginal orogens (Brazil). *Gondwana Res.* 93, 106–126. https://doi.org/10.1016/j.gr.2021.01.006

Galbraith, R.F. (1981). On statistical models for fission track counts. *J. Int. Assoc. Math. Geol.* 13, 471–478. https://doi.org/10.1007/BF01034498

Gallagher, K. (2012). Transdimensional inverse thermal history modeling for quantitative thermochronology. *J. Geophys. Res. Solid Earth* 117, B02408. https://doi.org/10.1029/2011JB008825

Gallagher, K., Charvin, K., Nielsen, S., Sambridge, M., Stephenson, J. (2009). Markov chain Monte Carlo (MCMC) sampling methods to determine optimal models, model resolution and model choice for Earth Science problems. *Mar. Pet. Geol.* 26, 525–535. https://doi.org/10.1016/j.marpetgeo.2009.01.003

Gautheron, C., Tassan-Got, L., Barbarand, J., Pagel, M. (2009). Effect of alpha-damage annealing on apatite (U-Th)/He thermochronology. *Chem. Geol.* 266, 157–170. https://doi.org/10.1016/j.chemgeo.2009.06.001

Gilchrist, A.R., Summerfield, M.A. (1990). Differential denudation and flexural isostasy in formation of rifted-margin upwarps. *Nature* 346, 739–742. https://doi.org/10.1038/346739a0

Gleadow, A.J.W., Duddy, I.R., Green, P.F., Hegarty, K.A. (1986). Fission track lengths in the apatite annealing zone and the interpretation of mixed ages. *Earth Planet. Sci. Lett.* 78, 245–254. https://doi.org/10.1016/0012-821X(86)90065-8

Green, P., Duddy, I., (2018) Apatite (U-Th-Sm)/He thermochronology on the wrong side of the tracks. *Chem. Geol.* 488, 21–33. https://doi.org/10.1016/j.chemgeo.2018.04.028

Green, P.F., Duddy, I.R., Laslett, G.M., Hegarty, K.A., Gleadow, A.J.W., Lovering, J.F. (1989). Thermal annealing of fission tracks in apatite 4. Quantitative modelling techniques and extension to geological timescales. *Chem. Geol. Isot. Geosci. Sect.* 79, 155–182. https://doi.org/10.1016/0168-9622(89)90018-3

Guadagnin, F., Chemale, F., Dussin, I.A., Jelinek, A.R., dos Santos, M.N., Borba, M.L., Justino, D., Bertotti, A.L., Alessandretti, L. (2010). Depositional age and provenance of the Itajaí Basin, Santa Catarina State, Brazil: Implications for SW Gondwana correlation. *Precambrian Res.* 180, 156–182. https://doi.org/10.1016/j.precamres.2010.04.002

Guenthner, W.R., Reiners, P.W., Ketcham, R.A., Nasdala, L., Giester, G. (2013). Helium diffusion in natural zircon: radiation damage, anisotropy, and the interpretation of zircon (U-TH)/He thermochronology. *Am. J. Sci.* 313, 145–198. https://doi.org/10.2475/03.2013.01

Harman, R., Gallagher, K., Brown, R., Raza, A., Bizzi, L. (1998). Accelerated denudation and tectonic/geomorphic reactivation of the craton of northeastern Brazil during the Late Cretaceous. *J. Geophys. Res.* 103, 27091–27105.

Hasui, Y. (2010). A grande colisão pré-cambriana do sudeste brasileiro e a estruturação regional, *Geociencias*.

Heilbron, M., de Morisson Valeriano, C., Peixoto, C., Tupinambá, M., Neubauer, F., Dussin, I., Corrales, F., Bruno, H., Lobato, M., Horta de Almeida, J.C., Guilherme do Eirado Silva, L. (2020). Neoproterozoic magmatic arc systems of the central Ribeira belt, SE-Brazil, in the context of the West-Gondwana pre-collisional history: A review. *J. South Am. Earth Sci.* 103, 102710. https://doi.org/10.1016/j.jsames.2020.102710

Heilbron, M., Eirado, L.G., Almeida, J. (2016). Mapa geológico e de recursos minerais do estado do Rio de Janeiro. Escala 1:400.000. *Programa Geol. do Bras.* CPRM.

Heilbron, M., Machado, N., 2003. Timing of terrane accretion in the Neoproterozoic-Eopaleozoic Ribeira Orogen (SE Brazil). Precambrian Res. 125, 87–112. https://doi.org/10.1016/S0301-9268(03)00082-2

Heilbron, Monica, Cordani, U.G., Alkmim, F.F. (2017a). The São Francisco Craton and Its Margins, in: Heilbron, M., Cordani, U.G., Alkmim, F.F. (Eds.), *São Francisco Craton, Eastern Brazil.* Springer, Cham, pp. 3–13. https://doi.org/10.1007/978-3-319-01715-0_1

Heilbron, Monica, Ribeiro, A., Valeriano, C.M., Paciullo, F. V, Almeida, J.C.H., Trouw, R.J.A., Tupinambá, M., Silva, L.G.E. (2017b). The Ribeira Belt, in: Heilbron, M., Cordani, U.G., Alkmim, F.F. (Eds.), *São Francisco Craton, Eastern Brazil.* Springer, Cham, pp. 277–302. https://doi.org/10.1007/978-3-319-01715-0

Hiruma, S.T., Riccomini, C., Modenesi-Gauttieri, M.C., Hackspacher, P.C., Neto, J.C.H., Franco-Magalhães, A.O.B. (2010). Denudation history of the Bocaina Plateau, Serra do Mar, southeastern Brazil: Relationships to Gondwana breakup and passive margin development. *Gondwana Res.* 18, 674–687. https://doi.org/10.1016/j.gr.2010.03.001

Hu, J., Liu, L., Faccenda, M., Zhou, Q., Fischer, K.M., Marshak, S., Lundstrom, C. (2018). Modification of the Western Gondwana craton by plume-lithosphere interaction. *Nat. Geosci.* 11, 203–210. https://doi.org/10.1038/s41561-018-0064-1

Hueck, M., Dunkl, I., Heller, B., Stipp Basei, M.A., Siegesmund, S. (2018a). (U-Th)/He Thermochronology and Zircon Radiation Damage in the South American Passive Margin: Thermal Overprint of the Paraná LIP? *Tectonics* 37, 4068–4085. https://doi.org/10.1029/2018TC005041

Hueck, M., Dunkl, I., Oriolo, S., Wemmer, K., Basei, M.A.S., Siegesmund, S. (2019). Comparing contiguous high- and low-elevation continental margins: New (U-Th)/He constraints from South Brazil and an integration of the thermochronological record of the southeastern passive margin of South America. *Tectonophysics* 770, 228222. https://doi.org/10.1016/j.tecto.2019.228222

Hueck, M., Oyhantçabal, P., Philipp, R.P., Basei, M.A.S., Siegesmund, S. (2018b). The Dom Feliciano Belt in Southern Brazil and Uruguay, in: Siegesmund, S., Basei, M.Â.S., Oyhantçabal, P., Oriolo, S. (Eds.), *Geology of Southwest Gondwana*. Springer, Cham, pp. 267–302. https://doi.org/10.1007/978-3-319-68920-3_11

Hurford, A.J. (2019). An Historical Perspective on Fission-Track Thermochronology. Springer International Publishing. https://doi.org/10.1007/978-3-319-89421-8_1

Hurford, A.J. (1990a). Standardization of fission track dating calibration: Recommendation by the Fission Track Working Group of the I.U.G.S. Subcommission on Geochronology. *Chem. Geol. Isot. Geosci.*

Sect. 80, 171–178. https://doi.org/10.1016/0168-9622(90)90025-8

Hurford, A.J., (1990b). International Union of Geological Sciences: Subcommission on Geochronology recommendation for the standardization of fission track dating calibration and data reporting. *Int. J. Radiat. Appl. Instrumentation.* Part 17, 233–236. https://doi.org/10.1016/1359-0189(86)90061-0

Hurford, A.J., Green, P.F. (1983). The zeta age calibration of fission-track dating. *Chem. Geol.* 41, 285–317. https://doi.org/10.1016/S0009-2541(83)80026-6

Jelinek, A.R., Chemale, F., van der Beek, P.A., Guadagnin, F., Cupertino, J.A., Viana, A. (2014). Denudation history and landscape evolution of the northern East-Brazilian continental margin from apatite fission-track thermochronology. *J. South Am. Earth Sci.* 54, 158–181. https://doi.org/10.1016/j.jsames.2014.06.001

Karl, M., Glasmacher, U.A., Kollenz, S., Franco-Magalhaes, A.O.B., Stockli, D.F., Hackspacher, P.C. (2013). Evolution of the South Atlantic passive continental margin in southern Brazil derived from zircon and apatite (U-Th-Sm)/He and fission-track data. *Tectonophysics* 604, 224–244. https://doi.org/10.1016/j.tecto.2013.06.017

Kasanzu, C.H. (2017). Apatite fission track and (U-Th)/He thermochronology from the Archean Tanzania Craton: Contributions to cooling histories of Tanzanian basement rocks. *Geosci. Front.* 8, 999–1007. https://doi.org/10.1016/j.gsf.2016.09.007

Kasanzu, C.H., Linol, B., de Wit, M.J., Brown, R., Persano, C., Stuart, F.M. (2016). From source to sink in central Gondwana: Exhumation of the Precambrian basement rocks of Tanzania and sediment accumulation in the adjacent Congo basin. *Tectonics* 35, 2034–2051. https://doi.org/10.1002/2016TC004147

Ketcham, R.A., Carter, A., Donelick, R.A., Barbarand, J., Hurford, A.J. (2007). Improved modeling of fission-track annealing in apatite. *Am. Mineral.* 92, 799–810. https://doi.org/10.2138/am.2007.2281

Krob, F.C., Glasmacher, U.A., Karl, M., Perner, M., Hackspacher, P.C., Stockli, D.F. (2019). Multi-chronometer thermochronological modelling of the Late Neoproterozoic to recent t-T-evolution of the SE coastal region of Brazil. *J. South Am. Earth Sci.* 92, 77–94. https://doi.org/10.1016/j.jsames.2019.02.012

Linol, B., de Wit, M. J., Milani, E.J., Guillocheau, F., Scherer, C. (2015). New Regional Correlation Between the Congo, Paraná and Cape-Karoo Basins of Southwest Gondwana, in: De Wit, Maarten J., Guillocheau, François, De Wit, M.C.J. (Eds.), *Geology and Resource Potential of the Congo Basin.* Springer, Berlin, Heidelberg, pp. 245–268. https://doi.org/10.1007/978-3-642-29482-2

Lippolt, H.J., Leitz, M., Wernicke, R.S., Hagedorn, B. (1994). (Uranium + thorium)/helium dating of apatite: experience with samples from different geochemical environments. *Chem. Geol.* 112, 179–191. https://doi.org/10.1016/0009-2541(94)90113-9

Macêdo Filho, A.A., Hollanda, M.H.B.M., Oliveira, A.L., Negri, F.A. (2023). Magma plumbing systems in the Parnaíba Basin: Geochemistry, geochronology, and regional correlations with Mesozoic large igneous provinces. *Lithos* 446–447, 107130. https://doi.org/10.1016/j.lithos.2023.107130

Machado, J.P.S.L., Jelinek, A.R., Bicca, M.M., Stephenson, R., Genezini, F.A. (2019). West Gondwana orogenies and Pangaea break-up: Thermotectonic effects on the southernmost Mantiqueira Province, Brazil. *J. Geol. Soc. London.* 176, 1056–1075. https://doi.org/10.1144/jgs2019-018

Martins-Ferreira, M.A.C., Dias, A.N.C., Chemale, F., Campos, J.E.G. (2020). Intracontinental uplift of the Brazilian Central Plateau linked to continental breakup, orogenies, and basin filling, supported by apatite and zircon fission-track data. *Arab. J. Geosci.* 13:891. https://doi.org/10.1007/s12517-020-05885-8

Milani, E.J., De Wit, M.J. (2014). Correlations between the classic Paraná and Cape-Karoo sequences of South America and southern Africa and their basin infills flanking the Gondwanides: Du Toit revisited. *Geol. Soc. Spec. Publ.* 294, 319–342. https://doi.org/10.1144/SP294.17

Milani, E.J., Faccini, U.F., Scherer, C.M., Araújo, L.M., Cupertino, J.A. (1998). Sequences and stratigraphic hierarchy of the Paraná Basin (Ordovician to Cretaceous), southern Brazil. *Bol. IG-USP. Série Científica* 29, 125–173. https://doi.org/https://doi.org/10.11606/issn.2316-8986.v29i0p125-173

Milani, E.J., Gonçalves De Melo, J.H., De Souza, P.A., Fernandes, L.A., França, A.B. (2007ª). Bacia do Paraná. *Bol. Geociencias da Petrobras* 15, 265–287.

Milani, E.J., Lana, M.C., Szatmari, P. (1988). Mesozoic rift basins around the northeast Brazilian microplate (Recôncavo – Tucano – Jatobá, Sergipe – Alagoas), in: W. Manspeizer (Ed.), *Developments in Geotectonics*. Elsevier, pp. 833–858. https://doi.org/10.1016/B978-0-444-42903-2.50039-7

Milani, E.J., Ramos, V.A. (1998). Paleozoic orogenies in southwestern Gondwana and the subsidence cycles of the Parana Basin. *Rev. Bras. Geociências* 28, 473–484.

Milani, E.J., Rangel, H.D., Bueno, G.V., Stica, J.M., Winter, W.R., Caixeta, J.M., Da Cruz Pessoa Neto, O. (2007b). Bacias sedimentares brasileiras - Cartas estratigráficas. *Bol. Geociencias da Petrobras* 15, 183–205.

Mohriak, W., Nemčok, M., Enciso, G. (2008). South Atlantic divergent margin evolution: Rift-border uplift and salt tectonics in the basins of SE Brazil. *Geol. Soc. Spec. Publ.* 294, 365–398. https://doi.org/10.1144/SP294.19

Moreira, J.L.P., Valdetaro, C.V., Gil, J.A., Machado, M.A.P. (2007). Bacia de Santos. *Bol. Geociencias da Petrobras* 15, 531–549.

Murray, K.E., Orme, D.A., Reiners, P.W. (2014). Effects of U-Th-rich grain boundary phases on apatite helium ages. *Chem. Geol.* 390, 135–151. https://doi.org/10.1016/j.chemgeo.2014.09.023

Novo, T.A., Fonte-boa, T.M.R., Rolim, J.M., Fonseca, A.C. (2021). The state of the art of low-temperature thermochronometry in Brazil. *J. Geol. Surv. Brazil* 4, 239–256. https://doi.org/https://doi.org/10.29396/jgsb.2021.v4.n3.4

Nürnberg, D., Müller, R.D. (1991). The tectonic evolution of the South Atlantic from Late Jurassic to present. *Tectonophysics* 191, 27–53. https://doi.org/10.1016/0040-1951(91)90231-G

Oriolo, S., Oyhantçabal, P., Basei, M.A.S., Wemmer, K., Siegesmund, S. (2016). The Nico Pérez Terrane (Uruguay): From Archean crustal growth and connections with the Congo Craton to late Neoproterozoic accretion to the Río de la Plata Craton. *Precambrian Res.* 280, 147–160. https://doi.org/10.1016/j.precamres.2016.04.014

Oyhantçabal, P., Cingolani, C.A., Wemmer, K., Siegesmund, S. (2018a). The Río de la Plata Craton of Argentina and Uruguay, in: Siegesmund, S., Basei, M.Â.S., Oyhantçabal, P., Oriolo, S. (Eds.), *Geology of Southwest Gondwana.* Springer, Cham, pp. 89–105. https://doi.org/10.1007/978-3-319-68920-3_4

Oyhantçabal, P., Oriolo, S., Philipp, R.P., Wemmer, K., Siegesmund, S. (2018b). The Nico Pérez Terrane of Uruguay and Southeastern Brazil, Regional G. ed, *Geology of Southwest Gondwana.* Springer, Cham. https://doi.org/10.1007/978-3-319-68920-3_7

Passarelli, C.R., Stipp Basei, M.A., Siga, J.O., Hara, O.M.M. (2018). The Luis Alves and Curitiba Terranes: Continental Fragments in the Adamastor Ocean, in: Siegesmund, S., Basei, M.Â.S., Oyhantçabal, P., Oriolo, S. (Eds.), *Geology of Southwest Gondwana.* Springer, Cham, pp. 189–215. https://doi.org/10.1007/978-3-319-68920-3

Pedrosa-Soares, A.C., Alkmim, F.F. de (2011). How Many Rifting Events Preceded the Development of the Araçuaí-West Congo Orogen? *Geonomos* 19, 244–251. https://doi.org/10.18285/geonomos.v19i2.56

Pedrosa-Soares, A.C., Alkmim, F.F., Tack, L., Noce, C.M., Babinski, M., Silva, L.C., Martins-Neto, M.A. (2008). Similarities and differences between the Brazilian and African counterparts of the Neoproterozoic Araçuaí-West Congo orogen. *Geol. Soc. Spec. Publ.* 294, 153–172. https://doi.org/10.1144/SP294.9

Pedrosa-Soares, A.C., Wiedemann-Leonardos, C.M. (2000). Evolution of Araçuaí Belt and its connection to the Ribeira Belt, eastern Brazil, in: Cordani, U.G., Milani, E.J., Thomaz-Filho, A., Campos, D.A. (Eds.), *Tectonic Evolution of South America.* 31st International Geological Congress, Rio de Janeiro, pp. 265–285. https://doi.org/10.13140/2.1.3802.5928

Perrota, M.M., Salvador, E.D., Lopes, R.C., D'Agostinho, L.Z., Peruffo, N., Gomes, S.D., Sachs, L.L.B., Meira, V.T., Garcia, M.G.M., Lacerda Filho, J. V. (2005). *Mapa Geológico do Estado de São Paulo*, escala 1:750.000. *Programa Geol. do Bras.* CPRM.

Philipp, R.P., Machado, R. (2005). The Late Neoproterozoic granitoid magmatism of the Pelotas Batholith, southern Brazil. *J. South Am. Earth Sci.* 19, 461–478. https://doi.org/10.1016/j.jsames.2005.06.010

Philipp, R.P., Pimentel, M.M., Chemale, F. (2016). Tectonic evolution of the Dom Feliciano Belt in Southern Brazil: Geological relationships and U-Pb geochronology. *Brazilian J. Geol.* 46, 83–104. https://doi.org/10.1590/2317-4889201620150016

Porada, H. (1989). Pan-African rifting and orogenesis in southern to equatorial Africa and eastern Brazil. *Precambrian Res.* 44, 103–136. https://doi.org/10.1016/0301-9268(89)90078-8

Price, P.B., Walker, R.M. (1963). Fossil Tracks of Charged Particles in Mica and the Age of Minerals. *J. Geophys. Res.* 68, 4847–4862. https://doi.org/10.1029/JZ068i016p04847

Queiroga, G.N., Pedrosa-Soares, A.C., Noce, C.M., Alkmim, F.F. de, Pimentel, M.M., Dantas, E., Martins, M., Castañeda, C., Suita, M.T. de F., Prichard, H. (2007). Age of the Ribeirão Da Folha Ophiolite, Araçuaí Orogen: the U-Pb Zircon (La-Icpms) Dating of a Plagiogranite. *Geonomos* 15, 61–65. https://doi.org/10.18285/geonomos.v15i1.107

Reiners, P.W. (2021). Thermochronology, *Encyclopedia of Geology*: Volume 1-6, Second Edition. https://doi.org/10.1016/B978-0-12-409548-9.12114-1

Reiners, P.W. (2005). Zircon (U-TH)/He thermochronometry. *Rev. Mineral. Geochemistry* 58, 151–179. https://doi.org/10.2138/rmg.2005.58.6

Reiners, P.W., Carlson, R.W., Renne, P.R., Cooper, K.M., Granger, D.E., McLean, N.M., Schoene, B. (2017). *Geochronology and Thermochronology*. Wiley-Blackwell. https://doi.org/10.1002/9781118455876

Reiners, P.W., Farley, K.A., Hickes, H.J. (2002). He diffusion and (U-Th)/He thermochronometry of zircon: Initial results from Fish Canyon Tuff and Gold Butte. *Tectonophysics* 349, 297–308. https://doi.org/10.1016/S0040-1951(02)00058-6

Reiners, P.W., Spell, T.L., Nicolescu, S., Zanetti, K.A. (2004). Zircon (U-Th)/He thermochronometry: He diffusion and comparisons with 40Ar/39Ar dating. *Geochim. Cosmochim. Acta* 68, 1857–1887. https://doi.org/10.1016/j.gca.2003.10.021

Reis, H.L.S., Alkmim, F.F., Fonseca, R.C.S., Nascimento, T.C., Suss, J.F., Prevatti, L.D. (2017). The São Francisco Basin, in: Heilbron, M., Cordani, U.G., Alkmim, F.F. (Eds.), *São Francisco Craton, Eastern Brazil.* Springer, Cham, pp. 117–143. https://doi.org/10.1007/978-3-319-01715-0_7

Riccomini, C. (1990). O Rift continental do sudeste do Brasil. Universidade de São Paulo.

Riccomini, C., Gomes, L., Anna, S. (2004). Evolução geológica do rift continental do sudeste do Brasil, in: Mantesso-Neto, V., Bartorelli, A., Carneiro, C.D.R., Brito-Neves, B.B. de (Eds.), *Geologia Do Continente Sul-Americano: Evolução Da Obra de Fernando Flávio de Almeida.* Beca, pp. 383–405.

Salomon, E., Passchier, C., Koehn, D. (2017). Asymmetric continental deformation during South Atlantic rifting along southern Brazil and Namibia. *Gondwana Res.* 51, 170–176. https://doi.org/10.1016/j.gr.2017.08.001

Sandwell, D.T., Müller, R.D., Smith, W.H.F., Garcia, E., Francis, R. (2014). New global marine gravity model from CryoSat-2 and Jason-1 reveals buried tectonic structure. *Science* (80-.). 346, 65–67. https://doi.org/10.1126/science.1258213

Scherer, C.M.S., Reis, A.D., Horn, B.L.D., Bertolini, G., Lavina, E.L.C., Kifumbi, C., Goso Aguilar, C. (2023). The stratigraphic puzzle of the permo-mesozoic southwestern Gondwana: The Paraná Basin record in geotectonic and palaeoclimatic context. *Earth-Science Rev.* 240, 104397. https://doi.org/10.1016/j.earscirev.2023.104397

Schmitt, R. da S., Fragoso, R. de A., Collins, A.S. (2018). Suturing Gondwana in the Cambrian: The Orogenic Events of the Final Amalgamation, in: Siegesmund, S., Basei, M.Â.S., Oyhantçabal, P., Oriolo, S. (Eds.), *Geology of Southwest Gondwana.* Springer, Cham, pp. 411–432. https://doi.org/10.1007/978-3-319-68920-3_15

Schmitt, R.D.S., Trouw, R., Van Schmus, W.R., Armstrong, R., Stanton, N.S.G. (2016). The tectonic significance of the Cabo Frio Tectonic Domain in the SE Brazilian margin: A Paleoproterozoic through Cretaceous saga of a reworked continental margin. *Brazilian J. Geol.* 46, 37–66. https://doi.org/10.1590/2317-4889201620150025

Sgarbi, G.N.C., Sgarbi, P.B. de A., Campos, J.E.G., Dardenne, M.A., Penha, U.C. (2001). Bacia Sanfranciscana: o registro Fanerozóico da Bacia do São Francisco, in: Pinto, C.P., Martins-Neto, M.A. (Eds.), *Bacia Do São Francisco: Geologia e Recursos Naturais.* SBG/MG, pp. 93–138.

Shuster, D.L., Flowers, R.M., Farley, K.A. (2006). The influence of natural radiation damage on helium diffusion kinetics in apatite. *Earth Planet. Sci. Lett.* 249, 148–161. https://doi.org/10.1016/j.epsl.2006.07.028

Silva, M.A., Pinto, C.P., Pinheiro, M.A.P., Marinho, M.S., Lombello, J.C., Pinho, J.M.M.P., Goulart, L.E.A., Magalhães, J.R. (2020). *Mapa Geológico do Estado de Minas Gerais*, Escala 1:1.000.000. *Programa Geol. do Bras.* CPRM.

Souza, M.E., de Souza Martins, M., Queiroga, G.N., Leite, M., Oliveira, R.G., Dussin, I., Pedrosa-Soares, A.C. (2019). Paleoenvironment, sediment provenance and tectonic setting of Tonian basal deposits of the Macaúbas basin system, Araçuaí orogen, southeast Brazil. *J. South Am. Earth Sci.* 96, 102393. https://doi.org/10.1016/j.jsames.2019.102393

Spiegel, C., Kohn, B., Belton, D., Berner, Z., Gleadow, A. (2009). Apatite (U-Th-Sm)/He thermochronology of rapidly cooled samples: The effect of He implantation. *Earth Planet. Sci. Lett.* 285, 105–114. https://doi.org/10.1016/j.epsl.2009.05.045

Stanton, N., Gordon, A., Cardozo, C., Kusznir, N. (2021). Morphostructure, emplacement and duration of the Abrolhos Magmatic Province: A geophysical analysis of the largest post-breakup magmatism of the South-Eastern Brazilian margin. *Mar. Pet. Geol.* 133, 105230. https://doi.org/10.1016/j.marpetgeo.2021.105230

Stockli, D.F., Farley, K.A., Dumitru, T.A. (2000). Calibration of the apatite (U-Th)/He thermochronometer on anexhumed fault block, White Mountains, California. *Geology* 28, 983–986. https://doi.org/10.1130/0091-7613(2000)28<983:COTAHT>2.0.CO;2

Szatmari, P., Milani, E.J. (2016). Tectonic control of the oil-rich large igneous-carbonate-salt province of the South Atlantic rift. *Mar. Pet. Geol.* 77, 567–596. https://doi.org/10.1016/j.marpetgeo.2016.06.004

Tagami, T., O'Sullivan, P.B. (2005). Fundamentals of fission-track thermochronology. *Rev. Mineral. Geochemistry* 58, 19–47. https://doi.org/10.2138/rmg.2005.58.2

Takenaka, L.B., Förster, M.W., Alard, O., Griffin, W.L., Jacob, D.E., Basei, M.A.S., O'Reilly, S.Y. (2023). Multi-mineral geochronology of kimberlites, kamafugites and alkaline-carbonatite rocks, SW São Francisco Craton, Brazil: Appraisal of intrusion ages. *Gondwana Res.* 124, 246–272. https://doi.org/10.1016/j.gr.2023.05.012

Tedeschi, M., Novo, T., Pedrosa-Soares, A., Dussin, I., Tassinari, C., Silva, L.C., Gonçalves, L., Alkmim, F., Lana, C., Figueiredo, C., Dantas, E., Medeiros, S., De Campos, C., Corrales, F., Heilbron, M. (2016). The Ediacaran Rio Doce magmatic arc revisited (Araçuaí-Ribeira orogenic system, SE Brazil). *J. South Am. Earth Sci.* 68, 167–186. https://doi.org/10.1016/j.jsames.2015.11.011

Thompson, R.N., Gibson, S.A., Mitghell, J.G., Dickin, A.P., Leonardos, O.H., Brod, J.A., Greenwood, J.G. (1998). Migrating Cretaceous-Eocene magmatism in the Serra do Mar Alkaline Province, SE Brazil: melts from the deflected Trindade mantle plume? *J. Petrol.* 39, 1493–1526. https://doi.org/10.1093/petroj/39.8.1493

Van Ranst, G., Pedrosa-Soares, A.C., Novo, T., Vermeesch, P., De Grave, J. (2020). New insights from low-temperature thermochronology into the tectonic and geomorphologic evolution of the south-eastern Brazilian highlands and passive margin. *Geosci. Front.* 11, 303–324. https://doi.org/10.1016/j.gsf.2019.05.011

Vauchez, A., Hollanda, M.H.B.M., Monié, P., Mondou, M., Egydio-Silva, M. (2019). Slow cooling and crystallization of the roots of the Neoproterozoic Araçuaí hot orogen (SE Brazil): Implications for rheology, strain distribution, and deformation analysis. *Tectonophysics* 766, 500–518. https://doi.org/10.1016/j.tecto.2019.05.013

Vaz, P.T., Rezende, N.G.A.M., Wanderley Filho, J.R., Silva Travassos, W.A. (2007). Bacia do Parnaíba. *Bol. Geociencias da Petrobras* 15, 253–263.

Vermeesch, P. (2009). RadialPlotter: A Java application for fission track, luminescence and other radial plots. *Radiat. Meas.* 44, 409–410. https://doi.org/10.1016/j.radmeas.2009.05.003

Wildner, W., Camozzato, E., Toniolo, J.A., Binotto, R.B., Iglesias, C.M.F., Laux, J.H. (2014). *Mapa Geológico do Estado de Santa Catarina*, Escala 1:500.000. *Programa Geol. do Bras.* CPRM.

Wolf, R.A., Farley, K.A., Kass, D.M. (1998). Modeling of the temperature sensitivity of the apatite (U-Th)/He thermochronometer. *Chem. Geol.* 148, 105–114. https://doi.org/10.1016/S0009-2541(98)00024-2

Wolf, R.A., Farley, K.A., Silver, L.T. (1996). Helium diffusion and low-temperature thermochronometry of apatite. *Geochim. Cosmochim. Acta* 60, 4231–4240. https://doi.org/10.1016/S0016-7037(96)00192-5

Zalán, P.V., De Oliveira, J.A.B. (2005). Origem e evolução estrutural do Sistema de Rittes Cenozóicos do Sudeste do Brasil (Origin and structural evolution of the Cenozoic Rift System of Southeastern Brasil). *Bol. Geociencias da Petrobras* 13, 269–300.

Zalán, P.V., Silva, P.C.R. (2007). Bacia do São Francisco. *Bol. Geociencias da Petrobras* 15, 561–571.

Zeitler, P.K., Herczeg, A.L., McDougall, I., Honda, M. (1987). U-Th-He dating of apatite: A potential thermochronometer. *Geochim. Cosmochim. Acta* 51, 2865–2868. https://doi.org/10.1016/0016-7037(87)90164-5

CAPÍTULO 5 – Thermal history along the Araçuaí Orogen and São Francisco Craton border, eastern Brazilian continental margin, based on low-temperature Thermochronologic data

Edgar do Amaral Santos [a,*], Andréa Ritter Jelinek [b], João Pacífico Machado [c], Daniel Stockli [d]

[a] Programa de Pós-Graduação em Geociências, Instituto de Geociências, Universidade Federal do Rio Grande do Sul, Brazil

[b] Instituto de Geociências, Universidade Federal do Rio Grande do Sul, Brazil

[c] CGA, Serviço Geológico Brasileiro (CPRM), Brazil

[d] University of Texas at Austin, United States

* Corresponding author. E-mail address: edgar.amaral@ufrgs.br (E. do Amaral Santos).

Nota explicativa

Este capítulo corresponde ao artigo publicado em 2022 no periódico *Tectonophysics*, que pode ser encontrado online acessando o link: *https://doi.org/10.1016/j.tecto.2022.229232*. Ao final do capítulo, encontra-se o email de aceite do artigo.

Abstract

Passive margins form in response to rifting affecting a continental area. Rifting evolution is dependent on structural and rheological inheritance, generally controlling differential denudation, and deposition. The Brazilian continental margin developed over a complex basement, composed of the orogenic lithosphere of the Brasiliano-Pan-African orogenic belts (e.g., the Araçuaí Orogen), and the cratonic lithosphere of the São Francisco Craton. In this work, we focus on the transitional zone between the warm and cold lithosphere of the northern segment of the Araçuaí Orogen to the São Francisco Craton. This study provides the first suite of two low-temperature thermochronometers, i.e., zircon and apatite (U–Th)/He, for the region. Using this approach, we examine the main cooling events, the geodynamic forces acting upon the lithosphere, the denudation rates affecting this region since West Gondwana amalgamation, and the correlation between thermochronology and structural inheritance. Our results indicate that ZHe corrected ages range from 483.1 ± 38.6 to 93.8 ± 7.5 Ma and eU concentrations vary from

10.91 to 632.51 μg/g. AHe corrected ages span from 129.9 ± 7.79 to 32.7 ± 1.96 Ma and eU concentrations range from 5.6 to 62.8 μg/g. Both ZHe and AHe ages display a positive correlation with eU concentration. Based on this dataset, we identify three cooling episodes, constrained from Lower Devonian to Carboniferous, Triassic/Jurassic to the present day, and Late Cretaceous/Paleocene to the present day. Additionally, two reheating episodes are constrained from Middle Jurassic to Early Cretaceous and from Late Cretaceous to Paleocene. Furthermore, we analyzed lineament directions in the orogenic, cratonic, and Cenozoic sedimentary cover domains to understand how structural inheritance affects the thermochronological record. Our observations reveal that reactivation of the Brasiliano NW-SE inherited structures during continental breakup up until the Paleocene possibly kept the AHe system open, resulting in the youngest AHe ages of our data set.

5.1 Introduction

Passive margins are landscapes that result from continental rifting that either end up forming oceans or finish as aborted rift segments (Braun and van der Beek, 2004; Misra and Mukherjee, 2015; Nemčok, 2016). The rift evolution strongly depends on basement properties (Buck, 1991), because rift geometry and development are largely controlled by the rheology (i.e., strength, thickness, and temperature) of the pre-rift lithosphere (Van Avendonk et al., 2009). Additionally, the composition of the lithosphere plays a fundamental role in rift formation and the development of passive margins (Kusznir and Park, 1987; Misra and Mukherjee, 2015).

The Brazilian passive margin started to form in the Early Cretaceous, through rifting in the far south that propagated northwards following the Brasiliano/Pan-African mobile belts formed during the assemblage of West Gondwana (Fig. 5.1a; Chang et al., 1992). These belts include the Dom Feliciano, Ribeira, and Araçuaí orogens, among several others (de Almeida et al., 1981). Rifting also affected the continental bridge between the Archean Cratons of São Francisco and Congo, located to the north of the Araçuaí Orogen, separating both landmasses between 120 and 112 Ma (Torsvik et al., 2009).

Several studies document the Phanerozoic evolution of the upper crust where the Brasiliano orogenic lithosphere interact with the São Francisco Craton lithosphere (Harman et al., 1998; De Morais Neto et al., 2007; Turner et al., 2008; Japsen et al., 2012;

Jelinek et al., 2014; Engelmann de Oliveira et al., 2016; Engelmann de Oliveira & Jelinek, 2017; Amaral-Santos et al., 2019; Van Ranst et al., 2020; Fonseca et al., 2021). These studies generally apply low-temperature thermochronology, such as apatite fission track and apatite (U–Th)/He to constrain thermal histories ranging mostly from the Mesozoic to the present day.

In this study, we constrain the Paleozoic to Cenozoic thermal histories of the Araçuaí Orogen and São Francisco Craton by combining, for the first time, zircon and apatite (U–Th)/He thermochronometers. Understanding of the controls on (U–Th)/He ages dispersion, the geodynamic forces driving the cooling and reheating episodes, and the denudation rates associated with each cooling phase are among our goals here. To this end, we analyze the lineaments of the orogenic, cratonic, and sedimentary cover domains to determine how structural inheritance may affect the thermochronological record in the area.

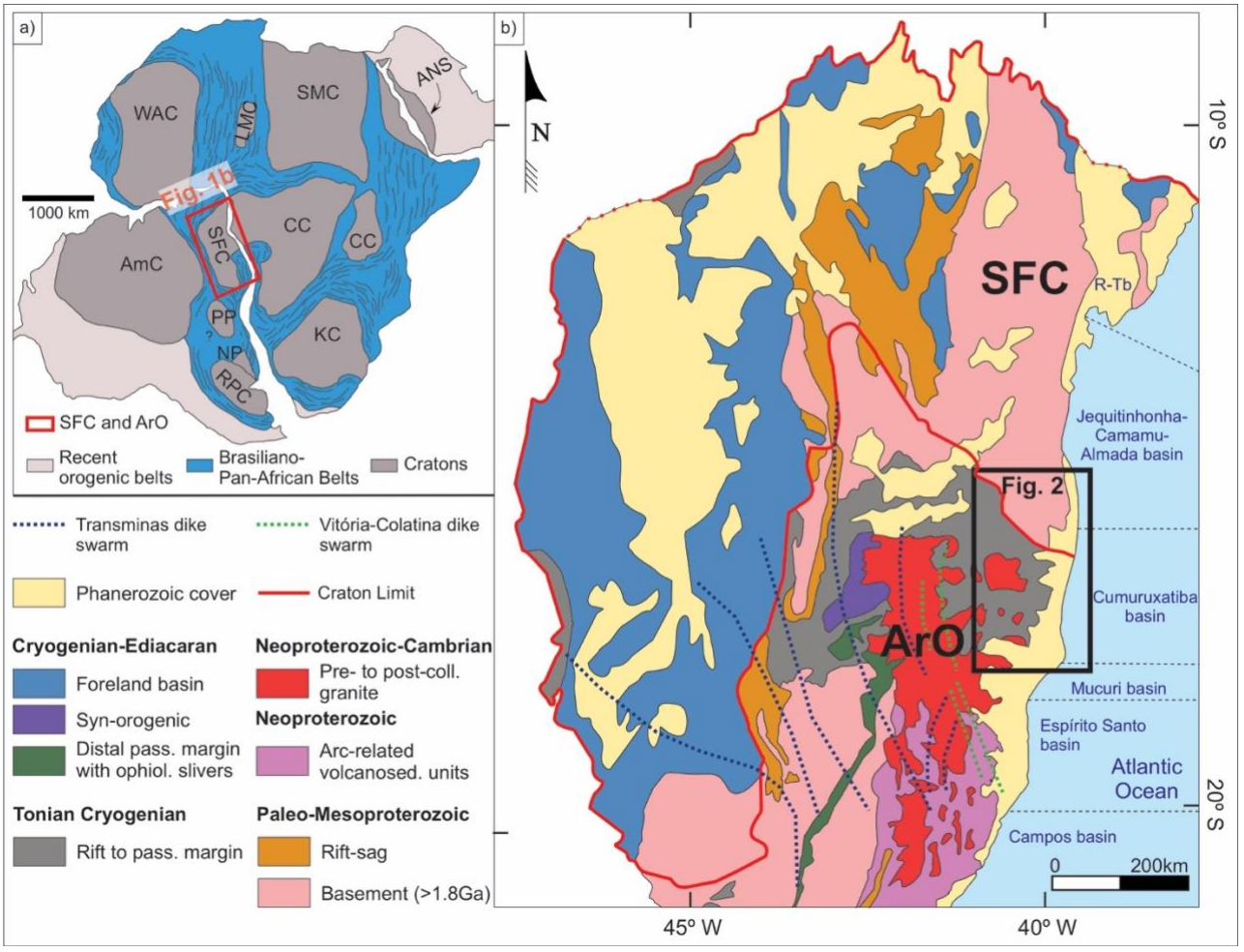

Figure 5. 1: a) West Gondwana map evidencing the cratonic nuclei, the Brasiliano/Pan-African belts, and the recent orogenic belts (after Oriolo et al., 2017). The red rectangle indicates the study area. Abbreviations are: SFC: São Francisco Craton; CC: Congo Craton; PP: Paranapanema Block; NP: Nico

Perez Terrane; RPC: Rio de la Plata Craton; AmC: Amazon Craton; WAC: West Africa Craton; LMC: Latea Metacraton; SMC: Sahara Metacraton; KC: Kalahari Craton; ANS: Arabian-Nubian Shield. b) Geologic map of the São Francisco Craton (SFC) and the Araçuaí Orogen (ArO) displaying the most important units in the selected area (after Almeida, 1981; De Alkmim, 2015; Alkmim et al., 2016) and the basins of the continental margin; R-Tb: Recôncavo-Tucano basins Volcanosed.: Volcanosedimentary; Pass.: passive; Ophiol.: ophiolite; Coll.: collisional. (For interpretation of the references to colour in this figure legend, the reader is referred to the web version of this article.)

5.2 Geological and geomorphological background

5.2.1 Geologic setting

The study area includes part of the São Francisco Craton and the Araçuaí Orogen (Figs. 5.1b and 5.2). The São Francisco Craton represents a Precambrian nucleus of the South American plate, encompassing rock assemblages that span from Paleoarchean to the Cenozoic (Heilbron et al., 2016a). In contrast, the Araçuaí Orogen comprises one of the several orogenic belts surrounding the São Francisco Craton (Fig. 5.1a). These belts were formed during the West Gondwana amalgamation and are mainly composed of Proterozoic to Cambrian igneous and metasedimentary rocks. Segments of both the São Francisco Craton and the Araçuaí Orogen constitute the basement of the Brazilian passive margin, formed after the breakup of Pangea in the Mesozoic (Rabinowitz and Labrecque, 1979; Torsvik et al., 2009). In our study area, the continental margin is marked by an expressive Cenozoic sedimentary cover, while Cenozoic igneous rocks are mostly submerged, with only a few scattered outcrops offshore.

The São Francisco and Congo Cratons, now separately located in South America and western-central Africa, were once part of a larger setting, in which their Archean nuclei were adjacent from the Archean to the Proterozoic (Heilbron et al., 2016b). During this period, several events shaped these landmasses through rifting and collisions. Lithological units older than 1.8 Ga (de Almeida, 1977) compose the main exposed basement assemblages, whereas units younger than 1.8 Ga constitute the cratonic cover (Fig. 5.1b; Teixeira et al., 2000; Barbosa and Sabaté, 2004; Pedrosa-Soares and de Alkmim, 2011; Alkmim and Martins-Neto, 2012; Cruz and Alkmim, 2016). During the end of the Neoproterozoic, subduction led to the amalgamation of West Gondwana through the inversion of rifts. The amalgamation also culminated in the closure of the Adamastor Ocean, among others, reuniting in a single continent several cratonic blocks that currently are part of South America and Africa (Pedrosa-Soares et al., 2008). The orogenic systems formed during this process are called Brasiliano/Pan-African orogens, with the

Araçuaí Orogen defining the southeast limit of the Sao Francisco Craton (de Almeida, 1977).

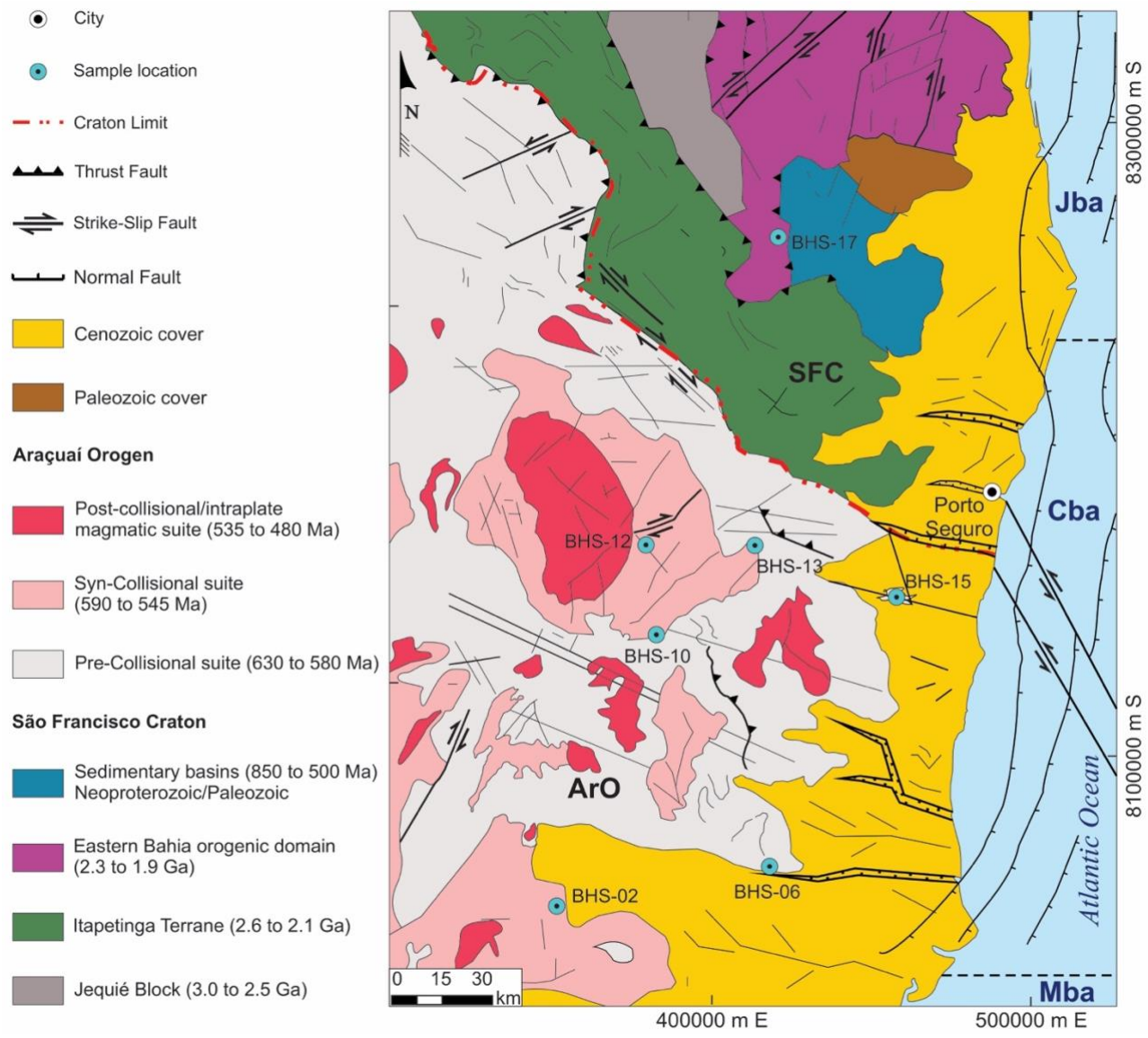

Figure 5. 2: Geologic map of the study area with sampling sites along the border of the São Francisco Craton (SFC) and the Araçuaí Orogen (ArO); Abbreviations are: Mba: Mucuri basin; Cba: Cumuruxatiba basin; Jba: Jequitinhonha basin.

The Araçuaí Orogen is currently interpreted as the external domain of the Araçuaí-West Congo confined orogen (AWCO), a region that was split into two different segments following the opening of the South Atlantic Ocean during the Cretaceous (Pedrosa-Soares and Wiedemann-Leonardos, 2000; Pedrosa-Soares et al., 2001; Alkmim et al., 2016). The Brazilian portion of the belt, i.e., the Araçuaí Orogen, inherited ophiolite slivers, suture zones, the entire magmatic arc, and the record of syn- to post-collisional magmatism (Pedrosa-Soares et al., 2008). The development of the Araçuaí Orogen lasted from ca. 590 to 530 Ma, with these ages representing the syn-metamorphic climax to the oldest

post-collisional/intraplate granitic plutons (Pedrosa-Soares et al., 2001; lkmim et al., 2016). Extensional structures vary in age from 530 to 480 Ma and mark the orogenic collapse, which is coeval to asthenosphere ascent (Pedrosa-Soares et al., 2011).

Following the Brasiliano/Pan-African cycle that resulted in the consolidation of the West Gondwana continent, there was a gradual decrease of the compression processes associated with the landmass assemblage, leading to generally stable intra-cratonic conditions (Carneiro et al., 2012). Although records of the early Paleozoic thermal history of both the São Francisco Craton and Araçuaí Orogen are scarce, 40Ar/39Ar ages of amphibole, muscovite, and biotite obtained in quartz-syenites from the Araçuaí Orogen document the last stages of the orogenic cycle. These ages range from 501 to 468 Ma and support regional low cooling rates (<5 ºC.My^{-1}; Petitgirard et al., 2009; Cavalcante et al., 2018; Vauchez et al., 2019), indicating the crossing of the 338–326 ºC isotherm at ca. 459 Ma. From the Ordovician to the Permian, several basins developed in the West Gondwana, including the Parnaíba, Sanfranciscana, Paraná, and Araripe basins, among others. Their sedimentary record suggests exhumation of the Brasiliano orogens, sea-level changes, and glaciation episodes, (Linol et al., 2015).

The emplacement of the Transminas mafic dike swarm during the Mesozoic, both in the São Francisco Craton and the Araçuaí Orogen, is considered a precursor of the South Atlantic Ocean opening (Fig. 5.1b). The dikes have whole-rock K–Ar ages varying from 220 to 170 Ma (Dussin, 1994; de Chaves, 2013; de Chaves and Neves, 2005). Seafloor spreading started in the southernmost South Atlantic during the Late Jurassic/Early Cretaceous (Buiter and Torsvik, 2014; Lovecchio et al., 2018). The rifting propagated northward, mainly following inherited Brasiliano/Pan-African structures (Heilbron et al., 2000; De Wit et al., 2008; Mohriak et al., 2008; Misra and Mukherjee, 2015; Salomon et al., 2017). Coeval to rifting, the emplacement of the Vitória-Colatina dike swarm resulted from the clockwise rotation of the southern South American relative to northern South America, as observed in other segments of the Brazilian passive continental margin (e.g., Milani and Ramos, 1998; Salomon et al., 2017; Hueck et al., 2018). To the east of study area, rifting affected the São Francisco Craton and Araçuaí Orogen basement at ca. 120 to 112 Ma (Torsvik et al., 2009), breaking the Bahia-Gabon cratonic bridge that originally connected both the Sao Francisco Craton to the Congo Craton. From the time of the rifting to the present-day, several basins developed along the Brazilian passive margin, with extensive sedimentary packages that record its evolution.

From Late Cretaceous to Paleocene, intense offshore volcanic activity records the emplacement of alkaline magmatism at ca. 50 Ma (Chang et al., 1992). These rocks are grouped in the Abrolhos Bank and have been associated with the Vitória-Trindade seamount chain (Cordani, 1970; Thompson et al., 1998). From Miocene to Pleistocene, several alluvial fan systems were deposited along the continental margin (Arai, 2006). These units comprise the youngest rocks near the study area and are grouped in the Barreiras Group.

5.2.2 Tectonism and physiography

The São Francisco Craton and Araçuaí Orogen domains show low-relief topography with average elevations of 300–400 m and with peak altitudes no higher than ca. 1200 m located farther inland (Fig. 5.3a). The drainage pattern in both domains is rectangular to dendritic, generally following the orientation of lineaments (Sampaio et al., 2002; Mesquita et al., 2021). The main rivers in the region are generally parallel to each other, flowing towards the east (Alcobaça, Jequitinhonha, and Pardo Rivers; Fig. 5.3a).

The structural fabric of the São Francisco Craton (Fig. 5.3b) is essentially inherited from a Paleoproterozoic orogeny, with the predominance of NNE-SSW, NW-SE, andENE-WSW-trending brittle structures (Fig. 5.3c). In contrast, the northern Araçuaí Orogen exhibits NE-SW and NW-SE-trending structures (Fig. 5.3c) inherited from the Brasiliano event (Sampaio et al., 2002; Oliveira et al., 2018; Mesquita et al., 2021) and mainly associated with dextral transpressive shear zones. Folds and thrusts verging towards the craton and the orogen core are also present, broadly defining a hemiflower structure. To the southwest of the study area, NE-SW-trending structures dominate, associated with both dextral and sinistral transcurrent shear zones marked by minor folding and the absence of thrusts (Sampaio et al., 2002).

The Cenozoic volcanic rocks deposited on top of the Sao Francisco Craton and Araçuaí Orogen comprise two large volcanic banks, namely the Abrolhos and Royal Charlotte Banks (Fig. 5.3a). In this setting, the continental shelf is composed of sedimentary and volcanic units that extend far into the sea and is surrounded to the north, east, and south by deep basins that reach down to 4000 m below sea level. The sedimentary Cenozoic cover is especially present as terraces along the coast, where deposition is possibly controlled by the reactivation of NW-SE-trending transcurrent and normal faults (Fig. 5.3b; Oliveira et al., 2018). Sea-level eustatic variations also seem to

control the deposition and erosion of the sedimentary rocks, resulting in prograding and retrograding shorelines (Mesquita et al., 2021). The structural trend in this domain is inherited from the crystalline basement broadly following WNW-ESE trends (Fig. 5.3c). As a result, the drainage in the Cenozoic domain is predominantly parallel, sub-parallel, and rectangular, with minor dendritic control (Fig. 5.3a; Mesquita et al., 2021). In addition to that, Cenozoic tectonics led to tilting of crustal blocks and the formation of graben-like structures, generating highly asymmetric basins (Sampaio et al., 2002).

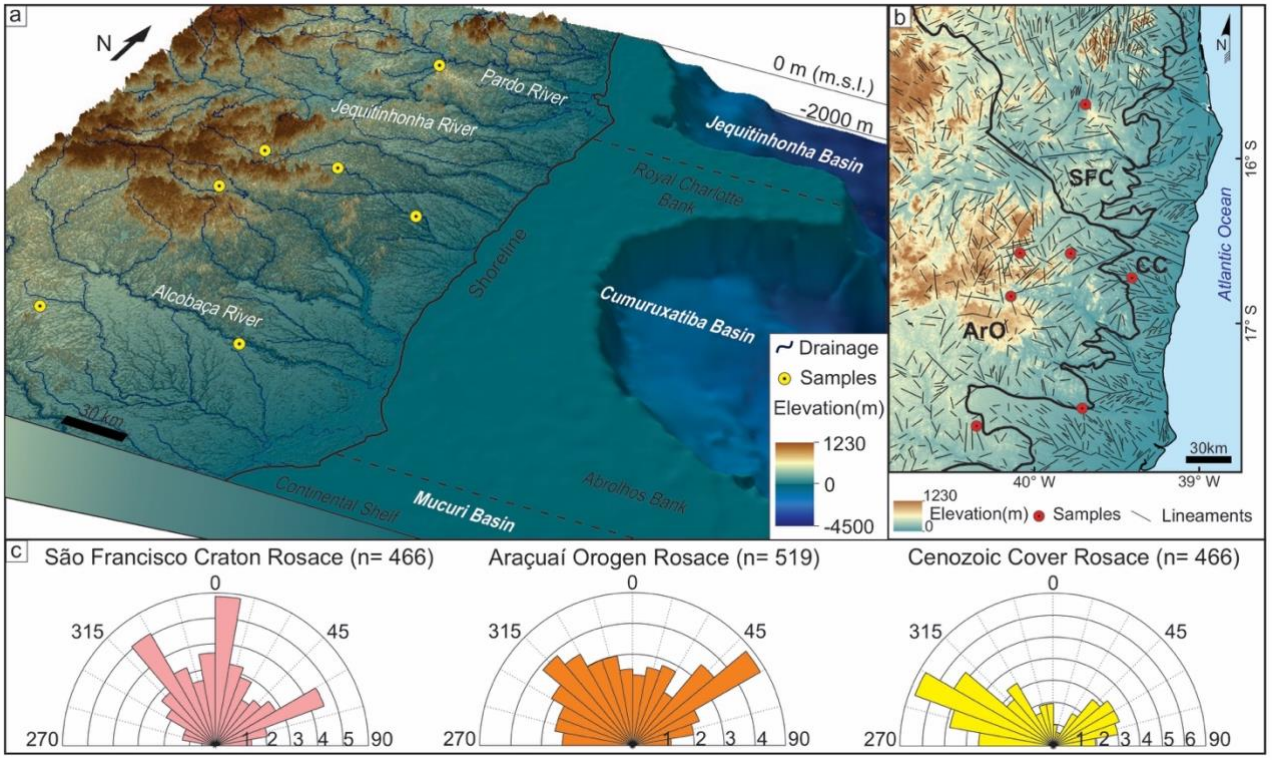

Figure 5. 3: a) Geomorphological 3d map of the study area displaying both land and undersea topography. The red dots indicate sampling sites and blue lines are the drainage network. b) Lineament map plotted over a hillshade of the study area, showing topography in 2d. Abbreviations are: SFC: São Francisco Craton; ArO: Araçuaí Orogen; CC: sedimentary Cenozoic cover; thin grey lines: lineaments. c) Rosace diagrams for the cratonic, orogenic, and Cenozoic cover domains evidencing the orientation of the manually traced lineaments and their frequency. (For interpretation of the references to colour in this figure legend, the reader is referred to the web version of this article.)

5.2.3 Existing thermochronology data

In the study region, several studies applied apatite fission-track thermochronology (Fig. 5.4) (Amaral et al., 1997; Japsen et al., 2012; Jelinek et al., 2014; Amaral-Santos et al., 2019; Van Ranst et al., 2020; Fonseca et al., 2021), and one study performed both apatite fission-track and apatite (U–Th)/He analysis (Van Ranst et al., 2020). These studies interpret the thermal history in terms of denudation phases constrained to the Permian-Early Triassic (Jelinek et al., 2014; Amaral-Santos et al., 2019; Fonseca et al.,

2021), Triassic-Jurassic (Amaral et al., 1997; Japsen et al., 2012), Early Cretaceous (Fonseca et al., 2021; Japsen et al., 2012; Jelinek et al., 2014), Late Cretaceous/Paleocene (Fonseca et al., 2021; Japsen et al., 2012; Jelinek et al., 2014; Van Ranst et al., 2020), and Neogene (Japsen et al., 2012; Jelinek et al., 2014; Amaral-Santos et al., 2019). Several hypotheses have been put forward to explain the cooling episodes and observed ages. Some of these hypotheses include the effect of local patterns, such as the role of drainage networks in inducing differential denudation (Van Ranst et al., 2020). Others suggest more broad and regional tectonic effects, such as differential denudation caused by contrasting rheology (cratonic vs non-cratonic lithosphere; Fonseca et al., 2021) and intraplate stresses from the Gondwanic orogenic cycle promoting cooling (Jelinek et al., 2014; Amaral-Santos et al., 2019).

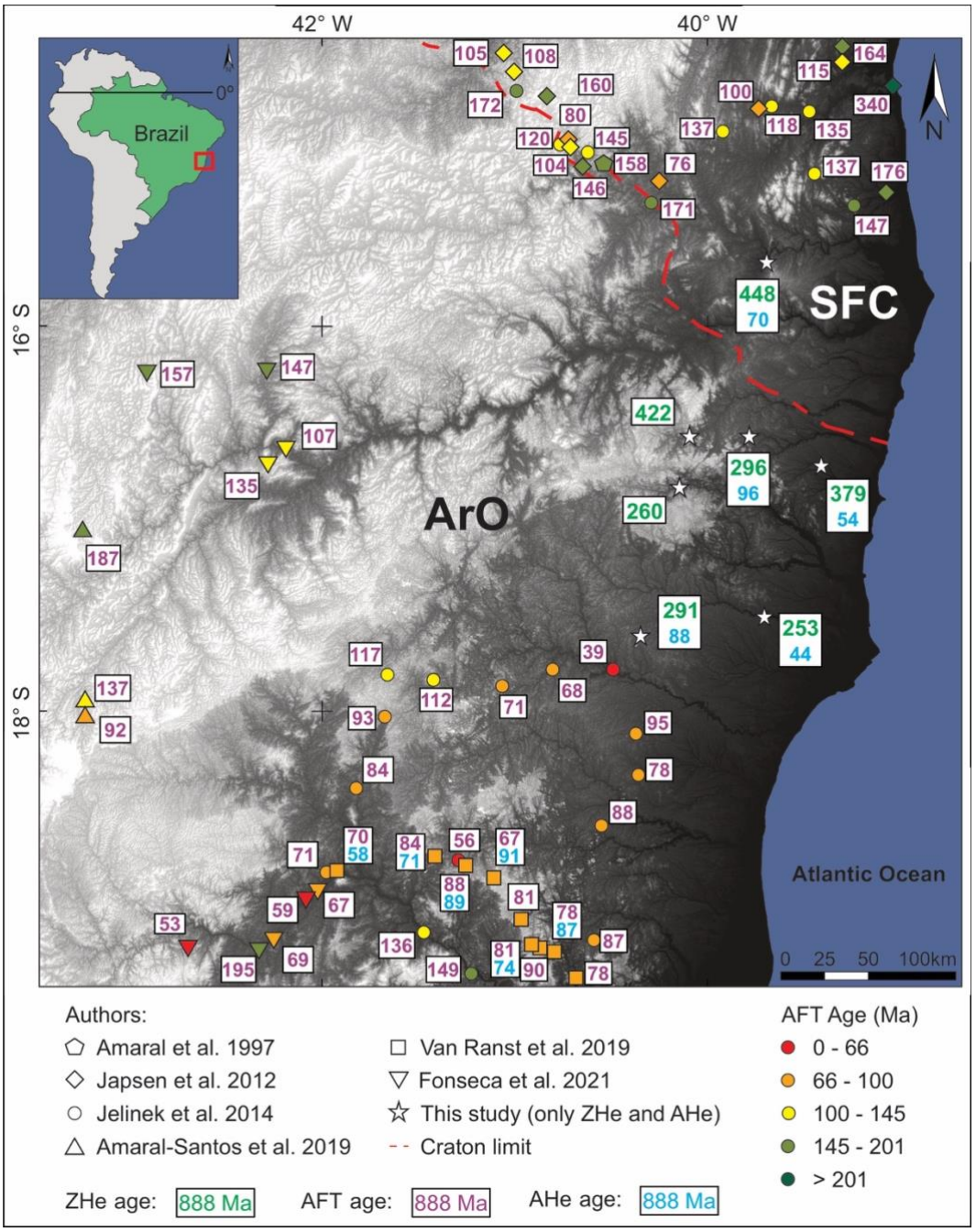

Figure 5. 4: Hillshade map displaying AFT central ages and AHe average ages available in the literature and ZHe and AHe average ages reported in this study. Data displayed in the figure indicate results from Amaral et al. (1997), Japsen et al. (2012), Jelinek et al. (2014), Amaral-Santos et al. (2019), Van Ranst et al. (2020), and Fonseca et al. (2021). Abbreviations are: SFC: São Francisco Craton; ArO: Araçuaí Orogen.

5.3 Sampling and analytical methods

5.3.1 Sampling strategy

For this study, we collected basement samples from seven outcrops across eastern Brazil covering two distinct terranes of Archean and Neoproterozoic ages, the São

Francisco Craton and the Araçuaí Orogen, respectively (Table 5.1). We preferably sampled lithologies rich in apatite and zircon, such as granite and gneiss, and we avoided locations sampled by previous studies. The study area presents low relief, which does not allow sampling along vertical profiles. Standard crushing, magnetic, and heavy liquids methods were used to obtain zircon and apatite crystals for (U–Th)/He analyzes. From seven samples, five samples provided aliquots for both mineral phases, while two samples only contained zircons crystals suited for (U–Th)/He analysis.

Table 5. 1: Details from samples analyzed in this study. N: Northing; E: Easting, coordinates in UTM zone 24 K, datum WGS84; m.a.s.l.: meters above sea level; Dist. Coast: The shortest distance to the Atlantic Ocean; Dist. Craton: the shortest distance to the São Francisco Craton. ZHe: Zircon (U–Th)/He dating; AHe: Apatite (U–Th)/He dating.

Sample	N (m)	E (m)	Lithology	Elevation (m.a.s.l.)	Dist. Coast (km)	Dist. Craton (km)	Domain	Method
BHS-02	8051869	357121	Gneiss	252	99	154	ArO	ZHe - AHe
BHS-06	8063640	425162	Granite	86	54	108	ArO	ZHe - AHe
BHS-10	8138101	378366	Metapelite	207	105	66	ArO	ZHe
BHS-12	8167574	383799	Granite	292	103	40	ArO	ZHe
BHS-13	8167297	416609	Granite	187	71	27	ArO	ZHe - AHe
BHS-15	8150790	456294	Gneiss	80	28	17	ArO	ZHe - AHe
BHS-17	8267569	425934	Tonalite	119	80	-	SFC	ZHe - AHe

5.3.2 Structural inheritance

To obtain the brittle structures for the structural inheritance analysis, a SRTM image with a spatial resolution of 1 arc-second (~30 m/pixel), horizontal Datum WGS84, was inspected using the software ArcGIS 10.3. The image was downloaded from the Earth Explorer internet page (www.earthexplorer.usgs.gov). Then, the lineaments were manually traced for each one of the geological domains, i.e., the São Francisco Craton (n = 466 lineaments), the Araçuaí Orogen (n = 519 lineaments), and the Cenozoic Cover (n = 466 lineaments), and had their lengths calculated based on their starting and ending points in the attribute table of the respective software. Next, a spreadsheet containing this information was imported into software Rockworks20, in which the rose diagrams were generated (Fig. 5.3c).

5.3.3 Apatite and Zircon (U-Th)/He analysis

The combined application of two low-temperature thermochronometers, ZHe and AHe, was the chosen technique to conduct this study. These methods are based on the

accumulation of ^{4}He within the crystals, which is produced by the radioactive decay chain of ^{238}U, ^{235}U, ^{232}Th, ^{147}Sm, and their intermediate daughter products, leading to stable ^{206}Pb, ^{207}Pb, ^{208}Pb, and ^{143}Nd (Reiners et al., 2017). At high temperatures, ^{4}He is lost by the apatite crystal through thermally activated volume diffusion (Zeitler et al., 1987; Wolf et al., 1998; Stockli et al., 2000; Farley, 2002) and the resulting apparent age is zero. Accumulation of radiation damage in apatite crystals strongly influences its helium diffusion kinetics as well (Flowers et al., 2009). Zircon ages are controlled by the accumulation of radiation damage within the crystal (Guenthner et al., 2013): for a single zircon crystal, progressive damage accumulation is dependent on the eU concentration (eU = [U] + 0.234* [Th] + 0.00463*[Sm]; Flowers et al., 2009; Reiners et al., 2017). He diffusivity can decrease by approximately three orders of magnitude as a result of increased disruption of c-axis parallel channels by radiation damage, and then increase by ten orders of magnitude (Guenthner et al., 2013, 2014).

The simultaneous production and loss of ^{4}He occur in lower temperatures and defines a zone denominated Partial Retention Zone (PRZ; Wolf et al., 1998). The apatite (U–Th)/He PRZ (AHePRZ) interval lies between ~40 and 70 ºC (Wolf et al., 1996, 1998; Stockli et al., 2000; Farley, 2002), defined by studies that did not take into account the effects of radiation damage. AHe ages can be affected by crystal size (Reiners and Farley, 2001; Brown et al., 2013), radiation damage accumulation (Shuster et al., 2006; Flowers et al., 2009), parent nuclide zonation (Farley, 2000; Reiners et al., 2017), U- and Th-rich micro-inclusions (Fitzgerald et al., 2006), neighboring grains with high U–Th content (Spiegel et al., 2009), and the cooling rates (Ault and Flowers, 2012; Reiners et al., 2017). Cooling rates have the potential to enhance the eU zonation effects when samples experience either slow monotonic cooling, have extended residence in the AHePRZ, or display protracted heating and cooling (Ault and Flowers, 2012). Differently, the zircon (U–Th)/He PRZ (ZHePRZ) retains ^{4}He at a higher temperature range than apatite. The lower and upper temperature bounds of the ZHePRZ are set at ~155 to 195 ºC (Reiners, 2005; Reiners et al., 2002, 2004, 2017). ZHePRZ is also affected by radiation damage (Guenthner et al., 2013) and the factors previously mentioned for apatite (Reiners et al., 2002, 2017; Reiners, 2005). Therefore, a combination of ZHe and AHe provides a robust and valuable tool to assess thermal events of the upper crust, since the temperature windows of these methods are complementary.

Four to six single-crystal aliquots were analyzed at the (U–Th)/He and U–Pb Geo-

Thermochronometry Laboratory of the University of Texas at Austin, for both zircon and apatite. The crystals were chosen based on morphology, size, and lack of visible inclusions and coating, using a customized Nikon SMZ-U/100 stereomicroscope. Crystals were also photographed with a digital Nikon camera and had their dimensions measured for alpha-ejection age correction (Ft; Farley et al., 1996).

Picked zircons were 203–544 μm long and 78–156 μm wide, whereas chosen apatites were 222–610 μm long and 128–335 μm wide. In most cases, the selected crystals had two terminations. The selected crystals were loaded in Pt tubes for degassing through heating with an Nd-YAG laser. The released gases were measured and quantified in a quadrupole mass spectrometer. Crystals were then recovered and dissolved for U, Th, and Sm determination in an Element2 HR-ICP-MS.

5.3.4 Thermal history modeling

Inverse thermal modeling was performed using QTQt 5.7.2 K (Gallagher, 2012). The software employs Bayesian transdimensional Markov Chain Monte Carlo, reducing problems related to over interpretation of the thermal histories. Radiation damage accumulation and annealing models of both ZHe (ZRDAAM; Guenthner et al., 2013) and AHe (RDAAM; Flowers et al., 2009) were considered when modeling all the thermal histories. The present-day temperature was constrained at 20 ± 10 ºC, since all samples are from outcrops. The prior for temperature was set at 100 ± 100 ºC, which encloses the maximum temperature interval relative to data information. The oldest uncorrected ZHe age of each sample was used as a prior for the time as to ± to. Additionally, we set the maximum $\partial T/\partial t$ as 30 ºC/m.y., which is broadly compatible with orogenic terranes and cratonic borders.

The MCMC algorithm initially ran 10,000 burn-in and 30,000 post-burn-in iterations in order to choose appropriate values for the MCMC parameters before longer runs. Acceptance rates were between 0.2 and 0.6 (QTQt User Guide). Then, we performed 10,000 burn-in and 200,000 post-burn-in iterations for each sample, combining both the

ZHe and AHe data for better constrain time-temperature paths. ZHe and AHe single-grain ages were modeled as if they were considered whole grains (Brown et al., 2013; Beucher et al., 2013). Neither age nor error were resampled for modeling. Expected models were analyzed in this study since they represent the weighted mean t-T-paths.

A combined inversion of samples BHS-02, BHS-06, BHS-13, and BHS-15 in a

single expected model was conceived as well. The main goal of this model was to assess differences on individual and combined thermal models. We select these samples because they belong to the same tectonic domain. Sample BHS-17 was not included in the modeling since it was collected in a different tectonic domain. Therefore, it may display a contrasting thermal history when compared to the samples of the Araçuaí Orogen.

5.4 Results

5.4.1 Lineament directions

Rose diagrams were generated for the São Francisco Craton, the Araçuaí Orogen, and the Cenozoic cover (Fig. 5.3c). The Sao Francisco Craton rose diagram suggests three major lineament orientations, i.e., NNE-SSW, NW-SE, and ENE-WSW. The Araçuaí Orogen diagram shows one major lineament orientation (NE-SW) followed by many lineaments near the NW-SE orientation. Finally, the Cenozoic Cover displays a predominance of WNW-ESE lineaments.

5.4.2 Results from ZHe and AHe data

ZHe and AHe dating results are presented in Table 5.2 and Table 5.3, respectively. A total of 41 zircon crystals were dated from seven different locations. Outliers were detected within the samples, and they were not considered for further analyzes and inversion (data in underscore italic on Tables 5.2 and 5.3). Upper outliers were determined by adding 1.5 times the interquartile range to the upper quartile, while lower outliers by subtracting 1.5 times the interquartile range to the lower quartile. Only a single outlier was detected in the whole zircon dataset, and it was discarded from the following analyzes and thermal modeling (Table 5.2).

The apparent uncorrected zircon ages are Paleozoic (72.5%) and Mesozoic (27.5%), ranging from 394.7 ± 31.6 to 81.9 ± 6.6 Ma, and ZHe corrected ages span from 483.1 ± 38.6 to 93.8 ± 7.5 Ma. The average corrected ZHe age obtained in the São Francisco Craton is the oldest age of this data set, 448.1 ± 21.9 Ma. On the other hand, the samples obtained for the Araçuaí Orogen show substantially younger ZHe corrected ages, spanning from 421.6 ± 31.1 to 253.0 ± 34.9 Ma. The standard deviation of ZHe ages ranges from 5.6 to 123.7 Ma (BHS-02 and BHS-10, respectively). Most uncertainties

(2σ) are within 1.9 and 20.5%, except for sample BHS-10 (63.2%). Zircon single grain eU concentrations span from 10.91 to 632.51 mg/g and ESR (Equivalent Spherical Radius) ranges from 50.61 to 103.02 μm. A positive correlation between eU and ZHe ages (Fig. 5.5a) is observed in the dataset, in contrast to other studies in both cratonic and near-cratonic environments (e.g. Powell et al., 2016; Machado et al., 2019, 2020). Conversely, the correlation between ESR and ZHe ages in our dataset is strongly negative (Fig. 5.5b). Intrasample and intersample ZHe age variation is discussed in section 5.1.1.

Single crystal AHe analysis yielded 26 apparent ages from five different locations. After removing the outlier ages (Table 5.3, underscore italic data), 23 apparent AHe ages were considered for the thermal modeling. The AHe uncorrected single-crystal ages are Mesozoic (61%) to Cenozoic (39%), spanning from 103.1 ± 6.2 to 25.6 ± 1.5 Ma. Considerable change occurs after applying the Ft correction (Farley et al., 1996), in which Mesozoic and Cenozoic ages correspond to 57% and 43% of the data, respectively, spanning from 129.9 ± 7.8 to 32.7 ± 2.0 Ma. Average corrected AHe ages in the Araçuaí domain range from 95.7 ± 19.1 to 43.9 ± 11.4 Ma, whereas the sample collected in the São Francisco Craton has an AHe age of 70.1 ± 9.2 Ma. The standard deviation of AHe ages ranges from 2.3 to 23.4 Ma (BHS-15 and BHS-13, respectively). Uncertainties (2σ) are within 4.8 and 26%. eU concentration range from 5.6 to 62.8 mg/g and ESR varies from 70.94 to 166.39 μm, typical values for apatite crystals. A positive correlation between eU and AHe ages (Fig. 5.6a) is observed in the dataset. On the other hand, this dataset suggests a sparse correlation between ESR and AHe ages (Fig. 5.6b). Intrasample and intersample AHe age dispersion are detailed in section 5.1.2.

*Table 5. 2: Summary of Zircon (U–Th)/He ages and parameters; Abbreviations are: eU: effective uranium, calculated as eUμg/g = [Uμg/g + (0.235*Thμg/g) + (0.00463*Smμg/g)]; ESR: Equivalent Spherical Radius; Ft: Correction Factor after (Farley et al., 1996); Corr.: Corrected; Aver.: Average; SD: Standard Deviation. Italic and underscore data refer to samples information that were not considered from discussion.*

Sample	Grain #	He (nmol/g)	U (∝g/g)	Th (∝g/g)	Sm (∝g/g)	eU (∝g/g)	ESR (∝m)	Raw Age (Ma)	± 2s (Ma)	Ft #	Corr. Age (Ma)	± 2s (Ma)	Aver. Corr. (Ma)	± 2s (Ma)	SD (Ma)
BHS-02	1	215.8	152.3	15.7	2.1	156.02	95.53	250.5	20.0	0.88	286.1	22.9	290.0	5.6	5.6
	3	295.3	206.8	23.1	2.3	212.19	94.45	252.1	20.2	0.87	288.2	23.1			
	4	271.2	193.1	49.1	3.8	204.65	68.57	240.3	19.2	0.83	290.5	23.2			
	5	*453.1*	*178.4*	*47.3*	*3.4*	*189.53*	*68.52*	*425.1*	*34.0*	*0.83*	*514.0*	*41.1*			
	6	431.4	308.3	26.2	1.7	314.44	69.40	248.6	19.9	0.83	298.9	23.9			
BHS-06	1	311.5	226.1	72.2	1.0	243.03	80.35	232.6	18.6	0.85	273.3	21.9	253.0	34.9	42.7
	2	147.5	118.4	31.1	0.7	125.70	96.22	213.3	17.1	0.88	243.8	19.5			
	3	88.0	86.6	30.4	1.3	93.69	76.16	171.5	13.7	0.84	203.6	16.3			
	4	103.6	103.8	29.9	1.5	110.81	72.72	170.8	13.7	0.87	204.2	16.3			
	5	239.6	151.2	60.3	1.3	165.33	94.19	262.3	21.0	0.87	301.2	24.1			
	6	280.5	184.1	55.8	1.0	197.17	103.02	257.5	20.6	0.88	291.7	23.3			
BHS-10	1	6.1	10.4	0.3	107.6	10.91	102.13	99.6	8.0	0.88	122.6	9.0	259.8	101.0	123.7
	2	203.6	108.5	37.7	1.5	117.35	72.10	312.4	25.0	0.83	374.5	30.0			
	3	262.2	154.2	60.0	4.6	168.26	78.88	281.5	22.5	0.85	332.1	26.6			
	4	217.0	126.2	33.1	1.2	133.90	78.80	292.4	23.4	0.85	344.5	27.6			
	5	507.9	343.7	57.4	22.7	357.19	80.71	257.4	20.6	0.85	301.5	24.1			
	6	8.0	17.0	0.2	126.4	17.59	92.11	81.9	6.6	0.87	93.8	7.5			
BHS-12	1	423.8	190.1	131.8	11.8	220.99	72.05	344.4	27.6	0.83	414.1	33.1	421.6	31.1	38.0
	2	566.7	302.3	169.6	23.3	342.07	53.56	298.8	23.9	0.78	383.7	30.7			
	3	407.6	193.7	112.6	28.6	220.19	50.61	332.6	26.6	0.77	433.8	34.7			
	4	239.1	128.6	68.5	6.7	144.69	57.52	298.1	23.8	0.79	375.7	30.1			
	5	1038.0	453.9	220.7	17.5	505.66	66.71	367.6	29.4	0.82	447.8	35.8			
	6	513.5	199.6	160.3	16.7	237.19	65.87	387.2	31.0	0.82	474.5	38.0			
BHS-13	1	333.2	186.3	51.7	1.8	198.40	68.81	302.7	24.2	0.83	365.6	29.3	296.4	60.7	74.3
	2	196.3	121.8	31.3	12.9	129.18	86.16	274.5	22.0	0.86	318.9	25.5			
	3	268.3	156.0	37.3	9.8	164.78	88.52	293.6	23.5	0.87	339.4	27.1			
	4	6.9	5.7	11.6	113.4	8.99	84.44	133.8	10.7	0.85	*157.2*	*12.6*			
	5	194.9	116.5	68.2	3.7	132.45	69.68	266.3	21.3	0.83	322.0	25.8			
	6	242.2	178.2	55.2	1.8	191.18	72.25	230.1	18.4	0.83	275.5	22.0			
BHS-15	1	1260.9	590.1	180.8	18.8	632.51	78.95	357.2	28.6	0.85	421.1	33.7	378.6	21.0	25.8
	2	673.9	363.8	168.3	14.6	403.24	67.85	301.3	24.1	0.82	365.7	29.3			
	3	869.3	460.6	141.8	13.5	493.83	69.42	316.7	25.3	0.83	382.2	30.6			
	4	490.5	274.8	139.1	5.7	307.40	71.99	288.1	23.0	0.83	345.9	27.7			
	5	594.0	307.4	139.4	2.3	340.06	61.42	314.5	25.2	0.81	390.0	31.2			
	6	770.1	435.5	140.0	12.0	468.27	61.52	296.6	23.7	0.81	367.1	29.4			
BHS-17	1	454.1	194.9	125.1	6.0	224.17	71.44	363.0	29.0	0.83	436.9	34.9	448.1	21.9	26.8
	2	583.0	268.3	131.9	15.9	299.27	52.95	349.5	28.0	0.78	449.7	36.0			
	3	824.1	411.4	235.2	24.7	466.58	53.41	317.9	25.4	0.78	408.5	32.7			
	4	522.3	203.8	142.7	15.3	237.25	72.84	393.3	31.5	0.83	471.9	37.7			
	5	582.7	248.1	150.1	29.3	283.36	76.01	368.2	29.5	0.84	438.1	35.0			
	6	651.1	255.6	166.7	13.4	294.65	65.84	394.7	31.6	0.82	483.1	38.6			

*Table 5. 3: Summary of Apatite (U–Th)/He ages and parameters; Abbreviations are eU: effective uranium, calculated as eUμg/g = [Uμg/g + (0.235*Thμg/g) +0.00463*Smμg/g); ESR: Equivalent Spherical Radius; Ft: Correction Factor after (Farley et al., 1996); Corr.: Corrected; Aver.: Average; SD: Standard Deviation. Italic and underscore data refer to samples information that were not considered from discussion.*

Sample	Grain #	He (nmol/g)	U (∝g/g)	Th (∝g/g)	Sm (∝g/g)	eU (∝g/g)	ESR ∝m	Raw Age (Ma)	± 2s (Ma)	Ft #	Corr. Age (Ma)	± 2s (Ma)	Aver. Corr. (Ma)	± 2s (Ma)	SD (Ma)
BHS-02	1	21.2	43.0	13.2	385.6	47.9	165.31	79.4	4.8	0.91	87.6	5.3	88.5	12.3	12.3
	2	*12.2*	*7.2*	*1.5*	*385.6*	*9.3*	*136.09*	*208.6*	*12.5*	*0.89*	*235.1*	*14.1*			
	3	32.2	58.6	9.2	444.9	62.8	119.53	92.1	5.5	0.87	105.4	6.3			
	4	3.7	7.3	0.2	323.8	8.9	152.41	68.5	4.1	0.90	76.0	4.6			
	5	13.0	25.7	1.3	595.6	28.8	166.39	77.3	4.6	0.91	85.0	5.1			
	6	*0.9*	*2.4*	*0.2*	*420.5*	*4.4*	*124.58*	*29.0*	*1.7*	*0.88*	*33.0*	*2.0*			
BHS-06	1	4.7	13.1	15.8	415.6	18.8	73.72	42.6	2.6	0.79	54.1	3.2	43.9	11.4	11.4
	2	1.8	4.4	1.2	313.7	6.1	114.41	46.2	2.8	0.87	53.4	3.2			
	3	1.1	3.9	3.7	337.3	6.3	74.11	28.1	1.7	0.79	35.5	2.1			
	4	0.9	3.4	3.2	310.1	5.6	70.94	25.6	1.5	0.78	32.7	2.0			
BHS-13	1	7.0	10.7	13.8	301.3	15.3	132.60	78.9	4.7	0.88	89.9	5.4	95.7	19.1	23.4
	2	15.7	20.1	26.9	464.8	28.5	88.53	96.0	5.8	0.82	117.0	7.0			
	3	13.5	15.4	22.1	421.3	22.5	76.82	103.1	6.2	0.79	129.9	7.8			
	4	5.8	12.7	16.5	317.8	18.1	104.23	55.8	3.4	0.85	66.0	4.0			
	5	9.9	16.8	27.2	460.7	25.3	81.07	67.6	4.1	0.80	84.1	5.1			
	6	9.5	15.2	26.4	410.8	23.2	82.98	70.6	4.2	0.81	87.4	5.2			
BHS-15	1	16.0	56.3	11.9	701.0	62.4	129.99	45.7	2.7	0.88	51.8	3.1	54.0	2.6	2.3
	2	9.7	32.7	5.2	431.5	35.9	142.29	48.1	2.9	0.89	53.8	3.2			
	3	*19.0*	*45.5*	*11.5*	*530.2*	*50.6*	*141.60*	*66.8*	*4.0*	*0.89*	*75.0*	*4.5*			
	4	12.9	41.5	5.7	445.9	44.9	164.32	51.1	3.1	0.91	56.4	3.4			
BHS-17	1	5.7	7.4	32.3	324.0	16.4	93.47	59.6	3.6	0.82	72.3	4.3	70.1	9.2	10.3
	2	7.3	9.8	41.7	388.7	21.3	82.19	59,0	3.5	0.80	73.6	4.4			
	3	7.4	10.8	33.2	522.5	21.0	84.99	59.6	3.6	0.81	73.7	4.4			
	4	5.8	9.7	42.0	401.4	21.4	68.73	46.8	2.8	0.77	61.2	3.7			
	5	9.3	11.0	49.6	389.6	24.4	74.09	65.8	3.9	0.78	84.3	5.1			
	6	5.4	9.8	41.4	415.2	21.4	76.08	43.5	2.6	0.79	55.3	3.3			

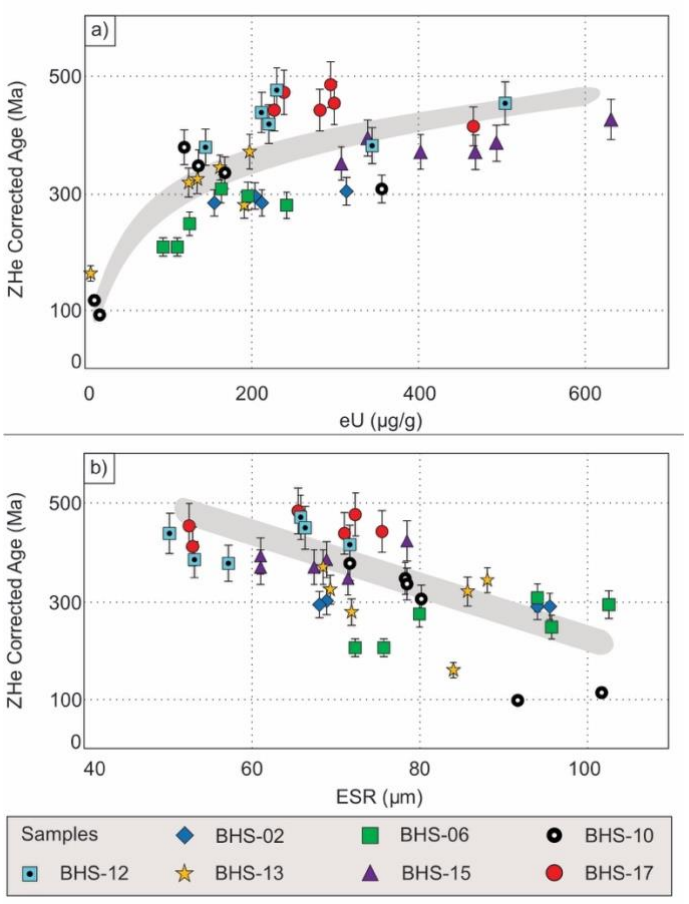

Figure 5. 5: ZHe corrected ages plotted against a) eU concentration and b) Equivalent Spherical Radius (ESR). The grey shading in both charts indicates the correlation between the parameters analyzed. Error bars (2σ) for each sample are displayed in the charts.

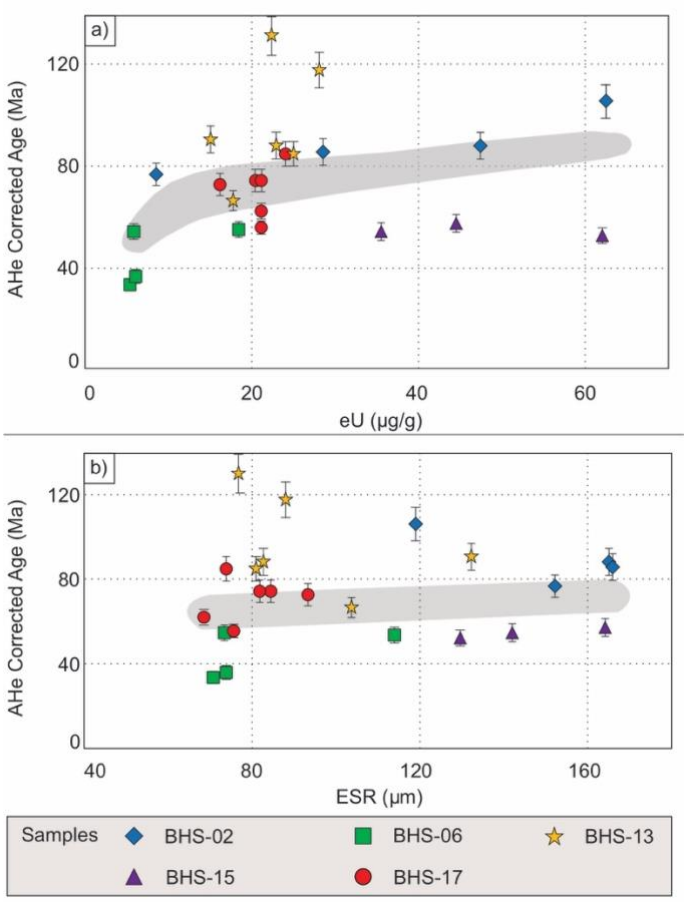

Figure 5. 6: AHe corrected ages plotted against a) eU concentration and b) Equivalent Spherical Radius (ESR). The grey shading in both charts indicates the correlation between the parameters analyzed. Error bars (2σ) for each sample are displayed in the charts.

5.4.3 Thermal inversion

The expected models for the seven samples are reported in Fig. 5.7. Models that incorporated both ZHe and AHe data are the most consistent, with a good agreement between observed and predicted ages. Samples relying only on ZHe information also exhibit a good agreement between the observed and predicted ages. However, the thermal history obtained for sample BHS-12 is poorly resolved. For this reason, this sample will not be considered in the following discussion. From the observed versus predicted age plots, it is noticeable that sample BHS-06 has observed ZHe ages far younger than its predicted ages, although its AHe ages plot on the 1:1 line. Sample BHS-17 also shows a similar behavior, however, to a lesser extent.

According to the plots provided in Fig. 5.7, the thermal history before ca. 250 ± 50 Ma is poorly constrained by the models, as demonstrated by the broad 95% confidence interval spanning for a significant temperature range (from ca. 200 to 20 ºC for ages >250 Ma). Although poorly constrained, we discuss the cooling episode observed during the

Paleozoic in section 5.3. Sample BHS-02 displays a minor cooling from 360 to 280 Ma followed by a slight reheating/stability up until 230 Ma. From 230 Ma to the present day, protracted cooling is registered in this sample.

Considering the weighted mean path and the relative probability displayed in the inverse thermal models, samples BHS-15 and BHS-17 indicate a long residence in temperatures equivalent to 100 to 140 ºC during the entire Paleozoic until the Lower-Middle Mesozoic (Fig. 5.7). From this time on, both samples suggest protracted cooling, evidenced by the high probability of the thermal model. Sample BHS-17 shows a cooling history from 130 ºC, at 230 Ma, to present-day surface temperatures. Sample BHS-15 remained at high temperature longer than sample BHS-17, and for this sample the onset of final cooling to surface conditions started at 120 Ma. Nonetheless, when the 95% confidence interval is considered, it becomes evident that these samples may have resided in a wide range of temperatures: BHS-15 have confidence intervals ranging from ca. 170 to 30 ºC at 450 Ma that narrow to nearly 130 to 90 ºC at 120 Ma, and BHS-17confidence intervals lie between 170 and 20 ºC at 460 Ma and narrow to 160 to 80 ºC at 230 Ma (Fig. 5.7).

Samples BHS-13 and BHS-06 show the most complex thermal history of our dataset (Fig. 5.7). Sample BHS-13 displays thermal stability at 100 ºC from 360 to 310 Ma, followed by reheating up to 130 ºC at 190 Ma. Since then, protracted cooling at two different fast cooling rates is observed. If the weighted mean path is considered, we can observe an accelerated cooling from 190 Ma to 130 Ma followed by a slower cooling phase from 130 Ma to the present day. In contrast to the weighted mean, the relative probability indicates a high probability of linear cooling from nearly 230 Ma to the present day. Sample BHS-06 registers cooling from 120 to 90 ºC that started at 400 Ma and lasted until 300 Ma, followed by reheating ranging from 90 to 140 ºC that spans from 300 to 120 Ma. Accelerated cooling brought the samples to the upper portion of the AHePRZ (40 ºC) from 120 to 70 Ma. If the weighted mean path is considered, a small reheating phase from 70 to 30 Ma with a temperature increment of 10 ºC is observed, succeeded by a final cooling to surface conditions at the present day.

BHS-10 is only constrained by ZHe. Still, the thermal history displays reheating of approximately 80 ºC, from 70 to 150 ºC, from at least 400 Ma to 120 Ma (Fig. 5.7). After this, accelerated cooling started around 100 Ma bringing the sample to surface conditions. The confidence intervals of this sample also suggest that reheating could have started

from near surface temperatures to approximately 130 ºC. At reheating peak, the paleotemperature varies from 150 to 120 ºC.

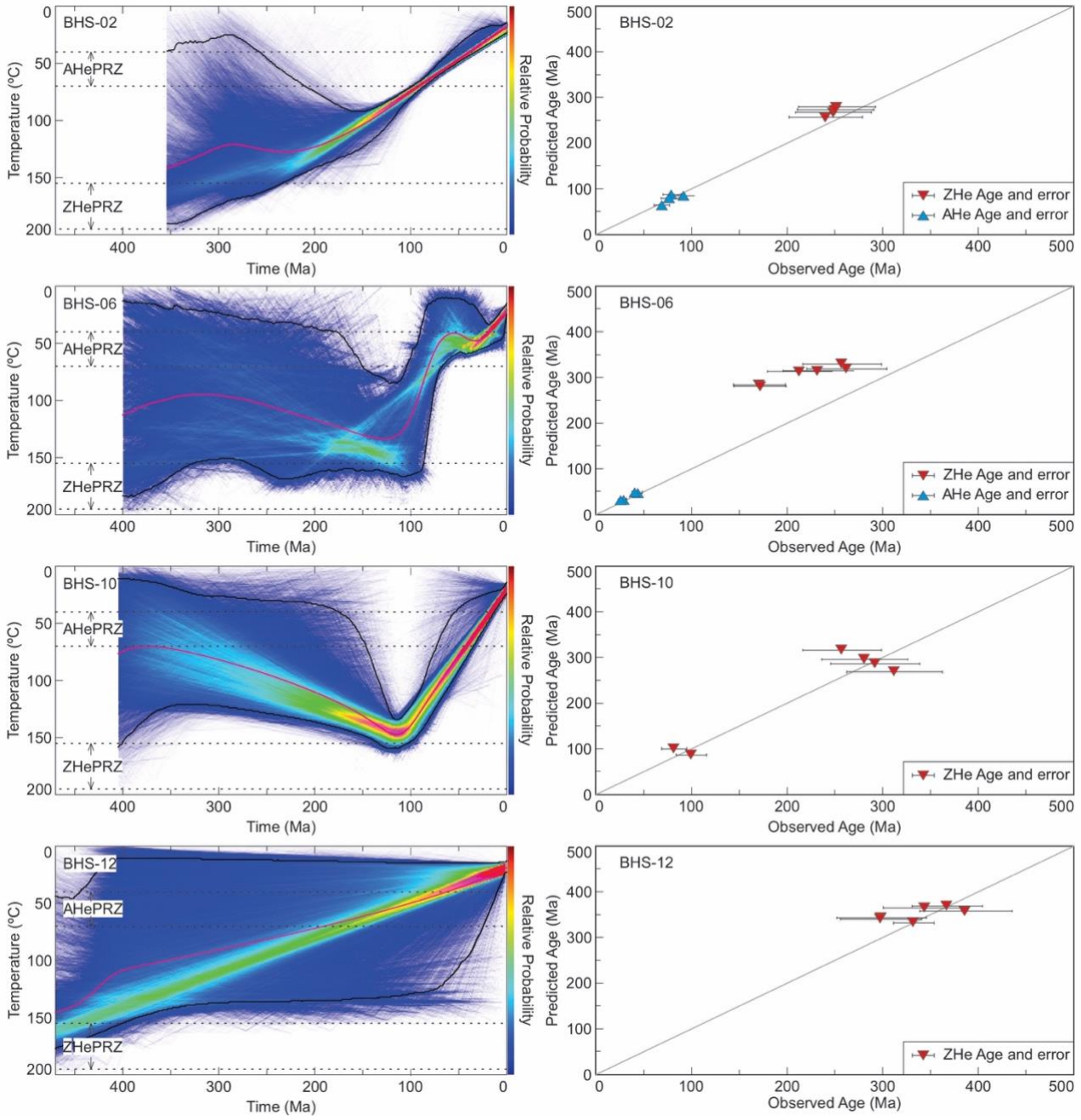

Figure 5. 7: Results of MCMC inverse modeling in QTQt (Gallagher, 2012) for samples BHS-02, BHS-06, BHS-10, BHS-12, BHS-13, BHS-15, and BHS-17. The expected model is defined by the range between both black curves (95% credible interval). The magenta curve represents the weighted mean path of the expected model. The dashed lines making a rectangle at the bottom and at the top of the time-temperature chart are the ZHePRZ and AHePRZ, respectively. The relative probability of time-temperature paths increases from blue to red, according to the scale bar next to the thermal history chart. Observed age versus Predicted age charts are shown on the right of the respective thermal history. ZHe single-crystal ages are plotted as upside down red triangles whereas upside pointing blue triangles are AHe single crystal ages. (For interpretation of the references to colour in this figure legend, the reader is referred to the web version of this article.)

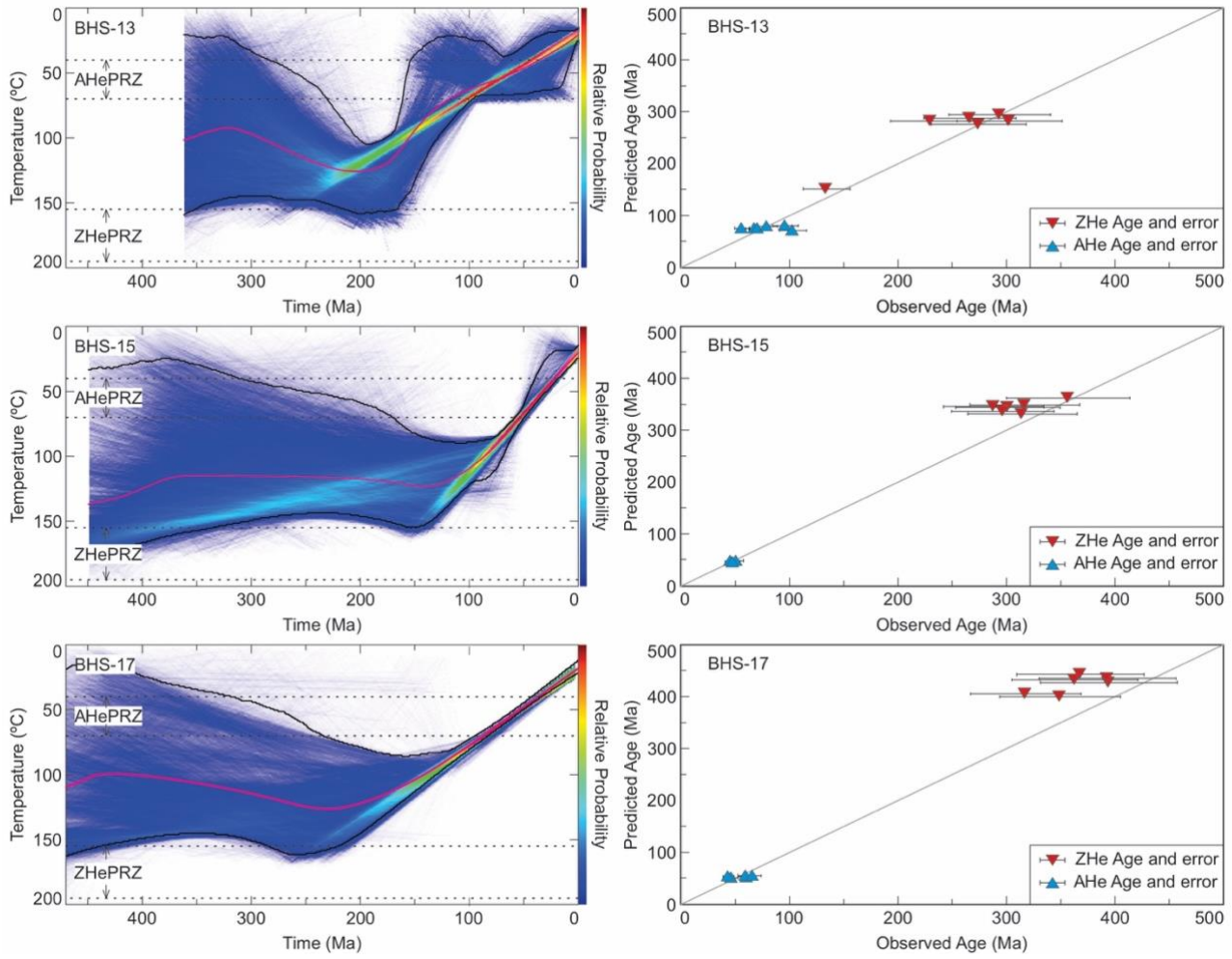

Figure 5. 7: (continued).

The combining AHe and ZHe thermal model for samples BHS-02, BHS-06, BHS-13, and BHS-15 is presented in Fig. 5.8a. This model indicates two reheating episodes separated by a cooling event and followed by a final cooling to current surface temperature in two contrasting rates. The first reheating episode is generally poorly constrained. Still, this phase suggests reheating from ca. 100 ºC, at 450 Ma, to ca. 150 ºC, at 220 Ma. Then, a cooling event brings samples from ca. 150 ºC to ca. 40 ºC between 220 and 160 Ma. From 160 to 90 Ma, another reheating event increases temperature from 40 to no more than 100 ºC, a temperature higher than the AHePRZ limit, which could cause complete loss of α particles on apatite samples. Finally, a cooling episode brought samples to surface conditions at two distinct exhumation rates. The first segment lasts 20 Ma, from 90 to 70 Ma, and shows a temperature decrease from 100 to 70 ºC, and the second starts at 70 Ma and brought the samples to surface conditions. Observed versus Predicted Age plot for the combined model (Fig. 5.8b) indicates an excellent correlation for most of the data set. Despite that, a few samples present a small

deviation from the 1:1 line, e.g., sample BHS-13, with AHe observed ages and associated errors older than predicted, despite its ZHe observed ages being plotted on the 1:1 line. Another example is sample BHS-06, which displays a good agreement between the observed and predicted AHe ages, although predicted ZHe ages are older than observed ones.

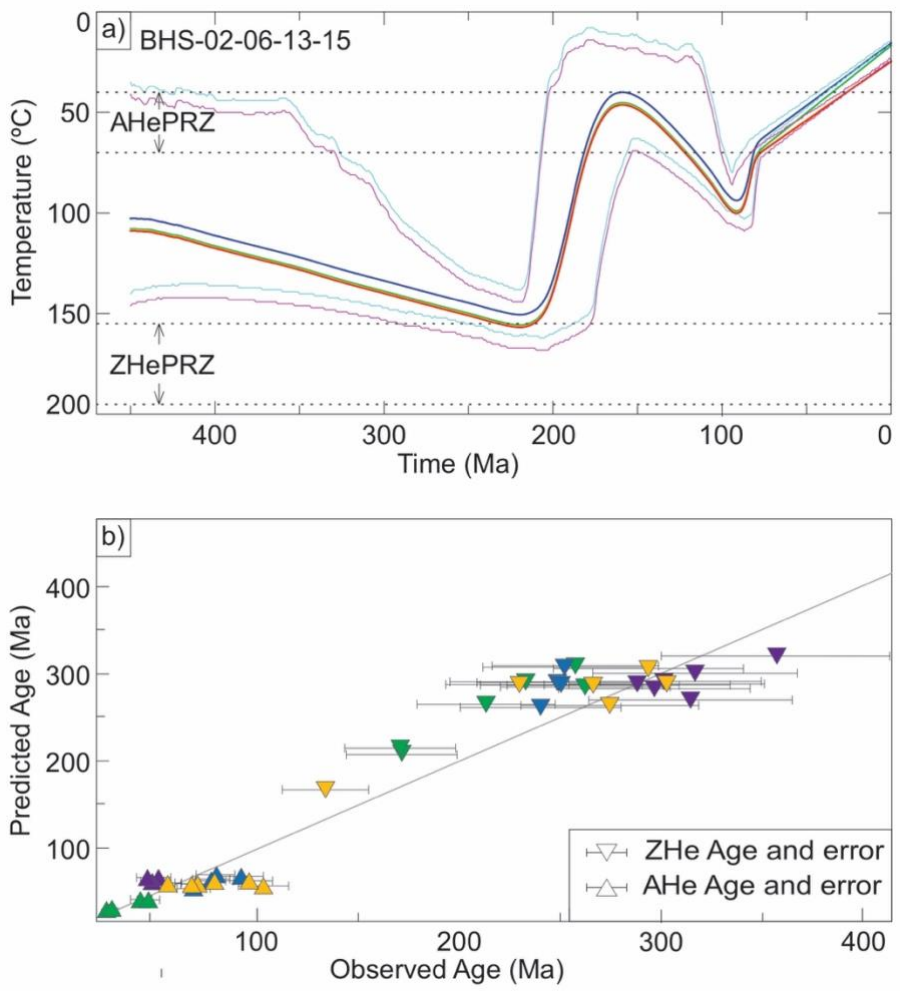

Figure 5. 8: a) Combined ZHe and AHe thermal model from samples BHS-02, BHS-06, BHS-13, and BHS-15. The dark blue curve is the weighted mean path of the BHS-02 sample; The yellow curve is the weighted mean path of the BHS-13 sample; The green and purple curves are the mean paths of the BHS-06 and BHS-15 samples, respectively. Light blue curves are the 95% confidence interval of the BHS-02 sample whereas magenta curves are the 95% credible interval of the BHS-15 sample (lower in the profile). b) Observed versus Predicted Age chart. Upside pointing triangles are AHe single-crystal ages and upsidedown triangles are ZHe single-crystal ages. Blue triangles represent BHS-02 ages, green triangles indicate BHS-06 ages, yellow triangles represent BHS-13 ages, and BHS-15 ages are indicated by purple triangles. (For interpretation of the references to colour in this figure legend, the reader is referred to the web version of this article.)

5.5 Discussion

5.5.1 Intra- and intersample variations

5.5.1.1 Zircon

Only minor intrasample/intersample age dispersion is observed in our data, which indicates that most of the samples experienced a similar thermal history within the ZHe thermal range. Cratonic and near cratonic environments usually exhibit negative correlations between eU and ZHe ages. In contrast, our dataset displays a positive correlation between these parameters (Fig. 5.5a), which can be interpreted as a result of damage at low alpha doses (Guenthner et al., 2013). Additionally, mostly relatively young zircons (10 to 100 Ma) and eU poor (10 to 1,500 μg/g) zircons present this positive correlation, indicating that damage in these minerals never exceeded a critical threshold. The studied zircons did not attain that amount of damage due to their low eU concentration, even though ZHe ages are hundreds of million years old (average corrected ages ranging from 253.0 to 448.0 Ma). Guenthner et al. (2013) also suggest that positive trends are expected for samples experiencing relatively slow, monotonic cooling, which is compatible with our samples to a certain extent.

The negative correlation between ESR and ZHe ages (Fig. 5.5b) may be another source of uncertainties and data dispersion, even though little information about negative trends is available from the literature. For apatite crystals, Brown et al. (2013) indicate that the lack of positive correlation between grain size and AHe age arises from the complex interplay between these factors with the possible influence of noise. If the zircon crystals obey similar rules, the negative trend observed in our results could suggest a complex interaction among ESR, ZHe age, and unknown additional sources of natural dispersion.

Finally, both the distance to the coast and sample elevation lack an evident correlation to ZHe corrected average ages (Fig. 5.9a and b, respectively). Conversely, the distance to the craton apparently plays a role in our zircon dataset (Fig. 5.9c), because old ZHe ages tend to be closer to the craton and have small ESR. This observation indicates that cratons are spared from exhumation when compared to orogenic belts (Nishiizumi et al., 1991; Flowers et al., 2006). Future investigations farther inland and to the south may corroborate our interpretations, where older ages are found closer to the craton.

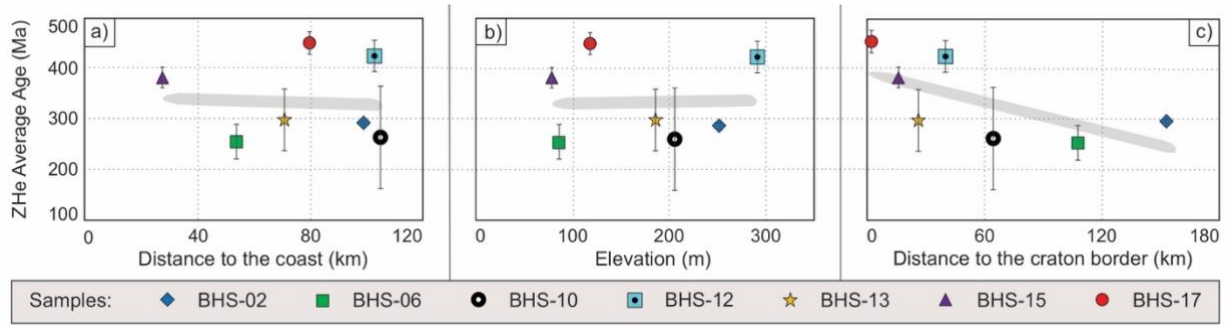

Figure 5. 9: ZHe Average Age plotted against a) Distance to the coast; b) Altitude (meters above sea level); c) Distance to the craton border. The grey shading refers to the trend observed on the charts. Error bars (2σ) for each sample are displayed in the charts.

5.5.1.2 Apatite

Apatite intrasample dispersion is substantial in samples BHS-06 and BHS-13. In the sampling process, we only selected grains free of mineral or fluid inclusions that may contain U and Th (Lippolt et al., 1994), such as zircon and monazite. This process diminishes the possibility of parentless ^{4}He that could be added into the apatite crystals. Another source of parentless ^{4}He includes the presence of U- and Th-rich mineral phases surrounding the apatite crystals, which could act as sources of ^{4}He (Spencer et al., 2004). In both cases, He implantation ultimately results in old AHe ages. Nonetheless, extremely old ages were not detected, allowing us to infer that the selected crystals were free of He implantation.

Another factor that adds to intrasample and intersample variation on AHe ages is radiation damage. This process influences He diffusion and can result in a variation of ten orders of magnitude of the apatite closure temperature (Flowers et al., 2009). For samples following an identical thermal history, the radiation damage induces high eU apatites to retain fractional He, resulting in older ages when compared to low eU apatites. A positive correlation between eU concentration and AHe ages is then expected for samples that experienced high retentivity, which is the case of this study. The correlation between eU concentration and AHe corrected ages in our dataset is slightly positive and non-linear (Fig. 5.6a), suggesting that apatites were exposed to slow cooling rates (Flowers et al., 2009) and/or have resided long time periods in the AHePRZ (Reiners and Farley, 2001).

Considering these results and the eU versus ZHe plot, we suggest that some samples experienced slow cooling in/near the AHePRZ, experienced protracted cooling, or even registered reheating, which is demonstrated by the thermal histories depicted in Fig. 5.7 and Fig. 5.8. The relationship between ESR and AHe ages suggests sparse

interdependence between these parameters, following an almost flat trend (Fig. 5.6b). The importance of evaluating ESR resides in the fact that grain size is potentially a source of AHe dispersion, because larger apatite crystals tend to hold a larger amount of radiogenic He (Reiners and Farley, 2001).

The intersample AHe age variation of this dataset may also be attributed to location, i.e., according to the distance to the coastline (Fig. 5.10a) and elevation (Fig. 5.10b), because older ages are associated with higher elevations and far from the shoreline. However, when comparing our AHe data with AHe ages obtained from samples of the Araçuaí Orogen by Van Ranst et al. (2020) (Fig. 5.4), it is noticeable an almost flat trend, suggesting no correlation between these parameters in a more regional context (Fig. 5.10a and b). Additionally, the distance to the craton border lacks visible correlation to AHe central ages, displaying a flat trend (Fig. 5.10c) similar to Van Ranst et al. (2020) data.

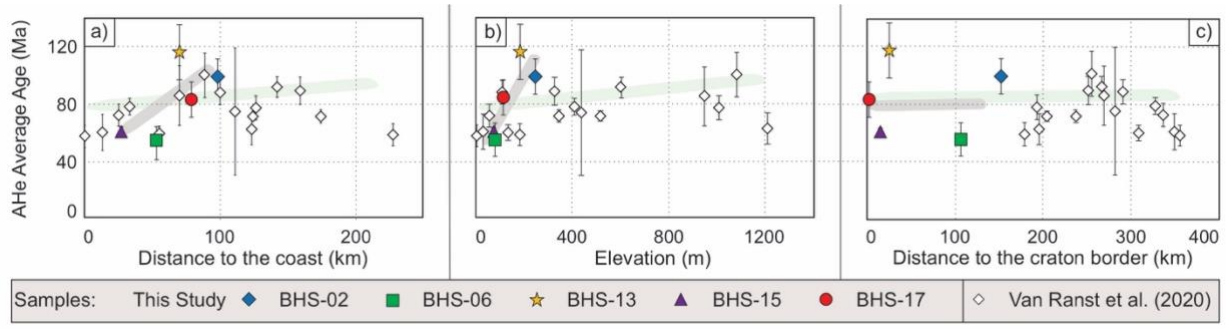

Figure 5. 10: AHe Average Age plotted against a) Distance to the coast; b) Altitude (meters above sea level); c) Distance to the craton border. These charts contain data from this study as well as apatite (U–Th)/He data from Van Ranst et al. (2020). The grey shading refers to the trend observed on the samples of this study whereas green shading encompasses the trend generated from this study and Van Ranst et al. (2020). Error bars (2σ) for each sample are displayed in the charts. (For interpretation of the references to colour in this figure legend, the reader is referred to the web version of this article.)

5.5.2 Cooling phases, geodynamic forces and denudation rates

5.5.2.1 End of the Brasiliano event (Early Paleozoic) to Pangea breakup

(Early Cretaceous)

The present-day geothermal gradient in the Araçuaí Orogen varies from 25 to 30 $^{o}C.km^{-1}$ (Schannor, 2018) and in the São Francisco Craton these values are between 18 and 42 $^{o}C.km^{-1}$ (Alexandrino and Hamza, 2008). To assess the denudation rates and the amount of erosion associated with cooling episodes from the end of the Brasiliano event to the present day, we attributed a mean geothermal gradient value of 25 ºC for both the

São Francisco Craton and the Araçuaí Orogen. Geothermal gradients vary over time, so we chose this value because it best represents typical geothermal gradients in ancient orogenic terranes and adjacent cratonic blocks (Burbank and Anderson, 2012; Lowell et al., 2014).

From Section 4.3, only two samples, BHS-02 and BHS-06, suggest a cooling phase during the Paleozoic (Fig. 5.7), although this event is poorly constrained, and the interpretations made about it are hypothetical. From the Lower Devonian to the Permian, these samples indicate a cooling of 20 to 30 ºC over the course of 80 to 100 m.y., which correspond to approximately 0.8 to 1.2 km of exhumation at denudation rates of 10 to 12 $m.Ma^{-1}$. This cooling event is interpreted as a result of the intraplate stresses associated with the Famatinian and Gondwanic orogenic cycles (Fig. 5.11; Milani and Ramos, 1998; Trouw and De Wit, 1999; Milani and De Wit, 2008). Previous apatite fission track data obtained in the São Francisco Craton (Jelinek et al., 2014; Fonseca et al., 2021) and in the southwestern border of the Araçuaí Orogen (Amaral-Santos et al., 2019) also record this cooling phase, which is generally attributed to orogenic processes. The study of Amaral-Santos et al. (2019) points to the exhumation of ca. 1.3 to 1.7 km in the northern segment of their study area, values that are broadly compatible with the results reported in this study. Additionally, other parts of West Gondwana also record this cooling event, suggesting a plate-wide effect (e.g., de Borba et al., 2002, 2003; Engelmann de Oliveira et al., 2016; Kasanzu et al., 2016; Dias et al., 2017; Alessio et al., 2019; Hueck et al., 2019; Machado et al., 2019; Martins-Ferreira et al., 2020). Although lacking high probability in the inversion models, the hypothesis made about the thermal history of these samples are supported by paleocurrent data from the Araripe basin that indicate sediment transport of NNW direction (Assine, 1994), which could point to the erosion of the Sao Francisco Craton and Araçuaí Orogen.

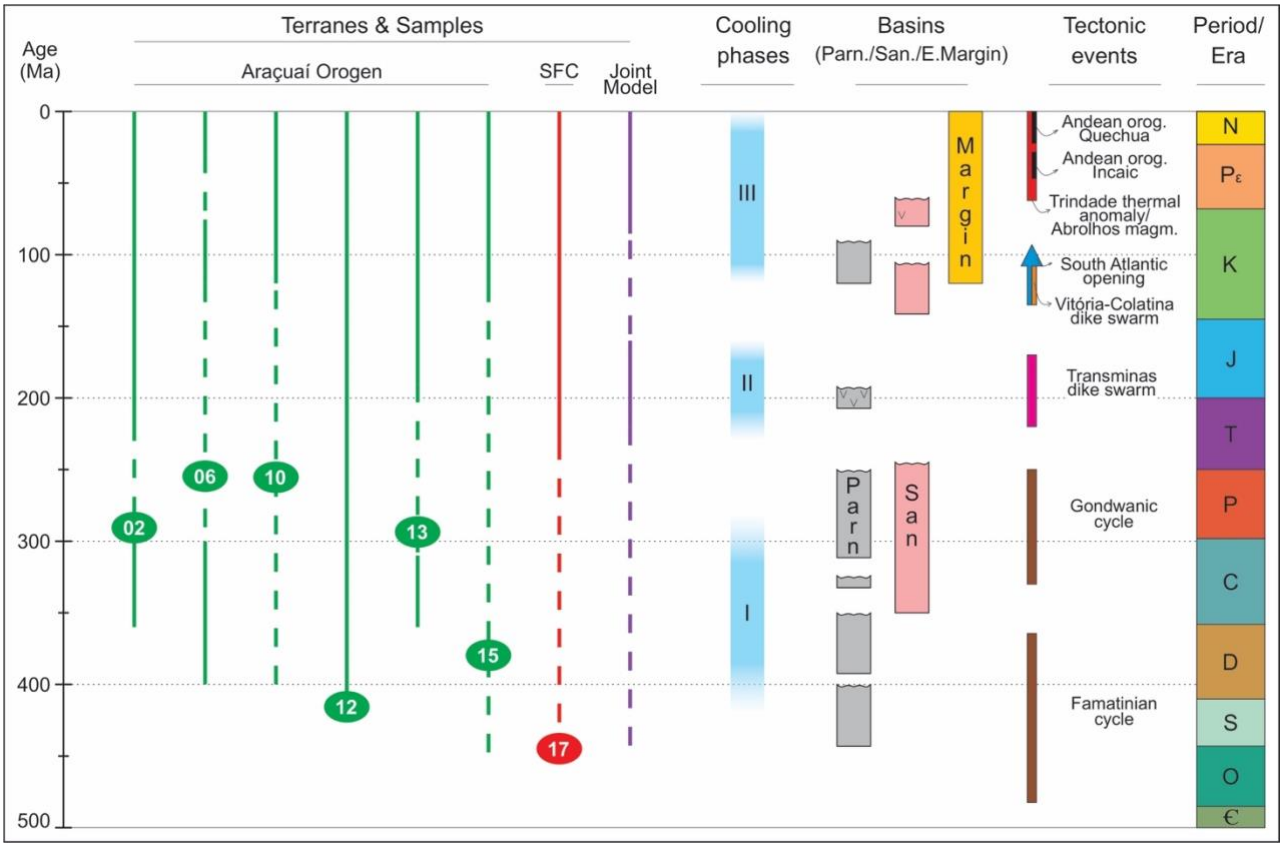

Figure 5. 11: Schematic chart evidencing thermal histories of this study, cooling phases, sedimentation in the surrounding basin depocenters, and major tectonic events associated with the chronostratigraphic chart. Continuous lines represent fast exhumation (>15 m.Ma^{-1}) and dashed lines slow exhumation (≤ 15 m.Ma^{-1}), steadystate, or reheating. Sample ID is placed on the mean corrected ZHe age. Abbreviations are: Parn.: Parnaíba basin; San.: Sanfranciscana basin; E. Margin: continental margin basins formed coevally to South Atlantic opening. v: intraplate magmatism (Parnaíba and Sanfranciscana basins); Andean Orog.: Andean orogeny.

At ca. 200 Ma, the relative probability of the thermal models increases significantly (BHS-06 and BHS-13; Fig. 5.7) and at 220 Ma the combined model exhibits a peak paleotemperature of 150 ºC (Fig. 5.5). These results suggest that the outcropping rocks in the northern segment of the Araçuaí Orogen were at temperatures near the lower temperature boundary of the ZHePRZ (~150 ºC). We estimate a denudation rate of 23 to 25 m.Ma^{-1} from the Ordovician to the Permian-Triassic transition for the northern Araçuaí Orogen (Fig. 5.10). These numbers suggest a total erosion of nearly 6.0 km, considering that Vauchez et al. (2019) assign the age of 459 Ma as the isothermal crossing of 338–326 ºC for the Araçuaí Orogen. Thermochronology data of other paleohighs in the West Gondwana interior seem to support the case for high denudation rates during this time, including the Sul-Rio-Grandense Shield (18 to 29 m.Ma^{-1}; e.g., Machado et al., 2019), the Tanzanian Craton (46 m.Ma^{-1}; Kasanzu, 2017; Kasanzu et al., 2016), and the Brasília Belt (ca.19 m.Ma^{-1}; Fonseca et al., 2020). Furthermore, the metamorphic rocks from

amphibolite to granulite facies (Uhlein et al., 1998; Belém, 2006) in northern Araçuaí Orogen indicate the removal of at least 15 to 20 km of the crustal section since the metamorphic peak during the Brasiliano orogenic cycle. The lack of the Gondwanides Orogeny signal in the Araçuaí Orogen for low-temperature thermochronometers, such as the apatite fission track suggested by Fonseca et al. (2021), also reinforces the removal of significant portions of the crust that once recorded this event. The 6.0 km estimate of sedimentary thickness for surrounding basin depocenters in West Gondwana also support the assumption of cooling and erosion (e.g., the Parnaíba, Araripe, Recôncavo-Tucano-Jatobá basins, among several others; Assine, 2007; Costa et al., 2007a; Costa et al., 2007b; Milani et al., 2007; Silva et al., 2007; Vaz et al., 2007).

From the Triassic/Lower Jurassic to the present-day, samples BHS-02, BHS-13, and BHS-17 (Fig. 5.7) register protracted cooling caused by exhumation until surface conditions (Fig. 5.11) at denudation rates varying from 15.7 to 23.2 $m.Ma^{-1}$ and the total erosion up to 4.4 km. The combined model suggests an accelerated cooling during this period, with similar values of erosion at a denudation rate of 73.3 $m.Ma^{-1}$. If we consider only the cooling registered prior to rifting, the amount of erosion ranges from 1.4 to nearly 2.0 km. Based on the available data, we correlate the onset of this cooling event to the end of the Gondwanic cycle (Cape-de la Ventana orogeny; Milani and De Wit, 2014), which is also observed in the Ribeira Belt farther south (Hiruma et al., 2010). Following exhumation, the sediments eroded were transported to a large-erg (Paraná basin) in the Pangea interior during the Jurassic-Cretaceous transition, to the Sanfranciscana basin, and to the pre-rift section of several basins in northeastern Brazil. The paleo-erg contains zircons of Neoproterozoic to Cambrian ages that are broadly compatible with the Brasiliano belts as its source area (Pinto et al., 2015), and paleowind directions from aeolian dunes are northerly (Moore et al., 1992; Linol et al., 2015). The paleocurrent from the adjacent Sanfranciscana basin also implicated the Araçuaí Orogen as a source area (Campos and Dardenne, 1997; Mescolotti et al., 2019). Finally, the pre-rift section in northeastern Brazil records northward sediment transportation (Kuchle et al., 2011) with a thickness of up to 0.9 km (Caixeta et al., 2007). Because cooling endured until the present day, initially the sediments accumulated in the continent interior and then migrated to the offshore basins that currently comprise the Brazilian continental margin.

Sample BHS-15 indicates a long residence at temperature of 120 ºC throughout the Paleozoic to the Early Cretaceous, which contrasts with the trends observed for the

other samples and requires additional sampling. Due to its proximity to the craton and following the observations of Fonseca et al. (2021) concerning the preservation of the upper crust in northern Araçuaí Orogen and the São Francisco Craton, slow cooling was expected for this sample. For these authors, the rigidity of the lithosphere increases towards the cratonic bridge, leading to differential denudation between the orogenic and cratonic lithospheres.

The combined model, on the other hand, exhibits a high temperature increment during the Middle Jurassic to the Early Cretaceous, which can be associated with the emplacement of either the Transminas or the Vitória-Colatina dike swarm at the southern end of the São Francisco Craton and the Araçuaí Orogen (Fig. 5.11; Novais et al., 2004; de Chaves and Neves, 2005; de Chaves, 2013; Belém, 2014; Coelho and Chaves, 2017). The combined model suggests temperatures high enough to completely reset the AHe ages during the emplacement of swarms, an important effect that has never been observed by previous works in the study region (Table 5.3; Amaral-Santos et al., 2019; Van Ranst et al., 2020).

5.5.2.2 Pangea breakup (Early Cretaceous) to present day

From the Early Cretaceous to the present day, both the individual and the combined thermal histories suggest cooling (Figs. 5.7, 5.8, and 5.11). The onset of cooling for samples BHS-06, BHS-10, and BHS-15 started during the Early Cretaceous, while for other samples it started by the end of the Triassic. Normal faulting and fragmentation of the upper crust were simultaneous to continental erosion, followed by sedimentation in the precursor South Atlantic oceanic basin (Mohriak et al., 2008). A total exhumation of 2 to 4 km from the time of breakup to the present day is constrained by our thermal models. These values are generally compatible to estimates of 3 to 7 km predicted by Harman et al. (1998) for samples collected in the São Francisco Craton and of 2.5 km suggested by Jelinek et al. (2014) for the Araçuaí Orogen. The main driving force for this cooling episode is related to rifting, since magma-poor continental margins experience flank uplift coeval to continental break (Nemčok, 2016). Turner et al. (2008), Jelinek et al. (2014), and Fonseca et al. (2021) also argue that this cooling phase observed in their studies in the Araçuaí Orogen and in the Sergipe-Alagoas basin could be related to the erosion of elevated rift shoulders. Additionally, the sedimentary record in the offshore Cumuruxatiba, Mucuri, and Jequitinhonha-Camamu-Almada basins can

range from 2.2 to nearly 7.8 km during the rift and transitional phases (França et al., 2007; Rangel et al., 2007; Rodovalho et al., 2007). These records suggest a continuous erosion of the continent that are compatible with the estimates reported in this study.

Sample BHS-06 shows a small reheating episode from 70 Ma to 30 Ma (Late Cretaceous to Paleocene), with a temperature increment of *ca.* 10 ºC (Fig. 5.7). Despite the low resolution of the thermal models for this period, we propose that this heating episode results from the Abrolhos magmatism and the Trindade thermal anomaly (Fig. 5.11). This hypothesis is based on the average corrected AHe age of 43.9 Ma for sample BHS-06. Additionally, sample BHS-15 also presents a young AHe age of 54 Ma, despite the absence of a heating trend in the thermal model. These are the youngest ages of our dataset, and the sample sites are located relatively close to the coast, where the volcanic deposits occur. The volcanism may have caused a locally increase of the geothermal gradient resetting the AHe system. The system remained opened until the temperature was low enough to allow the equilibrium between diffusion and generation of α particles, and finally cooling the sample below the AHePRZ.

The Late Cretaceous-Paleocene to present day cooling event records the denudation of nearly 2 km of rock succession, values in agreement with the offshore sedimentary record (e.g. Cumuruxatiba, Mucuri, Jequitinhonha-Camamu-Almada basins; França et al., 2007; Rangel et al., 2007; Rodovalho et al., 2007) and the estimates provided by Jelinek et al. (2014). A ubiquitous Late Cretaceous-Paleocene cooling is suggested for the region (e.g., Harman et al., 1998; De Morais Neto et al., 2007; Turner et al., 2008; Japsen et al., 2012; Jelinek et al., 2014; Van Ranst et al., 2020; Fonseca et al., 2021), and attributed to several causes. In the study area, the main causes include: (i) flexural isostasy caused by large-scale sedimentation and the Abrolhos magmatism in the offshore basins; (ii) thermal weakening of the crust due to the presence of the Trindade thermal anomaly. In special, the thermal weakening of the crust makes it susceptible to far compressional stresses propagated from the plate boundaries, i.e., the Andean Orogeny and ridge-push from the South Atlantic Ocean spreading center. Additional support for these claims is based on the enhanced buoyancy of the cratonic lithosphere caused by delamination (Hu et al., 2018), which is validated by the presence of the hot-spots of the Vitória-Trindade Seamount Chain (Skolotnev et al., 2010; Motoki et al., 2012) and the presence of multiple high-velocity anomalies below the South Atlantic margins (Hu et al., 2018). In summary, one or more factors listed above may have acted simultaneously as

the main geodynamic forces in the study area, causing the cooling observed in the thermal models.

Additional sampling for low-temperature thermochronology near the transition of the Araçuaí Orogen and the São Francisco Craton could enrich the understanding about the cooling episodes and amount of erosion. Also, sampling near the Transminas and Vitória-Colatina dike swarms could provide evidence for constraining reheating events, their maximum paleotemperatures, and the extent of their effect in the country rocks.

5.5.3 Structural and rheological inheritance

Structural inheritance is an important factor in the development of rifts because basement faults act as weak zones that concentrate deformation and allow reactivation. The study area sits in a transitional zone between two distinct rheological domains, a cratonic (cold) and a non-cratonic lithosphere (orogenic, hot). These domains have the potential to influence rift propagation (Nemčok, 2016; Salazar-Mora and Sacek, 2021), induce differential denudation (Fonseca et al., 2021), and deposition. To the north of the study area, the offshore Cretaceous to Cenozoic basins are emplaced on top of the cratonic basement, resulting in generally narrow and deep basins. In contrast, to the south the continental margin is wide and shallow, with volcano-sedimentary successions lying on top of the orogenic basement that was extended during rifting (Mohriak et al., 2008). This along-strike structural segmentation of the continental margin is also observed by Jelinek et al. (2014). These authors observe that the São Francisco Craton domain lacks an Early Cretaceous cooling coeval to rifting, while the Araçuaí Orogen displays accelerated denudation attributed to rift shoulder erosion. Our results reinforce the role of differential denudation between these domains, as previously observed by Fonseca et al. (2021).

The rose diagrams in Fig. 5.3c indicate that the NNE-SSW lineaments are the most frequent direction in the cratonic domain, inherited from a Paleoproterozoic orogen. These structural lineaments comprise weak zones that constrain the formation of faults parallel to the rift master faults and the present-day submerged grabens. They are also responsible for controlling the aborted Recôncavo-Tucano-Jatobá rift system, and the present-day coastline. Additionally, this trend is also parallel to the crustal weakness zone of intense ductile and brittle deformation described in southeastern Brazil (Giro et al., 2021).

In the Araçuaí Orogen, the lineament directions of the orogenic fabric displayed in the rose diagrams follows two distinct directions, NE-SW and NW-SE (Fig. 5.3c). NE-SW lineaments are parallel to orogen, while NW-SE structures are related to the northern curvature due to the confined nature of the Araçuaí Orogen against the São Francisco Craton. Also, NW-SE lineaments are linked to the clockwise rotation of the South American plate, as observed in other segments of the Brazilian continental margin (e.g.; Milani et al., 1998; Soares et al., 2007; Salomon et al., 2017; Hueck et al., 2018). These structures act as transfers faults in the Cumuruxatiba basin (Cretaceous to present), eastward of the study area, resulting in the development of zones of differential subsidence (Gontijo and Santos, 1992). Besides, NW-SE faults control the deposition of the Cenozoic sedimentary cover, possibly induced by flexural isostasy due to sedimentary and volcanic overload in the Cumuruxatiba basin.

As mentioned before, samples BHS-06 and BHS-15 present the youngest average corrected AHe ages of our data set, and these sample sites are placed next to the NW-SE lineaments. Therefore, we suggest that the reactivation of the NW-SE lineaments played an important role in the study area during the Cretaceous and Cenozoic by keeping the AHe system open for a longer period when compared to the other samples of our dataset. Our data reveals that lineaments and weakness zones in the upper crust not only control the deposition of sediments but also act as paths for fluid migration, keeping the temperatures high enough to allow diffusion of α particles. Future studies regarding the lineament directions discussed here and the analysis of fault planes and kinematic vectors are opportunities to correlate structural and rheological inheritance with low-temperature thermochronometers in a complex geologic transitional environment.

5.6 Conclusion

This study provides the first suite of combined zircon and apatite (U–Th)/He data across the continental margin along the transition between the Araçuaí Orogen and São Francisco Craton, on eastern Brazil. In this work, we analyzed 42 zircons and 26 apatites, which generated Paleozoic to Mesozoic and Mesozoic to Cenozoic ages, respectively. Zircon grains display a positive correlation between eU concentration and ages, attributed to low alpha doses due to low eU content. These crystals record relatively slow monotonic cooling from Cambrian to the transition between the Late Cretaceous and the Paleocene. ZHe ages are also controlled by the shortest distance to the craton, evidencing that

cratonic lithosphere is spared from exhumation when compared to orogenic terranes. Apatite crystals display a non-linear positive relationship between eU and AHe ages. This indicates that apatites were highly retentive and remained for long periods within the AHePRZ and/or underwent on slow cooling and experienced reheating. Both the elevation and the distance to the coast seems to locally control AHe ages.

Thermal histories obtained from modeling in the QTQt software produced several thermal histories that are summarized below:

(1) Cooling from Lower Devonian to Carboniferous: this hypothetical cooling event is attributed to the compressional stresses from the Gondwanic orogenic cycle. From the Ordovician to the end of the Permian, we suggest denudation rates of 23 to 25 $m.Ma^{-1}$ and a removal of 6.0 km. This value is similar to previous studies across West Gondwana.

(2) Cooling from Triassic/Jurassic to present day: we conclude that the onset of this cooling phase results from intraplate stresses coming from the Cape-de la Ventana orogeny, with sediment deposition in the Paraná and Sanfranciscana basins as well as in the pre-rift section of several basins in northeastern Brazil.

(3) Reheating from Middle Jurassic to Early Cretaceous: attributed to the emplacement of the Transminas and Vitória-Colatina mafic dike swarms in the São Francisco Craton and Araçuaí Orogen, prior to West Gondwana breakup.

(4) Reheating from Late Cretaceous to Paleocene: related to the Abrolhos Magmatism and the presence of the Trindade thermal anomaly. These events resulted in elevated thermal gradient that are recorded in samples closer to the coast. Younger AHe ages suggest an open AHe system and are mainly located near the coast.

(5) Cooling from Late Cretaceous-Paleocene to present day: a final cooling phase brings samples to surface conditions, with the removal of nearly 2 km of rock succession. This event could be connected to several geodynamic forces, such as flexural isostasy due to large scale sedimentation in the offshore basins and thermal weakening due to the Trindade thermal anomaly making the crust susceptible to compressional forces coming from the plate border (Andean orogeny and ridge-push from the Atlantic Ocean spreading center).

Finally, our results also suggest that the reactivation of NW-SE lineaments and faults helped keep the AHe system open for longer periods, resulting in a few anomalously young AHe ages. For other areas, coupling structural and rheological analyzes with zircon and apatite (U–Th)/He thermochronology could provide valuable

information about the upper crust processes and their relationship with the underlying tectonics.

5.7 Acknowledgments

E. Amaral-Santos thanks the support from Conselho Nacional de Desenvolvimento Científico e Tecnologico – CNPq, for the Ph.D scholarship (140775/2019-6). A.R. Jelinek thanks the support from CNPq (Project 309329/2020-5). We are grateful to the editor Dr. Zheng-Xiang Li and two anonymous reviewers that provided valuable considerations on an earlier version of this paper.

References

Alessio, B.L., Glorie, S., Collins, A.S., Jourdan, F., Jepson, G., Nixon, A., Siegfried, P.R., Clark, C., 2019. The thermo-tectonic evolution of the southern Congo Craton margin as determined from apatite and muscovite thermochronology. Tectonophysics 766, 398–415. https://doi.org/10.1016/j.tecto.2019.06.004

Alexandrino, C.H., Hamza, V.M., 2008. Estimates of heat flow and heat production and a thermal model of the São Francisco craton. Int. J. Earth Sci. 97, 289–306. https://doi.org/10.1007/s00531-007-0291-y

Alkmim, F.F. De, 2015. Geological Background: A tectonic panorama of Brazil, in: Vieira, B.C., Salgado, A.A.R., Santos, L.J.C. (Eds.), Landscapes and Landforms of Brazil. Springer, Dordrecht, pp. 9–18. https://doi.org/10.1007/978-94-017-8023-0

Alkmim, F.F., Kuchenbecker, M., Reis, H.L.S., 2016. The Araçuaí Belt, in: Heilbron, M., Cordani, U.G., Alkmim, F.F. (Eds.), São Francisco Craton, Eastern Brazil. Springer, Cham, pp. 255–276. https://doi.org/10.1007/978-3-319-01715-0

Alkmim, F.F., Martins-Neto, M.A., 2012. Proterozoic first-order sedimentary sequences of the São Francisco craton, eastern Brazil. Mar. Pet. Geol. 33, 127–139. https://doi.org/10.1016/j.marpetgeo.2011.08.011

Almeida, F.F.M. de, 1977. O Cráton do São Francisco. Rev. Bras. Geociências 7, 349–364.

Almeida, F.F.M., 1981. O Cráton do Paramirim e suas relações com o do São Francisco. Simpósio Sobre o Cráton do São Francisco e Suas Faixas Marginais. Salvador, 1981. SBG-Núcleo Bahia, Salvador, Anais, p. 1–10.

Amaral-Santos, E., Jelinek, A.R., Almeida-Abreu, P.A., Genezine, F.A., 2019. Phanerozoic cooling history of Archean/Paleoproterozoic basement in the southern Espinhaço Range, southeastern Brazil, through apatite fission-track analysis. J. South Am. Earth Sci. 96, 102352. https://doi.org/10.1016/j.jsames.2019.102352

Amaral, G., Born, H., Hadler, J.C.N., Iunes, P.J., Kawashita, K., Machado, D.L., Oliveira, E.P., Paulo, S.R., Tello, C.A.S., 1997. Fission track analysis of apatites from São Francisco craton and Mesozoic alcaline-carbonatite complexes from central and southeastern Brazil. J. South Am. Earth Sci. 10, 285–294. https://doi.org/10.1016/s0895-9811(97)00020-5

Arai, M., 2006. A grande elevação eustática do Mioceno e sua influência na origem do Grupo Barreiras. Geol. USP. Série Científica 6, 01–06. https://doi.org/10.5327/s1519-874x2006000300002

Assine, M.L., 1994. Paleocorrentes E Paleogeografia Na Bacia Do Araripe, Nordeste Do Brasil. Rev. Bras. Geociências 24, 223–232. https://doi.org/10.25249/0375-7536.1994223232

Ault, A.K., Flowers, R.M., 2012. Is apatite U-Th zonation information necessary for accurate interpretation of apatite (U-Th)/He thermochronometry data? Geochim. Cosmochim. Acta 79, 60–78.

https://doi.org/10.1016/j.gca.2011.11.037

Barbosa, J.S.F., Sabaté, P., 2004. Archean and Paleoproterozoic crust of the São Francisco Craton, Bahia, Brazil: Geodynamic features. Precambrian Res. 133, 1–27. https://doi.org/10.1016/j.precamres.2004.03.001

Belém, J., 2014. Geoquímica, Geocronologia E Contexto Geotectônico Do Magmatismo Máfico Associado Ao Feixe De Fraturas Colatina, Estado Do Espírito Santo. Universidade Federal de Minas Gerais.

Beucher, R., Brown, R.W., Roper, S., Stuart, F., Persano, C., 2013. Natural age dispersion arising from the analysis of broken crystals: Part II. Practical application to apatite (U-Th)/He thermochronometry. Geochim. Cosmochim. Acta 120, 395–416. https://doi.org/10.1016/j.gca.2013.05.042

Borba, A.W. de, Lima, E.F. de, Vignol-Lelarge, M.L.M., Mizusaki, A.M.P., Sparrenberg, I., Barros, C.E. de, 2003. Significance of Late Paleozoic fission-track ages in volcanic rocks from the Lavras Do Sul region, southernmost Brazil. Gondwana Res. 6, 79–88. https://doi.org/10.1016/S1342-937X(05)70645-6

Borba, A.W. de, Vignol-Lelarge, M.L.M., Mizusaki, A.M.P., 2002. Uplift and denudation of the Caçapava do Sul granitoids (southern Brazil) during Late Paleozoic and Mesozoic: Constraints from apatite fission-tract data. J. South Am. Earth Sci. 15, 683–692. https://doi.org/10.1016/S0895-9811(02)00086-X

Braun, J., van der Beek, P., 2004. Evolution of passive margin escarpments: What can we learn from low-temperature thermochronology? J. Geophys. Res. 109, F4009. https://doi.org/doi:10.1029/2004JF000147

Brown, R.W., Beucher, R., Roper, S., Persano, C., Stuart, F., Fitzgerald, P., 2013. Natural age dispersion arising from the analysis of broken crystals. Part I: Theoretical basis and implications for the apatite (U-Th)/He thermochronometer. Geochim. Cosmochim. Acta 122, 478–497. https://doi.org/10.1016/j.gca.2013.05.041

Buck, W.R., 1991. Modes of continental lithospheric extension. J. Geophys. Res. 96, 20161–20178. https://doi.org/10.1029/91jb01485

Buiter, S.J.H., Torsvik, T.H., 2014. A review of Wilson Cycle plate margins: A role for mantle plumes in continental break-up along sutures? Gondwana Res. 26, 627–653. https://doi.org/10.1016/j.gr.2014.02.007

Burbank, D.W., Anderson, R.S., 2012. Rates of Erosion and Uplift, in: Burbank, D.W., Anderson, R.S. (Eds.), Tectonic Geomorphology. Blackwell Publishing Ltd., pp. 195–242. https://doi.org/10.1002/9781444345063.ch7

Caixeta, J.M., Milhomem, P.S. Witzke, R.E., Dupuy, I.S.S, Gontijo, G.A., 2007. Bacia de Camamu. Boletim de Geociências da Petrobras 15(2), 455-461.

Campos, J.E.G., Dardenne, M.A., 1997. Estratigrafia E Sedimentação Da Bacia Sanfranciscana: Uma Revisão. Rev. Bras. Geociências 27, 269–282. https://doi.org/10.25249/0375-7536.1997269282

Carneiro, C.D.R., Almeida, F.F.M. de, Hasui, Y., Zalán, P. V., Teixeira, J.B.G., 2012. Estágios evolutivos do Brasil no Fanerozoico, in: Hasui, Y., Carneiro, C.D.R., Almeida, F.F.M. de, Bartorelli, A. (Eds.), Geologia Do Brasil. Beca, São Paulo, pp. 131–137.

Cavalcante, C., Hollanda, M.H., Vauchez, A., Kawata, M., 2018. How long can the middle crust remain partially molten during orogeny? Geology 46, 839–842. https://doi.org/10.1130/G45126.1

Chang, H.K., Kowsmann, R.O., Figueiredo, A.M.F., Bender, A.A., 1992. Tectonics and stratigraphy of the East Brazil Rift system: an overview. Tectonophysics 213, 97–138. https://doi.org/10.1016/0040-1951(92)90253-3

Chaves, A. de O., 2013. Enxames De Diques Máficos De Minas Gerais – O Estado Da Arte. Geonomos 21, 29–33. https://doi.org/10.18285/geonomos.v21i1.253

Chaves, A. de O., Neves, J.M.C., 2005. Radiometric ages, aeromagnetic expression, and general geology of mafic dykes from southeastern Brazil and implications for African-South American correlations. J. South Am. Earth Sci. 19, 387–397. https://doi.org/10.1016/j.jsames.2005.04.005

Coelho, R.M., Chaves, A.O., 2017. Diques máficos de Minas Gerais do Cretácio inferior: Idades Ar-Ar e correlação com a Província Ígnea Paraná-Etendeka. Geociências 36, 613–622.

Cordani, U.G., 1970. Idade do vulcanismo no Oceano Atlântico Sul. Bol. IGA 1, 9–75.

Costa, I.P., Bueno, G.V., Milhomem, P.S., Lima e Silva, H.S.R., Kosin, M.D., 2007b. Sub-bacia de Tucano Norte e Bacia de Jatobá. Boletim de Geociências da Petrobras 15(2), 445-453.

Costa, I.P., Milhomem, P.S., Bueno, G.V., Lima e Silva, H.S.R., Kosin, M.D., 2007a. Sub-bacias de Tucano Sul e Central. Boletim de Geociências da Petrobras 15(2), 433-443.

Cruz, S.C.P., Alkmim, F.F., 2016. The Paramirim Aulacogen, in: Heilbron, M., Cordani, U.G., Alkmim, F.F. (Eds.), São Francisco Craton, Eastern Brazil. Springer, Cham, pp. 97–115. https://doi.org/10.1007/978-3-319-01715-0_6

de Almeida, F.F.M., Hasui, Y., de Brito Neves, B.B., Fuck, R.A., 1981. Brazilian structural provinces: An introduction. Earth Sci. Rev. 17, 1–29. https://doi.org/10.1016/0012-8252(81)90003-9

De Wit, M.J., De Brito Neves, B.B., Trouw, R.A.J., Pankhurst, R.J., 2008. Pre-Cenozoic correlations across the South Atlantic region: “The ties that bind.” Geol. Soc. Spec. Publ. 294, 1–8. https://doi.org/10.1144/SP294.1

Dias, A.N.C., Moura, C.A.V., Milhomem Neto, J.M., Chemale, F., Girelli, T.J., Masuyama, K.M., 2017. Geochronology and thermochronology of the gneisses of the Brasiliano/Pan-African Araguaia Belt: Records of exhumation of West Gondwana and Pangea break up. J. South Am. Earth Sci. 80, 174–191. https://doi.org/10.1016/j.jsames.2017.09.027

Dussin, T.M., 1994. Associations volcano-plutoniques de l'Espinhaço Meridional (SE-Bresil). Master thesis. Univ. D'Orleans, France, pp. 177.

Engelmann de Oliveira, C.H., Jelinek, A.R., Chemale, F., Cupertino, J.A., 2016. Thermotectonic history of the southeastern Brazilian margin: Evidence from apatite fission track data of the offshore Santos Basin and continental basement. Tectonophysics 685, 21–34. https://doi.org/10.1016/j.tecto.2016.07.012

Farley, K.., Wolf, R.., Silver, L.., 1996. The effects of long alpha-stopping distances on (U-Th)/He ages. Geochim. Cosmochim. Acta 60, 4223–4229. https://doi.org/https://doi.org/10.1016/S0016-7037(96)00193-7

Farley, K. a, 2000. Helium diffusion from apatite, General behavior as illustrated by Durango fiuorapatite The implied He closure temperature for a grain. J. Geophys. Res. 105, 2903–2914.

Farley, K.A., 2002. (U-Th)/He dating: Techniques, calibrations, and applications. Rev. Mineral. Geochemistry 47, 819–844. https://doi.org/10.2138/rmg.2002.47.18

Fitzgerald, P.G., Baldwin, S.L., Webb, L.E., O’Sullivan, P.B., 2006. Interpretation of (U-Th)/He single grain ages from slowly cooled crustal terranes: A case study from the Transantarctic Mountains of southern Victoria Land. Chem. Geol. 225, 91–120. https://doi.org/10.1016/j.chemgeo.2005.09.001

Flowers, R.M., Bowring, S.A., Reiners, P.W., 2006. Low long-term erosion rates and extreme continental stability documented by ancient (U-Th)/He dates. Geology 34, 925–928. https://doi.org/10.1130/G22670A.1

Flowers, R.M., Ketcham, R.A., Shuster, D.L., Farley, K.A., 2009. Apatite (U-Th)/He thermochronometry using a radiation damage accumulation and annealing model. Geochim. Cosmochim. Acta 73, 2347–2365. https://doi.org/10.1016/j.gca.2009.01.015

Fonseca, A.C., Piffer, G.V., Nachtergaele, S., Van Ranst, G., De Grave, J., Novo, T.A., 2020. Devonian to Permian post-orogenic denudation of the Brasília Belt of West Gondwana: insights from apatite fission track thermochronology. J. Geodyn. 137, 101733. https://doi.org/10.1016/j.jog.2020.101733

Fonseca, A.C.L., Novo, T.A., Nachtergaele, S., Fonte-Boa, T.M.R., Van Ranst, G., De Grave, J., 2021. Differential Phanerozoic evolution of cratonic and non-cratonic lithosphere from a thermochronological perspective: São Francisco Craton and marginal orogens (Brazil). Gondwana Res. 93, 106–126. https://doi.org/10.1016/j.gr.2021.01.006

França, R.L., Del Rey, A.C., Tagliari, C.V., Brandão, J.R., Fontanelli, P.R., 2007. Bacia de Mucuri. Boletim de Geociências da Petrobras 15(2), 493-499.

Gallagher, K., 2012. Transdimensional inverse thermal history modeling for quantitative thermochronology. J. Geophys. Res. Solid Earth 117, B02408. https://doi.org/10.1029/2011JB008825

Giro, J.P., Almeida, J., Guedes, E., Bruno, H., 2021. Tectonic inheritances in rifts: The meaning of NNE lineaments in the continental rift of SE-Brazil. J. South Am. Earth Sci. 108, 103225. https://doi.org/10.1016/j.jsames.2021.103225

Gontijo, R.C., Santos, C.F. 1992. Compartimentação e alinhamentos estruturais transversais da Bacia de Cumuruxatiba (BA). In: SBG, Congresso Brasileiro de Geologia, 37, São Paulo, Anais, 1:564.

Guenthner, W.R., Reiners, P.W., Ketcham, R.A., Nasdala, L., Giester, G., 2013. Helium diffusion in natural zircon: radiation damage, anisotropy, and the interpretation of zircon (U-TH)/He thermochronology. Am. J. Sci. 313, 145–198. https://doi.org/10.2475/03.2013.01

Guenthner, W.R., Reiners, P.W., Tian, Y., 2014. Interpreting date-eU correlations in zircon (U-Th)/He datasets: A case study from the Longmen Shan, China. Earth Planet. Sci. Lett. 403, 328–339. https://doi.org/10.1016/j.epsl.2014.06.050

Harman, R., Gallagher, K., Brown, R., Raza, A., Bizzi, L., 1998. ccelerated denudation and tectonic/geomorphic reactivation of the craton of northeastern Brazil during the Late Cretaceous. J. Geophys. Res. 103, 27091–27105.

Heilbron, M., Cordani, U.G., Alkmim, F.F., Reis, H.L.S., 2016b. Tectonic Genealogy of a Miniature Continent, in: Heilbron, M., Cordani, U.G., Alkmim, F.F. (Eds.), São Francisco Craton, Eastern Brazil. Springer, Cham, pp. 321–331. https://doi.org/10.1007/978-3-319-01715-0_17

Heilbron, M., Mohriak, W., Valerianol, M., Milani, J., Almeida, J., Tupinambfil, M., Petreo, P., 2000. From Collision to Extension : The Roots of the Southeastern Continental Margin of Brazil to early Paleozoic marked by Late Jurassic, in: Mohriak, W., Taiwani, M. (Eds.), Atlantic Rifts and Continental Margins, Geophysical Monograph 115. American Geophysical Union, pp. 1–32.

Heilbron, Monica, Cordani, U.G., Alkmim, F.F., 2016a. The São Francisco Craton and Its Margins, in: Heilbron, M., Cordani, U.G., Alkmim, F.F. (Eds.), São Francisco Craton, Eastern Brazil. Springer, Cham, pp. 3–13. https://doi.org/10.1007/978-3-319-01715-0_1

Hiruma, S.T., Riccomini, C., Modenesi-Gauttieri, M.C., Hackspacher, P.C., Neto, J.C.H., Franco-Magalhães, A.O.B., 2010. Denudation history of the Bocaina Plateau, Serra do Mar, southeastern Brazil: Relationships to Gondwana breakup and passive margin development. Gondwana Res. 18, 674–687. https://doi.org/10.1016/j.gr.2010.03.001

Hu, J., Liu, L., Faccenda, M., Zhou, Q., Fischer, K.M., Marshak, S., Lundstrom, C., 2018. Modification of the Western Gondwana craton by plume-lithosphere interaction. Nat. Geosci. 11, 203–210. https://doi.org/10.1038/s41561-018-0064-1

Hueck, M., Dunkl, I., Heller, B., Stipp Basei, M.A., Siegesmund, S., 2018a. (U-Th)/He Thermochronology and Zircon Radiation Damage in the South American Passive Margin: Thermal Overprint of the Paraná LIP? Tectonics 37, 4068–4085. https://doi.org/10.1029/2018TC005041

Hueck, M., Dunkl, I., Oriolo, S., Wemmer, K., Basei, M.A.S., Siegesmund, S., 2019. Comparing contiguous high- and low-elevation continental margins: New (U-Th)/He constraints from South Brazil and an integration of the thermochronological record of the southeastern passive margin of South America. Tectonophysics 770, 228222. https://doi.org/10.1016/j.tecto.2019.228222

Japsen, P., Bonow, J.M., Green, P.F., Cobbold, P.R., Chiossi, D., Lilletveit, R., Magnavita, L.P., Pedreira, A., 2012. Episodic burial and exhumation in NE Brazil after opening of the South Atlantic. Bull. Geol. Soc. Am. 124, 800–816. https://doi.org/10.1130/B30515.1

Jelinek, A.R., Chemale, F., van der Beek, P.A., Guadagnin, F., Cupertino, J.A., Viana, A., 2014. Denudation history and landscape evolution of the northern East-Brazilian continental margin from apatite fission-track thermochronology. J. South Am. Earth Sci. 54, 158–181. https://doi.org/10.1016/j.jsames.2014.06.001

Kasanzu, C.H., 2017. Apatite fission track and (U-Th)/He thermochronology from the Archean Tanzania Craton: Contributions to cooling histories of Tanzanian basement rocks. Geosci. Front. 8, 999–1007. https://doi.org/10.1016/j.gsf.2016.09.007

Kasanzu, C.H., Linol, B., de Wit, M.J., Brown, R., Persano, C., Stuart, F.M., 2016. From source to sink in central Gondwana: Exhumation of the Precambrian basement rocks of Tanzania and sediment accumulation in the adjacent Congo basin. Tectonics 35, 2034–2051. https://doi.org/10.1002/2016TC004147

Kuchle, J., Scherer, C.M. dos S., Born, C.C., Alvarenga, R. dos S., Adegas, F., 2011. A contribution to regional stratigraphic correlations of the Afro-Brazilian depression - The Dom João Stage (Brotas Group and equivalent units - Late Jurassic) in Northeastern Brazilian sedimentary basins. J. South Am. Earth Sci. 31, 358–371. https://doi.org/10.1016/j.jsames.2011.02.007

Kusznir, N.J., Park, R.G., 1987. The extensional strength of the continental lithosphere: Its dependence on geothermal gradient, and crustal composition and thickness. Geol. Soc. Spec. Publ. 28, 35–52. https://doi.org/10.1144/GSL.SP.1987.028.01.04

Linol, B., de Wit, M. J., Milani, E.J., Guillocheau, F., Scherer, C., 2015. New Regional Correlation Between the Congo, Paraná and Cape-Karoo Basins of Southwest Gondwana, in: De Wit, Maarten J., Guillocheau, François, De Wit, M.C.J. (Eds.), Geology and Resource Potential of the Congo Basin. Springer, Berlin, Heidelberg, pp. 245–268. https://doi.org/10.1007/978-3-642-29482-2

Lippolt, H.J., Leitz, M., Wernicke, R.S., Hagedorn, B., 1994. (Uranium + thorium)/helium dating of apatite: experience with samples from different geochemical environments. Chem. Geol. 112, 179–191. https://doi.org/10.1016/0009-2541(94)90113-9

Lovecchio, J.P., Rohais, S., Joseph, P., Bolatti, N.D., Kress, P.R., Gerster, R., Ramos, V.A., 2018. Multistage rifting evolution of the Colorado basin (offshore Argentina): Evidence for extensional settings prior to the South Atlantic opening. Terra Nov. 30, 359–368. https://doi.org/10.1111/ter.12351

Lowell, R.P., Kolandaivelu, K., Rona, P.A., 2014. Hydrothermal Activity, in: Reference Module in Earth Systems and Environmental Sciences. Elsevier Inc., pp. 1–19. https://doi.org/10.1016/b978-0-12-409548-9.09132-6

Machado, J.P.S.L., Jelinek, A.R., Bicca, M.M., Stephenson, R., Genezini, F.A., 2019. West gondwana orogenies and pangaea break-up: Thermotectonic effects on the southernmost mantiqueira province, brazil. J. Geol. Soc. London. 176, 1056–1075. https://doi.org/10.1144/jgs2019-018

Machado, J.P.S.L., Jelinek, A.R., Stephenson, R., Gaucher, C., Bicca, M.M., Chiglino, L., Genezini, F.A., 2020. Low-temperature thermochronology of the South Atlantic margin along Uruguay and its relation to tectonic events in West Gondwana. Tectonophysics 784, 228439. https://doi.org/10.1016/j.tecto.2020.228439

Martins-Ferreira, M.A.C., Dias, A.N.C., Chemale, F., Campos, J.E.G., 2020. Intracontinental uplift of the Brazilian Central Plateau linked to continental breakup, orogenies, and basin filling, supported by apatite and zircon fission-track data. Arab. J. Geosci. 13:891. https://doi.org/10.1007/s12517-020-05885-8

Mescolotti, P.C., Varejão, F.G., Warren, L.V., Ladeira, F.S.B., Giannini, P.C.F., Assine, M.L., 2019. The sedimentary record of wet and dry eolian systems in the Cretaceous of Southeast Brazil: Stratigraphic and paleogeographic signifcance. Brazilian J. Geol. 49, e20190057. https://doi.org/10.1590/2317-4889201920190057

Mesquita, Á.F., Vieira, V.R.D.A., Arab, P.B., Bruch, A.F., Alves, T.N., 2021. Aspectos Morfoestruturais Da Margem Costeira Do Extremo Sul Da Bahia (Ne Brasil): Implicações Neotectônicas Na Evolução Geomorfológica Costeira. Rev. Bras. Geomorfol. 22, 47–64. https://doi.org/10.20502/rbg.v22i1.1798

Milani, E.J., De Wit, M.J., 2014. Correlations between the classic Paraná and Cape-Karoo sequences of South America and southern Africa and their basin infills flanking the Gondwanides: Du Toit revisited. Geol. Soc. Spec. Publ. 294, 319–342. https://doi.org/10.1144/SP294.17

Milani, E.J., Faccini, U.F., Scherer, C.M., Araújo, L.M., Cupertino, J.A., 1998. Sequences and stratigraphic hierarchy of

the Paraná Basin (Ordovician to Cretaceous), southern Brazil. Bol. IG-USP. Série Científica 29, 125–173. https://doi.org/https://doi.org/10.11606/issn.2316-8986.v29i0p125-173

Milani, E.J., Ramos, V.A., 1998. Paleozoic orogenies in southwestern Gondwana and the subsidence cycles of the Parana Basin\rOrogenias paleozoicas no dominio sul-ocidental do Gondwana e os cicios de subsidencia da bacia do Parana. Rev. Bras. Geociencias 28, 473–484.

Milani, E.J., Rangel, H.D., Bueno, G.V., Stica, J.M., Winter, W.R., Caixeta, J.M., Da Cruz Pessoa Neto, O., 2007. Bacias sedimentares brasileiras - Cartas estratigráficas. Bol. Geociencias da Petrobras 15, 183–205.

Misra, A.A., Mukherjee, S., 2015. Tectonic Inheritance in Continental Rifts and Passive Margins, Springer B. ed. Springer International Publishing. https://doi.org/DOI 10.1007/978-3-319-20576-2

Mohriak, W., Nemčok, M., Enciso, G., 2008. South Atlantic divergent margin evolution: Rift-border uplift and salt tectonics in the basins of SE Brazil. Geol. Soc. Spec. Publ. 294, 365–398. https://doi.org/10.1144/SP294.19

Moore, G.T., Hayashida, D.N., Ross, C.A., Jacobson, S.R., 1992. Paleoclimate of the Kimmeridgian/Tithonian (Late Jurassic) world: I. Results using a general circulation model. Palaeogeogr. Palaeoclimatol. Palaeoecol. 93, 113–150. https://doi.org/10.1016/0031-0182(92)90186-9

Morais Neto, J.M. De, Green, P.F., Karner, G.D., De Alkmim, F.F., 2007. Age of the Serra Do Martins formation, Borborema plateau, northeastern Brazil: Constraints from apatite and zircon fission track analysis. Bol. Geociencias da Petrobras 16, 23–52.

Motoki, A., Motoki, K.F., Melo, D.P. de, 2012. Caracterização Da Morfologia Submarina Da Cadeia Vitória-Trindade E Áreas Adjacentes, Es, Com Base Na Batimetria Predita Do Topo Versão 14.1. Rev. Bras. Geomorfol. 13, 151–170. https://doi.org/10.20502/rbg.v13i2.195

Nemčok, M., 2016. Rifts and Passive Margins: Structural Architecture, Thermal Regimes, and Petroleum Systems, Journal of Chemical Information and Modeling. Cambridge University Press, New York, NY.

Nishiizumi, K., Kohl, C.P., Arnold, J.R., Klein, J., Fink, D., Middleton, R., 1991. Cosmic ray produced 10Be and 26Al in Antarctic rocks: exposure and erosion history. Earth Planet. Sci. Lett. 104, 440–454. https://doi.org/10.1016/0012-821X(91)90221-3

Novais, L.C.C., Teixeira, L.B., Neves, M.T., Rodarte, J.B.M., Almeida, J.C.H., Valeriano, C. de M., 2004. Novas ocorrências de diques de diabásio na faixa Colatina-ES: estruturas rúpteis associadas e implicações tectônicas para as bacias de Campos e do Espírito Santo. Bol. Geociências da Petrobras 12, 191–194.

Oliveira, L.C., Oliveira, R.M.A.G., Pereira, E., 2018. Possível Controle Neotectônico sobre as Falésias do Litoral Sul da Bahia. Anuário do Inst. Geociências - UFRJ 41, 702–716. https://doi.org/10.11137/2018_3_702_716

Oriolo, S., Oyhantçabal, P., Wemmer, K., Siegesmund, S., 2017. Contemporaneous assembly of Western Gondwana and final Rodinia break-up: Implications for the supercontinent cycle. Geosci. Front. 8, 1431–1445. https://doi.org/10.1016/j.gsf.2017.01.009

Pedrosa-Soares, A.C., Alkmim, F.F. de, 2011. How Many Rifting Events Preceded the Development of the Araçuaí-West Congo Orogen? Geonomos 19, 244–251. https://doi.org/10.18285/geonomos.v19i2.56

Pedrosa-Soares, A.C., Alkmim, F.F., Tack, L., Noce, C.M., Babinski, M., Silva, L.C., Martins-Neto, M.A., 2008. Similarities and differences between the Brazilian and African counterparts of the Neoproterozoic Araçuaí-West Congo orogen. Geol. Soc. Spec. Publ. 294, 153–172. https://doi.org/10.1144/SP294.9

Pedrosa-Soares, A.C., Campos, C.P. DE, Noce, C., Silva, L.C., Novo, T., Roncato, J., Medeiros, S., Castañeda, C., Queiroga, G., Dantas, E., Dussin, I., Alkmim, F., 2011b. Late Neoproterozoic – Cambrian granitic magmatism in the Araçuaí orogen (Brazil), the Eastern Brazilian Pegmatite Province and related mineral resources. Geol. Soc. London, Spec. Publ. 350, 25–51.

Pedrosa-Soares, A.C., Noce, C.M., Wiedemann, C.M., Pinto, C.P., 2001. The Araçuaí-West-Congo Orogen in Brazil: An overview of a confined orogen formed during Gondwanaland assembly. Precambrian Res. 110, 307–323.

https://doi.org/10.1016/S0301-9268(01)00174-7

Pedrosa-Soares, A.C., Wiedemann-Leonardos, C.M., 2000. Evolution of Araçuaí Belt and its connection to the Ribeira Belt, eastern Brazil, in: Cordani, U.G., Milani, E.J., Thomaz-Filho, A., Campos, D.A. (Eds.), Tectonic Evolution of South America. 31st International Geological Congress, Rio de Janeiro, pp. 265–285. https://doi.org/10.13140/2.1.3802.5928

Petitgirard, S., Vauchez, A., Egydio-Silva, M., Bruguier, O., Camps, P., Monié, P., Babinski, M., Mondou, M., 2009. Conflicting structural and geochronological data from the Ibituruna quartz-syenite (SE Brazil): Effect of protracted “hot” orogeny and slow cooling rate? Tectonophysics 477, 174–196. https://doi.org/10.1016/j.tecto.2009.02.039

Pinto, V.M., Hartmann, L.A., Santos, J.O.S., McNaughton, N.J., 2015. Zircon ages delimit the provenance of a sand extrudite from the Botucatu Formation in the Paraná volcanic province, Iraí, Brazil. An. Acad. Bras. Cienc. 87, 1611–1622. https://doi.org/10.1590/0001-3765201520130222

Powell, J., Schneider, D., Stockli, D., Fallas, K., 2016. Zircon (U-Th)/He thermochronology of Neoproterozoic strata from the Mackenzie Mountains, Canada: Implications for the Phanerozoic exhumation and deformation history of the northern Canadian Cordillera. Tectonics 35, 663–689. https://doi.org/10.1002/2015TC003989

Rabinowitz, P.D., Labrecque, J., 1979. The Mesozoic South Atlantic ocean and evolution of its continental margins. J. Geophys. Res. 84, 5973–6002. https://doi.org/10.1029/JB084iB11p05973

Rangel, H.D., Flores De Oliveira, J.L., Caixeta, J.M., 2007. Bacia de Jequitinhonha. Bol. Geociencias da Petrobras 15, 475–483.

Read, G., Grutter, H., Winter, S., Luckman, N., Gaunt, F., Thomsen, F., 2004. Stratigraphic relations, kimberlite emplacement and lithospheric thermal evolution, Quiricó Basin, Minas Gerais State, Brazil. Lithos 77, 803–818. https://doi.org/10.1016/j.lithos.2004.04.011

Reiners, P.W., 2005. Zircon (U-TH)/He thermochronometry. Rev. Mineral. Geochemistry 58, 151–179. https://doi.org/10.2138/rmg.2005.58.6

Reiners, P.W., Carlson, R.W., Renne, P.R., Cooper, K.M., Granger, D.E., McLean, N.M., Schoene, B., 2017. Geochronology and Thermochronology. Wiley-Blackwell. https://doi.org/10.1002/9781118455876

Reiners, P.W., Farley, K.A., 2001. Influence of crystal size on apatite (U-Th)/He thermochronology: An example from the Bighorn Mountains, Wyoming. Earth Planet. Sci. Lett. 188, 413–420. https://doi.org/10.1016/S0012-821X(01)00341-7

Reiners, P.W., Farley, K.A., Hickes, H.J., 2002. He diffusion and (U-Th)/He thermochronometry of zircon: Initial results from Fish Canyon Tuff and Gold Butte. Tectonophysics 349, 297–308. https://doi.org/10.1016/S0040-1951(02)00058-6

Reiners, P.W., Spell, T.L., Nicolescu, S., Zanetti, K.A., 2004. Zircon (U-Th)/He thermochronometry: He diffusion and comparisons with 40Ar/39Ar dating. Geochim. Cosmochim. Acta 68, 1857–1887. https://doi.org/10.1016/j.gca.2003.10.021

Rodovalho, N., Gontijo, R.C., Santos, C.F., Milhomem, P.S., 2007. Bacia de Cumuruxatiba. Boletim de Geociências da Petrobras 15(2), 485-491.

Salazar-Mora, C.A., Sacek, V., 2021. Lateral flow of thick continental lithospheric mantle during tectonic quiescence. J. Geodyn. 145, 101830. https://doi.org/10.1016/j.jog.2021.101830

Salomon, E., Passchier, C., Koehn, D., 2017. Asymmetric continental deformation during South Atlantic rifting along southern Brazil and Namibia. Gondwana Res. 51, 170–176. https://doi.org/10.1016/j.gr.2017.08.001

Sampaio, A.R., Martins, A.A.M., Loureiro, H.C., Arcanjo, J.B., Moraes Filho, J.C., Souza, J.D. de;, Pereira, L.H.M., Couto, P.A.A., Santos, R.A. dos;, Melo, R.C., Bento, R.V., Borges, V.P., 2002. Programa levantamentos geológicos básicos do Brasil Projeto extremo sul da Bahia. Salvador.

Schannor, M., 2018. Geodynamic and Metamorphic Evolution of the Araçuaí Orogen (SE Brazil). PhD thesis. Dep. Geologia. Universidade Federal de Ouro Preto Online accessed on November 27th, 2018.

Shuster, D.L., Flowers, R.M., Farley, K.A., 2006. The influence of natural radiation damage on helium diffusion kinetics in apatite. Earth Planet. Sci. Lett. 249, 148–161. https://doi.org/10.1016/j.epsl.2006.07.028

Silva, O.B., Caixeta, J.M., Milhomem, P.S., Kosin, M.D., 2007. Bacia do Recôncavo. Boletim de Geociências da Petrobras 15(2), 423-431.

Skolotnev, S.G., Peyve, A.A., Turko, N.N., 2010. New data on the structure of the Vitoria-Trindade seamount chain (western Brazil basin, South Atlantic). Dokl. Earth Sci. 431, 435–440. https://doi.org/10.1134/S1028334X10040057

Soares, A.P., Soares, P.C., Bettú, D.F., Holz, M., 2007. Compartimentação estrutural da bacia do paraná: A questão dos lineamentos e sua influência na distribuição do Sistema Aquífero Guarani. Geociências 26, 297–311.

Spencer, A., Kohn, B., Gleadow, A., Norman, M., Belton, D., Carter, T., 2004. The importance of residing in a good neighborhood: rechecking the rules of the game for apatite (U-Th)/He thermochronology. In: Andressien, P. (ed.), 10th International Fission Track Dating, Amsterdam, p. 20.

Spiegel, C., Kohn, B., Belton, D., Berner, Z., Gleadow, A., 2009. Apatite (U-Th-Sm)/He thermochronology of rapidly cooled samples: The effect of He implantation. Earth Planet. Sci. Lett. 285, 105–114. https://doi.org/10.1016/j.epsl.2009.05.045

Stockli, D.F., Farley, K.A., Dumitru, T.A., 2000. Calibration of the apatite (U-Th)/He thermochronometer on anexhumed fault block, White Mountains, California. Geology 28, 983–986. https://doi.org/10.1130/0091-7613(2000)28<983:COTAHT>2.0.CO;2

Teixeira, W., Sabaté, P., Barbosa, J., Noce, C.M., Carneiro, M.A., 2000. Archean and Paleoproterozoic tectonic evolution of the São Francisco Craton, Brazil, in: Cordani, U.G., Milani, E.J., Thomaz Filho, A., Campos, D.A. (Eds.), Tectonic Evolution of South America. 31st International Geological Congress, Rio de Janeiro, pp. 101–137.

Thompson, R.N., Gibson, S.A., Mitghell, J.G., Dickin, A.P., Leonardos, O.H., Brod, J.A., Greenwood, J.G., 1998. Migrating Cretaceous-Eocene magmatism in the Serra do Mar Alkaline Province, SE Brazil: melts from the deflected Trindade mantle plume? J. Petrol. 39, 1493–1526. https://doi.org/10.1093/petroj/39.8.1493

Torsvik, T.H., Rousse, S., Labails, C., Smethurst, M.A., 2009. A new scheme for the opening of the South Atlantic Ocean and the dissection of an Aptian salt basin. Geophys. J. Int. 177, 1315–1333. https://doi.org/10.1111/j.1365-246X.2009.04137.x

Trouw, R.A.J., De Wit, M.J., 1999. Relation between the Gondwanide Orogen and contemporaneous intracratonic deformation. J. African Earth Sci. 28, 203–213. https://doi.org/10.1016/S0899-5362(99)00024-X

Turner, J.P., Green, P.F., Holford, S.P., Lawrence, S.R., 2008. Thermal history of the Rio Muni (West Africa)-NE Brazil margins during continental breakup. Earth Planet. Sci. Lett. 270, 354–367. https://doi.org/10.1016/j.epsl.2008.04.002

Uhlein, A., Egydio-Silva, M., Bouchez, J.L., Vauchez, A., 1998. The Rubim pluton (Minas Gerais, Brazil): a petrostructural and magnetic fabric study. J. South Am. Earth Sci. 11, 179–189. https://doi.org/10.1016/S0895-9811(98)00009-1

Van Avendonk, H.J.A., Lavier, L.L., Shillington, D.J., Manatschal, G., 2009. Extension of continental crust at the margin of the eastern Grand Banks, Newfoundland. Tectonophysics 468, 131–148. https://doi.org/10.1016/j.tecto.2008.05.030

Van Ranst, G., Pedrosa-Soares, A.C., Novo, T., Vermeesch, P., De Grave, J., 2020. New insights from low-temperature thermochronology into the tectonic and geomorphologic evolution of the south-eastern Brazilian highlands and passive margin. Geosci. Front. 11, 303–324. https://doi.org/10.1016/j.gsf.2019.05.011

Vauchez, A., Hollanda, M.H.B.M., Monié, P., Mondou, M., Egydio-Silva, M., 2019. Slow cooling and crystallization of the roots of the Neoproterozoic Araçuaí hot orogen (SE Brazil): Implications for rheology, strain distribution, and deformation analysis. Tectonophysics 766, 500–518. https://doi.org/10.1016/j.tecto.2019.05.013

Vaz, P.T., Rezende, N.G.A.M., Wanderley Filho, J.R., Travassos, W.A.S., 2007. Bacia do Parnaíba. Boletim de Geociências da Petrobras 15(2), 253-263.

Wolf, R.A., Farley, K.A., Kass, D.M., 1998. Modeling of the temperature sensitivity of the apatite (U-Th)/He thermochronometer. Chem. Geol. 148, 105–114. https://doi.org/10.1016/S0009-2541(98)00024-2

Wolf, R.A., Farley, K.A., Silver, L.T., 1996. Helium diffusion and low-temperature thermochronometry of apatite. Geochim. Cosmochim. Acta 60, 4231–4240. https://doi.org/10.1016/S0016-7037(96)00192-5

Zeitler, P.K., Herczeg, A.L., McDougall, I., Honda, M., 1987. U-Th-He dating of apatite: A potential thermochronometer. Geochim. Cosmochim. Acta 51, 2865–2868. https://doi.org/10.1016/0016-7037(87)90164-5

5.8 Email de aceite

Abaixo, segue a confirmação de que o artigo em questão foi aceito para publicação no periódico *Tectonophysics*.

Gmail — Edgar do Amaral Santos <santos.eas@gmail.com>

TECTO15114R2 - Editor's decision: accepted for publication
1 mensagem

Tectonophysics <em@editorialmanager.com> 24 de janeiro de 2022 às 04:33
Responder a: Tectonophysics <support@elsevier.com>
Para: Edgar do Amaral Santos <santos.eas@gmail.com>

Dear Mr. Amaral Santos,

I am pleased to inform you that the manuscript "Thermal history along the Araçuaí Orogen and São Francisco Craton border, eastern Brazilian continental margin, based on low-temperature thermochronologic data" (Mr. Edgar do Amaral Santos) has now been accepted by the editor for publication.

Your manuscript will soon be passed to the production department for further handling. Then you will receive further notice.

Your accepted manuscript will now be transferred to our production department and work will begin on creation of the proof. If we need any additional information to create the proof, we will let you know. If not, you will be contacted again in the next few days with a request to approve the proof and to complete a number of online forms that are required for publication.

Thank you for considering our journal for the publication of your research.

Kind regards,

Zheng-Xiang Li
Editor
Tectonophysics

CAPÍTULO 6 – Contrasting thermal histories in the Dom Feliciano Belt triggered by magmatism related to the Paraná-Etendeka LIP and fracture zone proximity

Edgar do Amaral Santos [a,*], *Andréa Ritter Jelinek* [b], *Daniel Stockli* [c], *Frederico Antônio Genezine* [d]

[a] Programa de Pós-Graduação em Geociências, Universidade Federal do Rio Grande do Sul, Brazil

[b] Instituto de Geociências, Universidade Federal do Rio Grande do Sul, Brazil

[c] University of Texas at Austin, United States of America

[d] Instituto de Pesquisas Energéticas e Nucleares, Centro do Reator de Pesquisas, Brazil

* Corresponding author. E-mail address: edgar.amaral@ufrgs.br (E. do Amaral Santos)

Nota explicativa

Este capítulo corresponde ao artigo aceito em 2023 para publicação no periódico *Tectonophysics*, que pode ser encontrado online acessando o link: https://doi.org/10.1016/j.tecto.2023.229841. Ao final do manuscrito encontra-se a carta de aceite da revista científica. Os dados suplementares presentes no artigo também podem ser obtidos acessando o link acima.

Abstract

The present-day southern Brazilian continental margin rests on top of the Dom Feliciano Belt (DFB) and adjacent cratons. This belt formed through the collision of the Rio de La Plata, Kalahari, Paranapanema, Congo and Luis Alves paleoplates in the Neoproterozoic. Several low-temperature thermochronology works were executed in the area, although none of them demonstrated how the basement temperature of the entire DFB evolved through time. To this end, this work aims to provide new Apatite Fission Track (AFT) and Apatite (U-Th)/He (AHe) ages for samples collected in the Catarinense Shield, in the northern DFB, and to perform inverse modeling in those samples. Besides, the collection of the basement temperature of 128 locations across the entire belt and adjacent cratons provided thermal information to create inverse-distance weighted interpolation maps documenting the progression of the temperature from 360 to 30 Ma. New AFT ages range from 126.6 ± 24.1 to 60.3 ± 6.03 Ma, whereas AHe ages span from 153.0 ± 9.2 to 62.5 ± 3.7 Ma. Mean track lengths are short to medium, suggesting complete thermal annealing

of apatite crystals. Apatite single-grain eU concentration range from 4.5 to 96 μg/g and display a sparse correlation with AHe ages. Interpolation maps evidence a contrasting temperature evolution of the northern DFB and bordering cratons relative to the southern segment and surrounding cratons. Near-surface exposure of the basement in the northern segment was possibly much earlier than in the south, followed by partial burial by the sedimentary successions of the Paraná Basin. The emplacement of volcanic rocks of the Paraná-Etendeka Large Igneous Province and associated dyke swarms and alkaline volcanic plugs related to the Florianópolis Fracture Zone raised and sustained higher basement temperatures until 30 Ma, resetting low-temperature thermochronometers in the northern DFB, which was minor to absent in the southern DFB.

6.1 Introduction

Before the opening of the South Atlantic Ocean during the Cretaceous, the southern continental margin of Brazil was in an intracontinental setting. The continent's interior was formed by several terranes of Archean to Proterozoic ages that were contiguous, such as the Rio de La Plata, Kalahari, Paranapanema, Congo, and Luis Alves cratons, forming the Dom Feliciano mobile belt during the Neoproterozoic and composing the West Gondwana paleocontinent (Basei et al., 2008; Hasui, 2010; Oriolo et al., 2017). The continent interior also recorded pulses of exhumation (Milani and De Wit, 2014), deposition of sedimentary successions (Milani et al., 2007a), magmatic and volcanic emplacement of igneous rocks (Stewart et al., 1996; Turner et al., 1994), and the rifting stages of the South Atlantic opening (Chang et al., 1992; Mohriak et al., 2008a). However, to this extent, it is not clear how the basement temperature of the entire Dom Feliciano Belt and adjacent cratons evolved in response to tectonic and magmatic processes during the Phanerozoic.

To investigate this question, we used two low-temperature thermochronometers to retrieve the ages and the thermal information of samples collected in the Catarinense Shield, located in the northern Dom Feliciano Belt, in southern Brazil. We present in this paper 13 new apatite fission track (AFT) ages, 30 single-grain apatite (U-Th)/He analyzes (AHe) and new thermal histories about this region through model inversion (Gallagher, 2012). In addition, interpolation maps for assessing the basement temperature of the entire Dom Feliciano Belt and surrounding cratons during the last 360 Ma were generated using the inverse distance weighted technique after compiling thermal history information of 128 locations. Additionally, we inspected track lengths and AHe-related parameters that

possibly control AHe ages. The new data presented in this study indicate complete thermal resetting of low-temperature thermochronometers from rifting to post-rifting coeval to post-rifting exhumation for samples located in the northern Dom Feliciano Belt. The data provided here also points to a complex thermal evolution for the Rio de La Plata and Luis Alves cratons as well as for the Dom Feliciano Belt, since there are multiple episodes of accelerated cooling as well as reheating episodes and slow cooling. Furthermore, several sources of heat seem to have raised the temperature of the northern Dom Feliciano Belt, which strongly contrasts with the southern segment of the belt.

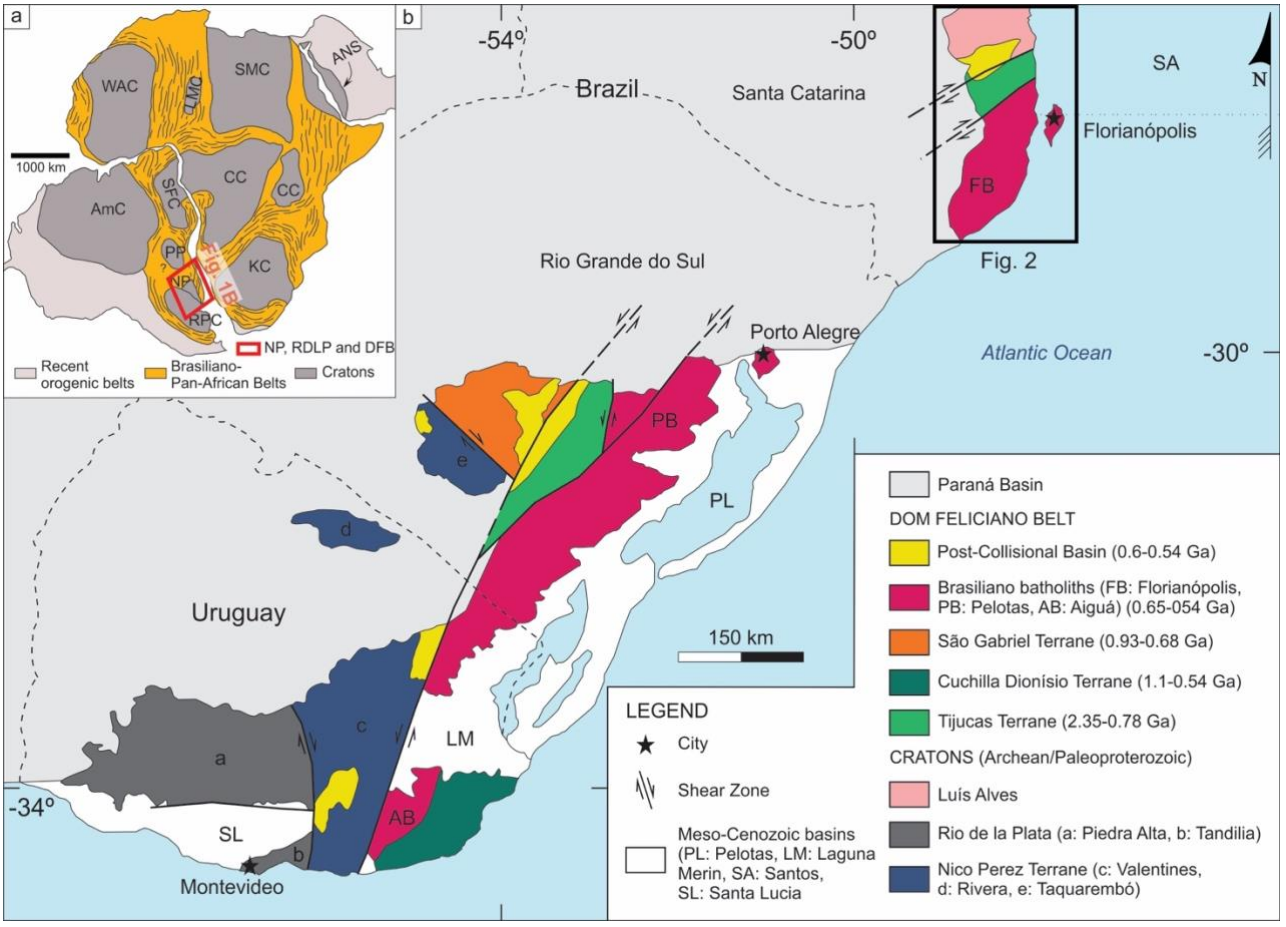

Figure 6. 1: a) West Gondwana map showing the cratonic nuclei, the belts formed in the Brasiliano/Pan-African event, and the recent orogenic belts (after Oriolo et al., 2017). Abbreviations are RDLP: Rio de La Plata Craton; NP: Nico Pérez Terrane; PP: Paranapanema Block; SFC: São Francisco Craton; AmC: Amazon Craton; KC: Kalahari Craton; CC: Congo Craton; LMC: Latea Metacraton; WAC: West Africa Craton; SMC: Sahara Metacraton; ANS: Arabian-Nubian Shield. b) The Dom Feliciano Belt and adjacent cratons along the continental margin of southern Brazil and Uruguay. After CPRM (2008) and Philipp et al. (2016).

6.2 Geological Background

During the Brasiliano/Pan-African orogenic cycle in the Neoproterozoic to the Ordovician, several paleocontinents and microplates of Archean to Proterozoic ages

interacted with each other forming the West Gondwana continent (de Almeida et al., 1981; Hasui, 2010; De Brito Neves and Fuck, 2013) (Fig. 6.1a). This process led to the formation of the Mantiqueira Province, which extends from Uruguay to eastern Brazil. The Dom Feliciano Belt corresponds to the southern segment of this province (Basei, 1985), which is limited by the Rio de La Plata craton and the Nico Perez Terrane to the southwest, the Luís Alves Craton to the north, the South Atlantic Ocean to the east, and the Paleo- to Mesozoic volcanosedimentary units of the Paraná Basin to the west (Hueck et al., 2018b) (Fig. 6.1b).

The Rio de La Plata Craton (RDLP) consists of voluminous granite-gneissic terrains and relics of supracrustal rocks of Paleoproterozoic age (2.2-2.1 Ga), metamorphosed under greenschist facies. The Piedra Alta Terrane corresponds to the main segment of the craton, whereas the Tandilla Terrane outcrops to a lesser extent (Fig. 6.1b) (Oyhantçabal et al., 2018a). The Nico Perez Terrane is subdivided into three blocks that outcrop in Uruguay and Brazil (Fig. 6.1b). These units are composed of orthogneisses, amphibolites, migmatites, mafic-ultramafic igneous rocks, and metasediments of Archean to Paleoproterozoic ages (e.g., Hartmann, 1998; Hartmann et al., 2001; Gaucher et al., 2011; Oriolo et al., 2016; Philipp et al., 2016; Oyhantçabal et al., 2018b). The Luís Alves Craton (LAC) (Fig. 6.1b), a microplate of Archean to Paleoproterozoic age, is composed of a tonalite-trondhjemite-granodiorite suite, mafic-ultramafic bodies and a few paragneisses metamorphosed under medium to high-grade metamorphic granulite (Basei et al., 1992, 1998). Additionally, Neoproterozoic units composed of volcanosedimentary basins and alkaline-peralkaline granitoids are found within the LAC (Passarelli et al., 2018).

The Dom Feliciano Belt (DFB) was assembled in the Neoproterozoic, during the Brasiliano/Pan-African orogenic cycle, when several terranes accreted, juxtaposed along shear zones (Philipp et al., 2016). In this context, the DFB is divided into four terranes and overlying sedimentary basins (Fig. 6.1b). The Cuchilla-Dionísio Terrane, also named Punta del Este Terrane, outcrops only in Uruguayan territory, and is composed of high-grade metamorphic rocks comprised by ortho- and para-derived granulites and migmatites of 800 and 770 Ma, with zircons containing metamorphic overgrowth of 650 Ma. The debate around this unit suggests it may correlate with orthogneisses of the Coastal Terrane in the Kaoko Belt (Basei et al., 2011; Oyhantçabal et al., 2011; Hueck et al., 2018b). The São Gabriel Terrane, located in southern Brazil, comprises two juvenile

arcs and a late-collisional basin, along with records of ophiolite slivers. The older arc developed between 890 and 860 Ma, whereas the younger one evolved between 770 and 720 Ma (Philipp et al., 2018), recording the first stages of the Brasiliano/Pan-African cycle. The Tijucas Terrane encompasses basement inliers of Peloproterozoic age, Statherian metagranites, Calymminian amphibolites, and Neoproterozoic metavolcano-sedimentary complexes (Philipp et al., 2016). The Neoproterozoic Brasiliano batholiths included in the DFB are named (i) Aiguá Batholith, in Uruguay; (ii) Pelotas Batholith on the border between Uruguay to the northeastern region of the Rio Grande do Sul State in Brazil; and (iii) Florianópolis Batholith in the Santa Catarina State in Brazil (Fig 6.1b). These batholiths were generated during and after the Dom Feliciano orogeny and emplaced along high-angle transcurrent shear zones (Philipp et al., 2016). The suites are composed of high-K calc-alkaline granitoids with metaluminous to peraluminous affinity and most intrusions were emplaced between 650 and 550 Ma (Philipp et al., 2016; Philipp and Machado, 2005). Late to post-collisional basins resting on top of the DFB are composed of volcanosedimentary successions dated between 600 and 540 Ma (Paim et al., 2000; Guadagnin et al., 2010), such as the Camaquã and Itajaí basins in Brazil, and Arroyo del Soldado Group in Uruguay. The Archean to Neoproterozoic terranes in Uruguay, Rio Grande do Sul and Santa Catarina are, respectively, named Uruguayan Shield, Sul-Rio-Grandense Shield (SRGS), and Catarinense Shield.

The compressional stresses that promoted the assembly of Gondwana ceased during the Paleozoic, which allowed the erosion and deposition of sediments, forming intracontinental basins. The Paraná Basin is one of these depocenters, composed of a volcanosedimentary package divided into six supersequences formed during the Paleozoic to the Mesozoic and reaching a thickness of nearly 7 km (Milani et al., 2007a). To the west of the study area (Fig. 6.2), the emplacement of the volcanic rocks of the Paraná-Etendeka Large Igneous Province (PELIP) – Serra Geral Formation, peaked at 134 Ma (Turner et al., 1994; Stewart et al., 1996; Janasi et al., 2011; Florisbal et al., 2014), covering most of the previous sedimentary successions of the Paraná Basin and possibly portions of the DFB.

Contemporaneous to the upper supersequences of the Paraná Basin, the opening of the South Atlantic Ocean in the Cretaceous (Nürnberg and Müller, 1991; Chang et al., 1992; Torsvik et al., 2009) led to the formation of several passive margin basins as well as important fracture zones. Eastward of the study area, the mostly offshore Pelotas and

Santos Basins developed on top of the Catarinense Shield, accumulating a thick sedimentary pile in the continental margin (Bueno et al., 2007; Milani et al., 2007b). The Pelotas Basin is mainly characterized as a volcanic margin, with thick wedges of seaward-dipping reflectors extending from the Florianópolis region to Argentina (Bueno et al., 2007b; Bueno, 2021). On the other hand, the Santos Basin lacks the expressive volcanism of the Pelotas Basin, although it has records of a thick evaporite layer that is absent in the Pelotas Basin (Talwani and Abreu, 2000; Milani et al., 2007b; Moreira et al., 2007). Significant fracture zones also developed simultaneously with the opening of the South Atlantic Ocean, such as the Florianópolis Fracture Zone (São Paulo ridge), in E-W direction (Gamboa and Rabinowitz, 1981), which is expressed as a volcanic high that extends from the oceanic crust towards the platform near Florianópolis (Mohriak et al., 2008b; Mohriak and Fainstein, 2012).

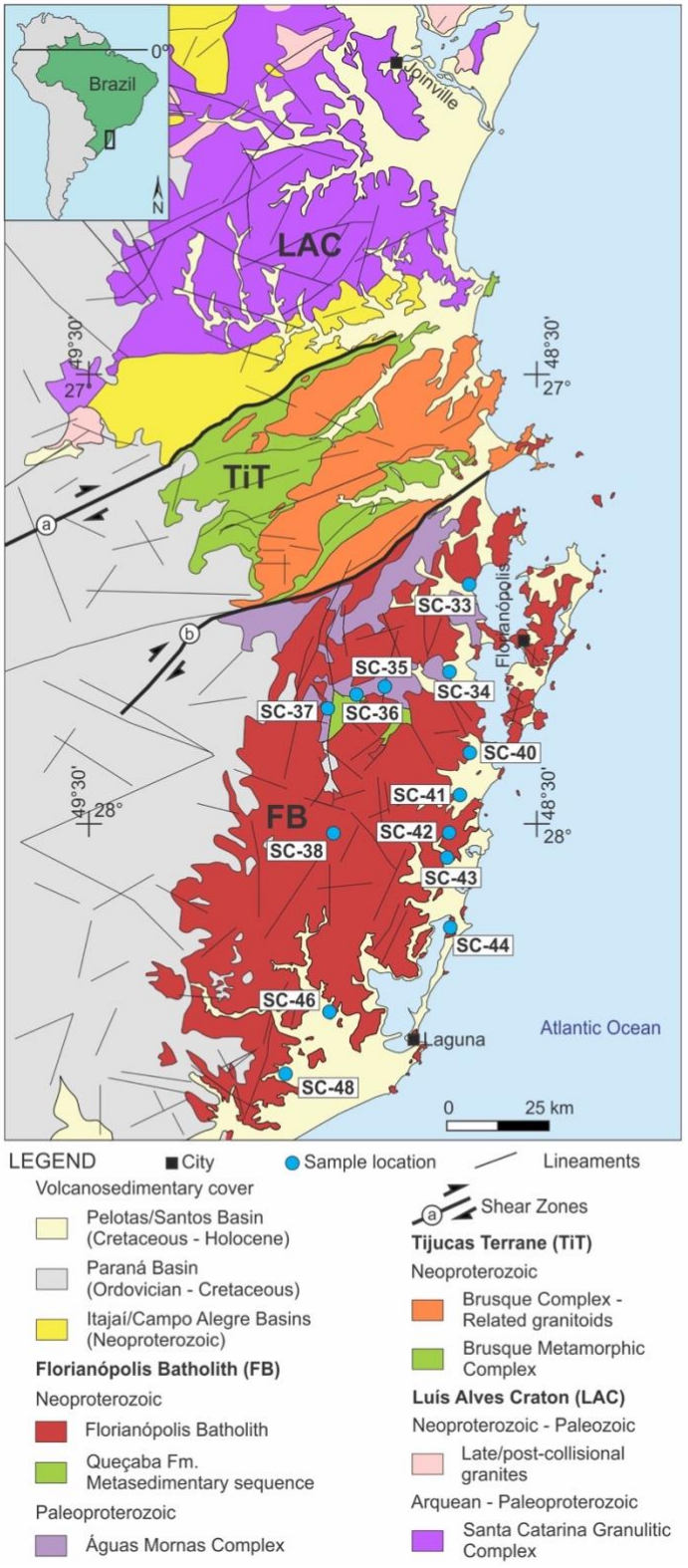

Figure 6. 2: The study area of this work comprises the Catarinense Shield and its main terranes. Sampling sites are shown in the figure and were restricted to the Florianópolis Batholith. Shear Zones: a: Itajaí-Perimbó Shear Zone; b: Major-Gercino Shear Zone. After CPRM (2014).

6.3 Sampling and analytical methods

6.3.1 Sampling approach

For this study, basement samples were collected from 13 outcrops over southern Brazil in the eastern portion of the Florianópolis Batholith in the Catarinense Shield, of Neoproterozoic age. We targeted lithologies rich in apatites (granites and gneisses) and we avoided locations that were already sampled in other studies. The collection of samples also followed two main transects of N-S and W-E direction to evaluate spatial variations in thermochronological results. Sampling along vertical profiles was not possible, because the study area presents low topographic prominence, where the average elevation is below 500 m and the highest peak is nearly 1.200 m above sea level. The details of the lithology, geographical location, elevation, shortest distance to the coast, and analytical methods performed in each sample are found in Table 6.1. Standard crushing, sieving, magnetic, heavy liquids, and hand-picking methods were performed to obtain the apatite crystal separates for both apatite fission track and apatite (U-Th)/He analyzes.

Table 6. 1: Details from samples analyzed in this study. Coordinates were acquired in UTM zone 22 J, datum WGS84; Dist. Coast: The distance to the Atlantic Ocean; m.a.s.l.: meters above sea level; AFT: Apatite Fission Track dating; AHe: Apatite (U–Th)/He dating.

Sample	Lithology	Easting	Northing	Elevation (m)	Dist. Coast (km)	Method
SC-33	Granitoid	732,808	6,958,339	12	0.07	AFT
SC-34	Granitoid	727,765	6,937,434	11	3.8	AFT, AHe
SC-35	Granitoid	713,930	6,933,863	150	17.9	AFT
SC-36	Granitoid	706,461	6,931,782	175	25.7	AFT, AHe
SC-37	Granitoid	700,942	6,929,205	162	31.7	AFT
SC-38	Granitoid	701,100	6,898,422	236	31.8	AFT, AHe
SC-40	Granitoid	732,504	6,917,226	3	3.5	AFT
SC-41	Granitoid	713,930	6,933,863	5	4.6	AFT, AHe
SC-42	Granitoid	726,544	6,898,593	63	6.5	AFT
SC-43	Granitoid	725,429	6,889,783	10	6.8	AFT
SC-44	Granitoid	725,542	6,873,041	17	2.6	AFT, AHe
SC-46	Granitoid	699,198	6,851,964	13	19.8	AFT, AHe
SC-48	Granitoid	690,289	6,839,148	5	14.6	AFT

6.3.2 Low-temperature thermochronometry

To investigate the Phanerozoic thermotectonic evolution of the Catarinense Shield and then compare it with the evolution of the entire DFB, this study applied a joint use of two low-temperature thermochronometers: apatite fission-track (AFT) and apatite (U-

Th)/He (AHe). These radio-isotopic systems have different temperatures in which the radiogenic isotopes or features retained within the crystal lattice. Such retention occurs in the temperature interval of ca. 120 and 40 ºC, which is compatible with the shallower portions of the crust. At temperatures higher than the specified range of each thermochronometer, radiogenic products are lost through diffusion/annealing and the apparent age tends to zero.

6.3.2.1 Apatite Fission-Track

The apatite fission-track method is based on the spontaneous fission of ^{238}U that generates linear defects in the apatite crystal lattice. The accumulation of these features is analyzed in terms of their areal density and length, providing the age and the thermal history that a sample has experienced (Price & Walker, 1963; Fleischer et al., 1975). At temperatures higher than 120 ºC apatites rapidly anneal, whereas they are stable in temperatures below 60 ºC in geological time scales. When apatites are in the temperature interval ranging from 120 to 60 ºC, their fission tracks shrink, specifying a temperature window called the apatite fission-track partial annealing zone (AFTPAZ - Gleadow & Duddy, 1981; Gleadow et al., 1986; Green et al., 1986). Temperature is the main factor controlling annealing, even though the apatite chemical composition and the radiation damage are also fundamental factors playing a role in track-fading (Carlson et al., 1999; Barbarand et al., 2003a; Tagami & O'Sullivan, 2005). The areal density of natural, spontaneous tracks relative to the areal density of induced tracks formed after neutron irradiation in a nuclear reactor will provide the apparent age for this sample (Tagami and O'Sullivan, 2005; Reiners et al., 2017). The track-length frequency obtained from horizontal confined fission tracks (Laslett et al., 1982), on the other hand, will provide information regarding the sample's thermal history (Barbarand et al., 2003b; Gleadow et al., 1986).

In this study, the external detector method (EDM; Hurford, 1990) was used. For that, aliquots of apatite crystals from 13 samples were mounted in epoxy resin, polished to expose internal surfaces, and chemically etched with 5.5M HNO3 at 21 ºC for 20 s to reveal the spontaneous fission tracks (Carlson et al., 1999). Low-uranium muscovite sheets were closely attached to the apatite crystals, U-doped glass dosimeters (CN5), and Durango age standards. Then, the mounts were placed in irradiation cans forming a stack and they were sent to be neutron-irradiated at the IEA-R1, IPEN-CNEN Reactor,

São Paulo, Brazil. Next, the muscovite sheets were etched in 48% HF at 20 ºC for 18 min to reveal the induced fission tracks (Fleischer and Price, 1964). Samples were dated at LabModel, a thermochronology facility in the Universidade Federal do Rio Grande do Sul. Leica CTR 6000 microscope paired with Leica Application Suite (LAS) software, at 1,000 x (dry) magnification, were used to conduct track-count and track-length measurements. AFT ages were calculated based on measurements of at least 20 grains whenever possible, although some samples did not attain that. Calibration of those ages was made according to the □-calibration method (Hurford and Green, 1983; Hurford, 1990) and reported as central ages (Galbraith and Laslett, 1993). Chi-squared test to evaluate the AFT ages homogeneity was carried (Galbraith, 1981; Galbraith and Green, 1990) using the RadialPlotter, version 9.4 (Vermeesch, 2009) and fission-track age errors are reported at the 1σ confidence level. With the purpose to analyze the thermal history, we aimed at measuring the length and the c-axis angles of 100 horizontal confined fission tracks in each sample, although most samples failed this criterion. Projection of horizontal confined tracks on the c-axis was also applied since the annealing rates are affected by the orientation of fission tracks relative to this axis (Donelick et al., 1999; Ketcham et al., 2007). The arithmetic mean of about 100 fission-track etch pit diameters (Dpar; e.g. Donelick et al., 2005) were measured as a proxy for apatite composition, which is also a contributing factor to the annealing of the fission tracks.

6.3.2.2 Apatite (U-Th)/He

The fundamentals of the (U-Th)/He dating rely on the radioactive decay of the ^{238}U, ^{235}U, ^{232}Th, and ^{147}Sm isotopes producing α nuclei (^{4}He), which are retained within the apatite lattice (Reiners et al., 2017). At high temperatures, the apatite crystal loses the radiogenic particle by thermally activated volume diffusion, consequently resulting in an age of zero. On the other hand, at lower temperatures, ^{4}He starts to accumulate, which is defined at ca. 70 ºC for the apatite (U-Th)/He thermochronometer. Concurrent production and loss of ^{4}He occurs in the temperature window of 70 to 40 ºC, defining the apatite (U-Th)/He partial retention zone (AHePRZ - Wolf et al., 1996, 1998; Stockli et al., 2000; Farley, 2002). Below 40 ºC, full retention of ^{4}He occurs. The apatite (U-Th)/He age and the limits of the AHePRZ may be affected by many factors, such as crystal size (e.g., Reiners and Farley, 2001; Brown et al., 2013), effective uranium concentration – eU (e.g., Flowers et al., 2009; Reiners et al., 2017), parent nuclide zonation (Farley, 2000; Reiners

et al., 2017), radiation damage (Shuster et al., 2006; Flowers et al., 2009), high U and Th content in the neighboring crystals (Spiegel et al., 2009; Murray et al., 2014), presence of micro-inclusions rich in U and Th (Fitzgerald et al., 2006), and cooling rates (Ault and Flowers, 2012; Reiners et al., 2017). Samples experiencing monotonic cooling and long residence within the AHePRZ may enhance the effects of the aforementioned factors, sometimes resulting in dispersed AHe ages (Ault and Flowers, 2012; Green and Duddy, 2018).

For the apatite (U-Th)/He technique, four to seven single crystals of six samples were analyzed at the University of Texas at Austin, in the UTChron – (U-Th)/He and U-Pb Geo-Thermochronometry Laboratory. A Nikon SMZ-U/100 stereomicroscope coupled with Nikon cameras was used to select the apatite crystals considering their size, morphology, and absence of visible inclusions and coating. Samples had their dimensions measured for alpha-eject correction (Ft; Farley et al., 1996) and crystals were photographed. Selected crystals were 94.86 to 302.57 μm long and 49.26 to 142.78 μm wide, in most cases having two terminations. The chosen aliquots were added in Pt tubes, followed by degassing under heating conditions imposed by the Nd-YAG laser. A quadrupole mass spectrometer then measured and quantified the extracted gas. Subsequently, the crystals were reclaimed and dissolved in 65% HNO3 for isotopic determination (U, Th, and Sm) in an Element2 HR-ICP-MS.

6.3.2.3 Thermal history inversion

In this study, the software QTQt, version 5.7.2K, was used for inverse modeling (Gallagher et al., 2009; Gallagher, 2012) that employs the Bayesian transdimensional Markov Chain Monte Carlo (MCMC) approach to data inversion. Dpar measurements and c-axis projection of horizontal confined fission tracks (Ketcham et al., 2007) were used to model AFT data, whereas the radiation damage accumulation and annealing model (RDAAM; Flowers et al., 2009) was applied to model AHe data. A single time-temperature constraint representing the present-day surface temperature was set at 20 ± 10 ºC. The prior for temperature was set at 70 ± 70 ºC. The prior for time (to ± to) was set as the oldest AFT age or raw AHe age of each sample. The maximum $\partial T/\partial t$ was set at 30 ºC/m.y.

Trial models containing only AFT data were performed at first because this method is more reliable and provides a more accurate description of the thermal history when

compared to AHe technique, as suggested by Green and Duddy (2018). Then, AHe data was incorporated into these models. Appropriate values for the MCMC algorithm were defined after initial runs of 30,000 iterations. These values were then applied for runs of at least 200,000 random paths.

6.3.2.4 Previous thermochronology studies and data integration

This study follows the work of Krob et al. (2019) and Machado et al. (2021) that used interpolated maps of temperature through time, integrating both data sets into a single study, coupled with new AFT and AHe data. Apatite fission track, apatite and zircon (U-Th)/He data associated with AFT data from both the northern and southern Dom Feliciano Belt and surrounding cratons as well associated thermal histories were compiled from Borba et al. (2002, 2003), Jelinek et al. (2003), Gomes (2011), Kollenz (2015), Oliveira et al. (2016), Gomes and Almeida (2019), Krob et al. (2019), and Machado et al. (2019, 2020). These studies provided the basement thermal information for 128 different locations across the DFB and Rio de la Plata and Luís Alves cratons ranging from 360 to 30 Ma (Supplementary Table 6.1). The compilation excluded AFT/AHe data collected from borehole samples and that did not have thermal models available. The T-t plots available in the literature list were not remodeled, but had their modelled temperatures compiled at specific time intervals. Most of the thermal histories reconstructed rely only on AFT data (e.g., although some others integrated AFT with zircon fission track, zircon (U-Th)/He, and apatite (U-Th)/He thermochronometers (e.g. Oliveira et al., 2016; Hueck et al., 2018; Machado et al., 2021). One study used numerical modeling combining low-temperature thermochronometers with K/Ar, 40Ar/39Ar, U-Pb, Sm-Nd, and Rb-Sr geochronological data for reconstructing the entire thermal history of the samples (Krob et al., 2019), which also incorporated a Paleozoic constraint acknowledging the sedimentary deposition of the Paraná Basin sequences, with temperatures similar to the present-day conditions.

From each thermal model available, the temperature at 12 specific times was obtained from the mean path. With these data for each point, interpolation maps were generated using the Inverse Distance Weighted (IDW) technique, from ArcToolbox, in the software ArcGIS 10.3. The main purpose of such interpolation maps is to have a broad view of the thermal evolution of southern Brazil and Uruguay as well as pinpoint any distinct thermal prints that may distinguish terranes, fault zones, or regions.

6.4 Results

6.4.1 Apatite Fission-Track

We present new AFT data results of 13 samples collected in the Florianópolis Batholith, northern DFB, summarized in Table 6.2. All AFT ages passed the χ^2 test ($P(\chi^2) > 0.05$) and the single grain ages showed no dispersion, indicating that the central ages correlate to a single population. AFT central ages of this study are displayed in Figure 6.3 along with AFT and AHe ages available in the literature. The new ages vary from 126.6 ± 24.1 to 60.3 ± 6.03 Ma, which are mostly Mesozoic (Lower to Upper Cretaceous) with the majority corresponding to the Upper Cretaceous Epoch. Sample SC-36 is the exception in this data set, since its AFT age is the youngest and the only one of the Paleocene Epoch. It was possible to acquire track-length and c-axis angle information from only 10 samples. Three samples lack information regarding AFT length/angle data and one sample did not yield sufficient lengths for a reliable representation of length distribution. Mean horizontal confined fission-track lengths (MTL) data are displayed in Table 6.2 and Fig. 6.4a. Overall, MTL is short to medium-sized (9.08 to 12.44 μm), showing unimodal distribution, and the standard deviation is narrow (Table 6.2 and Fig. 6.4b). MTL versus Standard Deviation shows a broad negative correlation between these parameters (Fig. 6.4c). Skewness is variable amongst samples: most of the data set is moderately negative, comprising five samples with values ranging between -0.94 and -0.55). Four samples are symmetrical, and their values span from -0.48 to 0.38, and one sample is moderately positive (value of 0.98). Dpar values range from 1.33 to 1.54 μm.

The trends of AFT ages versus elevation (Fig. 6.5a) and the shortest distance to the coastline (Fig. 6.5b) are essentially diffuse, suggesting that these parameters exert little influence on AFT ages of this data set.

Table 6. 2: New Apatite Fission Track data from the Catarinense Shield, in the northern Dom Feliciano Belt, southern Brazil. Underscore italic data are outliers, which were discarded from inversion.

Sample	**N**	**rs (Ns)**	**ri (Ni)**	**rd (Nd)**	**P (c2)**	**U**	**Centr. Age ± 1s**	**n**	**MTL**	**Std. Dev.**	**P.MTL**	**P.Std. Dev.**	**Dpar**	**Skewness**
	#	($x10^5$)	($x10^5$)	($x10^5$)	(%)	(∝g/g)	(Ma)	#	(∝m)	(∝m)	(∝m)	(∝m)	(∝m)	
SC-33	16	7.68 (53)	7.83 (54)	8.14 (16,276)	1	12.2	126.6 ± 24.1	*	*	*	*	*	*	*
SC-34	20	9.55 (85)	12.58 (112)	8.14 (16,276)	1	20.1	98.1 ± 14.7	16	11.59	1.89	13.39	1.44	1.41	-0,58
SC-35	20	17.75 (142)	15.88 (127)	6.06 (6,055)	0,99	33.3	107.5 ± 12.9	100	12.44	1.68	13.78	1.35	1.46	-0,94
SC-36	20	16.94 (144)	36.47 (310)	8.14 (16,276)	1	56.9	60.3 ± 6.0	100	12.24	1.66	13.75	1.13	1.37	-0,27
SC-37	20	10.69 (124)	19.14 (222)	8.14 (16,276)	0,98	29.9	72.4 ± 8.0	57	11.92	1.77	13.47	1.31	1.40	-0,55
SC-38	20	9.80 (98)	15.30 (153)	8.14 (16,276)	1	23.9	82.9 ± 10.8	76	11.93	1.88	13.49	1.41	1.54	-0,1
SC-40	20	7.08 (68)	8.85 (85)	8.14 (16,276)	0,98	13.8	103.4 ± 16.5	*	*	*	*	*	*	*
SC-41	20	13.00 (104)	13.38 (107)	6.06 (6,055)	1	28.1	93.6 ± 13.1	100	12.06	1.93	13.55	1.39	1.49	-0,63
SC-42	16	15.96 (217)	27.21 (370)	8.14 (16,276)	0,96	42.5	76.0 ± 6.8	16	11.81	1.56	13.48	1.3	1.33	-0,48
SC-43	20	7.15 (118)	8.30 (137)	8.14 (16,276)	0,96	13.0	111.3 ± 14.5	*	*	*	*	*	*	*
SC-44	20	15.50 (124)	22.75 (182)	8.14 (16,276)	0,89	35.5	88.2 ± 10.6	43	10.87	1.71	12.77	1.24	1.40	0,38
SC-46	20	13.75 (110)	17.75 (142)	8.14 (16,276)	1	27.7	100.2 ± 13.0	43	11.90	2.25	13.59	1.47	1.50	-0,81
SC-48	20	12.95 (101)	17.31 (135)	8.14 (16,276)	0,87	27.0	96.8 ± 12.6	6	9.08	2.90	11.83	2.12	1.37	0,98

N: number of apatite crystals analyzed to determine track densities; rs: measured spontaneous track density; Ns: number of spontaneous tracks counted; ri: measured induced track density; Ni: number of induced tracks counted; rd: track density measured in external detector adjacent to glass dosimeter during irradiation; Nd: number of tracks counted in determining rd; P (c2): chi-squared probability; n: number of confined track lengths measured; * no horizontal confined track length measured; Centr. Age: Central Age; Std. Dev.: Standard Deviation; P.MTL: Projected mean track length; P.Std. Dev.: Standard Deviation of Projected mean track length

Apatite ages calculated using a zeta of 320.24 ± 6.84 for CN5 glass on Brazil reactor.

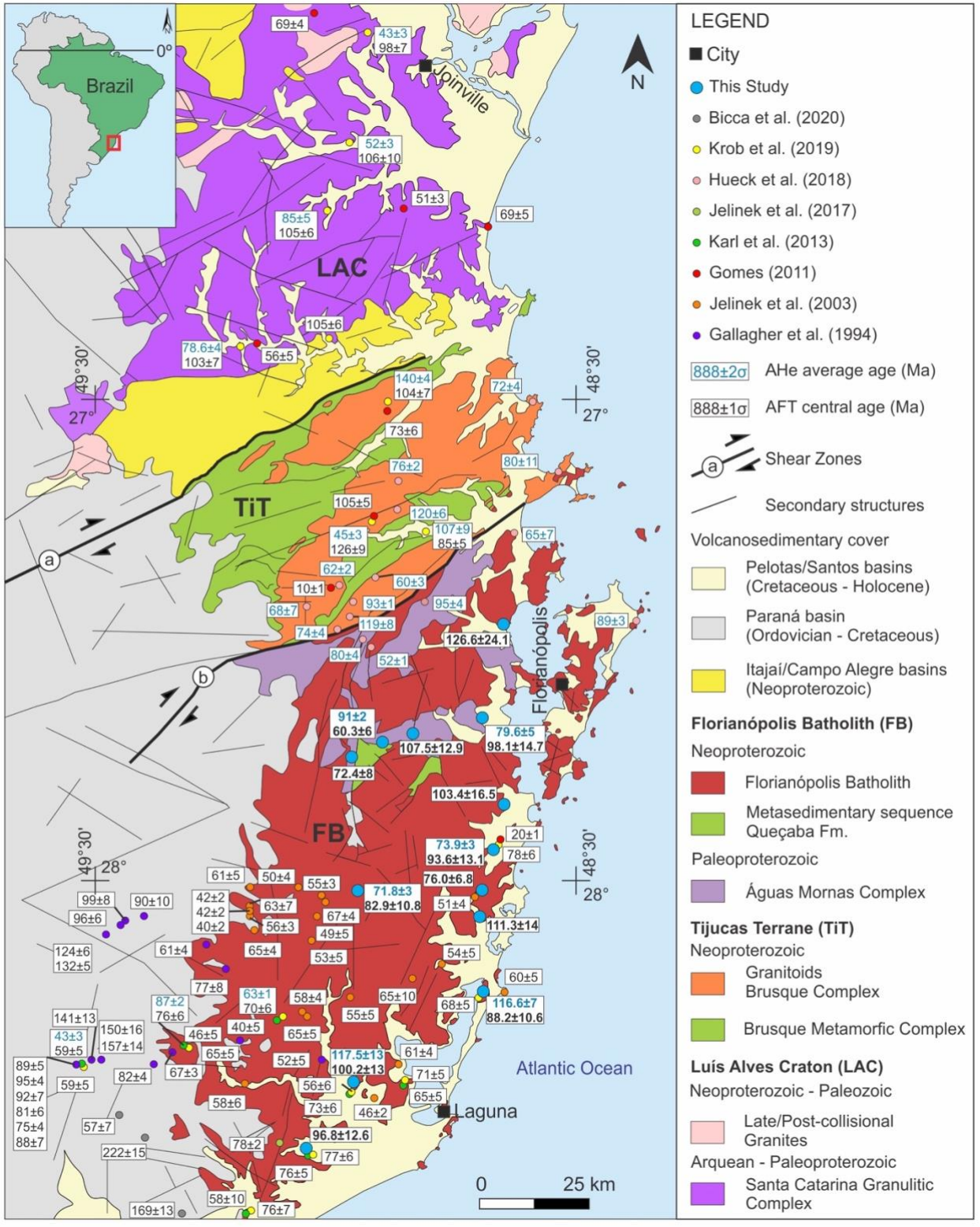

Figure 6. 3: Compilation of Apatite Fission Track and Apatite (U–Th)/He ages available for the Catarinense Shield and surrounding sediments. Results presented in this study are shown in bold. After CPRM (2014) and (Jelinek et al., 2021).

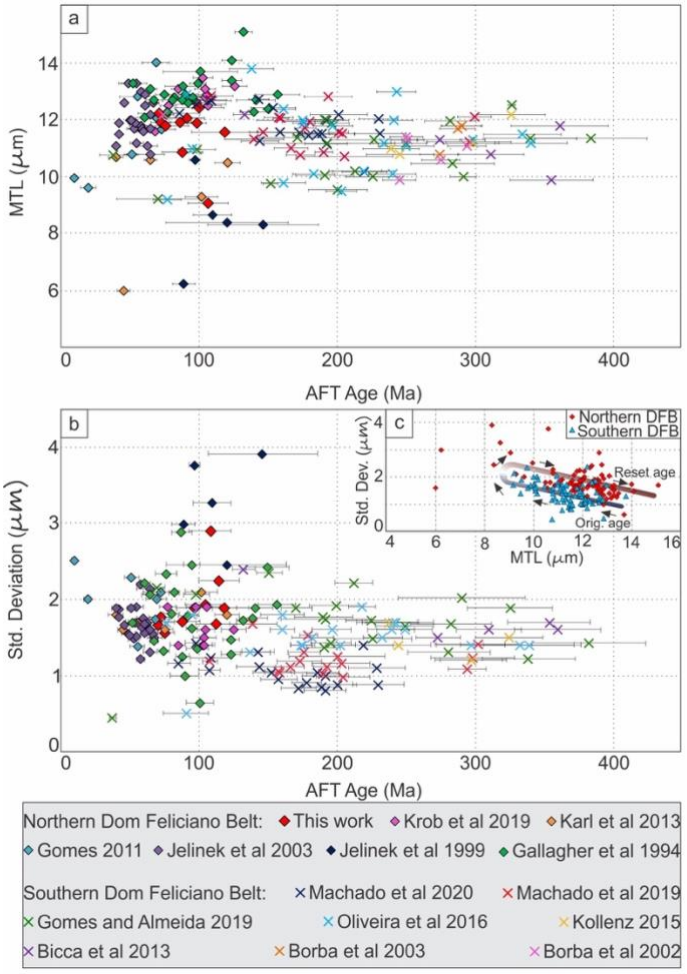

Figure 6. 4: Compiled Apatite Fission Track (AFT) ages of this study and from the literature plotted against a) Mean Track Length (MTL) and b) Standard Deviation (Std. Dev). c) Mean Track Lengths versus Standard Deviation. The AFT ages of the Uruguayan and Sul-Rio-Grandense shield are somewhat similar and grouped into the "Southern Dom Feliciano Belt" data set. AFT ages for the northern and southern Dom Feliciano Belt are shown as diamonds and X shapes, respectively. Error bars (1σ) are shown in the charts. Abbreviation is Orig. age: original age.

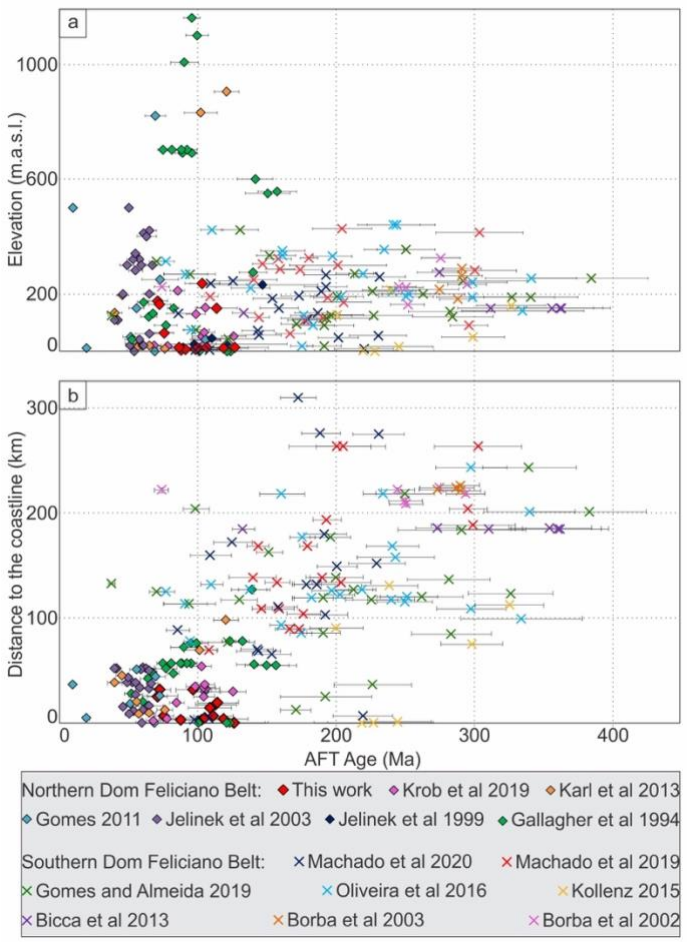

Figure 6. 5: Compiled central Apatite Fission Track ages (AFT) of this study and available in the literature plotted against a) Elevation; b) Distance to the coastline. Error bars (1σ) are shown in the charts. Abbreviation is: m.a.s.l.: meters above sea level.

6.4.2 Apatite (U-Th)/He

Table 6.3 presents the results of Apatite (U-Th)/He data. A sum of 34 apatite crystals was dated from six different locations. From this data set, four outliers were detected, were discarded from inversion and discussion (data in underscore italic on Table 6.3). Corrected AHe ages (Ft; Farley et al., 1996) are essentially Mesozoic (90%), spanning from 153.0 ± 9.2 to 62.5 ± 3.7 Ma. The standard deviation of AHe ages spans from 4.57 to 26.16 Ma and uncertainties (2σ) are within 2.5 and 11.1%. Apatite single grain eU concentration varies from 4.5 to 96 μg/g, lacking a correlation between this parameter and the corrected AHe ages (Fig. 6.5a). Equivalent Spherical Radius (ESR) ranges between 26.4 to 72.4 μm and its correlation with AHe ages is absent (Fig. 6.6b). The elevation and the distance to the coastline versus AHe ages produces a sparse correlation between these parameters (Fig. 6.6c and 6.6d).

*Table 6. 3: Summary of Apatite (U–Th)/He ages and parameters; The abbreviations reported in table are: eU: effective uranium, calculated as eUμg/g = [Uμg/g + (0.235*Thμg/ g) + 0.00463*Smμg/g)]; Ft: Correction Factor after (Farley et al., 1996); ESR: Equivalent Spherical Radius; Corr.: Corrected; SD: Standard Deviation; Aver.: Average. Italic and underscored data point to outlier samples (outliers) and discarded from inversion.*

Sample	Grain #	He (nmol/g)	U (∝g/g)	Th (∝g/g)	Sm (∝g/g)	eU (∝g/g)	Mass (∝g)	ESR (∝m)	Raw Age (Ma)	± 2s (Ma)	Ft #	Corr. Age (Ma)	± 2s (Ma)	Aver. Corr. (Ma)	± 2s (Ma)	SD (Ma)
SC-34	1	4,7	9,2	27,7	513,7	18,2	2,9	47,4	43,0	2,58	0,67	64,0	3,8	79,64	4,82	12,75
SC-34	2	3,1	5,4	17,1	371,4	11,2	4,1	47,7	46,1	2,77	0,67	68,4	4,1			
SC-34	3	1,9	2,9	7,6	191,3	5,6	2,6	45,0	56,4	3,38	0,66	85,7	5,1			
SC-34	4	2,7	5,1	15,0	321,4	10,1	1,9	41,0	43,9	2,63	0,63	70,0	4,2			
SC-34	6	4,5	6,8	17,9	384,8	12,8	3,1	50,7	58,4	3,51	0,69	84,3	5,1			
SC-34	7	1,8	1,9	7,8	154,1	4,5	1,8	43,2	64,4	3,86	0,64	100,3	6,0			
SC-34	8	4,1	6,4	20,3	397,2	13,0	1,7	40,2	52,6	3,16	0,62	84,8	5,1			
SC-36	*1*	*27,1*	*84,8*	*20,0*	*423,8*	*91,5*	*4,5*	*56,1*	*53,8*	*3,23*	*0,74*	*72,9*	*4,4*	91,05	2,29	4,57
SC-36	2	13,4	29,4	4,6	226,8	31,6	9,0	72,4	76,1	4,57	0,80	95,7	5,7			
SC-36	*3*	*27,9*	*55,7*	*11,0*	*337,8*	*59,9*	*2,9*	*47,6*	*84,2*	*5,05*	*0,70*	*120,8*	*7,2*			
SC-36	4	26,6	74,1	19,4	403,9	80,6	2,9	49,8	60,0	3,60	0,71	84,9	5,1			
SC-36	5	23,7	59,1	8,3	312,5	62,6	5,4	59,8	68,6	4,12	0,76	90,8	5,4			
SC-36	6	32,6	86,2	32,2	473,1	96,0	2,2	43,1	61,6	3,70	0,66	92,7	5,6			
SC-38	1	3,7	8,1	19,6	260,7	13,9	1,0	33,8	45,7	2,74	0,56	81,2	4,9	71,81	3,27	7,30
SC-38	3	8,4	16,1	47,1	480,9	29,3	2,4	45,7	50,1	3,00	0,66	75,6	4,5			
SC-38	4	5,4	10,0	34,6	452,4	20,2	5,0	59,5	45,8	2,75	0,73	62,5	3,7			
SC-38	5	4,0	7,3	26,0	313,6	14,9	3,4	50,4	46,2	2,77	0,69	67,0	4,0			
SC-38	6	11,6	21,2	67,0	670,7	40,0	3,3	51,3	50,6	3,03	0,69	72,8	4,4			
SC-38	*7*	*12,4*	*15,8*	*57,4*	*517,9*	*31,6*	*3,4*	*52,1*	*68,2*	*4,09*	*0,70*	*97,7*	*5,9*			
SC-41	1	3,7	6,6	14,1	259,1	11,1	3,8	50,2	56,4	3,38	0,69	81,6	4,9	73,97	2,82	6,29
SC-41	*2*	*7,2*	*10,9*	*27,0*	*427,9*	*19,3*	*2,5*	*41,8*	*64,0*	*3,84*	*0,64*	*100,7*	*6,0*			
SC-41	3	9,9	20,8	54,0	401,4	35,2	2,3	45,4	49,7	2,98	0,66	75,3	4,5			
SC-41	4	5,7	15,0	38,7	396,3	25,9	1,0	32,3	38,5	2,31	0,54	70,7	4,2			
SC-41	5	6,5	11,4	32,9	438,3	21,1	3,9	48,9	52,6	3,16	0,68	77,1	4,6			
SC-41	6	6,3	14,3	42,9	368,1	26,0	2,6	43,9	42,3	2,54	0,65	65,2	3,9			
SC-44	2	7,2	13,3	45,5	229,0	25,0	0,6	28,7	51,5	3,09	0,49	104,2	6,3	116,65	6,71	15,00
SC-44	5	10,5	14,1	51,5	359,5	27,8	1,6	41,8	66,1	3,97	0,63	104,5	6,3			
SC-44	6	25,4	31,6	123,0	548,8	62,6	0,7	30,2	71,8	4,31	0,51	139,9	8,4			
SC-44	7	20,1	23,5	91,9	453,0	46,9	2,5	48,3	75,7	4,54	0,68	112,0	6,7			
SC-44	8	7,1	10,2	24,9	186,7	16,9	1,3	38,1	74,1	4,45	0,60	122,6	7,4			
SC-46	1	14,1	16,7	54,5	381,7	31,2	3,2	49,0	79,5	4,77	0,68	116,7	7,0	117,55	13,08	26,16
SC-46	2	8,2	7,4	20,6	273,8	13,5	2,8	48,3	103,8	6,23	0,68	153,0	9,2			
SC-46	5	12,0	23,9	103,9	667,9	51,2	0,5	26,4	41,2	2,47	0,46	90,3	5,4			
SC-46	7	10,0	16,1	44,7	345,8	28,1	1,0	34,3	62,5	3,75	0,57	110,3	6,6			

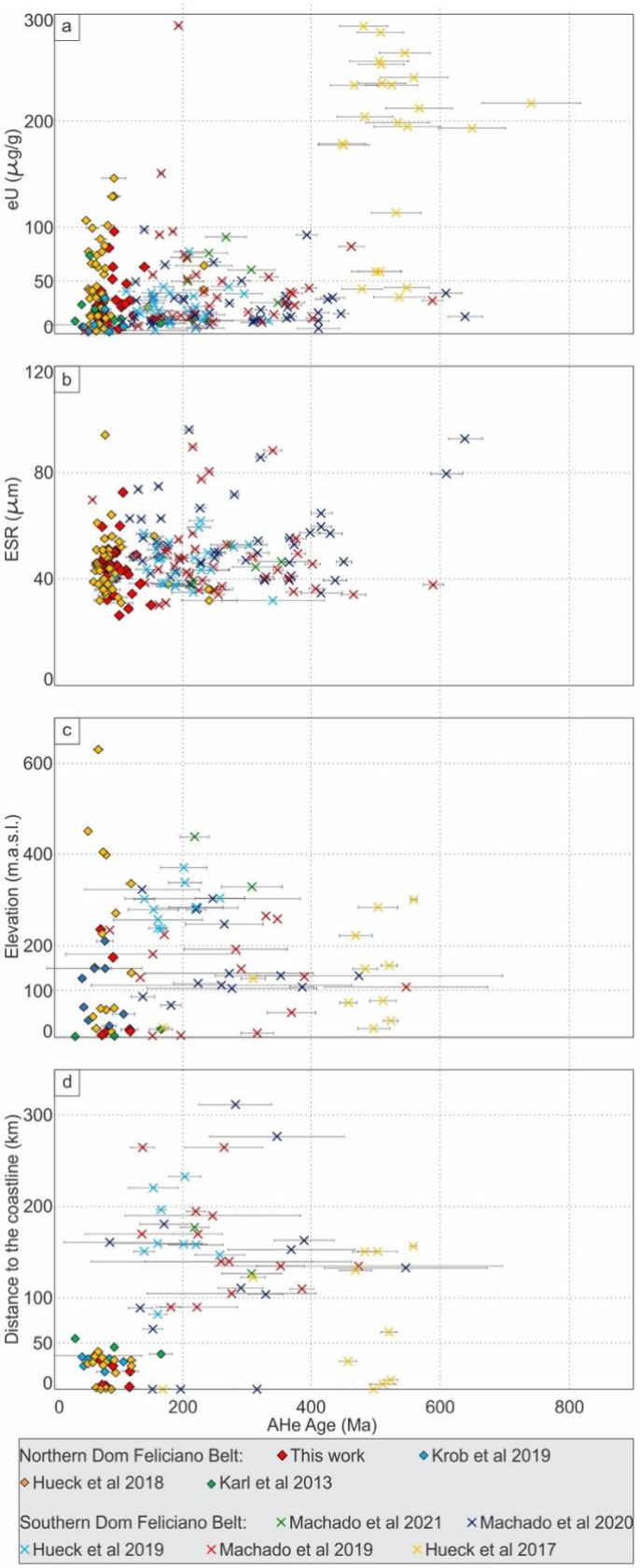
a
eU (μg/g)
300
200
100
50
0
b
ESR (μm)
120
80
40
0
c
Elevation (m.a.s.l.)
600
400
200
100
0
d
Distance to the coastline (km)
300
200
100
50
0
0
200
400
600
800
AHe Age (Ma)
Northern Dom Feliciano Belt:
This work
Krob et al 2019
Hueck et al 2018
Karl et al 2013
Southern Dom Feliciano Belt:
Machado et al 2021
Machado et al 2020
Hueck et al 2019
Machado et al 2019
Hueck et al 2017

Figure 6. 6: Apatite (U–Th)/He ages for all crystals analyzed in this study and available in the literature plotted against a) Effective uranium concentration (eU), b) Equivalent Spherical Radius (ESR). Mean Apatite (U–Th)/He ages in each sample of this study and in the literature plotted against c) Elevation and d) Distance to the coastline. Error bars (2σ) are shown for each sample.

6.4.3 Thermal history modeling

Fig. 6.7 presents the thermal histories modelled for 10 samples and the remaining samples were not modeled because they did not yield enough track length data. Models containing AFT and AHe data constrain both higher and lower portions of the time-temperature chart whereas some models for which there are less track-length data display thermal histories that contain large 95% credible envelopes. All samples display good agreement for AHe single grain ages, plotting in the 1:1 line or near it, though there are some exceptions. On the other hand, AFT observed ages are younger than the predicted ones, mostly falling off the 1:1 line

The thermal histories provided in Fig. 6.7 are poorly constrained before 150 ± 20 Ma, a period for which they display low relative probability. We analyzed both the weighted mean path and the relative probability indicated in the charts of Fig. 6.7. Based on that, the samples can be divided into three groups that present somewhat similar trajectories: the first group is comprised of samples SC-35, SC-36, SC-38, SC-44, and SC-46, the second group is comprised of samples SC-34 and SC-41, and the third group comprises samples SC-37 and SC-42. Sample SC-48 was not considered in any group because it failed to generate a constrained thermal history due to the lack of horizontal confined tracks.

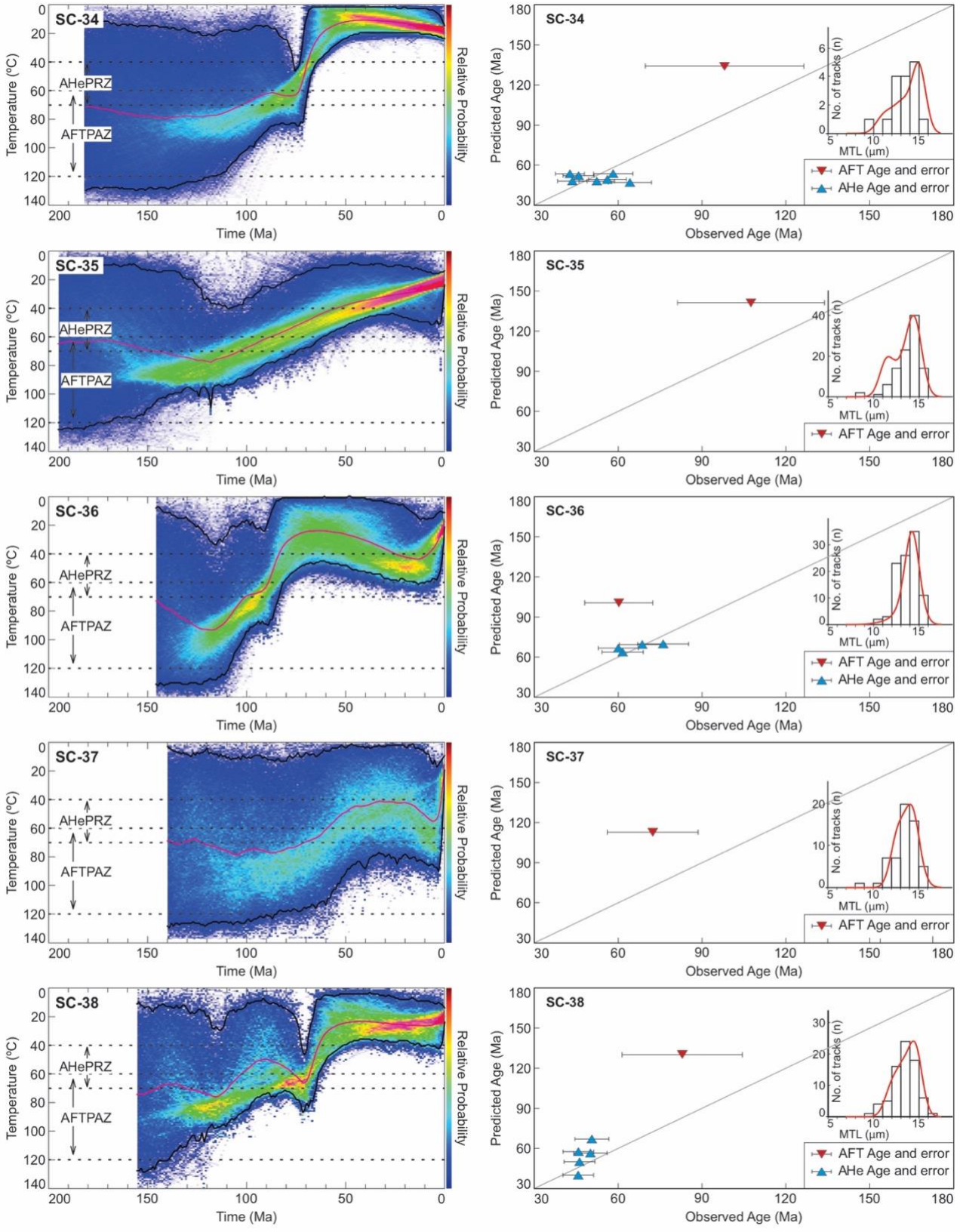

Figure 6. 7: Inverse modeling results generated in QTQt (Gallagher, 2012) for samples SC-34, SC-35, SC-36, SC-37, SC-38, SC-41, SC-42, SC-44, SC-46 and SC-48. The 95% credible interval defines the expected model (black curves). The weighted mean path is represented by the magenta curve. The range of the AFTPAZ and AHePRZ is defined by the dashed lines. The relative probability scale increases from blue to red. On the right of the thermal histories are shown observed versus predicted ages charts. Upside-

down red triangles indicate AFT ages whereas AHe single-crystal ages are displayed in upside-pointing blue triangles. The Mean Track Length (MTL) distribution of AFT data is represented as bars, with the red line indicating track lengths modeled. (For interpretation of the references to colour in this figure legend, the reader is referred to the web version of this article.)

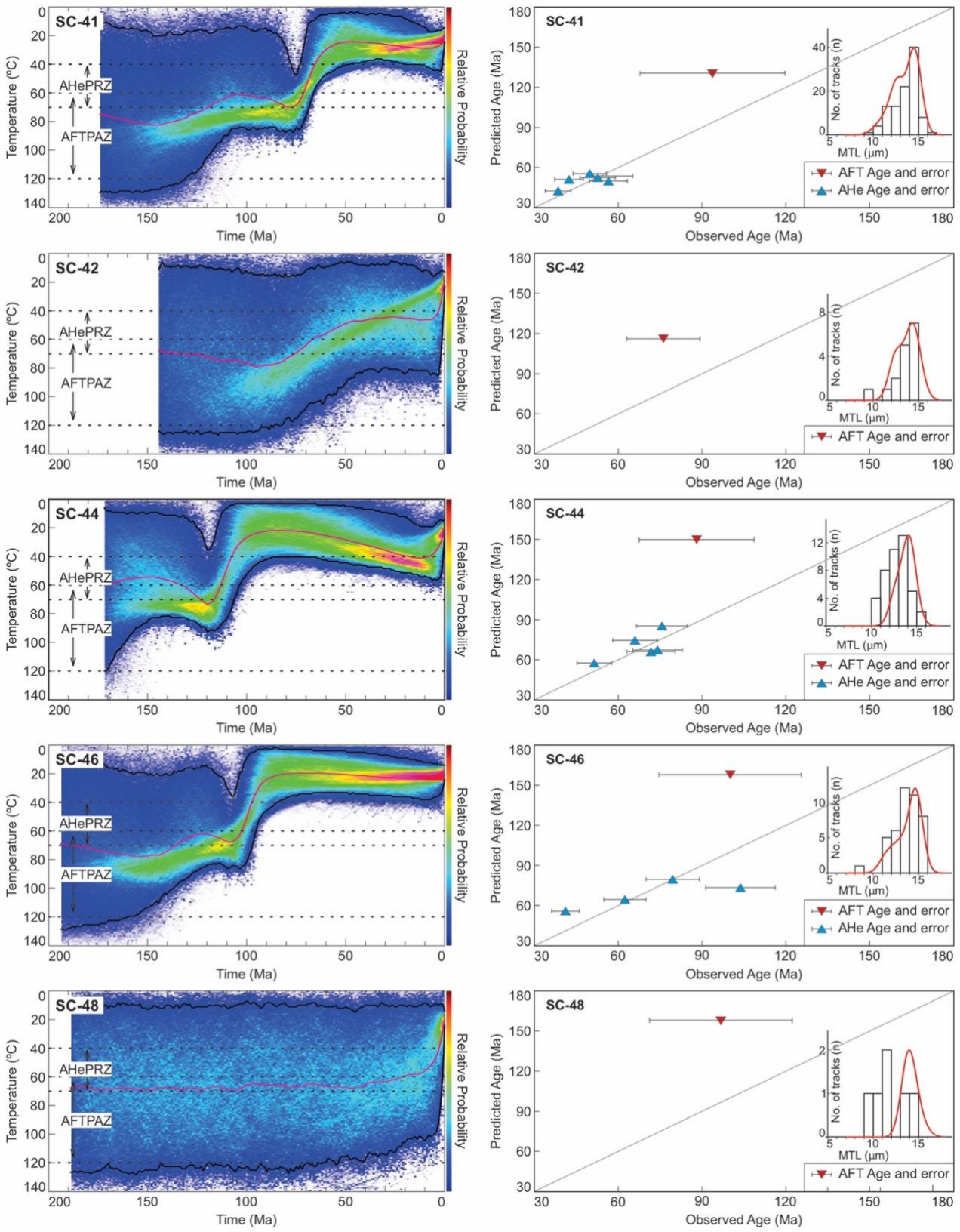

Figure 6. 7: (continued).

In general, Group 1 starts to cool between 120 and 110 Ma, from temperatures in the range of 95 to 70 ºC, with the samples cooling to present-day surface conditions, followed by some degree of reheating for most of them (Fig. 6.7). Samples SC-44 and SC-46 recorded accelerated cooling from 120 to 100 Ma and 110 to 90 Ma, respectively. Sample SC-44 recorded slow reheating of nearly 20 ºC to *ca.* 40 ºC from 100 until 15 Ma, followed by final cooling to a surface temperature of 20 ºC. Sample SC-46, on the contrary, remained at surface conditions since 90 Ma. Sample SC-36 recorded fast cooling as well, although lasting longer, from 120 to 80 Ma, until reaching 30 ºC. Then, a reheating of 20 ºC to *ca.* 50 ºC until 15 Ma was recorded, followed by final cooling to the present-day surface temperature. Sample SC-35 displays protracted continuous cooling from 120 Ma until the present day. Sample SC-38 cooled until 50 ºC at 90 Ma and reheated until 75 ºC at 70 Ma, although it displays a low relative probability. Next, this sample cooled to the present-day surface temperature at 50 Ma, remaining in this condition since then.

Belonging to Group 2, sample SC-34 displayed accelerated cooling from 80 to 60 Ma at temperatures of 65 to 15 ºC, remaining in this condition until the present day (Fig. 6.7). Sample SC-41 started to slowly cool from 150 Ma until 110 Ma from the temperature of 85 to 60 ºC, reheated until 70 ºC at 80 Ma also lacking high relative probability, and rapidly cooled from 70 to 25 ºC from 80 to 60 Ma, remaining in similar conditions to the present-day surface temperature since then.

Lastly, Group 3, composed of samples SC-37 and SC-42, started to cool at 100 until 50 Ma, from nearly 80 ºC to *ca.* 50 ºC. The temperature remained stable for nearly 30 Ma for sample SC-37, followed by reheating of 10 ºC and then cooling to the surface. Sample SC-42 remained at 50 ºC until 10 Ma and then cooled to present-day surface temperature (Fig. 6.7), although the inverse model lacks high probability, but presents a similar cooling trend with SC-35.

6.4.4 Basement temperatures assessment

The assessment of basement temperatures of the DFB and surrounding cratons since the beginning of the Carboniferous is presented in Fig. 6.8. These maps were generated using the Inverse Distance Weighted interpolation technique after reuniting thermal information of 128 locations.

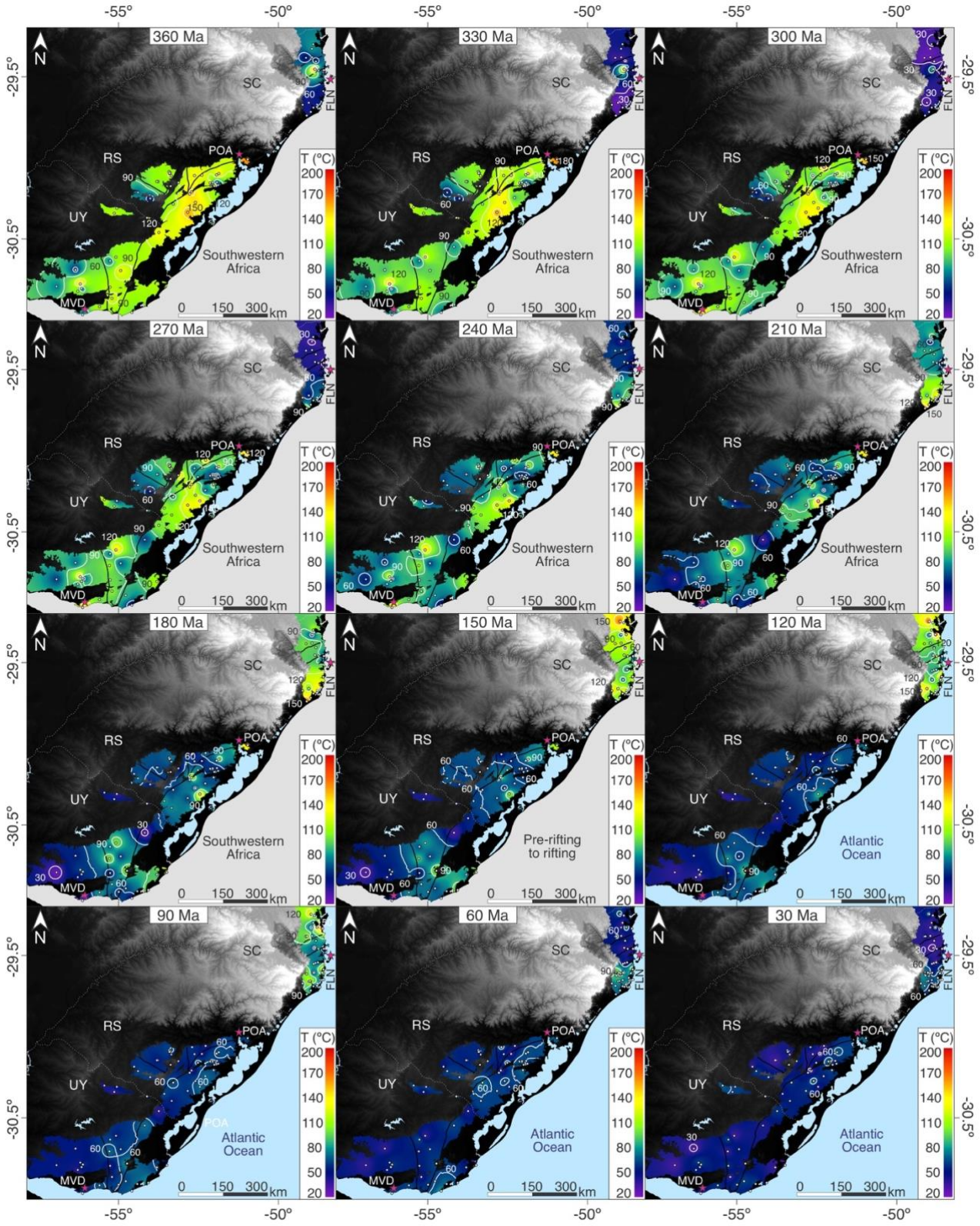

Figure 6. 8: Basement temperatures across the Dom Feliciano Belt and surrounding cratons from 360 to 30 Ma assessed by the Inverse Distance Weighted (IDW) interpolation technique. The time-temperature points were obtained from inverse models from this work and de Borba et al. (2002, 2003), Jelinek et al. (2003), Gomes (2011), Kollenz (2015), de Oliveira et al. (2016) Gomes and Almeida (2019), Krob et al. (2019), Machado et al. (2019, 2020) Red stars indicate the country or state capital city. Abbreviations are: SC: Santa Catarina State; RS: Rio Grande do Sul State; UY: Uruguay; FLN: Florianópolis; POA: Porto Alegre;

MVD: Montevideo. (For interpretation of the references to colour in this figure legend, the reader is referred to the web version of this article.)

The top row maps evidence the basement temperatures during the Carboniferous (Fig. 6.8). As it is shown, the temperatures of the DFB and adjacent cratons at the beginning of the Carboniferous Period were below 180 ºC. The Taquarembó Terrane and the western portion of the RDLP were cooler than the southern DFB to the east. However, the Catarinense Shield to the south of Florianópolis city in the northern DFB was at temperatures below 60 ºC. At 300 Ma, the rocks from this region were at their coolest temperature, residing on the surface or in extremely shallow portions of the crust, which is the result of the restriction imposed in the models of (Krob et al., 2019), forcing the models to run in low temperatures.

During the Permian, at 270 Ma, most of the RDLP, the southern end and central portions of the DFB, and the Taquarembó Terrane were at temperatures below 90 ºC. Surrounding these cooler portions, restrained regions of temperatures no higher than 120 ºC remained, as it is seen in the top end of the southern DFB near Porto Alegre city and close to the border between Uruguay and the Rio Grande do Sul state, both regions composing the Pelotas Batholith. In the northern DFB, a heating trend from north to south evidences that the Catarinense Shield had an increase in temperature to nearly 90 ºC. This pattern is maintained throughout the Triassic and Jurassic, reaching its higher temperature, 150 ºC, by 210 to 180 Ma (Fig. 6.8).

The southern DFB and the neighboring RDPL, on the other hand, remained in a cooling trend. At 180 Ma, temperatures in the region were cooler than 90 ºC, and in some locations even cooler than 30 ºC, such as the western portion of the RDPL and in the Pelotas Batholith in Uruguay. Before rifting at 150 Ma, most of the SRGS and Uruguayan Shields were at 60 ºC or less. Contrasting to this pattern, the northern DFB were at temperatures ranging from 150 to 60 ºC, at 150 Ma (Fig. 6.8).

From the opening of the South Atlantic Ocean, at 120 Ma, until 30 Ma, a distinct temperature pattern remains between the northern DFB and LAC in comparison with the southern DFB and RDLP. In the south, temperatures were no higher than 90 ºC at 120 Ma, cooling to nearly 30 ºC by the end of Paleogene. In the north, temperatures varied from 120 to 60º at 120 Ma, rapidly cooling to ~60-30 ºC at 30 Ma. It is noteworthy that to the south of Florianópolis city the temperature remained a little higher than 60 ºC until 30 Ma, contrasting to its neighboring craton and the whole SRGS and Uruguayan Shields

(Fig. 6.8).

6.5 Discussion

6.5.1 Distribution of Apatite Fission Track ages in the Northern and Southern Dom Feliciano Belt

In this work, we contributed 13 new AFT ages for the Catarinense Shield, located in the northern DFB (Table 6.2). The AFT ages presented here as well as a compilation of AFT ages of studies performed along the DFB and adjacent cratons are plotted against MTL (Fig. 6.4a) and standard deviation (Fig. 6.4b). The younger AFT ages, essentially from samples of the northern DFB, are mostly associated with long to intermediate tracks that are usually generated after rapid cooling or experienced a strong degree of annealing. The samples from this area present AFT ages younger than 150 Ma, suggesting that a reheating event raised temperatures high enough to reset AFT and AHe thermochronometers. The lack of well-defined thermal histories before 150 Ma is due to the complete thermal resetting of the AFT and AHe data used for thermal modeling. The thermal resetting in the northern DFB was caused by the emplacement of volcanic rocks belonging to the PELIP and associated feeding dyke swarms (Florisbal et al., 2014, 2018; Hueck et al., 2018a), causing a reheating event, raising the temperatures across the northern DFB. For the southern DFB, the fission track lengths are mostly short to intermediate, reflecting long residence at higher temperatures under some degree of annealing in the AFTPAZ. There is no apparent correlation between the standard deviation and AFT ages of samples analyzed. However, the samples of the northern DFB and LAC display values between 1 and 2.5 □m, whereas the southern DFB and RDLP exhibit values between 1 and 2 □m. According to Green (1986), as the annealing proceeds until total resetting, the older tracks fade, resulting in larger mean tracks and the reduction of the standard deviation values with a consequent AFT age reduction, generating distinct patterns in the standard deviation versus AFT age plot. Additionally, the plot of MTL versus standard deviation (Fig. 6.4c) shows that samples from the southern DFB and RDLP are clustered in the lower portion of the chart (Green, 1986), which may represent the “original age” of the AFT thermochronometer for this region. The “original age” in this case represents the age that the apatites would have if they were not disturbed by reheating events, representing original cooling ages. Considering this, the

samples from the northern DFB and LAC are, therefore, interpreted as reset AFT ages, which are plotted slightly above the samples from the Southern DFB in Fig. 6.4c. As said before, the northern DFB AFT ages represent reset ages, i.e., after the original cooling these samples were reheated in varying degrees until they were totally annealed. To corroborate our interpretation, the detrital AFT ages of rocks from the Paraná Basin located to the west to the Catarinense Shield exhibit Carboniferous ages similar to the AFT ages of the southern DFB (Bicca et al., 2020). Thus, we suggest that the Carboniferous ages may represent the timing of exposure of the shield to temperatures cooler than 60 ºC following the tectonic assembly of the shield.

The elevation and the shortest distance to the coastline are other criteria used to discuss AFT ages and their distribution. The data set presented here fails to demonstrate a correlation between these parameters with AFT ages, contrasting with the trends usually recognized for this thermochronometer in Brazil in specific studies (e.g. Amaral-Santos et al., 2019; Gallagher et al., 1994; Machado et al., 2019).

6.5.2 Apatite (U-Th)/He intra and intersample age variations

In this study, we presented 30 new AHe ages from six samples of the Catarinense Shield, in the northern DFB. Apatite (U-Th)/He intrasample age dispersion is small for most samples (see SD column in Table 6.3). For all samples the selected apatite crystals were free of inclusions, preventing parentless ^{4}He to be added to the apatite crystal lattice (Lippolt et al., 1994). U and Th-rich minerals that neighbor the apatite crystals are also other possible sources of He implantation. However, this data set does not exhibit any anomalously old AHe age, from which we deduce that these samples are free of He implantation.

Additionally to extraneous ^{4}He, the radiation damage plays a fundamental role as a source of intra- and intersample age variation, since it strongly influences He diffusion, inducing high-eU apatites to retain fractional He and producing old AHe ages. This effect is demonstrated by a positive non-linear correlation between these parameters (Flowers et al., 2009). This data set, however, shows a non-existent correlation between AHe ages and eU concentration (Fig. 6.6a), suggesting additional sources of noise that control the distribution of AHe ages. A monotonic fast cooling scenario that could explain the lack of correlation above is discarded because the western portion of the Florianópolis Batholith may have been exposed to surface conditions during the Paleozoic when the first units of

the Paraná Basin were deposited (Krob et al., 2019), as other parts of the Uruguayan and SRGS may have. Furthermore, this region probably experienced reheating during burial as well as reheating during the emplacement of the PELIP and associated feeding dykes (see 5.3 section) that reset both AHe and AFT thermochronometers, which argue against a monotonic cooling thermal history.

The grain size, referred to as ESR in this study, is also a parameter used to assess (U-Th)/He ages dispersion (Brown et al., 2013; Reiners and Farley, 2001). In this new data set, the AHe ages do not display a clear correlation with ESR (Fig. 6.6b). The lack of correlation can indicate simple rapid cooling in the range of this thermochronometer or overdispersion (Brown et al., 2013). Indeed, the thermal histories presented here display accelerated Meso-Cenozoic cooling. From a regional perspective, the relationship between the ESR and the AHe ages of samples collected in the northern and southern segments of the DFB and surrounding cratons fails to demonstrate a distinct correlation between these parameters. However, the northern DFB seems to relate to the first approach in which rapid cooling is the engine driving the lack of correlation, while in the southern DFB the driving mechanism is the overdispersion of ages (e.g., Hueck et al., 2017, 2018a, 2019; Machado et al., 2019, 2020).

The intersample AHe age variation, similar to AFT data, fails to correlate with elevation and the shortest distance to the coastline.

Dispersion amongst samples of this new data set also generated a pattern of inverted AFT and AHe ages, in which some of AHe ages are older than their AFT ones. These inverted ages are not explained by the analyzes performed in this study, nor by a series of works that have the same issues, which can be attributed to problems in understanding He diffusion systematics (Green and Duddy, 2018).

6.5.3 Timing and spatial patterns inferred from thermochronology and data interpolation

The new compilation presented in this study allows us to recognize and discuss regional trends for the studied area.

During the Carboniferous, the temperature of the entire DFB and adjacent cratons was below 180 °C (Fig. 6.8), with these rocks placed at mid to shallow portions of the upper crust. Exhumation of these rocks during the Paleozoic was affected by the

Gondwanic Orogenic Cycle (Milani and Ramos, 1998) through intraplate stress propagation, causing surface uplift and inducing erosion, as proposed for other West Gondwana intraplate environments (e.g., Jelinek et al., 2014; Engelmann de Oliveira et al., 2016; Amaral-Santos et al., 2019; Martins-Ferreira et al., 2020; do Amaral Santos et al., 2022). The Northern DFB and LAC were possibly exhumed by the Carboniferous as well, displaying temperatures compatible with near-surface conditions (Krob et al., 2019). These conditions exposed on our maps may be due to the constraints imposed before samples were modeled in the work of Krob et al. (2019). On the other hand, detrital AFT ages of sedimentary rocks from the Paraná basin range from Carboniferous to Miocene (Bicca et al., 2020), suggesting that older AFT ages may correlate with the northern DFB exhumation during the Carboniferous. AFT thermal modeling of these samples collected from boreholes to the west of Catarinense Shield advocates in favor of a surface to near-surface exposure from the end of the Paleozoic until the end of the Jurassic (Bicca et al., 2020). Detrital ZHe and ZFT ages of sedimentary samples of the Paraná basin (Karl et al., 2013) also suggest provenance ages related to the exhumation of the northern DFB and its partial exposure during the Carboniferous. By the end of this period, two supersequences of the Paraná Basin had already been deposited to the north of the LAC and the Gondwana I supersequence started its deposition during the Permian-Carboniferous, reaching a thickness of nearly 2.5 km (Milani et al., 2007a, 2007b). The units of the latter outcrop to the west and in some places within the Catarinense Shield, suggesting that the shield was, at least, partially covered by the sediments of the Paraná Basin. At that time, the sedimentary overload in the northern DFB reached nearly the thickness of 4 km, heating the basement, indicated by the reset of the AFT and AHe ages in the area, which is demonstrated by the maps shown in Fig. 6.8, from 300 to 210 Ma, and also advocated by Krob et al. (2019).

During the Triassic to the end of the Jurassic, both the Uruguayan and SRGS shields experienced gradual cooling, recording temperatures between 90 and 30 ºC (Fig. 6.8). Such trend suggests that before rifting, these shields were at low temperatures, in similar conditions to near-surface environments. Machado et al. (2021) suggested that the RDLP and the southern DFB likely cooled down between 110 and 60 ºC in the Mesozoic. For the same area, Hueck et al. (2017, 2019) proposed a hypothesis of near-surface exposure much earlier, by the Silurian, with possible reheating after that leading to samples remaining in temperatures higher than 60 ºC until the Triassic. Favoring the

assumption of near-surface conditions by the end of the Paleozoic to the Mesozoic advocated by Jelinek et al. (2021) and Machado et al. (2021), conglomerates and sandstones of the Sanga do Cabral Formation of Triassic age (Lavina, 1988) were deposited within the SRGS, suggesting that it was already exposed to near-surface conditions (low temperatures) during the Triassic. Considering that thermochronologic data is quite widespread, it is also important to emphasize that the thermal history recovered for the area is broad and that papers may have differences in what they highlight. In the Lower Cretaceous, the SRGS was cut by feeding dykes of the PELIP, even though only localized reheating was recorded by samples in the eastern Pelotas Batholith (Hueck et al., 2019; Machado et al., 2019). Moreover, Paleozoic AFT ages of the southern DFB and RDLP (Fig. 6.8) suggest minor to absent resetting caused the emplacement of the PELIP volcanic rocks, as suggested by Hueck et al. (2019).

On the other hand, the Catarinense Shield was at higher temperatures by the end of the Jurassic, with some locations recording 150 ºC (Fig. 6.8). The heating increment lasted until the Lower Cretaceous, with the emplacement of the PELIP at approximately 134 Ma (Turner et al., 1994; Stewart et al., 1996; Janasi et al., 2011). This extensive volcanic event induced reheating in the northern DFB and LAC, causing total annealing of the AFT and AHe thermochronometers (e. g., This work, Gallagher et al., 1994; Jelinek et al., 2003; Karl et al., 2013; Krob et al., 2019, 2020) and the partial to total resetting of ZHe and ZFT thermochronometers (Karl et al., 2013; Hueck et al., 2018; Krob et al., 2019). This is demonstrated by AFT and AHe ages similar or younger than the volcanic emplacement, thermal histories based on AFT data that do not span to times older than nearly 150 Ma, overly dispersed ZHe ages (Hueck et al., 2018a), and some Cretaceous ZFT and ZHe ages (Karl et al., 2013). Besides, the feeding dykes of the PELIP located in the Catarinense Shield (Florisbal et al., 2014, 2018; Wildner et al., 2014), in NE-SW direction, may also be responsible for elevating the geothermal gradient in the area, which would reinforce the annealing caused by the emplacement of the PELIP, as advocated by some authors (e.g., Hueck et al., 2018; Krob et al., 2019) and acknowledged in this study. Another possible source of heating during the Upper Jurassic to Lower Cretaceous is the alkaline-carbonatitic intrusions in the northern DFB (Anitápolis intrusion – ca. 132 Ma; Sonoki and Garda, 1988; Gibson et al., 2006; Ferreira et al., 2022) and to the north of the LAC, in the Ponta Grossa Arch region (Amaral et al., 1997). Some of these intrusions are found on or close to NW-SE lineaments, which acted as a conduit for the lavas of the

PELIP in a long and wide fissure zone (Riccomini et al., 2005). For all this, before rifting several sources of heating in the northern DFB and LAC were present, reshaping the geothermal gradient of the upper crust and resetting low-temperature thermochronometers, which completely opposes the processes operating in the southern DFB and RDLP.

The extrusions of the volcanic rocks of the PELIP were coeval to the opening of the southernmost South Atlantic basin in the Upper Jurassic to the Lower Cretaceous (Rabinowitz and Labrecque, 1979; Torsvik et al., 2009; Moulin et al., 2010; Heine et al., 2013) and preceded seafloor spreading located to the east of the Catarinense Shield, which occurred approximately between 120 and 115 Ma (Heine et al., 2013). The thermal histories presented in this study suggest that some samples experienced the onset of accelerated cooling following breakup and seafloor spreading (Fig. 6.7). A few AFT ages are contemporaneous with these tectonic processes (Table 6.2), suggesting that rifting may have induced exhumation of the Catarinense Shield. In addition to this, the temperature of the basement at 120 Ma ranged from 150 ºC to nearly 60 ºC, implying that some of the sources of heating mentioned earlier were still active. Conversely, the southern DFB and RDLP were in cooler temperatures during breakup as observed in the 120 Ma-map of Fig. 6.8.

Finally, during the Upper Cretaceous (90 Ma) to the Eocene (30 Ma) the drift phase of the South America plate was on course, recording the formation of sedimentary basins of the eastern Brazilian continental margin (e.g., Milani et al., 2007b; Mohriak et al., 2008b; Machado et al., 2021; Ferreira et al., 2022). Moreover, the emplacement of alkaline-carbonatitic intrusions in the SRGS, in the Catarinense Shield, and throughout the Mantiqueira Province were registered (Ferreira et al., 2022), implying sources of heat that Riccomini et al. (2005) attributed to long-lived mantle upwelling. Many AFT and AHe ages from this study and in the literature and some thermal models display fast cooling coeval to these events. Cogné et al. (2011), in their study in the Ribeira Belt to the north of the study area, related the Upper Cretaceous to the Paleogene cooling to a thermally weakened crust subject to plate-wide compression possibly associated with post-rifting magmatism or earlier mantle plume activity and structural inheritance. Important to notice, however, is that the mechanisms cited above were not only associated with cooling but also with post-rift uplift of the passive margin. However, in the northern DFB a prominent escarpment is somewhat absent while this geomorphic feature is completely absent in the

southern DFB. We, therefore, acknowledge this argument and we suggest that the prolonged higher temperature of the northern DFB and LAC in comparison with the southern DFB and RDLP (Fig. 6.8) is due to the closer proximity of the northern DFB to the Florianópolis Fracture Zone (Mohriak et al., 2010), of E-W direction. This fracture zone represents leaky faults related to the emplacement of volcanic plugs during the Upper Cretaceous to the Eocene (Mohriak et al., 2010) and, hence, a conduit for heating transport. Furthermore, a prominent NW-SE lineament named Cruzeiro do Sul is associated with the Florianópolis Fracture Zone and related to a major plate reorganization in the Paleogene to Neogene (Mohriak, 2004; Mohriak et al., 2010). At that time, several igneous plugs were emplaced both onshore and offshore in the Santos Basin, to the north of the study area, and, hence, could be a source of heat supply.

6.6. Conclusion

In this work, we contributed with 13 new AFT ages and 30 new apatite (U-Th)/He ages of samples collected in the Catarinense Shield, in the northern Dom Feliciano Belt. Both AFT and corrected AHe ages are essentially Mesozoic and MTL are short to medium associated with reset AFT ages.

Additionally, we assessed the basement temperatures for 128 locations across the entire DFB and adjacent cratons – Rio de La Plata and Luís Alves – since the Carboniferous, presented in 12 maps. Since the Paleozoic, the northern and southern DFB experienced contrasting thermal histories. The southern DFB was possibly exhumed to near-surface temperatures by the end of the Permian, being subject to minor reheating only in a few places until the present day. Conversely, the northern DFB was probably exposed to near-surface conditions in the Carboniferous and partially buried by the sediments of the Paraná basin megasequences, interpreted from data compiled from the literature that used constraints that forced models to run in low temperatures and from detrital AFT, ZFT and ZHe ages to the west of the study area. From the Mesozoic to the Eocene, the region was strongly reheated by the (1) emplacement of the volcanic rocks of the Paraná-Etendeka Large Igneous Province; (2) presence of a feeding dyke system of the same LIP, and (3) intrusion of alkaline-carbonatitic rocks mostly associated with the Florianópolis Fracture Zone, of E-W direction. Therefore, we suggest that the northern DFB and Luís Alves Craton region recorded a series of mutual events responsible for keeping the temperature high enough to induce the annealing of the fission tracks and the

diffusion of particles in apatite, causing age dispersion and resetting partial to totally these low-temperature thermochronometers, completely contrasting to the Meso-Cenozoic thermal history of the southern Dom Feliciano Belt and Rio de La Plata craton.

Several issues remain open and should be answered in future works; for example, (1) the extent of annealing conditions for AFT and AHe thermochronometers to the north of the locations sampled in this study; (2) the trends of AFT age versus elevation/distance to the coastline for samples located to the continent interior and at higher elevations; (3) the role of E-W and NW-SE fracture zones affecting the thermochronological record, such as the Florianópolis Fracture Zone exemplified in this study.

6.7 Acknowledgments

E. Amaral-Santos thanks the Ph.D scholarship provided by the Conselho Nacional de Desenvolvimento Científico e Tecnológico – CNPq, for (140775/2019-6). A.R. Jelinek thanks to the Conselho Nacional de Desenvolvimento Científico e Tecnológico - CNPq (Project 309329/2020-5). The authors thank M.M. Bicca for assistance with AFT data. The authors thank the Tectonophysics Editor Dr. Zheng-Xiang Li, the reviewer Dr. Mathias Hueck, and an anonymous reviewer that helped to improve an earlier version of this manuscript.

References

Amaral-Santos, E., Jelinek, A.R., Almeida-Abreu, P.A., Genezine, F.A., 2019. Phanerozoic cooling history of Archean/Paleoproterozoic basement in the southern Espinhaço Range, southeastern Brazil, through apatite fission-track analysis. J. South Am. Earth Sci. 96, 102352. https://doi.org/10.1016/j.jsames.2019.102352

Amaral, G., Born, H., Hadler, J.C.N., Iunes, P.J., Kawashita, K., Machado, D.L., Oliveira, E.P., Paulo, S.R., Tello, C.A.S., 1997. Fission track analysis of apatites from São Francisco craton and Mesozoic alcaline-carbonatite complexes from central and southeastern Brazil. J. South Am. Earth Sci. 10, 285–294. https://doi.org/10.1016/s0895-9811(97)00020-5

Ault, A.K., Flowers, R.M., 2012. Is apatite U-Th zonation information necessary for accurate interpretation of apatite (U-Th)/He thermochronometry data? Geochim. Cosmochim. Acta 79, 60–78. https://doi.org/10.1016/j.gca.2011.11.037

Barbarand, J., Carter, A., Wood, I., Hurford, T., 2003a. Compositional and structural control of fission-track annealing in apatite. Chem. Geol. 198, 107–137. https://doi.org/10.1016/S0009-2541(02)00424-2

Barbarand, J., Hurford, T., Carter, A., 2003b. Variation in apatite fission-track length measurement:

Implications for thermal history modelling. Chem. Geol. 198, 77–106. https://doi.org/10.1016/S0009-2541(02)00423-0

Basei, M.Â.S., 1985. O Cinturão Dom Feliciano em Santa Catarina. University of São Paulo.

Basei, M.A.S., Frimmel, H.E., Nutman, A.P., Preciozzi, F., 2008. West Gondwana amalgamation based on detrital zircon ages from Neoproterozoic Ribeira and Dom Feliciano belts of South America and comparison with coeval sequences from SW Africa. Geol. Soc. Spec. Publ. 294, 239–256. https://doi.org/10.1144/SP294.13

Basei, M.A.S., McReath, I., Siga, O., 1998. The Santa Catarina Granulite Complex of Southern Brazil: A Review. Gondwana Res. 1, 383–391. https://doi.org/10.1016/S1342-937X(05)70854-6

Basei, M.A.S., Peel, E., Bettucci, L.S., Preciozzi, F., Nutman, A.P., 2011. The basement of the Punta del Este Terrane (Uruguay): An African Mesoproterozoic fragment at the eastern border of the South American Río de La Plata craton. Int. J. Earth Sci. 100, 289–304. https://doi.org/10.1007/s00531-010-0623-1

Basei, M.A.S., Siga Jr., O., Machiavelli, A., Mancini, F., 1992. Evolução Tectônica Dos Terrenos Entre Os Cinturões Ribeira E Dom Feliciano (Pr-Sc). Rev. Bras. Geociências 22, 216–221. https://doi.org/10.25249/0375-7536.1992216221

Bicca, M.M., Kalkreuth, W., da Silva, T.F., de Oliveira, C.H.E., Genezini, F.A., 2020. Thermal and depositional history of Early-Permian Rio Bonito Formation of southern Paraná Basin – Brazil. Int. J. Coal Geol. 228, 103554. https://doi.org/10.1016/j.coal.2020.103554

Borba, A.W. de, Lima, E.F. de, Vignol-Lelarge, M.L.M., Mizusaki, A.M.P., Sparrenberg, I., Barros, C.E. de, 2003. Significance of Late Paleozoic fission-track ages in volcanic rocks from the Lavras Do Sul region, southernmost Brazil. Gondwana Res. 6, 79–88. https://doi.org/10.1016/S1342-937X(05)70645-6

Borba, A.W. de, Vignol-Lelarge, M.L.M., Mizusaki, A.M.P., 2002. Uplift and denudation of the Caçapava do Sul granitoids (southern Brazil) during Late Paleozoic and Mesozoic: Constraints from apatite fission-tract data. J. South Am. Earth Sci. 15, 683–692. https://doi.org/10.1016/S0895-9811(02)00086-X

Brown, R.W., Beucher, R., Roper, S., Persano, C., Stuart, F., Fitzgerald, P., 2013. Natural age dispersion arising from the analysis of broken crystals. Part I: Theoretical basis and implications for the apatite (U-Th)/He thermochronometer. Geochim. Cosmochim. Acta 122, 478–497. https://doi.org/10.1016/j.gca.2013.05.041

Bueno, G.V., 2021. Bacia de Pelotas em retrospectiva. In: Jelinek, A.R., Sommer, C.A. (Eds.), Contribuições à Geologia Do Rio Grande Do Sul e de Santa Catarina. Compasso Lugar-Cultura, Porto Alegre, pp. 389-402.

Bueno, G.V., Zacharias, A.A., Oreiro, S.G., Cupertino, J.A., Falkenhein, F.U.H., Martins-Neto, M.A., 2007. Bacia de Pelotas. Bol. Geociencias da Petrobras 15, 551–559.

Carlson, W.D., Donelick, R.A., Ketcham, R.A., 1999. Variability of apatite fission-track annealing kinetics: I. Experimental results. Am. Mineral. 84, 1213–1223. https://doi.org/10.2138/am-1999-0901

Chang, H.K., Kowsmann, R.O., Figueiredo, A.M.F., Bender, A.A., 1992. Tectonics and stratigraphy of the East Brazil Rift system: an overview. Tectonophysics 213, 97–138. https://doi.org/10.1016/0040-

1951(92)90253-3

Cogné, N., Gallagher, K., Cobbold, P.R., 2011. Post-rift reactivation of the onshore margin of southeast Brazil: Evidence from apatite (U–Th)/He and fission-track data. Earth Planet. Sci. Lett. 309, 118–130. https://doi.org/10.1016/j.epsl.2011.06.025

CPRM, 2008. Mapa Geológico do Estado do Rio Grande do Sul. Porto Alegre, Programa Geologia do Brasil, escala 1:750.000.

CPRM, 2014. Mapa Geológico do estado de Santa Catarina. Porto Alegre, Programa Geologia do Brasil, escala 1:500.000.

de Almeida, F.F.M., Hasui, Y., de Brito Neves, B.B., Fuck, R.A., 1981. Brazilian structural provinces: An introduction. Earth Sci. Rev. 17, 1–29. https://doi.org/10.1016/0012-8252(81)90003-9

De Brito Neves, B.B., Fuck, R.A., 2013. Neoproterozoic evolution of the basement of the South-American platform. J. South Am. Earth Sci. 47, 72–89. https://doi.org/10.1016/j.jsames.2013.04.005

do Amaral Santos, E., Jelinek, A.R., Machado, J.P., Stockli, D., 2022. Thermal history along the Araçuaí Orogen and São Francisco Craton border, eastern Brazilian continental margin, based on low-temperature thermochronologic data. Tectonophysics 825, 229232. https://doi.org/10.1016/j.tecto.2022.229232

Donelick, R.A., Ketcham, R.A., Carlson, W.D., 1999. Variability of apatite fission-track annealing kinetics: II. Crystallographic orientation effects. Am. Mineral. 84, 1224–1234. https://doi.org/10.2138/am-1999-0902

Donelick, R.A., O'Sullivan, P.B., Ketcham, R.A., 2005. Apatite fission-track analysis, in: Reiners, P.W., Ehlers, T.A. (Eds.), Reviews in Mineralogy and Geochemistry. pp. 49–94. https://doi.org/10.2138/rmg.2005.58.3

Engelmann de Oliveira, C.H., Jelinek, A.R., Chemale, F., Cupertino, J.A., 2016. Thermotectonic history of the southeastern Brazilian margin: Evidence from apatite fission track data of the offshore Santos Basin and continental basement. Tectonophysics 685, 21–34. https://doi.org/10.1016/j.tecto.2016.07.012

Farley, K.., Wolf, R.., Silver, L.., 1996. The effects of long alpha-stopping distances on (U-Th)/He ages. Geochim. Cosmochim. Acta 60, 4223–4229. https://doi.org/https://doi.org/10.1016/S0016-7037(96)00193-7

Farley, K. a, 2000. Helium diffusion from apatite, General behavior as illustrated by Durango fiuorapatite The implied He closure temperature for a grain. J. Geophys. Res. 105, 2903–2914.

Farley, K.A., 2002. (U-Th)/He dating: Techniques, calibrations, and applications. Rev. Mineral. Geochemistry 47, 819–844. https://doi.org/10.2138/rmg.2002.47.18

Ferreira, A.C.D., Conceição, R.V., Mizusaki, A.M.P., 2022. Mesozoic to Cenozoic alkaline and tholeiitic magmatism related to West Gondwana break-up and dispersal. Gondwana Res. 106, 15–33. https://doi.org/10.1016/j.gr.2022.01.005

Fitzgerald, P.G., Baldwin, S.L., Webb, L.E., O'Sullivan, P.B., 2006. Interpretation of (U-Th)/He single grain ages from slowly cooled crustal terranes: A case study from the Transantarctic Mountains of southern Victoria Land. Chem. Geol. 225, 91–120. https://doi.org/10.1016/j.chemgeo.2005.09.001

Fleischer, R.L., Price, P.B., 1964. Techniques for geological dating of minerals by chemical etching of

fission fragment tracks. Geochim. Cosmochim. Acta 28, 1705–1714. https://doi.org/10.1016/0016-7037(64)90017-1

Fleischer, R. L., Price, P. B., Walker, R. M., 1975. Nuclear tracks in Solids: Principles and Applications. University of California Press, California.

Florisbal, L.M., Heaman, L.M., de Assis Janasi, V., de Fatima Bitencourt, M., 2014. Tectonic significance of the Florianópolis Dyke Swarm, Paraná-Etendeka Magmatic Province: A reappraisal based on precise U-Pb dating. J. Volcanol. Geotherm. Res. 289, 140–150. https://doi.org/10.1016/j.jvolgeores.2014.11.007

Florisbal, L.M., Janasi, V.A., Bitencourt, M.F., Nardi, L.V.S., Marteleto, N.S., 2018. Geological, geochemical and isotope diversity of ~ 134 Ma dykes from the Florianópolis Dyke Swarm, Paraná Magmatic Province: Geodynamic controls on petrogenesis. J. Volcanol. Geotherm. Res. 355, 181–203. https://doi.org/10.1016/j.jvolgeores.2017.08.002

Flowers, R.M., Ketcham, R.A., Shuster, D.L., Farley, K.A., 2009. Apatite (U-Th)/He thermochronometry using a radiation damage accumulation and annealing model. Geochim. Cosmochim. Acta 73, 2347–2365. https://doi.org/10.1016/j.gca.2009.01.015

Galbraith, R.F., 1981. On statistical models for fission track counts. J. Int. Assoc. Math. Geol. 13, 471–478. https://doi.org/10.1007/BF01034498

Galbraith, R.F., Green, P.F., 1990. Estimating the component ages in a finite mixture. Int. J. Radiat. Appl. Instrumentation. Part 17, 197–206. https://doi.org/10.1016/1359-0189(90)90035-V

Galbraith, R.F., Laslett, G.M., 1993. Statistical models for mixed fission track ages. Int. J. Radiat. Appl. Instrumentation. Part 21, 459–470. https://doi.org/10.1016/1359-0189(93)90185-C

Gallagher, K., 2012. Transdimensional inverse thermal history modeling for quantitative thermochronology. J. Geophys. Res. Solid Earth 117, B02408. https://doi.org/10.1029/2011JB008825

Gallagher, K., Charvin, K., Nielsen, S., Sambridge, M., Stephenson, J., 2009. Markov chain Monte Carlo (MCMC) sampling methods to determine optimal models, model resolution and model choice for Earth Science problems. Mar. Pet. Geol. 26, 525–535. https://doi.org/10.1016/j.marpetgeo.2009.01.003

Gallagher, K., Hawkesworth, C.J., Mantovani, M.S.M., 1994. The denudation history of the onshore continental margin of SE Brazil inferred from apatite fission track data. J. Geophys. Res. 99, 117–145. https://doi.org/10.1029/94jb00661

Gamboa, L.A.P., Rabinowitz, P.D., 1981. The Rio Grande fracture zone in the western South Atlantic and its tectonic implications. Earth Planet. Sci. Lett. 52, 410–418. https://doi.org/10.1016/0012-821X(81)90193-X

Gaucher, C., Frei, R., Chemale, F., Frei, D., Bossi, J., Martínez, G., Chiglino, L., Cernuschi, F., 2011. Mesoproterozoic evolution of the Río de la Plata Craton in Uruguay: At the heart of Rodinia? Int. J. Earth Sci. 100, 273–288. https://doi.org/10.1007/s00531-010-0562-x

Gibson, S.A., Thompson, R.N., Day, J.A., 2006. Timescales and mechanisms of plume-lithosphere interactions: 40Ar/39Ar geochronology and geochemistry of alkaline igneous rocks from the Paraná-Etendeka large igneous province. Earth Planet. Sci. Lett. 251, 1–17. https://doi.org/10.1016/j.epsl.2006.08.004

Gleadow, A.J.W., Duddy, I.R., 1981. A natural long-term track annealing experiment for apatite. Nucl. Tracks 5, 169–174. https://doi.org/10.1016/0191-278X(81)90039-1

Gleadow, A.J.W., Duddy, I.R., Green, P.F., Hegarty, K.A., 1986. Fission track lengths in the apatite annealing zone and the interpretation of mixed ages. Earth Planet. Sci. Lett. 78, 245–254. https://doi.org/10.1016/0012-821X(86)90065-8

Gomes, C.H., 2011. História Térmica Das Regiões Sul E Sudeste Da América Do Sul: Implicações Na Compartimentação Geotectônica Do Gondwana. Cristiane Heredia Gomes. Universidade Federal do Rio Grande do Sul.

Gomes, C.H., Almeida, D., 2019. New insights into the Gondwana breakup at the Southern South America by apatite fission-track analyses. Adv. Geosci. 47, 1–15. https://doi.org/10.5194/adgeo-47-1-2019

Green, P., Duddy, I., 2018. Apatite (U-Th-Sm)/He thermochronology on the wrong side of the tracks. Chem. Geol. 488, 21–33. https://doi.org/10.1016/j.chemgeo.2018.04.028

Green, P.F., 1986. On the thermo-tectonic evolution of Northern England: Evidence from fission track analysis. Geol. Mag. 123, 493–506. https://doi.org/10.1017/S0016756800035081

Green, P.F., Duddy, I.R., Gleadow, A.J.W., Tingate, P.R., Laslett, G.M., 1986. At an early stage in the development of fission-track dating , Fleischer et al . (1965) showed that of various environmental param- eters which could possibly affect the long term stability of fission tracks , temperature is by far the dominant factor . Chem. Geol. Isot. Geosci. Sect. 59, 237–253. https://doi.org/http://dx.doi.org/10.1016/0168-9622(86)90074-6

Guadagnin, F., Chemale, F., Dussin, I.A., Jelinek, A.R., dos Santos, M.N., Borba, M.L., Justino, D., Bertotti, A.L., Alessandretti, L., 2010. Depositional age and provenance of the Itajaí Basin, Santa Catarina State, Brazil: Implications for SW Gondwana correlation. Precambrian Res. 180, 156–182. https://doi.org/10.1016/j.precamres.2010.04.002

Hartmann, L.A., 1998. Deepest exposed crust of Brazil - Geochemistry of paleoproterozoic depleted Santa Maria Chico granulites. Gondwana Res. 1, 331–341. https://doi.org/10.1016/S1342-937X(05)70849-2

Hartmann, L.A., Campal, N., Santos, J.O.S., McNaughton, N.J., Bossi, J., Schipilov, A., Lafon, J.M., 2001. Archean crust in the Rio de la Plata Craton, Uruguay - SHRIMP U-Pb zircon reconnaissance geochronology. J. South Am. Earth Sci. 14, 557–570. https://doi.org/10.1016/S0895-9811(01)00055-4

Hasui, Y., 2010. A grande colisão pré-cambriana do sudeste brasileiro e a estruturação regional, Geociencias.

Heine, C., Zoethout, J., Müller, R.D., 2013. Kinematics of the South Atlantic rift. Solid Earth 4, 215–253. https://doi.org/10.5194/se-4-215-2013

Hueck, M., Dunkl, I., Heller, B., Stipp Basei, M.A., Siegesmund, S., 2018a. (U-Th)/He Thermochronology and Zircon Radiation Damage in the South American Passive Margin: Thermal Overprint of the Paraná LIP? Tectonics 37, 4068–4085. https://doi.org/10.1029/2018TC005041

Hueck, M., Dunkl, I., Oriolo, S., Wemmer, K., Basei, M.A.S., Siegesmund, S., 2019. Comparing contiguous high- and low-elevation continental margins: New (U-Th)/He constraints from South Brazil and an integration of the thermochronological record of the southeastern passive margin of South America.

Tectonophysics 770, 228222. https://doi.org/10.1016/j.tecto.2019.228222

Hueck, M., Oriolo, S., Dunkl, I., Wemmer, K., Oyhantçabal, P., Schanofski, M., Basei, M.Â.S., Siegesmund, S., 2017. Phanerozoic low-temperature evolution of the Uruguayan Shield along the South American passive margin. J. Geol. Soc. London. 174, 609–626. https://doi.org/10.1144/jgs2016-101

Hueck, M., Oyhantçabal, P., Philipp, R.P., Basei, M.A.S., Siegesmund, S., 2018b. The Dom Feliciano Belt in Southern Brazil and Uruguay, in: Siegesmund, S., Basei, M.Â.S., Oyhantçabal, P., Oriolo, S. (Eds.), Geology of Southwest Gondwana. Springer, Cham, pp. 267–302. https://doi.org/10.1007/978-3-319-68920-3_11

Hurford, A.J., 1990. Standardization of fission track dating calibration: Recommendation by the Fission Track Working Group of the I.U.G.S. Subcommission on Geochronology. Chem. Geol. Isot. Geosci. Sect. 80, 171–178. https://doi.org/10.1016/0168-9622(90)90025-8

Hurford, A.J., Green, P.F., 1983. The zeta age calibration of fission-track dating. Chem. Geol. 41, 285–317. https://doi.org/10.1016/S0009-2541(83)80026-6

Janasi, V. de A., de Freitas, V.A., Heaman, L.H., 2011. The onset of flood basalt volcanism, Northern Paraná Basin, Brazil: A precise U-Pb baddeleyite/zircon age for a Chapecó-type dacite. Earth Planet. Sci. Lett. 302, 147–153. https://doi.org/10.1016/j.epsl.2010.12.005

Jelinek, A.R., Bastos Neto, A.C., Poupeau, G., 2003. Análise Por Traços De Fissão Em Apatitas Do Distrito Fluorítico De Santa Catarina: Relações Entre Hidrotermalismo E Evolução Da Margem Continental. Rev. Bras. Geociências 33, 289–298. https://doi.org/10.25249/0375-7536.2003333289298

Jelinek, A.R., Chemale, F., van der Beek, P.A., Guadagnin, F., Cupertino, J.A., Viana, A., 2014. Denudation history and landscape evolution of the northern East-Brazilian continental margin from apatite fission-track thermochronology. J. South Am. Earth Sci. 54, 158–181. https://doi.org/10.1016/j.jsames.2014.06.001

Jelinek, A.R., Machado, J.P.S.L., Santos, E. do A., 2021. Evolução termocronológica do Cinturào Dom Feliciano: implicações na geodinâmica da margem continental sul do Brasil, in: Jelinek, A.R., Sommer, C.A. (Eds.), Contribuições à Geologia Do Rio Grande Do Sul e de Santa Catarina. Compasso Lugar-Cultura, Porto Alegre, pp. 185–202.

Karl, M., Glasmacher, U.A., Kollenz, S., Franco-Magalhaes, A.O.B., Stockli, D.F., Hackspacher, P.C., 2013. Evolution of the South Atlantic passive continental margin in southern Brazil derived from zircon and apatite (U-Th-Sm)/He and fission-track data. Tectonophysics 604, 224–244. https://doi.org/10.1016/j.tecto.2013.06.017

Ketcham, R.A., Carter, A., Donelick, R.A., Barbarand, J., Hurford, A.J., 2007. Improved modeling of fission-track annealing in apatite. Am. Mineral. 92, 799–810. https://doi.org/10.2138/am.2007.2281

Kollenz, S., 2015. Long-term landscape evolution, cooling and exhumation history of the South American passive continental margin in NE Argentina & SW Uruguay. Ruprecht-Karls-Universität.

Krob, F.C., Glasmacher, U.A., Bunge, H.-P., Friedrich, A.M., Hackspacher, P.C., 2020. Application of stratigraphic frameworks and thermochronological data on the Mesozoic SW Gondwana intraplate environment to retrieve the Paraná-Etendeka plume movement. Gondwana Res. 84, 81–110. https://doi.org/10.1016/j.gr.2020.02.010

Krob, F.C., Glasmacher, U.A., Karl, M., Perner, M., Hackspacher, P.C., Stockli, D.F., 2019. Multi-

chronometer thermochronological modelling of the Late Neoproterozoic to recent t-T-evolution of the SE coastal region of Brazil. J. South Am. Earth Sci. 92, 77–94. https://doi.org/10.1016/j.jsames.2019.02.012

Laslett, G.M., Kendall, W.S., Gleadow, A.J.W., Duddy, I.R., 1982. Bias in measurement of fission-track length distributions. Nucl. Tracks Radiat. Meas. 6, 79–85. https://doi.org/10.1016/0735-245X(82)90031-X

Lavina, E.L., 1988. The Passa Dois Group. In: Internation Gondwana Symposium, 7. 1988. São Paulo. Field excursion guide book. São Paulo: Instituto de Geociências, 24-30.

Lippolt, H.J., Leitz, M., Wernicke, R.S., Hagedorn, B., 1994. (Uranium + thorium)/helium dating of apatite: experience with samples from different geochemical environments. Chem. Geol. 112, 179–191. https://doi.org/10.1016/0009-2541(94)90113-9

Machado, J.P., Jelinek, A.R., Stephenson, R., O'Sullivan, P., 2021. Thermochronology of South America passive margin between Uruguay and southern Brazil: A lengthy and complex cooling history based on (U–Th)/He and fission tracks. J. South Am. Earth Sci. 106, 103019. https://doi.org/10.1016/j.jsames.2020.103019

Machado, J.P.S.L., Jelinek, A.R., Bicca, M.M., Stephenson, R., Genezini, F.A., 2019. West gondwana orogenies and pangaea break-up: Thermotectonic effects on the southernmost mantiqueira province, brazil. J. Geol. Soc. London. 176, 1056–1075. https://doi.org/10.1144/jgs2019-018

Machado, J.P.S.L., Jelinek, A.R., Stephenson, R., Gaucher, C., Bicca, M.M., Chiglino, L., Genezini, F.A., 2020. Low-temperature thermochronology of the South Atlantic margin along Uruguay and its relation to tectonic events in West Gondwana. Tectonophysics 784, 228439. https://doi.org/10.1016/j.tecto.2020.228439

Machado, J.P.S.L., Stephenson, R., Jelinek, A.R., Abdallah, R., 2021. Sismoestratigrafia e evolução da Bacia de Pelotas, in: Jelinek, A.R., Sommer, C.A. (Eds.), Contribuições à Geologia Do Rio Grande Do Sul e de Santa Catarina. Editora Compasso, Porto Alegre, pp. 403–419. https://doi.org/10.29327/537860.1-24

Martins-Ferreira, M.A.C., Dias, A.N.C., Chemale, F., Campos, J.E.G., 2020. Intracontinental uplift of the Brazilian Central Plateau linked to continental breakup, orogenies, and basin filling, supported by apatite and zircon fission-track data. Arab. J. Geosci. 13:891. https://doi.org/10.1007/s12517-020-05885-8

Milani, E.J., De Wit, M.J., 2014. Correlations between the classic Paraná and Cape-Karoo sequences of South America and southern Africa and their basin infills flanking the Gondwanides: Du Toit revisited. Geol. Soc. Spec. Publ. 294, 319–342. https://doi.org/10.1144/SP294.17

Milani, E.J., Gonçalves De Melo, J.H., De Souza, P.A., Fernandes, L.A., França, A.B., 2007a. Bacia do paraná. Bol. Geociencias da Petrobras 15, 265–287.

Milani, E.J., Ramos, V.A., 1998. Paleozoic orogenies in southwestern Gondwana and the subsidence cycles of the Parana Basin. Rev. Bras. Geociências 28, 473–484.

Milani, E.J., Rangel, H.D., Bueno, G.V., Stica, J.M., Winter, W.R., Caixeta, J.M., Da Cruz Pessoa Neto, O., 2007b. Bacias sedimentares brasileiras - Cartas estratigráficas. Bol. Geociencias da Petrobras 15, 183–205.

Mohriak, W.U., 2004. Recursos energéticos associados à ativação tectônica mesozóica-cenozóica da América do Sul. In: Mantesso-Neto, V., Bartorelli, A., Carneiro, C.D.R., Brito-Neves, B.B. (eds). Geologia do Continente Sul-Americano: Evolução da obra de Fernando Flávio Marques de Almeida. Beca Produções Culturais Ltda., São Paulo, XVII, 293-318.

Mohriak, W., Nemčok, M., Enciso, G., 2008a. South Atlantic divergent margin evolution: Rift-border uplift and salt tectonics in the basins of SE Brazil. Geol. Soc. Spec. Publ. 294, 365–398. https://doi.org/10.1144/SP294.19

Mohriak, W., Nemčok, M., Enciso, G., 2008b. South Atlantic divergent margin evolution: Rift-border uplift and salt tectonics in the basins of SE Brazil. Geol. Soc. Spec. Publ. 294, 365–398. https://doi.org/10.1144/SP294.19

Mohriak, W.U., Fainstein, R., 2012. Phanerozoic regional geology of the eastern Brazilian margin, in: Roberts, D.G., Bally, A.W. (Eds.), Regional Geology and Tectonics: Phanerozoic Passive Margins, Cratonic Basins and Global Tectonic Maps. Elsevier, Boston, pp. 222–282. https://doi.org/10.1016/B978-0-444-56357-6.00006-8

Mohriak, W.U., Nóbrega, M., Odegard, M.E., Gomes, B.S., Dickson, W.G., 2010. Geological and geophysical interpretation of the Rio Grande Rise, south-eastern Brazilian margin: Extensional tectonics and rifting of continental and oceanic crusts. Pet. Geosci. 16, 231–245. https://doi.org/10.1144/1354-079309-910

Moreira, J.L.P., Valdetaro, C.V., Gil, J.A., Machado, M.A.P., 2007. Bacia de Santos 2007. Bol. Geociencias da Petrobras 15, 531–549.

Moulin, M., Aslanian, D., Unternehr, P., 2010. A new starting point for the South and Equatorial Atlantic Ocean. Earth-Science Rev. 98, 1–37. https://doi.org/10.1016/j.earscirev.2009.08.001

Murray, K.E., Orme, D.A., Reiners, P.W., 2014. Effects of U-Th-rich grain boundary phases on apatite helium ages. Chem. Geol. 390, 135–151. https://doi.org/10.1016/j.chemgeo.2014.09.023

Nürnberg, D., Müller, R.D., 1991. The tectonic evolution of the South Atlantic from Late Jurassic to present. Tectonophysics 191, 27–53. https://doi.org/10.1016/0040-1951(91)90231-G

Oliveira, C.H.E. de, Jelinek, A.R., Chemale, F., Bernet, M., 2016. Evidence of post-Gondwana breakup in Southern Brazilian Shield: Insights from apatite and zircon fission track thermochronology. Tectonophysics 666, 173–187. https://doi.org/10.1016/j.tecto.2015.11.005

Oriolo, S., Oyhantçabal, P., Basei, M.A.S., Wemmer, K., Siegesmund, S., 2016. The Nico Pérez Terrane (Uruguay): From Archean crustal growth and connections with the Congo Craton to late Neoproterozoic accretion to the Río de la Plata Craton. Precambrian Res. 280, 147–160. https://doi.org/10.1016/j.precamres.2016.04.014

Oriolo, S., Oyhantçabal, P., Wemmer, K., Siegesmund, S., 2017. Contemporaneous assembly of Western Gondwana and final Rodinia break-up: Implications for the supercontinent cycle. Geosci. Front. 8, 1431–1445. https://doi.org/10.1016/j.gsf.2017.01.009

Oyhantçabal, P., Cingolani, C.A., Wemmer, K., Siegesmund, S., 2018a. The Río de la Plata Craton of Argentina and Uruguay, in: Siegesmund, S., Basei, M.Â.S., Oyhantçabal, P., Oriolo, S. (Eds.), Geology of Southwest Gondwana. Springer, Cham, pp. 89–105. https://doi.org/10.1007/978-3-319-68920-3_4

Oyhantçabal, P., Oriolo, S., Philipp, R.P., Wemmer, K., Siegesmund, S., 2018b. The Nico Pérez Terrane of Uruguay and Southeastern Brazil, Regional G. ed, Geology of Southwest Gondwana. Springer, Cham. https://doi.org/10.1007/978-3-319-68920-3_7

Oyhantçabal, P., Siegesmund, S., Wemmer, K., Passchier, C.W., 2011. The transpressional connection between Dom Feliciano and Kaoko Belts at 580-550 Ma. Int. J. Earth Sci. 100, 379–390. https://doi.org/10.1007/s00531-010-0577-3

Paim, P.S.G., Chemale Jr, F., Lopes, R. da C., 2000. A Bacia do Camaquã, in: Holz, M., De Ros, L.F. (Eds.), Geologia Do Rio Grande Do Sul. CIGO/UFRGS, Porto Alegre, pp. 231–274.

Passarelli, C.R., Stipp Basei, M.A., Siga, J.O., Hara, O.M.M., 2018. The Luis Alves and Curitiba Terranes: Continental Fragments in the Adamastor Ocean, in: Siegesmund, S., Basei, M.Â.S., Oyhantçabal, P., Oriolo, S. (Eds.), Geology of Southwest Gondwana. Springer, Cham, pp. 189–215. https://doi.org/10.1007/978-3-319-68920-3

Philipp, R.P., Machado, R., 2005. The Late Neoproterozoic granitoid magmatism of the Pelotas Batholith, southern Brazil. J. South Am. Earth Sci. 19, 461–478. https://doi.org/10.1016/j.jsames.2005.06.010

Philipp, R.P., Pimentel, M.M., Basei, M.A.S., 2018. The Tectonic Evolution of the São Gabriel Terrane, Dom Feliciano Belt, Southern Brazil: The Closure of the Charrua Ocean, in: Siegesmund, S., Basei, M.Â.S., Oyhantçabal, P., Oriolo, S. (Eds.), Geology of Southwest Gondwana. Springer, Cham, pp. 243–265. https://doi.org/10.1007/978-3-319-68920-3_10

Philipp, R.P., Pimentel, M.M., Chemale, F., 2016. Tectonic evolution of the Dom Feliciano Belt in Southern Brazil: Geological relationships and U-Pb geochronology. Brazilian J. Geol. 46, 83–104. https://doi.org/10.1590/2317-4889201620150016

Price, P.B., Walker, R.M., 1963. Fossil Tracks of Charged Particles in Mica and the Age of Minerals. J. Geophys. Res. 68, 4847–4862. https://doi.org/10.1029/JZ068i016p04847

Rabinowitz, P.D., Labrecque, J., 1979. The Mesozoic South Atlantic ocean and evolution of its continental margins. J. Geophys. Res. 84, 5973–6002. https://doi.org/10.1029/JB084iB11p05973

Reiners, P.W., Carlson, R.W., Renne, P.R., Cooper, K.M., Granger, D.E., McLean, N.M., Schoene, B., 2017. Geochronology and Thermochronology. Wiley-Blackwell. https://doi.org/10.1002/9781118455876

Reiners, P.W., Farley, K.A., 2001. Influence of crystal size on apatite (U-Th)/He thermochronology: An example from the Bighorn Mountains, Wyoming. Earth Planet. Sci. Lett. 188, 413–420. https://doi.org/10.1016/S0012-821X(01)00341-7

Riccomini, C., Velázquez, V.F., Gomes, C.B., 2005. Tectonic controls of the Mesozoic and Cenozoic alkaline magmatism in the central- southeastern Brazilian Platform. Mesozoic to Cenozoic Alkaline Magmat. Brazilian Platf. 31–57.

Shuster, D.L., Flowers, R.M., Farley, K.A., 2006. The influence of natural radiation damage on helium diffusion kinetics in apatite. Earth Planet. Sci. Lett. 249, 148–161. https://doi.org/10.1016/j.epsl.2006.07.028

Sonoki, I.K., Garda, G.M., 1988. Idades K-Ar de rochas alcalinas do Brasil meridional e Paraguai oriental: compilação e adaptação às novas constantes de decaimento. Bol. IG-USP. Série Científica 19, 63–85. https://doi.org/10.11606/issn.2316-8986.v19i0p63-85

Spiegel, C., Kohn, B., Belton, D., Berner, Z., Gleadow, A., 2009. Apatite (U-Th-Sm)/He thermochronology of rapidly cooled samples: The effect of He implantation. Earth Planet. Sci. Lett. 285, 105–114. https://doi.org/10.1016/j.epsl.2009.05.045

Stewart, K., Turner, S., Kelley, S., Hawkesworth, C., Kirstein, L., Mantovani, M., 1996. 3-D, 40Ar-39Ar geochronology in the Paraná continental flood basalt province. Earth Planet. Sci. Lett. 143, 95–109. https://doi.org/10.1016/0012-821x(96)00132-x

Stockli, D.F., Farley, K.A., Dumitru, T.A., 2000. Calibration of the apatite (U-Th)/He thermochronometer on anexhumed fault block, White Mountains, California. Geology 28, 983–986. https://doi.org/10.1130/0091-7613(2000)28<983:COTAHT>2.0.CO;2

Tagami, T., O'Sullivan, P.B., 2005. Fundamentals of fission-track thermochronology. Rev. Mineral. Geochemistry 58, 19–47. https://doi.org/10.2138/rmg.2005.58.2

Talwani, M., Abreu, V., 2000. Inferences regarding Initiation of Oceanic Crust Formation From the U.S. East Coast Margin and Conjugate South Atlantic Margins, in: Mohriak, W.U., Talwani, M. (Eds.), In Atlantic Rifts and Continental Margins. American Geophysical Union, Washington, p. 115. https://doi.org/https://doi.org/10.1029/GM115p0211

Torsvik, T.H., Rousse, S., Labails, C., Smethurst, M.A., 2009. A new scheme for the opening of the South Atlantic Ocean and the dissection of an Aptian salt basin. Geophys. J. Int. 177, 1315–1333. https://doi.org/10.1111/j.1365-246X.2009.04137.x

Turner, S., Regelous, M., Kelley, S., Hawkesworth, C., Mantovani, M., 1994. Magmatism and continental break-up in the South Atlantic: high precision 40Ar39Ar geochronology. Earth Planet. Sci. Lett. 121, 333–348. https://doi.org/10.1016/0012-821X(94)90076-0

Vermeesch, P., 2009. RadialPlotter: A Java application for fission track, luminescence and other radial plots. Radiat. Meas. 44, 409–410. https://doi.org/10.1016/j.radmeas.2009.05.003

Wildner, W., Camozzato, E., Toniolo, J.A., Binotto, R.B., Iglesias, C.M.F., Laux, J.H., 2014. Mapa geológico do Estado de Santa Catarina. Porto Alegre: CPRM. Escala 1:500.000. Programa Geologia do Brasil. Subprograma de Cartografia Geológica Regional.

Wolf, R.A., Farley, K.A., Kass, D.M., 1998. Modeling of the temperature sensitivity of the apatite (U-Th)/He thermochronometer. Chem. Geol. 148, 105–114. https://doi.org/10.1016/S0009-2541(98)00024-2

Wolf, R.A., Farley, K.A., Silver, L.T., 1996. Helium diffusion and low-temperature thermochronometry of apatite. Geochim. Cosmochim. Acta 60, 4231–4240. https://doi.org/10.1016/S0016-7037(96)00192-5

6.8 Email de aceite

Abaixo, segue a confirmação de que o artigo em questão foi aceito para publicação no periódico *Tectonophysics*.

Gmail **Edgar do Amaral Santos <santos.eas@gmail.com>**

TECTO15956R2 - Editor's decision: accepted for publication
1 mensagem

Tectonophysics <em@editorialmanager.com> 17 de abril de 2023 às 02:17
Responder a: Tectonophysics <support@elsevier.com>
Para: Edgar do Amaral Santos <santos.eas@gmail.com>

Dear Mr. do Amaral Santos,

I am pleased to inform you that the manuscript "Contrasting thermal histories in the Dom Feliciano Belt triggered by magmatism related to the Paraná-Etendeka LIP and fracture zone proximity" (Mr. Edgar do Amaral Santos) has now been accepted by the editor for publication.

Your manuscript will soon be passed to the production department for further handling. Then you will receive further notice.

Your accepted manuscript will now be transferred to our production department and work will begin on creation of the proof. If we need any additional information to create the proof, we will let you know. If not, you will be contacted again in the next few days with a request to approve the proof and to complete a number of online forms that are required for publication.

Thank you for considering our journal for the publication of your research.

We encourage authors of original research papers to share the research objects – including raw data, methods, protocols, software, hardware and other outputs – associated with their paper. More information on how our open access Research Elements journals can help you do this is available at https://www.elsevier.com/authors/tools-and-resources/research-elements-journals?dgcid=ec_em_research_elements_email.

Kind regards,

Zheng-Xiang Li
Editor
Tectonophysics

CAPÍTULO 7 – Contrasting behavior and dynamics of lithospheric processes in São Francisco Craton and adjacent belts: Insights from thermochronological analysis

Edgar do Amaral Santos [a,], Andréa Ritter Jelinek [b], Frederico Antônio Genezine [c], Daniel Stockli [d]*

[a] Programa de Pós-Graduação em Geociências, Universidade Federal do Rio Grande do Sul, Brazil

[b] Instituto de Geociências, Universidade Federal do Rio Grande do Sul, Brazil

[c] Instituto de Pesquisas Energéticas e Nucleares, Centro do Reator de Pesquisas, Brazil

[d] University of Texas at Austin, United States of America

* Corresponding author. E-mail address: edgar.amaral@ufrgs.br (E. do Amaral Santos)

Nota explicativa

Este capítulo corresponde ao artigo submetido em 2023 no periódico *Gondwana Research.* Ao final do manuscrito encontra-se a carta de submissão na revista científica. Os dados suplementares desse artigo estarão disponíveis quando do aceite deste artigo, visto que é composto por tabelas bastante extensas.

Abstract

The South American Platform hosts the São Francisco Craton (SFC) and the Araçuaí and Ribeira orogenic belt in southeastern to northeastern Brazil. These geologic domains hold records of differential exhumation, sedimentation, volcanic activity, and post-rift reactivation of faults and shear zones. Therefore, these terrains are excellent places to scrutinize the dynamics of lithospheric processes since they are characterized by the transition of a cratonic to an orogenic lithosphere. To investigate the processes involved in the contrasting behavior of the upper crust, we provide 23 new Apatite Fission Track (AFT) ages and thermal histories. Then, we compiled thermal information from 357 sites and constructed inverse distance weighted maps that depict the spatial distribution of AFT ages and the temperature evolution from 360 to 30 Ma. The AFT ages range from 154.4 ± 20.1 to 37.1 ± 3.0Ma. Results reveal that the SFC experienced exhumation before adjacent orogenic terranes. At the same time, the Araçuaí and Ribeira Belts underwent Mesozoic to Cenozoic cooling from temperatures cooler than 110 ºC, indicating rift to post-rift reactivation and reheating. Our work demonstrates the importance of considering

rheology when analyzing regional exhumation patterns, particularly in cratonic and non-cratonic lithosphere cases. Furthermore, the structural fabric of orogenic belts is vital for reactivating faults and shear zones during a post-rift phase of a continental margin, generating local heating and exhumation. Furthermore, this work exposes that volcanism can disrupt the thermal record, inducing crustal reheating and keeping the low-temperature thermochronometers open, generating young AFT ages.

7.1 Introduction

A series of mechanisms that operate from deep within the Earth, such as mantle dynamics (Dávila et al., 2023) and tectonics (Val et al., 2018), to surface climate conditions (Jepson et al., 2021) govern lithospheric processes. These mechanisms are influenced by rheology (Fonseca et al., 2021), the presence of crustal discontinuities (do Amaral Santos et al., 2022), and volcanism (Hueck et al., 2018; do Amaral Santos et al., 2023).

A primary lithospheric transitional zone where we can investigate the dynamics of lithospheric processes is in southeastern to northeastern Brazil. The São Francisco Craton (SFC), which is a cratonic peninsula that once was part of the Congo Craton (Heilbron et al., 2017a), and two orogenic belts formed through the interaction of these cratons during the Neoproterozoic to Cambrian characterize this region: The Araçuaí (Alkmim et al., 2017) and Ribeira Belts (Heilbron et al., 2017b). The former represents an orogenic belt formed in a cratonic embayment (Pedrosa-Soares et al., 2011; Alkmim et al., 2017), whereas several micro-continents accreted to a continental margin constitute the latter (Heilbron et al., 2017b). Additionally, these terranes act as basement to the continental margin developed from the Cretaceous onward since the opening of the South Atlantic Ocean (Nürnberg and Müller, 1991; Chang et al., 1992; Torsvik et al., 2009). Considering this geologic context, we chose the Apatite Fission Track (AFT) method (Donelick et al., 2005; Price and Walker, 1963) because it records the thermal information within the upper few kilometers of the crust from depths spanning from 5 to 2 km and temperatures ranging from *ca.* 120 to 60 ºC, respectively (Gleadow and Duddy, 1981; Gleadow et al., 1986; Green et al., 1986), making it a valuable tool for investigating geodynamic processes.

We collected 23 basement samples in the Araçuaí Belt and SFC and performed AFT analyses to achieve this. This contribution presents 23 new AFT ages and obtained new

thermal histories for the analyzed samples. Additionally, we compiled all AFT ages available in the literature and thermal information from 357 samples distributed across the Ribeira and Araçuaí Belts and the SFC to create inverse distance-weighted (IDW) maps. One of these maps depicts the spatial distribution of AFT ages, while 12 maps illustrate the temperature evolution from 360 to 30 Ma throughout the region. These maps were further analyzed and discussed along with geological data available in the literature, focusing on local and regional lithospheric processes. Our study aims to understand how the spatial distribution of AFT ages behaves in this transitional zone, how the thermal history recorded evolved through time and temperature, and which cooling and reheating events the area recorded. Then, we looked for evidence for the control of rheology, reactivation of crustal discontinuities, and volcanism on crustal exhumation, considering a regional geodynamic perspective.

7.2 Geologic Framework

The study area of this work extends from southeastern to northeastern Brazil, encompassing cratonic and orogenic terranes known as SFC and Araçuaí and Ribeira Belts, respectively, along with the continental margin to the east (Fig. 7.1).

The SFC, a cratonic fragment within the South American plate, was once part of the Congo Craton. These cratons remained intact until their dispersal during the opening of the South Atlantic Ocean in the Lower Cretaceous (Alkmim and Martins-Neto, 2012; Heilbron et al., 2017a). The exposed basement units of the SFC are older than 1.8 Ga, while the cratonic cover consists of sequences younger than 1.8 Ga (Almeida, 1977). Archean TTG-gneisses, granitoids, greenstone belts, Paleoproterozoic plutons, and supracrustal successions characterize the basement units. The cratonic cover encompasses Proterozoic and Phanerozoic sedimentary sequences (Alkmim and Marshak, 1998; Alkmim and Martins-Neto, 2012). Surrounding this craton are the Brasiliano belts, a series of orogenic systems formed during the amalgamation of the West Gondwana continent. This work analyzed the orogenic belts located southeast and south of the craton, namely the Araçuaí and Ribeira Belts, respectively (Almeida, 1977).

The Araçuaí Belt formed during the Neoproterozoic to the Cambrian through the interaction of the SFC and the Congo Craton in a confined setting, where these cratons formed an embayment (Alkmim et al., 2006; Heilbron et al., 2017a; Pedrosa-Soares et al., 2008, 2011). The belt represents the external domain of the Araçuaí-West Congo Orogen,

characterized by thick-skinned deformation (Alkmim et al., 2017). In the Brazilian portion of the orogen, known as the Araçuaí Belt, there are basement units older than 1.8 Ga, Paleo to Mesoproterozoic rif to rift-sag successions of the Espinhaço Supergroup, Neoproterozoic-Cambrian passive margin units (Macaúbas Group; Souza et al., 2019), syn-orogenic sequences, and crustal-derived granitic intrusions. The syn-metamorphic climax of the granitic plutons dates to *ca.* 590 to 530 Ma (Alkmim et al., 2017; Pedrosa-Soares et al., 2001; Pedrosa-Soares and Wiedemann-Leonardos, 2000).

Located southward of the SFC, the Ribeira Belt resulted from multiple collisional episodes during the Neoproterozoic to Cambrian (Heilbron and Machado, 2003). This belt consists of four tectono-stratigraphic terranes, including a reworked cratonic basement of the external sector along with intra-cratonic basins and a passive margin unit, active margin sequences, continental magmatic arcs, and a series of granites that intruded the basement, and supracrustal units (Heilbron et al., 2020). Terrane docking and reworking have played a significant role in this orogen. At the same time, the structural fabric of this belt is characterized by shear zones and large-scale folds, with metamorphic imprints ranging from 630 to 510 Ma (Heilbron et al., 2017b).

Several basin depocenters developed within the Gondwana continent from the Ordovician onwards, such as the Paraná, Parnaíba, and Sanfranciscana basins (Linol et al., 2015). The Parnaíba basin started its subsidence during the Silurian, related to the final stages of the Brasiliano-Pan-African Orogenic Cycle (Vaz et al., 2007), and it is constituted of five supersequences related to fluctuations of eustatic epicontinental sea levels. The Paraná Basin, located southwest of the study area, consists of six supersequences separated by regional unconformities. Transgressive-regressive cycles characterize the first three sequences of Ordovician to Permian/Triassic ages, and the last three sequences comprise continental volcano-sedimentary units of Triassic to Cretaceous ages (Milani et al., 1998, 2007a; Scherer et al., 2023). Last, the Sanfranciscana basin, located within the SFC, developed from the Carboniferous/Permian to the Cretaceous, comprising glacial-marine and continental desertic environments associated with volcanic extrusions (Campos and Dardenne, 1997; Sgarbi et al., 2001; Zalán and Silva, 2007).

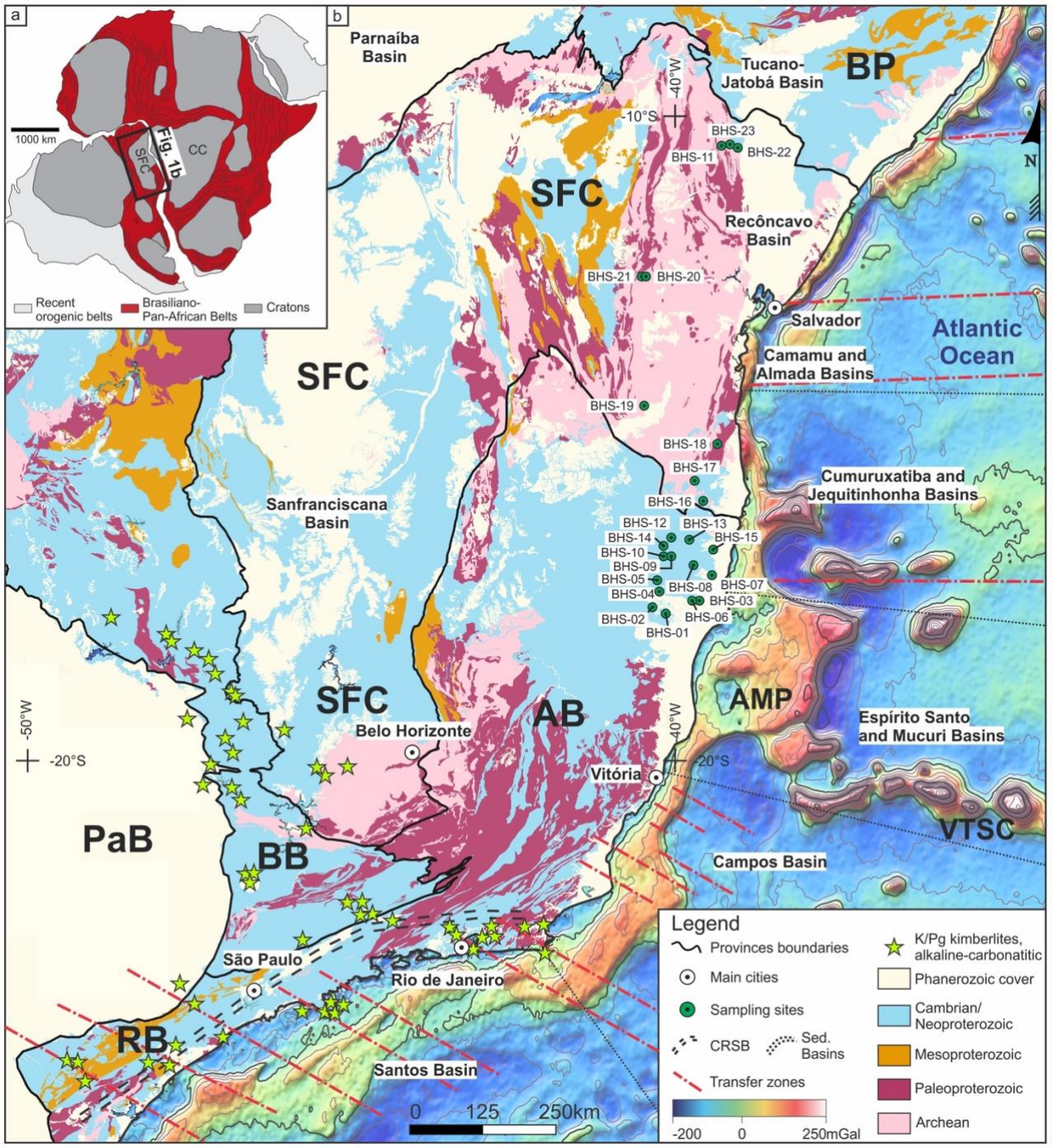

Figure 7. 1: a) West Gondwana map depicting the cratons, some orogenic belts formed during the West Gondwana amalgamation, and the recent orogenic belts (after Oriolo et al., 2017). SFC: São Francisco Craton; CC: Congo Craton. b) Geologic map of the study area in southeastern to northeastern Brazil (after Leite et al., 2004), evidencing the limits of the São Francisco Craton and the adjacent Araçuaí Belt (AB), Ribeira Belt (RB), Brasília Belt (BB), the Borborema Province (BP), and the intracratonic Paraná (PaB), Parnaíba, Sanfranciscana, Recôncavo-Tucano-Jatobá Basins, as well as the Continental Rift of Southeastern Brazil (CRSB) (Riccomini et al., 2004) and the Cretaceous/Paleogene kimberlites and alkaline-carbonatitic rocks. The offshore region displays the gravity anomaly map of the South Atlantic Ocean seafloor (Sandwell et al., 2014) eastward of the study area, evidencing the Abrolhos Magmatic Province (AMP), the Vitória-Trindade seamount chain (VTSC), and the Cretaceous/Cenozoic marginal basins (Mohriak and Fainstein, 2012).

The formation of the continental margin to the east of the SFC, Araçuaí Belt, and

Ribeira Belts coincided with the opening of the South Atlantic Ocean during the Lower Cretaceous (Mohriak et al., 2008). Both segments, composed of cratonic or non-cratonic rocks as basements, comprise Cretaceous to Cenozoic sedimentary sequences and Paleocene to Eocene volcanic rocks (Mohriak and Fainstein, 2012). The volcanic record in the region is notable for the significant Abrolhos Magmatic Province (Stanton et al., 2021), as well as the Vitória-Trindade seamount chain. Additionally, a series of kimberlite and alkaline-carbonatitic plutons that intruded both the margin and the interior of the continent in southeastern Brazil during the Cretaceous and Paleogene (Takenaka et al., 2023).

Furthermore, during the Paleogene, the Continental Rift of Southeastern Brazil (CRSB) developed, forming an elongated narrow trough nearly 900 km long (Riccomini, 1990; Riccomini et al., 2004; Zalán and De Oliveira, 2005). This lithospheric feature is mainly parallel to the present-day coastline and the Neoproterozoic shear zones of the Ribeira Belt. These shear zones were reactivated as normal faults, generating sedimentary basins and as strike-slip afterward, producing tectonic deformation. Additionally, volcanic alkaline emplacement near the border of the rift occurred as the rift developed (Riccomini et al., 2004, 2005).

7.3 Methods

For AFT thermochronology analysis, this study collected 23 basement samples from the Araçuaí Belt and SFC regions. Our focus was on lithologies rich in apatite such as granites and gneisses. Some of these samples had previously undergone analysis for zircon and apatite (U-Th)/He thermochronology (do Amaral Santos et al., 2022), which this study integrated (Supplementary Data S1). Table 7.1 contains detailed information regarding the lithology, sample locations, altitudes, and the methods employed.

The AFT method relies on the accumulation of fission tracks resulting from the spontaneous fission of ^{238}U (Price and Walker, 1963; Fleischer and Price, 1964). By analyzing the areal density and length of these tracks, we can determine the AFT age and reconstruct the thermal history experienced by each sample (Reiners et al., 2017). These tracks remain preserved below 120 °C over geological timescales, corresponding to upper crustal temperatures. However, at temperatures between 120 and 60 °C (Green et al., 1989b), the tracks undergo shrinkage due to thermal annealing, with the temperature, chemical composition, and radiation damage acting as controlling factors (Donelick et al.,

2005; Tagami and O'Sullivan, 2005), defining the Apatite Partial Annealing Zone.

Table 7. 1: Details from samples analyzed in this study. Coordinates in decimal degree; AHe and ZHe data published in do Amaral Santos et al. (2022) and available in Supplementary Data S1. AFT: Apatite Fission Track; AHe: Apatite (U-Th)-He dating; ZHe: Zircon (U-Th)/He dating.

Sample	Lithology	Latitude (º S)	Longitude (º W)	Elevation (m)	Method
BHS-01	Granitoid	17.717500	40.141111	169	AFT
BHS-02	Granitoid	17.615278	40.346667	252	AFT, ZHe, AHe
BHS-03	Granitoid	17.515278	39.650556	24	AFT
BHS-04	Granitoid	17.371667	40.231667	149	AFT
BHS-05	Granitoid	17.188889	40.280556	227	AFT
BHS-06	Granitoid	17.512222	39.705000	86	AFT, ZHe, AHe
BHS-07	Granitoid	17.131667	39.433333	36	AFT
BHS-08	Granitoid	16.957222	39.716111	82	AFT
BHS-09	Granitoid	16.827500	40.056667	197	AFT
BHS-10	Granitoid	16.837222	40.141667	207	AFT, Zhe
BHS-11	Granitoid	10.468889	39.268611	450	AFT
BHS-12	Granitoid	16.571111	40.089167	292	AFT, ZHe
BHS-13	Granitoid	16.575000	39.781667	187	AFT, ZHe, AHe
BHS-14	Granitoid	16.659167	40.175278	293	AFT
BHS-15	Granitoid	16.725278	39.410000	80	AFT, ZHe, AHe
BHS-16	Granitoid	15.968889	39.561944	82	AFT
BHS-17	Granitoid	15.668889	39.691111	119	AFT, ZHe, AHe
BHS-18	Granitoid	15.083333	39.340556	90	AFT
BHS-19	Granitoid	14.493333	40.467222	838	AFT
BHS-20	Granitoid	12.509167	40.449444	305	AFT
BHS-21	Granitoid	12.493333	40.506667	317	AFT
BHS-22	Granitoid	10.489444	39.067778	385	AFT
BHS-23	Granitoid	10.465000	39.146111	449	AFT

Standard crushing, sieving, and hand-picking techniques concentrated the apatite crystals (Kohn et al., 2019). This study utilized the external detector method (EDM; Hurford, 1990) and neutron irradiation in the CNEN-IPEN reactor in São Paulo, Brazil. The apatite crystals were embedded in epoxy resin, polished, and subjected to chemical etching with HNO_3 5.5 M at 21 °C for 20 seconds (Carlson et al., 1999; Donelick et al., 2005) to reveal spontaneous tracks. Low-U muscovite sheets were affixed to the apatite

mounts, U-doped glass dosimeters (CN5), and Durango age standards. To expose induced tracks, 48 % HF at 20 °C for 18 minutes etched the mica sheets.

AFT dating and track length measurements were conducted at the Labmodel, a thermochronology facility at the Universidade Federal do Rio Grande do Sul, Brazil. The analysis was assisted using a Leica CTR 6000 microscope at a magnification of 1,000x (dry). A minimum of 20 grains were used for AFT age calculation, with only one sample not meeting this criterion. The ζ calibration method was employed to calibrate the AFT ages (Hurford and Green, 1983), and age homogeneity was evaluated using the chi-squared test (Galbraith, 1981) in RadialPlotter 9.4 (Vermeesch, 2009). A length-frequency histogram of AFT data (n>50) was obtained for 19 representative samples, while less representative histograms (50>n>10) were obtained for three samples.

Inverse modeling was performed for 22 samples using the QTQt 5.8.0 software (Gallagher, 2012), with Dpar and c-axis projection (Ketcham et al., 2007) employed as parameters to model AFT data (Ketcham et al., 2007). For inverse modeling, the radiation damage accumulation and annealing models for zircon (Guenthner et al., 2013) and apatite (Flowers et al., 2009) were utilized to model (U-Th)/He data of zircon and apatite, respectively.

The present-day surface temperature was constrained to 20 ± 10 °C. When considering only AFT data, the prior temperature was set at 70 ± 70 °C, whereas it was set at 100 ± 100 °C when including ZHe data. The oldest AFT or ZHe/AHe age of each sample was used as a prior for time with an uncertainty of $t_o \pm t_o$, and the maximum gradient ($\partial T/\partial t$) was set at 30 °C/m.y. Initial runs of 30,000 iterations were used to define the values for the MCMC algorithm. Runs of at least 200,000 post-burn-in iterations were then defined with the appropriate values for inverse modeling.

To evaluate the AFT age of all available samples in the literature across SFC, Araçuaí, and Ribeira Belts and to assess the evolution of basement temperature in this region, we employed inverse distance weighted (IDW) maps created using ArcGIS 10.3. The map illustrating the AFT ages was constructed based on the AFT central ages of 728 sites (Supplementary Data S2). The IDW maps depicting the temperature evolution were generated using temperature data at 12 specific time intervals (360 to 30Ma) acquired from 357 sites, including thermal models created in this study and those available in the literature (Supplementary Data S3). The analysis of thermal histories predominantly relied on AFT; however, some studies integrated this thermochronometer with other

geochronometers and thermochronometers, such as AHe, ZHe, U-Pb in zircon (Franco et al., 2005; Hiruma et al., 2010; Cogné et al., 2011, 2012; Doranti-Tiritan, 2013; Jelinek et al., 2014, 2020; Engelmann de Oliveira et al., 2016; Soares et al., 2016; Amaral-Santos et al., 2019; Krob et al., 2019; Van Ranst et al., 2020; Fonseca et al., 2021, 2022, 2023; Gezatt et al., 2021; Costa, 2022; do Amaral Santos et al., 2022). Notably, one study used constraints to replicate present-day temperature conditions for modeling in low-temperature environments, which may bias the models to force low-temperature paths (Krob et al., 2019).

7.4 Results

7.4.1 Spatial distribution of AFT ages and MTL

The new AFT data from 23 analyzed sites in the northern Araçuaí Belt and SFC are summarized in Table 7.2 and Figure 7.2. The AFT ages were calculated using a zeta of 134.41 ± 6.19 for CN5 glass on the Brazil reactor, and all samples passed the χ^2 test ($P(\chi^2) > 0.05$), which represents single age populations.

The new AFT central ages vary from 154.4 ± 20.1 to 37.1 ± 3.0Ma (Fig. 7.2), which are Jurassic to Eocene Epoch. The AFT ages of samples collected in the orogenic domain vary from 125.6 to 37.1 Ma and are younger. In contrast, the cratonic area exhibits older ages, spanning from 154.4 to 103.8 Ma, except for two samples recording 77 and 77.2 Ma (Fig. 7.2). This data set displays a positive correlation between AFT ages and the distance to the coast as well as a positive correlation between AFT ages and Dpar (Supplementary Data S4, Figs. S1 and S2). Additionally, the samples BHS-02 and BHS-13 display AFT ages younger than their AHe ones.

Track-length and c-axis angle data were acquired from 22 samples, while only one sample lacked this information (Table 7.2). Nineteen samples have more than 60 horizontal confined fission-track lengths measured, whereas three samples have yet to reach 40 tracks measured. The MTL falls within the short to intermediate range (10.91 to 13.20 mm), with most tracks measuring 11 to 12 mm, and exhibits a unimodal distribution with narrow standard deviation and negative skewness (Supplementary Data S4). This data set displays a negative correlation between AFT ages and MTL (Fig. S3).

Table 7. 2: New Apatite Fission Track data from the Araçuaí Belt and the São Francisco Craton, in southeastern to northeastern Brazil.

Sample	N	r s (Ns)	r i (Ni)	r d (Nd)	P (c2)	U	Centr. Age ± 1s	n	MTL	Std. Dev.	P.MTL	P.Std. Dev.	Dpar	Skewness
	#	($x10^5$)	($x10^5$)	($x10^5$)	(%)	(∝g/g)	(Ma)	#	(∝m)	(∝m)	(∝m)	(∝m)	(∝m)	#
BHS-01	25	10.68 (156)	13.01 (190)	21.30 (27164)	0.99	7.8	116.5 ± 14.0	100	12.08	1.71	13.51	1.34	1.51	-0.14
BHS-02	25	6.04 (330)	12.77 (697)	14.54 (18586)	0.97	11.1	46.1 ± 3.7	100	12.47	1.58	13.72	1.26	1.52	-0.13
BHS-03	25	12.65 (148)	27.52 (322)	21.30 (27164)	0.79	16.4	65.5 ± 7.2	11	12.73	1.92	13.62	1.87	1.46	-1.09
BHS-04	25	15.99 (331)	41.98 (869)	14.54 (18586)	1.00	36.7	37.1 ± 3.0	101	11.27	1.87	13.11	1.25	1.43	-0.19
BHS-05	25	5.53 (142)	10.82 (278)	14.54 (18586)	0.95	9.4	49.7 ± 5.5	77	12.71	1.61	13.95	1.14	1.48	-0.66
BHS-06	25	4.15 (164)	5.22 (206)	14.54 (18586)	0.99	4.6	77.3 ± 8.5	70	13.20	1.80	14.34	1.26	1.5	-0.61
BHS-07	25	7.09 (317)	15.28 (683)	14.54 (18586)	0.88	13.3	45.2 ± 3.6	100	12.78	1.59	13.92	1.10	1.45	-0.65
BHS-08	25	13.84 (256)	10.97 (203)	14.54 (18586)	0.5	9.6	122.1 ± 12.2	100	11.56	1.97	13.16	1.41	1.7	-0.12
BHS-09	25	10.68 (156)	13.01 (190)	21.30 (27164)	1.00	7.8	116.5 ± 14.0	70	12.26	1.93	13.48	1.65	1.61	-0.24
BHS-10	25	16.92 (330)	17.54 (342)	14.54 (18586)	0.89	15.3	93.6 ± 8.4	100	12,00	1.69	13.28	1.32	1.63	-0.03
BHS-11	25	13.29 (299)	15.73 (354)	21.30 (27164)	0.96	9.4	119.8 ± 10.8	100	10.91	1.68	12.60	1.33	1.59	0.03
BHS-12	14	8.38 (88)	8.38 (88)	14.54 (18586)	0.50	7.3	97.0 ± 15.5	*	*	*	*	*	*	*
BHS-13	25	7.40 (290)	9.21 (361)	14.54 (18586)	0.61	8.0	78.0 ± 7.0	100	12.37	1.59	13.69	1.10	1.65	-0.53
BHS-14	25	6.94 (460)	7.828 (519)	21.30 (27164)	0.28	4.7	125.6 ± 10.0	66	12.34	1.88	13.55	1.53	1.65	-0.84
BHS-15	25	14.73 (383)	36.31 (944)	21.30 (27164)	0.72	21.6	57.8 ± 4.6	100	12.56	1.61	13.92	1.13	1.61	-0.41
BHS-16	25	6.11 (113)	6.70 (124)	21.30 (27164)	1.00	4.0	129.2 ± 18.1	15	11.79	1.56	13.19	1.20	1.77	-0.1
BHS-17	25	7.81 (225)	7.36 (212)	21.30 (27164)	0.97	4.4	150.2 ± 16.5	101	11.86	1.75	13.33	1.33	1.58	-0.16
BHS-18	25	7.26 (283)	9.13 (356)	14.54 (18586)	0.944	8.0	77.2 ± 6.9	72	11.45	1.91	13.05	1.36	1.53	0.08
BHS-19	25	22.00 (220)	30.10 (301)	21.30 (27164)	0.95	17.9	103.8 ± 10.4	76	11.91	1.89	13.44	1.24	1.54	-0.37
BHS-20	25	22.90 (229)	42.30 (423)	21.30 (27164)	1.00	25.2	77.0 ± 6.9	100	11.54	1.67	12.92	1.54	1.46	-0.06
BHS-21	25	20.75 (220)	18.02 (191)	14.54 (18586)	1.00	15.7	111.6 ± 12.3	100	11.19	1.67	12.95	1.25	1.48	0.24
BHS-22	25	24.20 (242)	18.80 (188)	14.54 (18586)	1.00	16.4	124.6 ± 13.7	37	11.24	2.07	12.96	1.26	1.49	0.34
BHS-23	25	13.08 (187)	8.18 (117)	14.54 (18586)	1.00	7.1	154.4 ± 20.1	99	11.77	1.66	13.07	1.40	1.48	0.13

N: number of apatite crystals analyzed to determine track densities; r s: measured spontaneous track density; Ns: number of spontaneous tracks counted; r i: measured induced track density; Ni: number of induced tracks counted; r d: track density measured in external detector adjacent to glass dosimeter during irradiation; Nd: number of tracks counted in determining r d; P (c2): chi-squared probability; n: number of confined track lengths measured; * no horizontal confined track length measured; Centr. Age: Central Age; Std. Dev.: Standard Deviation; P.MTL: Projected mean track length; P.Std. Dev.: Standard Deviation of Projected mean track length

Apatite ages calculated using a zeta of 134.41 ± 6.19 for CN5 glass on Brazil reactor. Analyst: Edgar do Amaral Santos

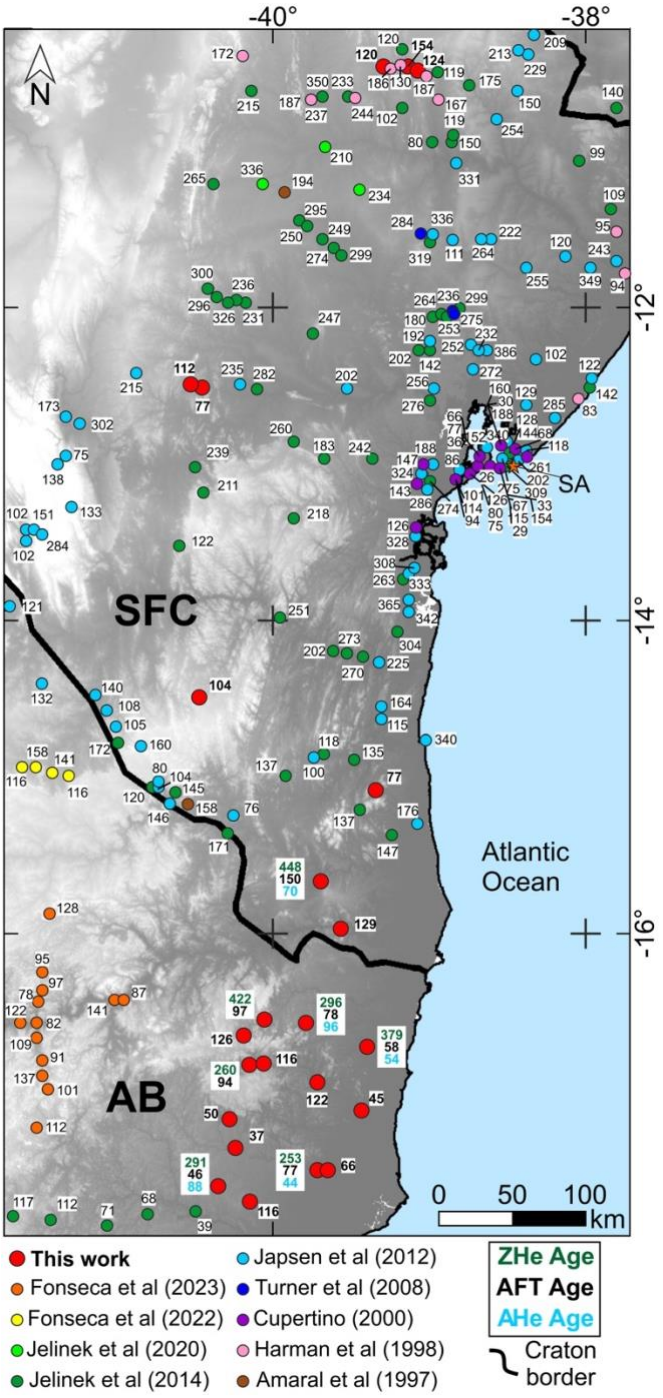

Figure 7. 2: Distribution of the new AFT ages of this data set along with AFT, AHe, and ZHe ages available in the literature from the northern Araçuaí Belt (AB) and the São Francisco Craton (SFC) (Amaral et al., 1997; Harman et al., 1998; Cupertino, 2000; Turner et al., 2008; Japsen et al., 2012; Jelinek et al., 2014, 2020; do Amaral Santos et al., 2022; Fonseca et al., 2022, 2023). Results of this study are displayed in bold and is the only work to incorporate both ZHe and AHe data in the area.

The AFT age spatial distribution depicted in Fig. 7.3 reveals older AFT ages in both northern and southern segments of the SFC. The northern portion displays Permian to Triassic ages, while the southern region primarily encompasses ages within the Triassic to Jurassic. Jurassic to Lower Cretaceous ages characterize the transitional region from

the craton to the adjacent belts.

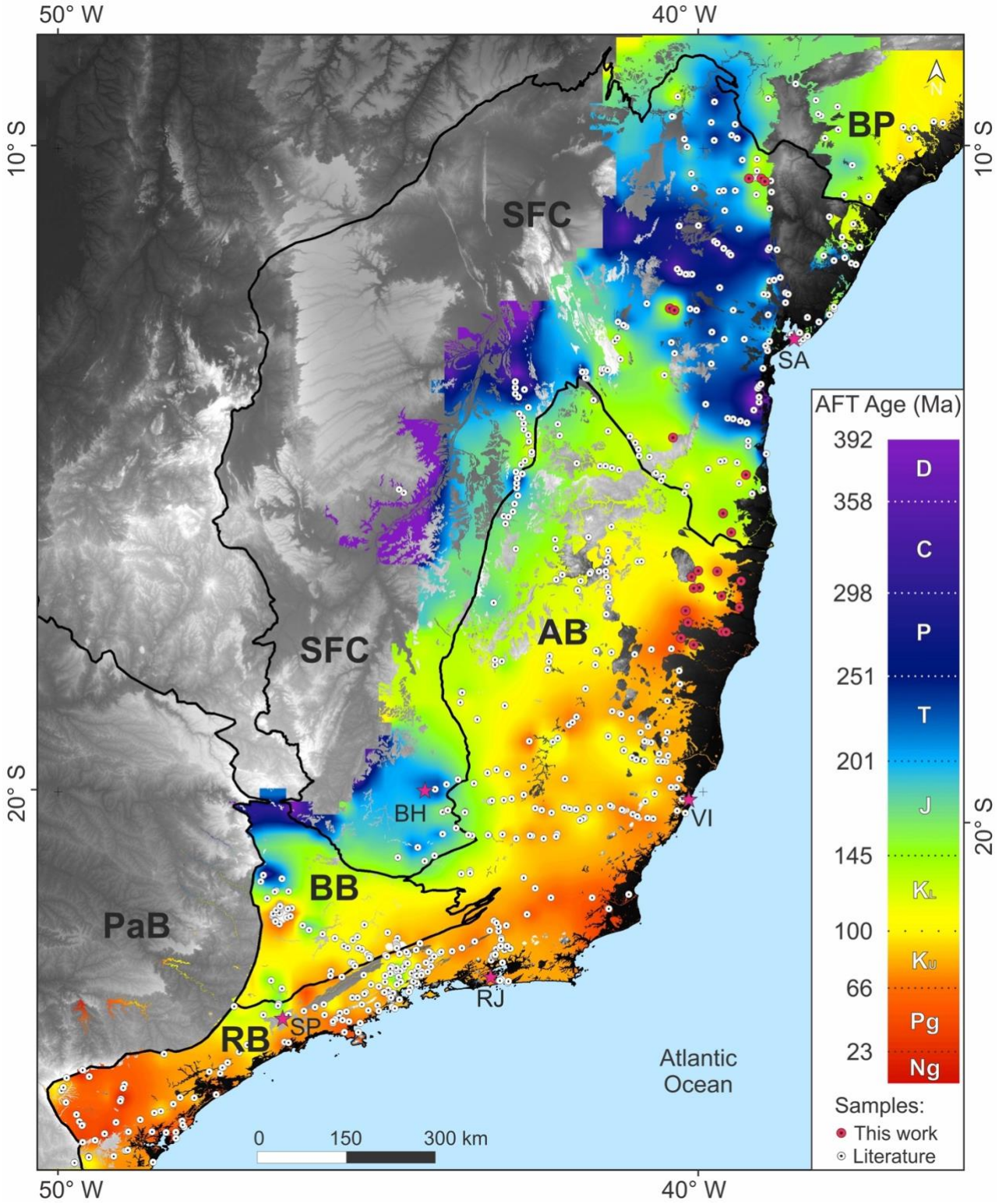

Figure 7. 3: a) Inverse distance weighted (IDW) map displaying the spatial distribution of Apatite Fission Track central ages in southeastern to northeastern Brazil. The interpolation process considered samples from Gallagher et al. (1994), Amaral et al. (1997), Harman et al. (1998), Cupertino (2000), Oliveira et al. (2000), Hadler et al. (2001), Tello Saenz et al. (2003), Carmo (2005), Franco et al. (2005), Ribeiro et al. (2005, 2011), Silva (2006), Hackspacher et al. (2007), Genaro (2008), Turner et al., (2008), Franco-Magalhaes et al. (2010, 2014), Hiruma et al. (2010), Gomes (2011), Cogné et al. (2012), Japsen et al.

(2012), Doranti-Tiritan (2013), Karl et al. (2013), Jelinek et al. (2014, 2020), Souza et al. (2014), Engelmann de Oliveira et al. (2016), Soares et al. (2016), Amaral-Santos et al. (2019), Krob et al. (2019), Van Ranst et al. (2020), Fonseca et al. (2020, 2021, 2022, 2023), Gezatt et al. (2021), and Costa, (2022). Samples from the Phanerozoic cover were not considered for interpolation. Abbreviations are: SFC: São Francisco Craton; AB: Araçuaí Belt; RB: Ribeira Belt; BB: Brasília Belt; BP: Borborema Province; PaB: Paraná Basin; RJ: Rio de Janeiro City; SA: Salvador City; BH: Belo Horizonte City. After Engelmann de Oliveira and Jelinek (2017), Hueck et al. (2019), and Novo et al. (2021).

The inland portion of the Araçuaí Belt displays Lower to Upper Cretaceous ages, which are broadly compatible with the shape of the SFC limits. The samples closer to the margin exhibit Upper Cretaceous to Paleogene ages, and some samples located to the northwest of latitude 20° S and longitude 40° W record ages varying from the Lower to Upper Cretaceous.

Furthermore, the Araçuaí and the Ribeira Belts demonstrate a noticeable trend of increasing AFT ages towards the coast, ranging from the Lower Cretaceous to the Neogene. Contrasting to the overall ages of the Araçuaí Belt, the Ribeira Belt mainly displays Upper Cretaceous to Paleogene ages, with some Neogene ages in its southern portion. Some localized sites within the Ribeira Belt display AFT ages from the Lower Cretaceous.

Finally, the intersection between the Ribeira and the southern Brasília belts displays Jurassic to Lower Cretaceous ages, except its northerly region, which records Paleozoic and Triassic ages, and a site of Upper Cretaceous ages in the Brasília Belt near an alkaline massif (Fig. 7.1).

7.4.2 Thermal history patterns and temperature variations: insights from thermal models and data kriging

Based on the thermal models, three distinct groups were identified (Supplementary Data S4 and Fig. 7.4):

(i) Slow continuous cooling from the Paleozoic onwards (BHS-01, 09, 14, and 16), with some samples lacking thermal signals before 110 Ma (BHS-03, 05, 07, and 15).

(ii) The onset of slow cooling from the Paleozoic to the Upper Cretaceous, followed by a rapid cooling event during the Paleogene-Neogene (BHS-04, 08, 11, and 19 to 23).

(iii) An initial cooling episode succeeded by reheating 10 to 25 °C and, subsequently, a final cooling to present-day surface conditions (BHS-02, 06, 10, 13, 17, and 18).

Considering the IDW maps (Figs. 7.4, 7.5, and 7.6) and thermal models, limited thermal information is available for certain regions preceding the Mesozoic, with relatively low probability.

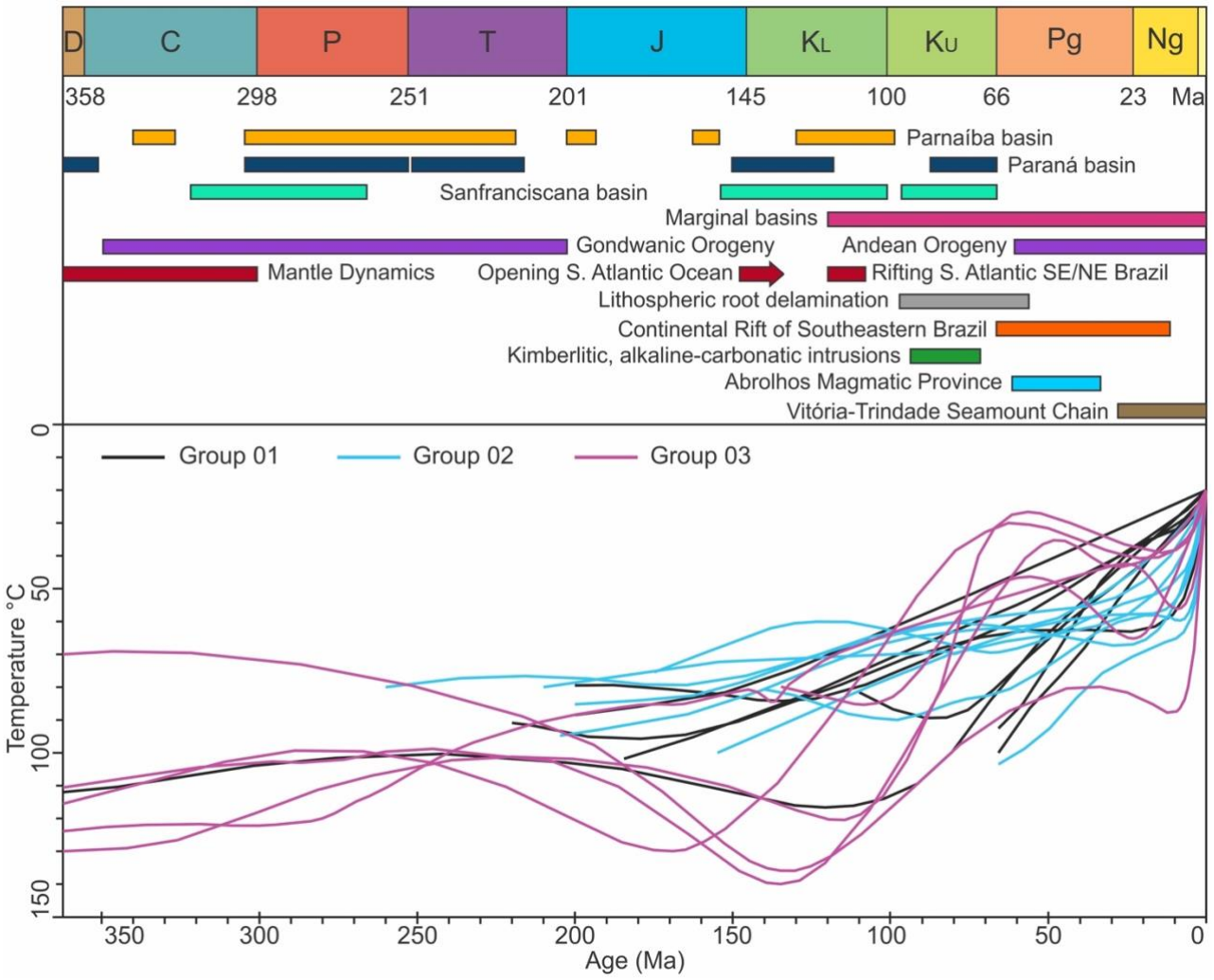

Figure 7. 4: Chronological chart evidencing the expected model's weighted mean trajectories of the new thermal histories provided in this study, along with the leading local and regional events (sedimentary deposition, tectonism, mantle dynamics, and magmatism).

The SFC has consistently exhibited temperatures below 120°C since the Paleozoic. Its southern segment has experienced temperatures lower than 80°C since at least the Carboniferous, contrasting to the neighboring orogenic belts. On the other hand, the northern SFC recorded temperatures ranging from 110 to 70°C during the Paleozoic. During the Triassic to Jurassic, the temperature of the northern SFC was between 80 and 50 ºC. In contrast, the transitional region of the craton with the northern Araçuaí Belt near the margin remained at temperatures varying from 120 and 80 °C. From the Cretaceous (150 Ma map) onwards, the craton slowly cooled until the present-day surface conditions.

The portion of the Araçuaí Belt near the present-day margin lacks thermal information before 180-150 Ma. On the other hand, the thermal history of the continent's interior dates to the Carboniferous, with temperatures below 120-110°C. Localized sites within the transitional region of the northern Araçuaí Belt and SFC also exhibit

temperatures close to 110°C from 210 to 150 Ma. During the Mesozoic to Cenozoic, from 150 to 60 Ma, some sites were in higher temperatures, nearly 110 °C, while others cooled down to 50 °C. Finally, from 60 to 30 Ma, the northern Araçuaí Belt and the Ribeira Belt display localized sites recording temperatures of approximately 90 ºC while the remaining portions of these belts and the SFC display temperatures of approximately 50 ºC or less.

The temperature signals in the Ribeira Belt varied from 20°C to over 180°C during the Carboniferous to Triassic periods. The southern region had near-surface temperatures, while the northern region had higher temperatures of around 120°C. During the Mesozoic, the contrasting temperatures between the northern and southern portions of the belt remained. From 150 Ma onwards, some portions of this belt display a temperature increment towards the Paraná Basin and then cooling, while some segments kept the temperatures nearly 90 °C until 90 to 60 Ma.

7.5 Thermotectonic assessment of the São Francisco Craton and surrounding orogens

7.5.1 The Northern Araçuaí Belt and São Francisco Craton: the new AFT data set

This study presents 23 new AFT central ages distributed across the northern Araçuaí Belt and the SFC (Tab. 7.2 and Fig. 7.2). We also provide 22 inverse thermal models (Supplementary Data S4 and Fig. 7.4).

The new AFT ages are Mesozoic to Cenozoic, of which the Araçuaí Belt mainly records younger AFT ages, and the SFC holds older AFT ages. This AFT data set negatively correlates to MTL and may represent the left portion of a boomerang plot (Green, 1986), indicating reset ages. The samples having MTL larger than 12 μm, i.e., intermediate to long track lengths and noticeably young ages, characterize the samples that were reset. We attribute the emplacement of the Abrolhos Magmatic Province during the Paleocene to the Eocene as the cause of the reset, evidenced by the AFT data presented here. This volcanic event may be responsible for keeping temperatures high enough to induce thermal annealing, producing young AFT and AHe ages.

Additionally, the negative skewing of most samples can correlate to a brief reheating time in the upper portion of the APAZ or extended residence in the lower portion of the APAZ since existing tracks fade while new long tracks form when samples are under

temperatures of approximately 60 ºC. Considering this information, if reheating occurs, the extended residence in upper crustal levels leads apatites to be more retentive for α particles, causing their retention zone to undergo a temperature increment (Flowers et al., 2009). This drives the AHe thermochronometer to hold slightly similar temperature boundaries with the AFT method and, therefore, to cause apatites to record similar ages in both methods and even to invert AHe and AFT ages (Flowers and Kelley, 2011), which is the case of a few samples in this study (BHS-02 and BHS-13) and some samples of Van Ranst et al. (2020) collected in the Araçuaí Belt.

The intermediate to long MTL of samples of this study and their narrow standard deviation may be indicative of fast cooling, which the thermal histories of samples BHS-02, 03, 04, 06, 08, 10, 13, and 15 during the Cenozoic. Some of these samples, such as BHS-02, 06, 10, and 15, along with BHS-09 and 18, display accelerated cooling that is compatible with the time of rifting at 120 Ma, causing exhumation and sediment deposition in the new basins formed (Fig. 7.4).

Samples BHS-04, 08, 11, and 16 to 23 (Fig. 7.4), mainly located within the São Francisco Craton or close to its borders, exhibit a Paleogene-Neogene cooling event, which finds support in increased sedimentary thickness in the marginal basins (e.g. Jelinek et al., 2014).

7.5.2 The São Francisco Craton and surrounding belts: regional assessment

7.5.2.1 Carboniferous to Triassic

In this study, we compiled AFT data from 728 sites to create a IDW map illustrating the distribution of AFT ages (Fig. 7.3) in southeastern Brazil. Furthermore, for 357 samples, the thermal history (Fig. 7.4) allowed the compilation of thermal information to construct 12 IDW maps covering the time range from 360 to 30 Ma (Figs. 7.5, 7.6, and 7.7). The novel compilation highlighted in this research facilitates identifying and analyzing regional cooling patterns within the studied area.

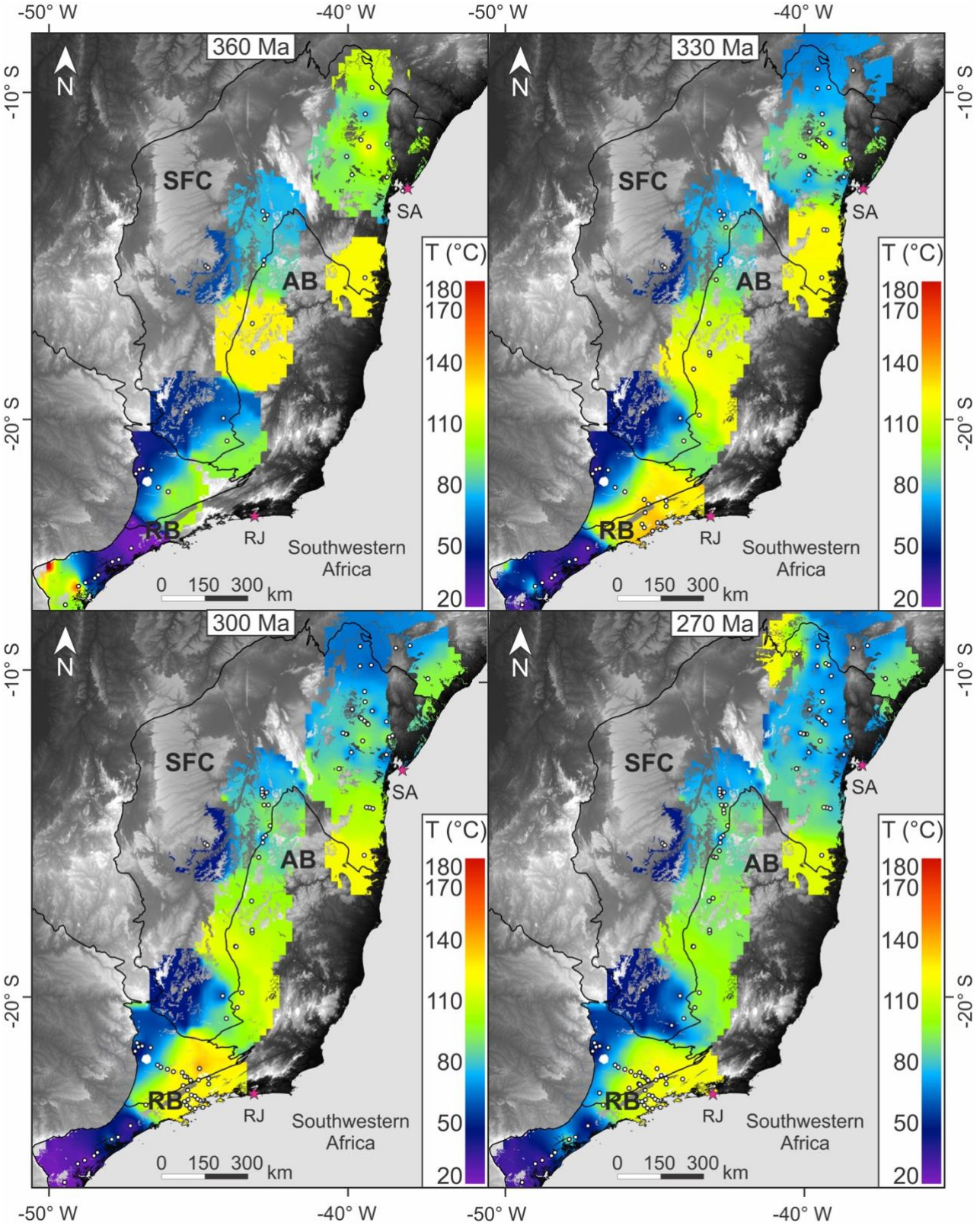

Figure 7. 5: Inverse distance weighted maps created through the interpolation of data collected from thermal models of basement samples across the São Francisco Craton (SFC), Araçuaí Belt (AB), and Ribeira Belt (RB) from 360 to 270 Ma. The time-temperature points collected from this work and samples available in the literature are displayed in Supplementary Data S3. Pink stars refer to the state capital city. Abbreviations are: RJ: Rio de Janeiro City; SA: Salvador City; BH: Belo Horizonte City.

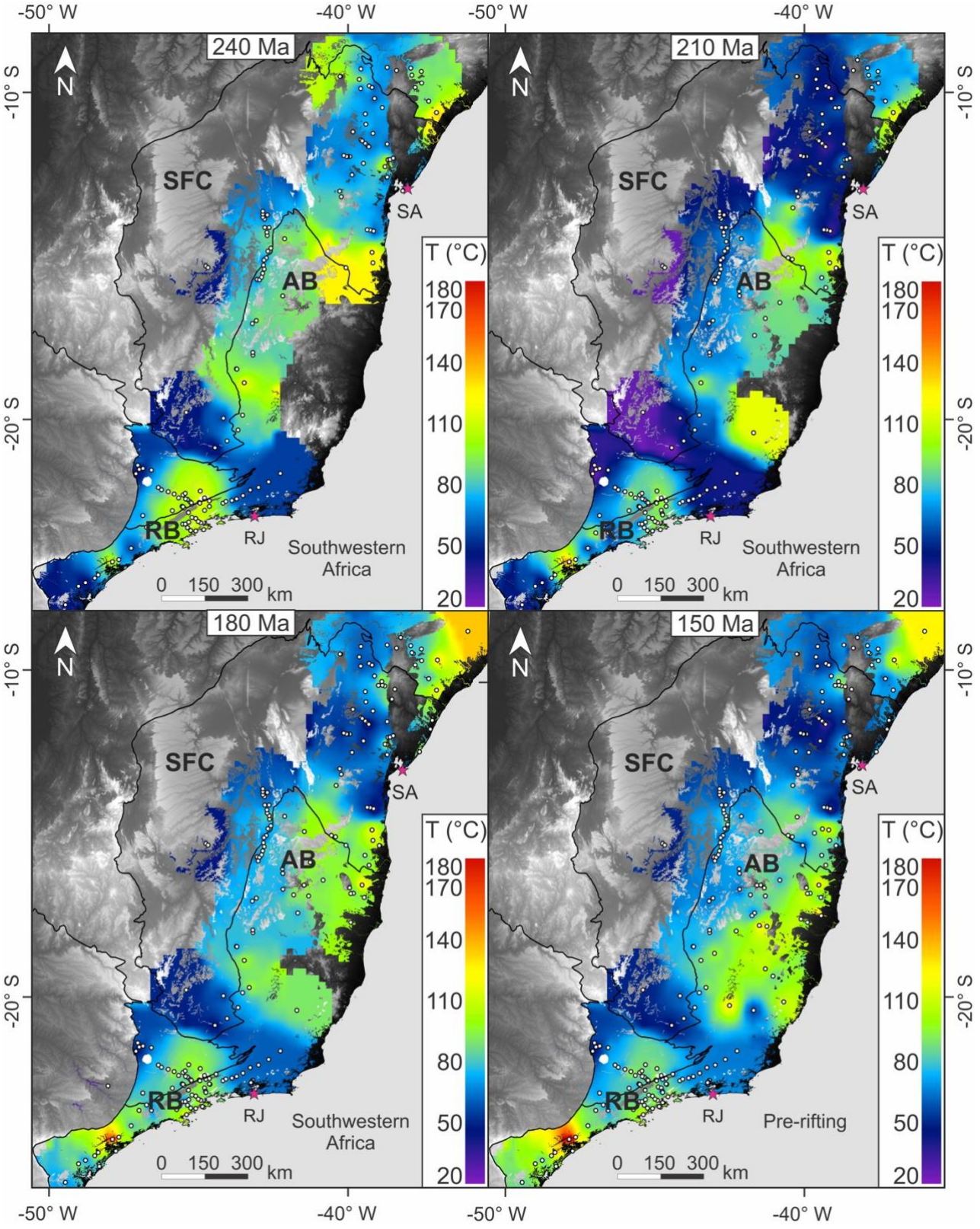

Figure 7. 6: Inverse distance weighted maps created through the interpolation of data collected from thermal models of basement samples across the São Francisco Craton (SFC), Araçuaí Belt (AB), and Ribeira Belt (RB) from 240 to 150 Ma. The time-temperature points collected from this work and samples available in the literature are displayed in Supplementary Data S3. Pink stars refer to the state capital city. Abbreviations are: RJ: Rio de Janeiro City; SA: Salvador City; BH: Belo Horizonte City.

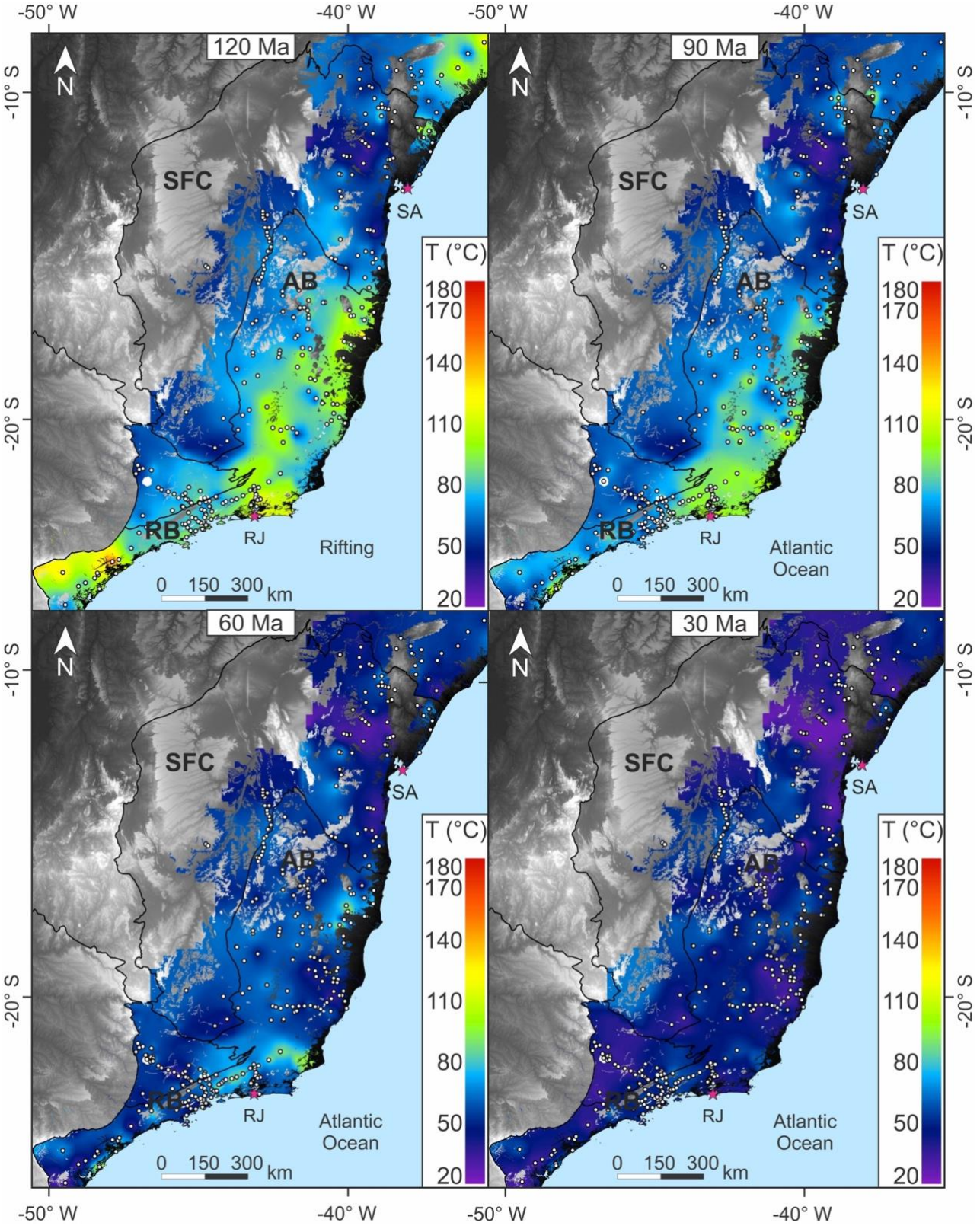

Figure 7. 7: Inverse distance weighted maps created through the interpolation of data collected from thermal models of basement samples across the São Francisco Craton (SFC), Araçuaí Belt (AB), and Ribeira Belt (RB) from 120 to 30 Ma. The time-temperature points collected from this work and samples available in the literature are displayed in Supplementary Data S3. Pink stars refer to the state capital city. Abbreviations are: RJ: Rio de Janeiro City; SA: Salvador City; BH: Belo Horizonte City.

During the Carboniferous to the Triassic, the SFC and its adjacent belts (e.g. Jelinek et al., 2014; Amaral-Santos et al., 2019; Fonseca et al., 2021; do Amaral Santos et al., 2022), along with other segments of West Gondwana (e.g., Kasanzu et al., 2016; Machado et al., 2019; Martins-Ferreira et al., 2020; do Amaral Santos et al., 2023), underwent cooling and erosion due to (1) intraplate stresses of the Gondwanic Orogenic Cycle (Fig. 7.4; Milani and Ramos, 1998) and (2) uplift caused by mantle dynamics (Dávila et al., 2023). During this time, the Santa Fé Group, the initial unit of the intracontinental Sanfranciscana Basin (Figs. 7.1 and 7.4), was deposited (Campos and Dardenne, 1997). This unit, dating back to the Carboniferous-Permian, consists of formations associated with periglacial environments (Sgarbi et al., 2001; Zalán and Silva, 2007), and its sediments were transported from the adjacent Brasiliano belts (Linol et al., 2015). The IDW map recording the Paleozoic thermal signals (Fig. 7.5) provides supporting evidence that the majority of the SFC had already reached temperatures below 100 °C, with specific nuclei registering temperatures of 50 °C or below, indicating shallow portions of the crust or even surface exposure in the region where these samples were collected. The AFT ages spatial distribution (Fig. 7.3) within the SFC also sheds light on the cooling, as these ages represent the oldest data in the analyzed data set, reinforcing that the SFC remained relatively unaffected by rapid exhumation since at least the Carboniferous. Furthermore, the new MTL data of this study depict short to intermediate fission tracks for most of the SFC, suggesting long residence within the thermal range of the AFT method, thus implying slow cooling (samples BHS-11 and 16 to 23; Fig. 7.4).

The lithosphere of the Araçuaí Belt adjacent to the SFC exhibits intermediate AFT ages compared to the coastal region, which shows younger AFT ages (Figs. 7.2 and 7.3). This disparity can be attributed to the gradual and slow continuous cooling observed in the inland portion of the Araçuaí Belt towards the SFC, as evidenced by the temperature variations from the Carboniferous to the Permian (Fig. 7.5). In contrast, the eastern segment of the belt, including the northern Ribeira Belt, displays significantly younger AFT ages and lacks the thermal signal that low-temperature thermochronometers, particularly the AFT method, are capable of recording. This behavior arises due to temperatures exceeding 120 °C, surpassing the closure temperature of the AFT thermochronometer. Notably, the contrasting AFT ages between the SFC and the adjacent belts depict a cooling control based on rheology, where the robust cratonic lithosphere tends to erode slowly. In contrast, the warmer and weaker orogenic lithosphere is rapidly removed

(Fonseca et al., 2021).

The IDW maps (Fig. 7.5) also reveal a Paleozoic cooling in the basement of the Ribeira Belt during the Carboniferous to the end of the Permian in a region adjacent to the Paraná Basin (Fig. 7.4). This basin served as an intracontinental depocenter in the West Gondwana continent during the Paleozoic to Upper Cretaceous (Milani et al., 2007a). The western portion of the Ribeira Belt and the central Brasilia Belt experienced temperatures comparable to the present-day surface conditions and then underwent erosion. The sediments from these regions contributed to the formation of the lower supersequences within the Paraná Basin (Milani et al., 2007a). In contrast, the eastern portion of the Ribeira Belt and the southern tip of the Brasília Belt were exposed to higher temperatures, delineating a boundary between the Santos Block to the north and the Peruíbe Block to the south due to the segmentation of these blocks by transfer zones (Fig. 7.1; Krob et al., 2019; Meisling et al., 2001). The basement near-surface exposure of the southern/central Ribeira Belt can also be attributed to time-temperature constraints imposed during the inversion process, which compel the models to operate in low temperatures (Krob et al., 2019), which, in this case, we disregard, considering the geologic data record mentioned above.

7.5.2.2 Triassic to Jurassic

During the Triassic to Jurassic (240–180 Ma maps, Fig. 7.6), certain sections of the Araçuaí Belt still experienced temperatures higher than the detectable range of the AFT thermochronometer (Fig. 7.6). The absence of thermal signals from both the AFT and AHe methods indicates significant crustal erosion, where the shallow portion of the crust was continually eroded, along with the accompanying thermal records it once held. This hypothesis finds support in the exposure of high-grade metamorphic rocks, such as amphibolites to granulites, which form the crystalline core of the Araçuaí Orogen (Uhlein et al., 1998).

The thermal records pointed out by do Amaral Santos et al. (2022) and Hiruma et al. (2010) suggest that the end of the Gondwanic cycle may lead to exhumation and cooling in some portions of the Ribeira and Araçuaí Belt, bringing samples to shallow portions of the crust. After cooling, these samples started recording the AFT method, observed in the 150 Ma-map (Figs. 7.4 and 7.6).

Since 240 Ma, an estimated exhumation of 3,000-4,000 m can be inferred in the

transition area of the northern Araçuaí Belt and the SFC considering the temperatures observed in the compiled data (Fig. 7.6). The sediments resulting from this exhumation were deposited in nearby basin depocenters, including the Sanfranciscana, Parnaíba, Recôncavo-Tucano-Jatobá basins (Milani et al., 2007b). These estimates align with those provided by Harman et al. (1998), Jelinek et al. (2014), and do Amaral Santos et al. (2022).

7.5.2.3 Late Jurassic-Early Cretaceous and Cenozoic

Starting from 150 Ma onwards, most of the samples examined in this study detected the thermal signal of the AFT. Samples BHS-14 and BHS-16 (Supplementary Data S4 and Fig. 7.4) recorded AFT central ages dating from the Upper Jurassic to Lower Cretaceous, suggesting that the AFT thermochronometer was already within the APAZ. The interpolated maps (Figs. 7.3, 7.6, and 7.7) illustrate a distinct temperature and AFT age spatial distribution pattern attributed to the rheological difference between cratonic and non-cratonic lithosphere, as previously proposed by Fonseca et al. (2021, 2022) and supported in this study, which evidence differential cooling and exhumation. This pattern is evident in the contrasting temperatures of the Araçuaí Belt and the craton: the northeastern Araçuaí Belt and transitional SFC displayed higher temperatures (110-80 ºC), with localized sites exceeding this temperature range. In contrast, the inland Araçuaí Belt and most of the SFC experienced lower temperatures (80-50 ºC) (Fig. 7.3). The Borborema Province and the southern/central Ribeira Belt exhibited higher temperatures than the SFC, supporting the assumption of differential exhumation based on rheology, since they are also composed of orogenic lithosphere. As stated in section 4.1, the AFT central age spatial distribution is another source of validation for the hypothesis of contrasting rheology leading to differential lithospheric exhumation.

The IDW maps (Figs. 7.6 and 7.7) also indicate a temperature increment from 150 to 120 Ma in the transitional region of the Araçuaí-Ribeira Belt. This artifact can be attributed to the interpolation process, which did not consider several samples with temperatures exceeding 120 ºC at 150 Ma, as they could not record any thermal information before that time. Subsequently, at 120 Ma, these samples entered the APAZ, registering elevated temperatures (110-100 ºC). As a result, these high-temperature samples influenced the resulting interpolation maps to display a generalized reheating phase in this region, which we disregard and attribute to a software artifact.

From 120 to 90 Ma (Fig. 7.7), the region extending from Rio de Janeiro city to the north, up to the border with the SFC, underwent rapid cooling from 120 ºC to nearly 70 ºC. The new data set here displays AFT ages that correlate to this event, which is the case of samples BH-01, BHS-08, BHS-09, and BHS-14. This accelerated cooling event is primarily attributed to the erosion of the rift shoulders formed in the Araçuaí Belt (Jelinek et al., 2014; do Amaral Santos et al., 2022). The uplifted crystalline rocks, which comprise the shoulders, contributed sediments that were subsequently deposited in the adjacent basins – Campos, Espírito Santo, and Mucuri basins – within the newly opened Atlantic Ocean (Fig. 7.4). These sediments formed a sedimentary pile that reached a thickness of up 4,400 m (França et al., 2007a, 2007b; Winter et al., 2007). It is essential to notice that some samples of the cratonic domain also display AFT ages that can correlate to the Lower Cretaceous cooling event (samples BHS-11 and BHS-21), pointing to local cooling and erosion of the cratonic lithosphere to a lesser extent than observed for the orogenic lithosphere.

During the transition from the Mesozoic to the Cenozoic era at 60 Ma, the IDW map presented in this study (Fig. 7.7) shows temperatures of 70 ºC, indicating shallow crust portions. Since then, the SFC and its southeastern surrounding orogenic belts have undergone approximately 2,000 m of exhumation. These exhumed rocks contributed sediments to the passive margin basins that developed atop the Late Precambrian-Cambrian crystalline basement east of the South American continent (Mohriak and Fainstein, 2012). However, certain regions still exhibited higher temperatures, reaching nearly 100 ºC (Fig. 7.3). This is observed in the Continental Rift of Southeastern Brazil (Riccomini et al., 2004) and the onshore region near the Abrolhos Magmatic Province (Stanton et al., 2021) (Figs. 7.1 and 7.4).

In the Ribeira Belt, the CRSB installation zone experienced tectonic stress, potentially resulting in higher temperatures than its surroundings. Near the coast, temperatures of 90-100 ºC are indicative of the Paleogene tectonism of the Guaraqueçaba, Cananéia, and Sete Barras grabens (Fig. 7.1 and 7.7; Souza et al., 1996; Riccomini et al., 2004; Nascimento, 2013). Moreover, although the CRSB is primarily controlled by NE-SW shear zones, the Guaraqueçaba region exhibits multiple NW-SE lineaments associated with the Ponta Grossa Arch (Santos et al., 2023) in the southern Ribeira Belt, which influence the drainage pattern and exhibit incised river channels (Nascimento, 2013). Furthermore, Hiruma et al. (2010) also argue that tectonism and fault

reactivation caused changes in the drainage network and river capture during the Neogene, resulting in progressive denudation in the central Ribeira Belt. In the northern Ribeira Belt near the CRSB, reactivation of the shear zones caused the high-temperature regime observed in the IDW map at 60 Ma (Fig. 7.7), which also could be caused by sedimentation of the Cenozoic basins, as argued by Krob et al. (2019), and the presence of alkaline intrusions (Fig. 7.1) heating its vicinity. Therefore, we propose that both the southern and northern Ribeira Belt experienced higher temperatures, as indicated by noticeably young AFT ages (Fig. 7.3), due to post-rift reactivation of these lineaments and shear zones during CRSB development and locally increased temperatures due to kimberlitic and alkaline-carbonatitic plutons emplaced nearby.

The onshore region of the northern Araçuaí Belt adjacent to the Abrolhos Magmatic Province (Fig. 7.1) depicts higher temperatures at 60 Ma (Fig. 7.7), evidencing cooling since then, and it contains some of the younger AFT samples of the Araçuaí Belt (Table 7.2; samples BHS-02 to BHS-05, BHS-07, and BHS-15 in this study), ranging from 65 to 37 Ma. These young ages and high temperatures can be attributed to offshore volcanism in the Abrolhos Magmatic Province, primarily occurring between 56 and 37 Ma (Stanton et al., 2021) along with the presence of NW-SE lineaments that may have been reactivated and acted as conduits for heat transport, keeping the low-temperature thermochronometers opened, as previously advocated by do Amaral Santos et al. (2022) and supported by our findings.

During the Upper Cretaceous onward, the South American plate was under a state of compression: at the Pacific margin, the plate changed its state from extension to compression, inducing shortening and exhumation in the Andes (Ramos, 2010); at the South Atlantic spreading center, the half-spreading rate increased, resulting in accentuated ridge-push (Torsvik et al., 2009). Coeval to this far-field stresses, in southeastern Brazil, numerous high-temperature intrusions, alkaline bodies, and kimberlites emplaced surrounding the São Francisco Craton (Ferreira et al., 2022; Gernon et al., 2023; Takenaka et al., 2023). Additionally, by the end of the Paleogene to Neogene, the Vitória-Trindade Seamount Chain located offshore in the Atlantic Ocean started its emplacement. These magmatic records suggest an increased heat flow in the area, making the crust thermally weak (Cogné et al., 2012; Japsen et al., 2012) and promoting surface uplift, which is also attributed to delamination of deep lithospheric roots (Hu et al., 2018). These heat sources, along with the combined far-field effects of plate

borders and intraplate tectonism/epeirogeny, lead to deformation across the continent, driving exhumation, cooling, and sedimentary deposition in the marginal basins (Cogné et al., 2012).

At 30 Ma, the continental margin, mainly the interior of the SFC, and the inland section of the adjacent orogenic belts were exposed at shallow to near-surface levels (Fig. 7.7). Using the methods employed in this study and those documented in the literature, an estimated exhumation of approximately 1,000 m has occurred from 30 Ma to the present. However, based on stratigraphic data, this thickness can vary from 500 m to more than 2,000 m, with the most significant sedimentary accumulation in the Espírito Santo Basin (França et al., 2007b), located to the east of the Araçuaí Belt, and more minor accumulations the Camamu and Almada basins close to Salvador city and to the east of the SFC (Caixeta et al., 2007; Gontijo et al., 2007). To constrain the basement cooling during the last 30 Ma, thus, thus at shallow depths and cool temperatures, a lower-temperature thermochronometer would be required, such as Monazite Fission Track dating (Jones et al., 2021), which can lead to potential future studies in the area to constrain the time of rapid and slow cooling in the continent.

The results presented in this work, both new and compiled data, reinforce the importance of studying the transitional region of the SFC and Araçuaí Belt, along with the Ribeira Belt, taking into account the effects of differing rheology on the spatial distribution of AFT ages and exhumation. Specifically, the SFC's strong and cold cratonic lithosphere contrasts with the weak and warm orogenic lithosphere of the Araçuaí and Ribeira Belts. It is essential to highlight that certain regions, such as the southern Ribeira Belt and the continental margin near the Abrolhos Magmatic Province, may exhibit local rapid exhumation and reheating episodes (Fig. 7.7). These phenomena can be attributed to post-rift tectonism through fault reactivation and the effects of volcanic emplacement and heating transport along faults, as well as other far-field stresses that were coevally acting upon the lithosphere, ranging from ridge-push in the South Atlantic spreading center to compression in the Pacific margin of the South American plate.

7.6 Conclusion

In conclusion, our research has shed light on several critical aspects of the thermochronological evolution and exhumation history of the São Francisco Craton and the adjacent Araçuaí and Ribeira Belts. Through the analysis of Apatite Fission Track

ages, ranging from 154.4 ± 20.1 to 37.1 ± 3.0Ma, and temperature data, we have identified significant variations in the thermal history of these regions, which have been instrumental in understanding the tectonic processes and geological evolution that have shaped them.

One key finding is the contrasting behavior between the cratonic lithosphere of the São Francisco Craton and the orogenic lithosphere of the Araçuaí and Ribeira Belts. The strong and cold cratonic lithosphere erodes slowly, while the weak and warm orogenic lithosphere is continuously removed. This stark contrast is reflected in the AFT ages and thermal records, providing valuable insights into the dynamics of lithospheric processes.

Additionally, volcanic activity and fault reactivation have played crucial roles in the thermal evolution of specific areas. Firstly, during the rift phase of the South Atlantic Ocean opening, the exhumation of elevated rift shoulders caused cooling in the Araçuaí and Ribeira Belts. Offshore volcanism in the Abrolhos Magmatic Province, located to the west of the Araçuaí Belt and SFC, between 56 and 37 Ma, has contributed to elevated temperatures in the onshore region of the northern Araçuaí Belt. Additionally, post-rift tectonic processes, including fault reactivation and volcanic emplacement near the Continental Rift of Southeastern Brazil, as well as emplacement of kimberlitic, alkaline-carbonatitic intrusions and the Vitória-Trindade Seamount Chain have led to local rapid exhumation and reheating episodes both in the Ribeira Belt and the continental margin near the Abrolhos Magmatic Province.

These findings contribute to a better understanding of the geodynamic evolution of the São Francisco Craton and Araçuaí and Ribeira Belts and have implications for regional tectonic models and the exploration of natural resources in these areas. The observed variations in thermal history provide valuable insights into the dynamics of lithospheric processes, highlighting the need for comprehensive studies that integrate thermochronological data with other geological and geophysical observations.

In summary, our research has contributed novel insights into the thermochronological evolution and exhumation history of the São Francisco Craton and the Araçuaí and Ribeira Belts. Rheological contrasts, erosion of rift shoulders, volcanic activity, and fault and shear zone reactivation have emerged as crucial factors shaping these regions. Further investigations combining multiple data sources and techniques will continue to enhance our knowledge of these complex geological systems.

7.7 Acknowledgments

E. Amaral Santos thanks the Ph.D. scholarship provided by the Conselho Nacional de Desenvolvimento Científico e Tecnológico – CNPq (140775/2019-6). A.R. Jelinek thanks to the Conselho Nacional de Desenvolvimento Científico e Tecnológico - CNPq (Project 309329/2020-5). The authors thank the Associate Editor of Gondwana Research, Dr. Andrea Festa, and two anonymous reviewers who contributed enormously to improving this work's early version.

While preparing this work, the authors used ChatGPT to review the English grammar and word spelling. After using this service, the authors reviewed and edited the content as needed and took full responsibility for the publication's content.

References

Alkmim, F.F., Kuchenbecker, M., Reis, H.L.S., 2017. The Araçuaí Belt, in: Heilbron, M., Cordani, U.G., Alkmim, F.F. (Eds.), São Francisco Craton, Eastern Brazil. Springer, Cham, pp. 255–276. https://doi.org/10.1007/978-3-319-01715-0

Alkmim, F.F., Marshak, S., 1998. Transamazonian Orogeny in the Southern São Francisco Craton Region, Minas Gerais, Brazil: Evidence for Paleoproterozoic collision and collapse in the Quadrilátero Ferrífero. Precambrian Res. 90, 29–58. https://doi.org/10.1016/s0301-9268(98)00032-1

Alkmim, F.F., Marshak, S., Pedrosa-Soares, A.C., Peres, G.G., Cruz, S.C.P., Whittington, A., 2006. Kinematic evolution of the Araçuaí-West Congo orogen in Brazil and Africa: Nutcracker tectonics during the Neoproterozoic assembly of Gondwana. Precambrian Res. 149, 43–64. https://doi.org/10.1016/j.precamres.2006.06.007

Alkmim, F.F., Martins-Neto, M.A., 2012. Proterozoic first-order sedimentary sequences of the São Francisco craton, eastern Brazil. Mar. Pet. Geol. 33, 127–139. https://doi.org/10.1016/j.marpetgeo.2011.08.011

Almeida, F.F.M. de, 1977. O Cráton do São Francisco. Rev. Bras. Geociências 7, 349–364.

Amaral-Santos, E., Jelinek, A.R., Almeida-Abreu, P.A., Genezine, F.A., 2019. Phanerozoic cooling history of Archean/Paleoproterozoic basement in the southern Espinhaço Range, southeastern Brazil, through apatite fission-track analysis. J. South Am. Earth Sci. 96, 102352. https://doi.org/10.1016/j.jsames.2019.102352

Amaral, G., Born, H., Hadler, J.C.N., Iunes, P.J., Kawashita, K., Machado, D.L., Oliveira, E.P., Paulo, S.R., Tello, C.A.S., 1997. Fission track analysis of apatites from São Francisco craton and Mesozoic alcaline-carbonatite complexes from central and southeastern Brazil. J. South Am. Earth Sci. 10, 285–294. https://doi.org/10.1016/s0895-9811(97)00020-5

Caixeta, J.M., Da Silva Milhomem, P., Witzke, R.E., Siqueira Dupuy, I.S., Gontijo, G.A., 2007. Bacia de Camamu. Bol. Geociencias da Petrobras 15, 455–461.

Campos, J.E.G., Dardenne, M.A., 1997. Estratigrafia E Sedimentação Da Bacia Sanfranciscana: Uma Revisão. Rev. Bras. Geociências 27, 269–282. https://doi.org/10.25249/0375-7536.1997269282

Carlson, W.D., Donelick, R.A., Ketcham, R.A., 1999. Variability of apatite fission-track annealing kinetics: I. Experimental results. Am. Mineral. 84, 1213–1223. https://doi.org/10.2138/am-1999-0901

Carmo, I.D., 2005. Geocronologia do intemperismo Cenozoico no Sudoeste do Brasil. Dep. Geol. Universidade Federal do Rio de Janeiro.

Chang, H.K., Kowsmann, R.O., Figueiredo, A.M.F., Bender, A.A., 1992. Tectonics and stratigraphy of the East Brazil Rift system: an overview. Tectonophysics 213, 97–138. https://doi.org/10.1016/0040-1951(92)90253-3

Cogné, N., Gallagher, K., Cobbold, P.R., 2011. Post-rift reactivation of the onshore margin of southeast Brazil: Evidence from apatite (U–Th)/He and fission-track data. Earth Planet. Sci. Lett. 309, 118–130. https://doi.org/10.1016/j.epsl.2011.06.025

Cogné, N., Gallagher, K., Cobbold, P.R., Riccomini, C., Gautheron, C., 2012. Post-breakup tectonics in southeast Brazil from thermochronological data and combined inverse-forward thermal history modeling. J. Geophys. Res. B Solid Earth 117, 1–16. https://doi.org/10.1029/2012JB009340

Costa, D., 2022. Late Cretaceous exhumation of the Doce River valley and the Colatina Fracture Zone,

Southeastern Brazil: implications from apatite fission-track data. Universidade Federal de Minas Gerais.
Cupertino, J.A., 2000. Evolução tectono-climática na fase Rifte das bacias de Camamu, parte norte, e sul do Recôncavo, com ênfase na utilização de isótopos estáveis e traços de fissão. Universidade Federal do Rio Grande do Sul.
Dávila, F.M., Martina, F., Ávila, P., Ezpeleta, M., 2023. Mantle contribution to Late Paleozoic glaciations of SW Gondwana. Glob. Planet. Change 220, 104018. https://doi.org/10.1016/j.gloplacha.2022.104018
do Amaral Santos, E., Jelinek, A.R., Machado, J.P., Stockli, D., 2022. Thermal history along the Araçuaí Orogen and São Francisco Craton border, eastern Brazilian continental margin, based on low-temperature thermochronologic data. Tectonophysics 825, 229232. https://doi.org/10.1016/j.tecto.2022.229232
do Amaral Santos, E., Jelinek, A.R., Stockli, D., Genezine, F.A., 2023. Contrasting thermal histories in the Dom Feliciano Belt triggered by magmatism related to the Paraná-Etendeka LIP and fracture zone proximity. Tectonophysics 857, 229841. https://doi.org/10.1016/j.tecto.2023.229841
Donelick, R.A., O'Sullivan, P.B., Ketcham, R.A., 2005. Apatite fission-track analysis, in: Reiners, P.W., Ehlers, T.A. (Eds.), Reviews in Mineralogy and Geochemistry. pp. 49–94. https://doi.org/10.2138/rmg.2005.58.3
Doranti-Tiritan, C., 2013. Evolução geomórfica e modelagem termocinemática 3D da região do planalto de Poços de Caldas (SP/MG). Universidade Estadual Paulista.
Engelmann de Oliveira, C.H., Jelinek, A.R., 2017. História termotectônica da margem continental Brasileira a partir de dados de traços de fissão em apatita. Pesqui. em Geociencias 44, 387–400. https://doi.org/10.22456/1807-9806.83263
Engelmann de Oliveira, C.H., Jelinek, A.R., Chemale, F., Cupertino, J.A., 2016. Thermotectonic history of the southeastern Brazilian margin: Evidence from apatite fission track data of the offshore Santos Basin and continental basement. Tectonophysics 685, 21–34. https://doi.org/10.1016/j.tecto.2016.07.012
Ferreira, A.C.D., Conceição, R.V., Mizusaki, A.M.P., 2022. Mesozoic to Cenozoic alkaline and tholeiitic magmatism related to West Gondwana break-up and dispersal. Gondwana Res. 106, 15–33. https://doi.org/10.1016/j.gr.2022.01.005
Fleischer, R.L., Price, P.B., 1964. Techniques for geological dating of minerals by chemical etching of fission fragment tracks. Geochim. Cosmochim. Acta 28, 1705–1714. https://doi.org/10.1016/0016-7037(64)90017-1
Flowers, R.M., Kelley, S.A., 2011. Interpreting data dispersion and "inverted" dates in apatite (U-Th)/He and fission-track data sets. Geochim. Cosmochim. Acta 75, 5169–5186. https://doi.org/10.1016/j.gca.2011.06.016
Flowers, R.M., Ketcham, R.A., Shuster, D.L., Farley, K.A., 2009. Apatite (U-Th)/He thermochronometry using a radiation damage accumulation and annealing model. Geochim. Cosmochim. Acta 73, 2347–2365. https://doi.org/10.1016/j.gca.2009.01.015
Fonseca, A., Cruz, S., Novo, T., He, Z., De Grave, J., 2022. Differential exhumation of cratonic and non-cratonic lithosphere revealed by apatite fission-track thermochronology along the edge of the São Francisco craton, eastern Brazil. Sci. Rep. 12, 2728. https://doi.org/10.1038/s41598-022-06419-w
Fonseca, A., Novo, T., Fonte-Boa, T., Kuchenbecker, M., Fragoso, D.G.C., Peifer, D., Pedrosa-Soares, A.C., De Grave, J., 2023. Control of inherited structural fabric on the development and exhumation of passive margins – Insights from the Araçuaí Orogen (Brazil). Geosci. Front. 14, 101628. https://doi.org/10.1016/j.gsf.2023.101628
Fonseca, A.C., Piffer, G.V., Nachtergaele, S., Van Ranst, G., De Grave, J., Novo, T.A., 2020. Devonian to Permian post-orogenic denudation of the Brasília Belt of West Gondwana: insights from apatite fission track thermochronology. J. Geodyn. 137, 101733. https://doi.org/10.1016/j.jog.2020.101733
Fonseca, A.C.L., Novo, T.A., Nachtergaele, S., Fonte-Boa, T.M.R., Van Ranst, G., De Grave, J., 2021. Differential Phanerozoic evolution of cratonic and non-cratonic lithosphere from a thermochronological perspective: São Francisco Craton and marginal orogens (Brazil). Gondwana Res. 93, 106–126. https://doi.org/10.1016/j.gr.2021.01.006
França, R.L., Del Rey, A.C., Tagliari, C.V., Brandão, J.R., De Rossi Fontanelli, P., 2007a. Bacia de Mucuri. Bol. Geociencias da Petrobras 15, 493–499.
França, R.L., Del Rey, A.C., Tagliari, C.V., Brandão, J.R., De Rossi Fontanelli, P., 2007b. Bacia do Espírito Santo. Bol. Geociencias da Petrobras 15, 501–509.
Franco-Magalhaes, A.O.B., Cuglieri, M.A.A., Hackspacher, P.C., Saad, A.R., 2014. Long-term landscape evolution and post-rift reactivation in the southeastern Brazilian passive continental margin: Taubaté basin. Int. J. Earth Sci. 103, 441–453. https://doi.org/10.1007/s00531-013-0967-4
Franco-Magalhaes, A.O.B., Hackspacher, P.C., Glasmacher, U.A., Saad, A.R., 2010. Rift to post-rift evolution of a "passive" continental margin: The Ponta Grossa Arch, SE Brazil. Int. J. Earth Sci. 99, 1599–1613. https://doi.org/10.1007/s00531-010-0556-8
Franco, A.O.B., Hackspacher, P.C., Godoy, D.F., Ribeiro, L.F.B., Guedes, S., 2005. História Térmica do Maciço Alcalino de Poços de Caldas (SP/MG) e adjacências através da análise de datação por traços de fissão em apatitas. Rev. Bras. Geociências 35, 351–358.
Galbraith, R.F., 1981. On statistical models for fission track counts. J. Int. Assoc. Math. Geol. 13, 471–478.

https://doi.org/10.1007/BF01034498
Gallagher, K., 2012. Transdimensional inverse thermal history modeling for quantitative thermochronology. J. Geophys. Res. Solid Earth 117, B02408. https://doi.org/10.1029/2011JB008825
Gallagher, K., Hawkesworth, C.J., Mantovani, M.S.M., 1994. The denudation history of the onshore continental margin of SE Brazil inferred from apatite fission track data. J. Geophys. Res. 99, 117–145. https://doi.org/10.1029/94jb00661
Genaro, D.T., 2008. Contrubuição ao Conhecimento de Processos Atuantes no Rifteamento Continental, por Traços de Fissão em Zircões e Apatitas, Aplicados no Rift Continental do Sudeste do Brasil, Bacias de Taubaté, Resende, Volta Redonda e Circunvizinhanças. Universidade Estadual Paulista.
Gernon, T.M., Jones, S.M., Brune, S., Hincks, T.K., Palmer, M.R., Schumacher, J.C., Primiceri, R.M., Field, M., Griffin, W.L., O'Reilly, S.Y., Keir, D., Spencer, C.J., Merdith, A.S., Glerum, A., 2023. Rift-induced disruption of cratonic keels drives kimberlite volcanism. Nature 620. https://doi.org/10.1038/s41586-023-06193-3
Gezatt, J.N., Macdonald, D.I.M., Stephenson, R., Jelinek, A.R., Carter, A., 2021. South Atlantic passive margin evolution: A thermochronology case study from the Rio de Janeiro-Três Rios section, SE Brazil. J. South Am. Earth Sci. 106, 103051. https://doi.org/10.1016/j.jsames.2020.103051
Gleadow, A.J.W., Duddy, I.R., 1981. A natural long-term track annealing experiment for apatite. Nucl. Tracks 5, 169–174. https://doi.org/10.1016/0191-278X(81)90039-1
Gleadow, A.J.W., Duddy, I.R., Green, P.F., Hegarty, K.A., 1986. Fission track lengths in the apatite annealing zone and the interpretation of mixed ages. Earth Planet. Sci. Lett. 78, 245–254. https://doi.org/10.1016/0012-821X(86)90065-8
Gomes, C.H., 2011. História Térmica Das Regiões Sul E Sudeste Da América Do Sul: Implicações Na Compartimentação Geotectônica Do Gondwana. Cristiane Heredia Gomes. Universidade Federal do Rio Grande do Sul.
Gontijo, G.A., Da Silva Milhomem, P., Caixeta, J.M., Siqueira Dupuy, I.S., De Lemos Menezes, P.E., 2007. Bacia de Almada. Bol. Geociencias da Petrobras 15, 463–473.
Green, P.F., 1986. On the thermo-tectonic evolution of Northern England: Evidence from fission track analysis. Geol. Mag. 123, 493–506. https://doi.org/10.1017/S0016756800035081
Green, P.F., Duddy, I.R., Gleadow, A.J.W., Tingate, P.R., Laslett, G.M., 1986. Thermal Annealing of Fission Tracks in Apatite: 1. A Qualitative Description. Chem. Geol. Isot. Geosci. Sect. 59, 237–253. https://doi.org/http://dx.doi.org/10.1016/0168-9622(86)90074-6
Green, P.F., Duddy, I.R., Laslett, G.M., Hegarty, K.A., Gleadow, A.J.W., Lovering, J.F., 1989. Thermal annealing of fission tracks in apatite 4. Quantitative modelling techniques and extension to geological timescales. Chem. Geol. Isot. Geosci. Sect. 79, 155–182. https://doi.org/10.1016/0168-9622(89)90018-3
Guenthner, W.R., Reiners, P.W., Ketcham, R.A., Nasdala, L., Giester, G., 2013. Helium diffusion in natural zircon: radiation damage, anisotropy, and the interpretation of zircon (U-TH)/He thermochronology. Am. J. Sci. 313, 145–198. https://doi.org/10.2475/03.2013.01
Hackspacher, P.C., Godoy, D.F. de, Ribeiro, L.F.B., Hadler Neto, J.C., Franco, A.O.B., 2007. Modelagem térmica e geomorfologia da borda sul do Cráton do São Francisco: termocronologia por traços de fissão em apatita. Rev. Bras. Geociências 37, 76–86. https://doi.org/10.25249/0375-7536.200737s47686
Hadler, J.C., Paulo, S.R., Iunes, P.J., Tello, S.C.A., Balestrieri, M.L., Bigazzi, G., Curvo, E.A.C., Hackspacher, P., 2001. A PC compatible Brazilian software for obtaining thermal histories using apatite fission track analysis. Radiat. Meas. 34, 149–154. https://doi.org/10.1016/S1350-4487(01)00141-X
Harman, R., Gallagher, K., Brown, R., Raza, A., Bizzi, L., 1998. Accelerated denudation and tectonic/geomorphic reactivation of the craton of northeastern Brazil during the Late Cretaceous. J. Geophys. Res. 103, 27091–27105.
Heilbron, M., de Morisson Valeriano, C., Peixoto, C., Tupinambá, M., Neubauer, F., Dussin, I., Corrales, F., Bruno, H., Lobato, M., Horta de Almeida, J.C., Guilherme do Eirado Silva, L., 2020. Neoproterozoic magmatic arc systems of the central Ribeira belt, SE-Brazil, in the context of the West-Gondwana pre-collisional history: A review. J. South Am. Earth Sci. 103, 102710. https://doi.org/10.1016/j.jsames.2020.102710
Heilbron, M., Machado, N., 2003. Timing of terrane accretion in the Neoproterozoic-Eopaleozoic Ribeira Orogen (SE Brazil). Precambrian Res. 125, 87–112. https://doi.org/10.1016/S0301-9268(03)00082-2
Heilbron, Monica, Cordani, U.G., Alkmim, F.F., 2017a. The São Francisco Craton and Its Margins, in: Heilbron, M., Cordani, U.G., Alkmim, F.F. (Eds.), São Francisco Craton, Eastern Brazil. Springer, Cham, pp. 3–13. https://doi.org/10.1007/978-3-319-01715-0_1
Heilbron, Monica, Ribeiro, A., Valeriano, C.M., Paciullo, F. V, Almeida, J.C.H., Trouw, R.J.A., Tupinambá, M., Silva, L.G.E., 2017b. The Ribeira Belt, in: Heilbron, M., Cordani, U.G., Alkmim, F.F. (Eds.), São Francisco Craton, Eastern Brazil. Springer, Cham, pp. 277–302. https://doi.org/10.1007/978-3-319-01715-0
Hiruma, S.T., Riccomini, C., Modenesi-Gauttieri, M.C., Hackspacher, P.C., Neto, J.C.H., Franco-Magalhães, A.O.B., 2010. Denudation history of the Bocaina Plateau, Serra do Mar, southeastern Brazil: Relationships to Gondwana breakup and passive margin development. Gondwana Res. 18, 674–687.

https://doi.org/10.1016/j.gr.2010.03.001
Hu, J., Liu, L., Faccenda, M., Zhou, Q., Fischer, K.M., Marshak, S., Lundstrom, C., 2018. Modification of the Western Gondwana craton by plume-lithosphere interaction. Nat. Geosci. 11, 203–210. https://doi.org/10.1038/s41561-018-0064-1
Hueck, M., Dunkl, I., Heller, B., Stipp Basei, M.A., Siegesmund, S., 2018. (U-Th)/He Thermochronology and Zircon Radiation Damage in the South American Passive Margin: Thermal Overprint of the Paraná LIP? Tectonics 37, 4068–4085. https://doi.org/10.1029/2018TC005041
Hueck, M., Dunkl, I., Oriolo, S., Wemmer, K., Basei, M.A.S., Siegesmund, S., 2019. Comparing contiguous high- and low-elevation continental margins: New (U-Th)/He constraints from South Brazil and an integration of the thermochronological record of the southeastern passive margin of South America. Tectonophysics 770, 228222. https://doi.org/10.1016/j.tecto.2019.228222
Hurford, A.J., 1990. International Union of Geological Sciences: Subcommission on Geochronology recommendation for the standardization of fission track dating calibration and data reporting. Int. J. Radiat. Appl. Instrumentation. Part 17, 233–236. https://doi.org/10.1016/1359-0189(86)90061-0
Hurford, A.J., Green, P.F., 1983. The zeta age calibration of fission-track dating. Chem. Geol. 41, 285–317. https://doi.org/10.1016/S0009-2541(83)80026-6
Japsen, P., Bonow, J.M., Green, P.F., Cobbold, P.R., Chiossi, D., Lilletveit, R., Magnavita, L.P., Pedreira, A., 2012. Episodic burial and exhumation in NE Brazil after opening of the South Atlantic. Bull. Geol. Soc. Am. 124, 800–816. https://doi.org/10.1130/B30515.1
Jelinek, A.R., Chemale, F., van der Beek, P.A., Guadagnin, F., Cupertino, J.A., Viana, A., 2014. Denudation history and landscape evolution of the northern East-Brazilian continental margin from apatite fission-track thermochronology. J. South Am. Earth Sci. 54, 158–181. https://doi.org/10.1016/j.jsames.2014.06.001
Jelinek, A.R., Corrêa-Gomes, L.C., Bicca, M.M., 2020. Evolução termotectônica fanerozoica da margem continental na área do Rifte Recôncavo-Tucano-Jatobá. Pesqui. em Geociências 47, e0823. https://doi.org/10.22456/1807-9806.101330
Jepson, G., Carrapa, B., Gillespie, J., Feng, R., DeCelles, P.G., Kapp, P., Tabor, C.R., Zhu, J., 2021. Climate as the Great Equalizer of Continental-Scale Erosion. Geophys. Res. Lett. 48, e2021GL095008. https://doi.org/10.1029/2021GL095008
Jones, S., Gleadow, A., Kohn, B., 2021. Thermal annealing of implanted 252Cf fission tracks in monazite. Geochronology 3, 89–102. https://doi.org/10.5194/gchron-3-89-2021
Karl, M., Glasmacher, U.A., Kollenz, S., Franco-Magalhaes, A.O.B., Stockli, D.F., Hackspacher, P.C., 2013. Evolution of the South Atlantic passive continental margin in southern Brazil derived from zircon and apatite (U-Th-Sm)/He and fission-track data. Tectonophysics 604, 224–244. https://doi.org/10.1016/j.tecto.2013.06.017
Kasanzu, C.H., Linol, B., de Wit, M.J., Brown, R., Persano, C., Stuart, F.M., 2016. From source to sink in central Gondwana: Exhumation of the Precambrian basement rocks of Tanzania and sediment accumulation in the adjacent Congo basin. Tectonics 35, 2034–2051. https://doi.org/10.1002/2016TC004147
Ketcham, R.A., Carter, A., Donelick, R.A., Barbarand, J., Hurford, A.J., 2007. Improved modeling of fission-track annealing in apatite. Am. Mineral. 92, 799–810. https://doi.org/10.2138/am.2007.2281
Kohn, B., Chung, L., Gleadow, A., 2019. Fission-Track Analysis: Field Collection, Sample Preparation and Data Acquisition. Springer International Publishing. https://doi.org/10.1007/978-3-319-89421-8_2
Krob, F.C., Glasmacher, U.A., Karl, M., Perner, M., Hackspacher, P.C., Stockli, D.F., 2019. Multi-chronometer thermochronological modelling of the Late Neoproterozoic to recent t-T-evolution of the SE coastal region of Brazil. J. South Am. Earth Sci. 92, 77–94. https://doi.org/10.1016/j.jsames.2019.02.012
Leite, C.A.S., Perrotta, M.M., Silva, M.A., Heineck, C.A., Salvador, E.D., Vieira, V.S., Lopes, R.C., Silva, M.G.M., Drumond, J.B.V., Malouf, R.F., Lacerda Filho, J.V., Valente, C.R., Gomes, S.D., Sachs, L.L.B., Oliveira, I.W.B., Ramgrab, G.E., Netto, C., Junqueira, P.A., Paes, V.J.C., 2004. Cartas Geológicas Brasil ao Milionésimo - Folha Rio de Janeiro.
Linol, B., de Wit, M. J., Milani, E.J., Guillocheau, F., Scherer, C., 2015. New Regional Correlation Between the Congo, Paraná and Cape-Karoo Basins of Southwest Gondwana, in: De Wit, Maarten J., Guillocheau, François, De Wit, M.C.J. (Eds.), Geology and Resource Potential of the Congo Basin. Springer, Berlin, Heidelberg, pp. 245–268. https://doi.org/10.1007/978-3-642-29482-2
Machado, J.P.S.L., Jelinek, A.R., Bicca, M.M., Stephenson, R., Genezini, F.A., 2019. West Gondwana orogenies and Pangaea break-up: Thermotectonic effects on the southernmost Mantiqueira Province, Brazil. J. Geol. Soc. London. 176, 1056–1075. https://doi.org/10.1144/jgs2019-018
Martins-Ferreira, M.A.C., Dias, A.N.C., Chemale, F., Campos, J.E.G., 2020. Intracontinental uplift of the Brazilian Central Plateau linked to continental breakup, orogenies, and basin filling, supported by apatite and zircon fission-track data. Arab. J. Geosci. 13:891. https://doi.org/10.1007/s12517-020-05885-8
Meisling, K.E., Cobbold, P.R., Mount, V.S., 2001. Reactivation of an obliquely rifted margin, Campos and Santos basins, southeastern Brazil. Am. Assoc. Pet. Geol. Bull. 85, 1903–1924. https://doi.org/10.1306/8626d0b3-173b-11d7-8645000102c1865d

Milani, E.J., Faccini, U.F., Scherer, C.M., Araújo, L.M., Cupertino, J.A., 1998. Sequences and stratigraphic hierarchy of the Paraná Basin (Ordovician to Cretaceous), southern Brazil. Bol. IG-USP. Série Científica 29, 125–173. https://doi.org/https://doi.org/10.11606/issn.2316-8986.v29i0p125-173

Milani, E.J., Gonçalves De Melo, J.H., De Souza, P.A., Fernandes, L.A., França, A.B., 2007a. Bacia do Paraná. Bol. Geociencias da Petrobras 15, 265–287.

Milani, E.J., Ramos, V.A., 1998. Paleozoic orogenies in southwestern Gondwana and the subsidence cycles of the Parana Basin. Rev. Bras. Geociências 28, 473–484.

Milani, E.J., Rangel, H.D., Bueno, G.V., Stica, J.M., Winter, W.R., Caixeta, J.M., Da Cruz Pessoa Neto, O., 2007b. Bacias sedimentares brasileiras - Cartas estratigráficas. Bol. Geociencias da Petrobras 15, 183–205.

Mohriak, W., Nemčok, M., Enciso, G., 2008. South Atlantic divergent margin evolution: Rift-border uplift and salt tectonics in the basins of SE Brazil. Geol. Soc. Spec. Publ. 294, 365–398. https://doi.org/10.1144/SP294.19

Mohriak, W.U., Fainstein, R., 2012. Phanerozoic regional geology of the eastern Brazilian margin, in: Roberts, D.G., Bally, A.W. (Eds.), Regional Geology and Tectonics: Phanerozoic Passive Margins, Cratonic Basins and Global Tectonic Maps. Elsevier, Boston, pp. 222–282. https://doi.org/10.1016/B978-0-444-56357-6.00006-8

Nascimento, E.R. do, 2013. Morfotectônica E Origem Das Morfoestruturas Da Serra Do Mar Paranaense. Universidade Federal do Paraná.

Novo, T.A., Fonte-boa, T.M.R., Rolim, J.M., Fonseca, A.C., 2021. The state of the art of low-temperature thermochronometry in Brazil. J. Geol. Surv. Brazil 4, 239–256. https://doi.org/https://doi.org/10.29396/jgsb.2021.v4.n3.4

Nürnberg, D., Müller, R.D., 1991. The tectonic evolution of the South Atlantic from Late Jurassic to present. Tectonophysics 191, 27–53. https://doi.org/10.1016/0040-1951(91)90231-G

Oliveira, S.G. de, Hackspacher, P.C., Hadler Neto, J.C., Iunes, P.J., Paulo, S.R. de, Ribeiro, L.F.B., Tello Saenz, C.A., 2000. Constraints on the Evolution and Thermal History of the Continental Platform of Southeast Brazil, São Paulo State, Using Apatite Fission Track Analysis (Afta). Rev. Bras. Geociências 30, 107–109. https://doi.org/10.25249/0375-7536.2000301107109

Oriolo, S., Oyhantçabal, P., Wemmer, K., Siegesmund, S., 2017. Contemporaneous assembly of Western Gondwana and final Rodinia break-up: Implications for the supercontinent cycle. Geosci. Front. 8, 1431–1445. https://doi.org/10.1016/j.gsf.2017.01.009

Pedrosa-Soares, A.C., Alkmim, F.F., Tack, L., Noce, C.M., Babinski, M., Silva, L.C., Martins-Neto, M.A., 2008. Similarities and differences between the Brazilian and African counterparts of the Neoproterozoic Araçuaí-West Congo orogen. Geol. Soc. Spec. Publ. 294, 153–172. https://doi.org/10.1144/SP294.9

Pedrosa-Soares, A.C., Campos, C.P. DE, Noce, C., Silva, L.C., Novo, T., Roncato, J., Medeiros, S., Castañeda, C., Queiroga, G., Dantas, E., Dussin, I., Alkmim, F., 2011. Late Neoproterozoic – Cambrian granitic magmatism in the Araçuaí orogen (Brazil), the Eastern Brazilian Pegmatite Province and related mineral resources. Geol. Soc. London, Spec. Publ. 350, 25–51.

Pedrosa-Soares, A.C., Noce, C.M., Wiedemann, C.M., Pinto, C.P., 2001. The Araçuaí-West-Congo Orogen in Brazil: An overview of a confined orogen formed during Gondwanaland assembly. Precambrian Res. 110, 307–323. https://doi.org/10.1016/S0301-9268(01)00174-7

Pedrosa-Soares, A.C., Wiedemann-Leonardos, C.M., 2000. Evolution of Araçuaí Belt and its connection to the Ribeira Belt, eastern Brazil, in: Cordani, U.G., Milani, E.J., Thomaz-Filho, A., Campos, D.A. (Eds.), Tectonic Evolution of South America. 31st International Geological Congress, Rio de Janeiro, pp. 265–285. https://doi.org/10.13140/2.1.3802.5928

Price, P.B., Walker, R.M., 1963. Fossil Tracks of Charged Particles in Mica and the Age of Minerals. J. Geophys. Res. 68, 4847–4862. https://doi.org/10.1029/JZ068i016p04847

Ramos, V.A., 2010. The tectonic regime along the Andes: Present-day and Mesozoic regimes. Geol. J. 45, 2–25. https://doi.org/10.1002/gj.1193

Reiners, P.W., Carlson, R.W., Renne, P.R., Cooper, K.M., Granger, D.E., McLean, N.M., Schoene, B., 2017. Diffusion and thermochronologic interpretations, in: Reiners, P.W., Carlson, R.W., Renne, P.R., Cooper, K.M., Granger, D.E., McLean, N.M., Schoene, B. (Eds.), Geochronology and Thermochronology. Wiley, pp. 83–126. https://doi.org/10.1002/9781118455876.ch5

Ribeiro, L.F.B., Hackspacher, P.C., Ribeiro, M.C.S., Hadler Neto, J.C., Tello, S.C.A., Iunes, P.J., Franco, A.O.B., Godoy, D.F., 2005. Thermotectonic and fault dynamic analysis of Precambrian basement and tectonic constraints with the Parana basin. Radiat. Meas. 39, 669–673. https://doi.org/10.1016/j.radmeas.2004.09.007

Ribeiro, M.C.S., Hackspacker, P.C., Ribeiro, L.F.B., Hadler Neto, J.C., 2011. Evolução Tectônica E Denudacional Da Serra Do Mar (Se/Brasil) No Limite Entre O Cretáceo Superior E Paleoceno, Utilizando Análises De Traços De Fissão E U-Th/He Em Apatitas. Rev. Bras. Geomorfol. 12, 3–14. https://doi.org/10.20502/rbg.v12i0.254

Riccomini, C., 1990. O Rift continental do sudeste do Brasil. Universidade de São Paulo.

Riccomini, C., Gomes, L., Anna, S., 2004. Evolução geológica do rift continental do sudeste do Brasil, in: Mantesso-Neto, V., Bartorelli, A., Carneiro, C.D.R., Brito-Neves, B.B. de (Eds.), Geologia Do Continente Sul-Americano: Evolução Da Obra de Fernando Flávio de Almeida. Beca, pp. 383–405.

Riccomini, C., Velázquez, V.F., Gomes, C.B., 2005. Tectonic controls of the Mesozoic and Cenozoic alkaline magmatism in the central- southeastern Brazilian Platform. Mesozoic to Cenozoic Alkaline Magmat. Brazilian Platf. 31–57.

Sandwell, D.T., Müller, R.D., Smith, W.H.F., Garcia, E., Francis, R., 2014. New global marine gravity model from CryoSat-2 and Jason-1 reveals buried tectonic structure. Science (80-.). 346, 65–67. https://doi.org/10.1126/science.1258213

Santos, J.M. dos, Salamuni, E., Morales, N., de Castro, L.G., Lima da Silva, C., de Souza, I.A., Gimenez, V.B., Oliveira, S.P., 2023. Aeromagnetic and structural characterization of dyke swarms in southeast Brazil: Evidence for Cenozoic reactivation of the Guapiara lineament, Ponta Grossa Arch. J. South Am. Earth Sci. 129, 104523. https://doi.org/10.1016/j.jsames.2023.104523

Scherer, C.M.S., Reis, A.D., Horn, B.L.D., Bertolini, G., Lavina, E.L.C., Kifumbi, C., Goso Aguilar, C., 2023. The stratigraphic puzzle of the permo-mesozoic southwestern Gondwana: The Paraná Basin record in geotectonic and palaeoclimatic context. Earth-Science Rev. 240, 104397. https://doi.org/10.1016/j.earscirev.2023.104397

Sgarbi, G.N.C., Sgarbi, P.B. de A., Campos, J.E.G., Dardenne, M.A., Penha, U.C., 2001. Bacia Sanfranciscana: o registro Fanerozóico da Bacia do São Francisco, in: Pinto, C.P., Martins-Neto, M.A. (Eds.), Bacia Do São Francisco: Geologia e Recursos Naturais. SBG/MG, pp. 93–138.

Silva, L.G.A.F., 2006. A interação entre os eventos tectônicos e a evolução geomorfológica da Serra da Bocaina, Sudeste do Brasil. Universidade do Estado do Rio de Janeiro.

Soares, C.J., Guedes, S., Jonckheere, R., Hadler, J.C., Passarella, S.M., Dias, A.N.C., 2016. Apatite fission-track of Cretaceous alkaline rocks of Ponta Grossa and Alto Paranaíba Arches, Brazil. Geol. J. 51, 805–810. https://doi.org/10.1002/gj.2694

Souza, D.H. de, Hackspacher, P.C., Doranti-Tiritan, C., De Godoy, D.F., 2014. Comparação Da Dinâmica Evolutiva, a Longo E Curto Prazo, Entre O Planalto De Poços De Caldas E O Planalto De São Pedro De Caldas. Rev. Bras. Geomorfol. 15, 251–272. https://doi.org/10.20502/rbg.v15i2.481

Souza, L.A.P. de, Tessler, M.G., Galli, V.L., 1996. O Gráben De Cananéia. Rev. Bras. Geociências 26, 139–150. https://doi.org/10.25249/0375-7536.1996139150

Souza, M.E., de Souza Martins, M., Queiroga, G.N., Leite, M., Oliveira, R.G., Dussin, I., Pedrosa-Soares, A.C., 2019. Paleoenvironment, sediment provenance and tectonic setting of Tonian basal deposits of the Macaúbas basin system, Araçuaí orogen, southeast Brazil. J. South Am. Earth Sci. 96, 102393. https://doi.org/10.1016/j.jsames.2019.102393

Stanton, N., Gordon, A., Cardozo, C., Kusznir, N., 2021. Morphostructure, emplacement and duration of the Abrolhos Magmatic Province: A geophysical analysis of the largest post-breakup magmatism of the South-Eastern Brazilian margin. Mar. Pet. Geol. 133, 105230. https://doi.org/10.1016/j.marpetgeo.2021.105230

Tagami, T., O'Sullivan, P.B., 2005. Fundamentals of fission-track thermochronology. Rev. Mineral. Geochemistry 58, 19–47. https://doi.org/10.2138/rmg.2005.58.2

Takenaka, L.B., Förster, M.W., Alard, O., Griffin, W.L., Jacob, D.E., Basei, M.A.S., O'Reilly, S.Y., 2023. Multi-mineral geochronology of kimberlites, kamafugites and alkaline-carbonatite rocks, SW São Francisco Craton, Brazil: Appraisal of intrusion ages. Gondwana Res. 124, 246–272. https://doi.org/10.1016/j.gr.2023.05.012

Tello Saenz, C.A., Hackspacher, P.C., Hadler Neto, J.C., Iunes, P.J., Guedes, S., Ribeiro, L.F.B., Paulo, S.R., 2003. Recognition of Cretaceous, Paleocene, and Neogene tectonic reactivation through apatite fission-track analysis in Precambrian areas of southeast Brazil: Association with the opening of the South Atlantic Ocean. J. South Am. Earth Sci. 15, 765–774. https://doi.org/10.1016/S0895-9811(02)00131-1

Torsvik, T.H., Rousse, S., Labails, C., Smethurst, M.A., 2009. A new scheme for the opening of the South Atlantic Ocean and the dissection of an Aptian salt basin. Geophys. J. Int. 177, 1315–1333. https://doi.org/10.1111/j.1365-246X.2009.04137.x

Turner, J.P., Green, P.F., Holford, S.P., Lawrence, S.R., 2008. Thermal history of the Rio Muni (West Africa)-NE Brazil margins during continental breakup. Earth Planet. Sci. Lett. 270, 354–367. https://doi.org/10.1016/j.epsl.2008.04.002

Uhlein, A., Egydio-Silva, M., Bouchez, J.L., Vauchez, A., 1998. The Rubim pluton (Minas Gerais, Brazil): a petrostructural and magnetic fabric study. J. South Am. Earth Sci. 11, 179–189. https://doi.org/10.1016/S0895-9811(98)00009-1

Val, P., Venerdini, A.L., Ouimet, W., Alvarado, P., Hoke, G.D., 2018. Tectonic control of erosion in the southern Central Andes. Earth Planet. Sci. Lett. 482, 160–170. https://doi.org/10.1016/j.epsl.2017.11.004

Van Ranst, G., Pedrosa-Soares, A.C., Novo, T., Vermeesch, P., De Grave, J., 2020. New insights from low-temperature thermochronology into the tectonic and geomorphologic evolution of the south-eastern Brazilian highlands and passive margin. Geosci. Front. 11, 303–324.

https://doi.org/10.1016/j.gsf.2019.05.011
Vaz, P.T., Rezende, N.G.A.M., Wanderley Filho, J.R., Silva Travassos, W.A., 2007. Bacia do Parnaíba. Bol. Geociencias da Petrobras 15, 253–263.
Vermeesch, P., 2009. RadialPlotter: A Java application for fission track, luminescence and other radial plots. Radiat. Meas. 44, 409–410. https://doi.org/10.1016/j.radmeas.2009.05.003
Winter, W.R., Jahnert, R.J., França, A.B., 2007. Bacia de Campos. Bol. Geociencias da Petrobras 15, 511–529.
Zalán, P.V., De Oliveira, J.A.B., 2005. Origem e evolução estrutural do Sistema de Rittes Cenozóicos do Sudeste do Brasil (Origin and structural evolution of the Cenozoic Rift System of Southeastern Brasil). Bol. Geociencias da Petrobras 13, 269–300.
Zalán, P.V., Silva, P.C.R., 2007. Bacia do São Francisco. Bol. Geociencias da Petrobras 15, 561–571.

7.8 Email de confirmação de submissão

Abaixo, segue a confirmação de que o artigo em questão foi submetido no periódico *Gondwana Research*.

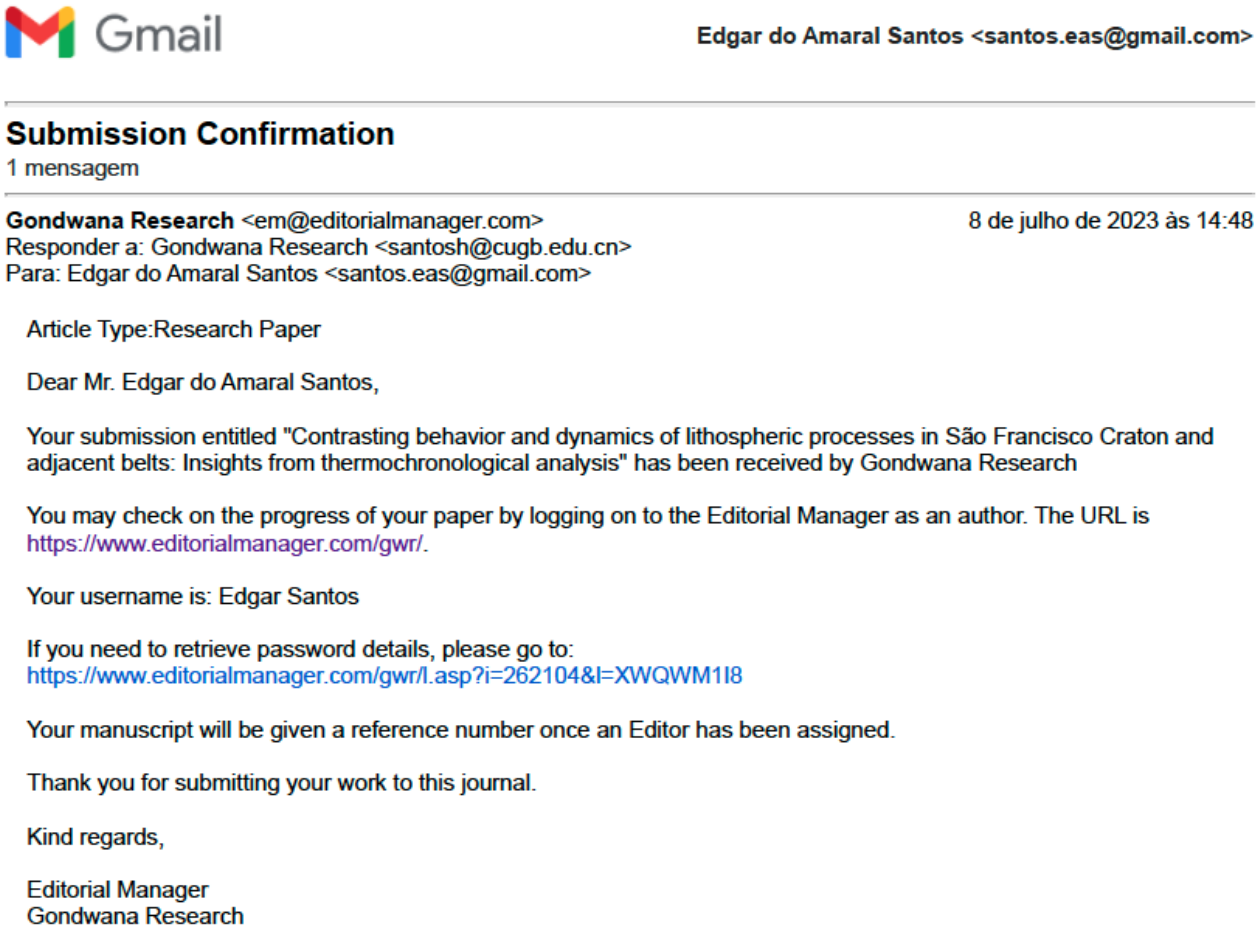

Gmail — Edgar do Amaral Santos <santos.eas@gmail.com>

Submission Confirmation
1 mensagem

Gondwana Research <em@editorialmanager.com> 8 de julho de 2023 às 14:48
Responder a: Gondwana Research <santosh@cugb.edu.cn>
Para: Edgar do Amaral Santos <santos.eas@gmail.com>

Article Type:Research Paper

Dear Mr. Edgar do Amaral Santos,

Your submission entitled "Contrasting behavior and dynamics of lithospheric processes in São Francisco Craton and adjacent belts: Insights from thermochronological analysis" has been received by Gondwana Research

You may check on the progress of your paper by logging on to the Editorial Manager as an author. The URL is https://www.editorialmanager.com/gwr/.

Your username is: Edgar Santos

If you need to retrieve password details, please go to:
https://www.editorialmanager.com/gwr/l.asp?i=262104&l=XWQWM1I8

Your manuscript will be given a reference number once an Editor has been assigned.

Thank you for submitting your work to this journal.

Kind regards,

Editorial Manager
Gondwana Research

APÊNDICES

A.1 – XII South American Symposium on Isotope Geology – 2022

SSAGI
XII South American Symposium on Isotope Geology
3-6 July 2022, Santiago de Chile, Chile
ssagi.science

Dispersion of apatite and zircon (U-Th)/He ages and their relationship with eU concentration, craton border proximity, elevation, and shoreline distance: A case study in eastern Brazil

Edgar do Amaral Santos[1], Andréa Ritter Jelinek[2], Daniel Stockli[3]

(1) Programa de Pós-Graduação em Geociências - Universidade Federal do Rio Grande do Sul
(2) Instituto de Geociências - Universidade Federal do Rio Grande do Sul
(3) Jackson School of Geosciences - The University of Texas in Austin

From the Neoproterozoic to the Cambrian, several cratonic fragments amalgamated into a large landmass called Gondwana continent. The mobile belts formed in this process register the opening and closure of oceans and the collision of the stable cratonic blocks, such as the Araçuaí Belt situated to the southeast of the São Francisco Craton, in Eastern Brazil. After ceasing the stresses related to the convergence of the cratons, the Gondwana paleocontinent interior became subject to weathering and erosion. The thermal history of this region indicates cooling during the Paleozoic recorded in low-temperature thermochronometers, such as zircon and apatite (U-Th)/He. These thermochronometers together record the thermal history of temperatures lower than ~190 to nearly 40 ºC, which corresponds to the upper crust ~10 km. However, these methods provide not only the thermal history itself, but also cooling ages. Therefore, this study aims to understand the main factors controlling the cooling ages obtained for both thermochronometers. For that, seven samples were analyzed, of which five were subject to both zircon (ZHe) and apatite (AHe) (U-Th)/He analyses. ZHe corrected cooling ages vary from 483.1 ± 38.6 to 93.8 ±7.5 Ma and eU concentration on zircon crystals range from 10.91 to 632.51 ug/g. On the other hand, AHe corrected cooling ages range from 129.9 ± 7.8 to 32.7 Ma and the eU concentration of apatite crystals spans from 5.6 to 62.8 ug/g. Both ZHe and AHe correlate positively with eU concentration in a non-linear trend, suggesting relatively slow, monotonic cooling and/or long residence in temperatures between 70 to 40 ºC. The Equivalent Spherical Radius (ESR) of zircon ranges from 50.61 to 103.02 um, whereas apatite crystals have values spanning from 70.94 to 166.39 um. ESR and ZHe ages present a negative correlation, suggesting unknown sources of natural dispersion. Conversely, the ESR and AHe ages correlation is sparse, suggesting little interdependence between these parameters in this study. The distance to the coastline and elevation in relation to ZHe and AHe ages are also another source of possible control. This control only seems to be legit for apatite locally, with older ages far from the shore and at higher elevations. When analyzing regional trends, however, the correlation is sparse. It is also absent any correlation between elevation and the distance to the shoreline and ZHe ages. Finally, the distance to the craton border was also analyzed, evidencing that it controls the ZHe ages, but fails to control AHe ones. These results suggest that the samples of the Araçuaí Belt and the São Francisco Craton were subject to slow, monotonic cooling, and that none of these parameters act as a single age controlling source, at least locally. Therefore, more studies are required to investigate the additional parameters that control the age dispersion in northern Araçuaí Belt and São Francisco Craton.

Financing: Edgar do Amaral Santos: Conselho Nacional de Desenvolvimento Científico e Tecnológico – CNPq, Ph.D scholarship (140775/2019-6). Andrea Ritter Jelinek: CNPq (Project 309329/2020-5).

A.2 – XII South American Symposium on Isotope Geology – 2022

SSAGI
XII South American Symposium on Isotope Geology
3-6 July 2022, Santiago do Chile, Chile

Preliminary results of the control sources of apatite (U-Th)/He ages obtained in the Catarinense Shield, Northern Dom Feliciano Belt

Edgar do Amaral Santos[1], Andréa Ritter Jelinek[2], Daniel Stockli[3]

(1) Programa de Pós-Graduação em Geociências - Universidade Federal do Rio Grande do Sul
(2) Instituto de Geociências - Universidade Federal do Rio Grande do Sul
(3) Jackson School of Geosciences - The University of Texas in Austin

The Dom Feliciano Belt (DFB) is an orogenic belt located to the south of the Mantiqueira Province, extending for about 1200 km, from Uruguay to southern Brazil. The DFB was formed by the convergence of several terrains and cratonic blocks during the Neoproterozoic, composing the southern portion of the Gondwana paleocontinent. After ceasing the compressive phase responsible for the consolidation of this paleocontinent, this belt became subject to weathering and erosive processes. One of the ways to understand in detail the evolution of the DFB during the Phanerozoic is using low-temperature thermochronometers, such as (U-Th)/He in apatite (AHe). This thermochronometer is based on accumulation of a particles (^{4}He) generated from the radioactive decay of U, Th and Sm and it provides the cooling age of rocks, generally restricted to low temperatures and more superficial portions of the crust. Aiming understand the control sources in the AHe ages of the Catarinense Shield, northern portion of the DFB, rock samples of granitic composition were collected. The samples were submitted to mineral separation processes to obtain apatite concentrates. Subsequently, the methodology of (U-Th)/He in apatite was used in the separated mineral aliquots as follows: (i) measurements of the length and width of the crystals were taken; (ii) the apatites were subjected to He extraction in a vacuum chamber with subsequent measurement of the concentration of this isotope in a quadrupole mass spectrometer; (iii) the apatites were dissolved to obtain the concentration of U, Th and Sm isotopes. The results obtained indicate uncorrected single crystal AHe ages that range from 38.5 ± 2.3 to 103.8 ± 6.2 Ma, with a predominance of Cenozoic ages. After F_t correction, AHe ages range from 62.5 ± 3.7 to 153 ± 9.2 Ma, predominantly Mesozoic (Cretaceous). The concentration of eU varies between 4.5 and 96 ug/g and its correlation with AHe ages is slightly positive and non-linear. Equivalent spherical radius (ESR) measurements of apatites are between 26.4 and 59.8 um and the correlation of this parameter with AHe ages is slightly negative. The correlation between AHe ages and distance from the coastline and altitude is also negative, with the oldest ages being at low altitudes and close to the coastline. These results will be combined with inverse numerical modeling in QTQt software to obtain the thermal histories recorded in these samples, which will provide a better understanding of the main controls of the AHe ages and the thermal evolution of the Santa Catarina Shield during the Phanerozoic.

Financing: Edgar do Amaral Santos: CNPq PhD scholarship - (140775/2019-6)Andréa Ritter Jelinek: CNPq - (Project 309329/2020-5).

A.3 – IV Semana Acadêmica dos Pós-Graduandos do Instituto de Geociências – SAPIGEO – 2022

TERMOCRONOLOGIA DE BAIXA TEMPERATURA APLICADA ÀS ROCHAS DA FAIXA ARAÇUAÍ E DO CRÁTON SÃO FRANCISCO, MARGEM CONTINENTAL LESTE BRASILEIRA

Edgar do Amaral Santos[1], Andréa Ritter Jelinek[2]

[1] Programa de Pós-Graduação em Geociências - Universidade Federal do Rio Grande do Sul
[2] Instituto de Geociências - Universidade Federal do Rio Grande do Sul

Resumo: Margens passivas se formam em resposta ao rifteamento de uma área continental. A evolução do rifte é dependente tanto da herança estrutural, quanto da herança tectônica, o que geralmente controla a denudação diferencial e, consequentemente, a deposição de sedimentos. O embasamento cristalino sobre o qual a margem continental leste brasileira se assenta apresenta uma variedade litológica bastante complexa composta pela litosfera orogênica dos cinturões Brasilianos-Pan-Africanos, como a Faixa Araçuaí, e pela litosfera cratônica do Cráton São Francisco. Este trabalho concentrou-se na zona transicional entre as litosferas distintas da porção norte da Faixa Araçuaí e do referido cráton, consideradas quente e fria, respectivamente. Foram empregados, pela primeira vez nesta região, os termocronômetros de baixa temperatura (U-Th)/He em zircão e apatita. Estes termocronômetros fornecem a idade de resfriamento das rochas, geralmente restritas a porções mais superficiais da crosta. Com essa perspectiva, foram examinados os principais eventos de resfriamento, as forças geodinâmicas que atuaram na litosfera desta zona transicional, as taxas de denudação que afetaram essa região desde a formação do continente Gondwana Ocidental e a correlação entre a termocronologia e a herança estrutural. Os resultados indicam que as idades de He em zircão (ZHe) corrigidas variam entre 483,1 ± 38,6 a 93,8 ± 7,5 Ma e as concentrações de urânio efetivo (eU) variam entre 10,91 a 632,51 mg/g. Conforme esperado, as idades de He em apatita (AHe) corrigidas são mais jovens, variando entre 129,9 ± 7,79 e 32,7 ±1,96 Ma. A concentração de eU nas apatitas se situam entre 5,6 e 62,8 mg/g. Ambas idades de ZHe e AHe apresentam correlação positiva com a concentração de eU. Foram identificadas três fases de resfriamento, restringidas entre o Devoniano Inferior ao Carbonífero, Triássico/Jurássico ao presente e Neocretáceo/Paleoceno ao presente e dois episódios de reaquecimento, entre o Jurássico Médio ao Eocretáceo e do Neocretáceo ao Paleoceno. Adicionalmente, foram analisadas as direções dos lineamentos nos domínios cratônico, orogênico e da cobertura sedimentar para entender como a herança estrutural afeta o registro termocronológico. Constatou-se que as estruturas NW-SE herdadas do ciclo Brasiliano e reativadas durante a ruptura continental entre o Cretáceo e o Paleoceno possivelmente foram responsáveis por manter o sistema (U-Th)/He em apatita aberto, o que resultou nas idades mais jovens do conjunto de dados obtidos.

Palavras-chave: *Cráton São Francisco, Faixa Araçuaí, Termocronologia por (U-Th)/He em apatita e zircão.*

A.4 – 50º Congresso Brasileiro de Geologia – 2021

50º CONGRESSO BRASILEIRO DE GEOLOGIA
28 a 30 | junho de 2021 | Brasília - DF

THERMOTECTONIC EVOLUTION OF THE ARAÇUAÍ OROGENY REVEALED BY ZIRCON AND APATITE U-TH/HE THERMOCHRONOLOGY

Amaral-Santos, E.[1]; *Jelinek, A.R.*[1]; *Machado, J.P.S.L.*[1]; *Stockli, D.*[2]
[1]Universidade Federal do Rio Grande do Sul; [2]University of Texas;

ABSTRACT: The Gondwana landmass was assembled between the Neoproterozoic and the Cambrian, when several cratonic fragments interspersed by mobile belts were amalgamated. The Araçuaí Orogeny, one of the orogenic belts surrounding the São Francisco Craton, was formed during these collisions and is characterized by a unique geodynamic setting, where the orogen is confined to a cratonic embayment. The onset of this orogenic event is of Ediacaran age, whereas post-collisional magmatism persisted until ca. 500 Ma. In order to understand the cooling history of the Araçuaí Orogeny, thermochronometry analyses of U-Th/He on zircon (ZHe) and apatite (AHe) were conducted, since this technique registers the events occurring in the upper crust (the upper ~10 kilometers), making it a valuable tool for assessing cooling and/or reheating events, denudation, and epirogenic movements, among others. The closure temperature for ZHe is ca. 190 ºC and for AHe is ca. 60 ºC. Considering this, 12 thermochrnometry analyses were made in the Araçuaí Orogeny and São Francisco Craton domains, being seven ZHe and five AHe. Preliminary results point to ZHe cooling ages varying from 621.5 to 107.5 Ma on zircon with effective uranium concentration (eU) ranging from 631.8 to 9.0 ppm. For AHe, the apparent ages vary from 163.5 to 37.5 Ma and the eU ranges between 62.9 and 4.5 ppm. AHe and ZHe are positively correlated to eU. The samples collected in the Araçuaí domain present younger ages than the samples of the São Francisco Craton, what can be preliminary interpreted as two different patterns of denudation. These results, combined with thermal modeling to be developed, can better constrain the cooling history of this portion on the Brazilian territory, improving our comprehension about the Phanerozoic evolution of the region, especially regarding the events that led to the opening of South Atlantic Ocean during the Mesozoic.

KEYWORDS: ZIRCON U-TH/HE THERMOCHRONOLOGY, APATITE U-TH/HE THERMOCHRONOLOGY, ARAÇUAÍ OROGENY.

ISBN | 978-65-992688-1-6

A.5 – 50º Congresso Brasileiro de Geologia – 2021

50º CONGRESSO BRASILEIRO DE GEOLOGIA
28 a 30 | junho de 2021 | Brasília - DF

A SEMANA ACADÊMICA DOS PÓS-GRADUANDOS DO INSTITUTO DE GEOCIÊNCIAS – SAPIGEO, E O DIÁLOGO COM O DIVERSO

Oliveira, E.J.[1]; Massuda, A.J.[1]; Santos, A.C.S.[1]; Silva, A.F.[1]; Padilha, D.F.[1]; Santos, E.A.[1]; Oliveira, E.B.[1]; Costa, E.O.[1]; Rios, F.R.[1]; Battista, F.[1]; Andres, F.G.[1]; Amarante, F.B.[1]; Rockenbach, I.A.[1]; Silva, I.C.R.[1]; Maia, J.A.[1]; Tononi, L.L.[1]; Pereira, L.M.C.[1]; Rocha, M.X.[1]; Silva, M.D.[1]; Xavier, P.L.A.[1]; Maahs, R.[1]; Gonçalves, T.F.[1]; Santos, T.B.[1]
[1]Universidade Federal do Rio Grande do Sul

RESUMO: A Semana Acadêmica dos Pós-Graduandos do Instituto de Geociências – SAPIGEO, é um evento criado e organizado pelos discentes dos Programas de Pós-Graduação em Geociências (PPGGEO) e Geografia (POSGEA) da Universidade Federal do Rio Grande do Sul-UFRGS. O qual tem o objetivo de divulgar as pesquisas desenvolvidas na universidade, promovendo a integração entre pesquisadores e a comunidade. Com edições bienais realizadas nos anos de 2015, 2017 e 2019, a SAPIGEO teve início a partir da percepção dos discentes sobre um ambiente desprovido de articulação entre os pares, bem como da necessidade de se pensar o processo formativo em conjunto. Nestas edições buscou-se estabelecer diálogos, internos e externos, compreendendo-se a riqueza da troca e da exposição das ideias em ambiente acadêmico. A estrutura programática da SAPIGEO conta com apresentações de forma oral e pôster para os discentes exporem seus projetos de pesquisa, reservando espaços para debate de pautas de interesse comum tendo como convidados professores, profissionais e público externo em mesas redondas e palestras. Também é reservado o espaço para o encontro informal entre os participantes ocupando o espaço dos centros acadêmicos, integrando e motivando a participação dos alunos da graduação. Ao longo dos eventos são construídos olhares críticos, para além da técnica e das demandas de mercado, questionando as dimensões que envolvem o pós-graduando e acolhendo como ele se expressa. Com duração de 3 a 5 dias, e uma comissão organizadora variando de quatorze a vinte e duas pessoas, em três edições alcançou-se cento e setenta e nove inscritos com igual número de trabalhos apresentados. Estes números expressam o existente desejo de comunicação e aproximação entre os pós-graduandos afora as atividades ordinárias previstas na estrutura programática, criando assim um espaço de colaboração que enriquece o processo formativo profissional e acadêmico. Ao se observar a criação de espaços de diálogo com o diverso, percebe-se a celebração dos princípios indissociáveis da educação superior. Neste diapasão, a institucionalização destes espaços visa convergir as expectativas dos PPG's junto à comunidade interna e externa. Em tempos de urgência de ações extensionistas por parte da comunidade científica a abertura ao diálogo pode melhorar não somente a leitura do mundo, mas a leitura pelo mundo da comunidade acadêmica enquanto sociedade.

PALAVRAS-CHAVE: COMUNICAÇÃO GEOCIENTÍFICA, SEMANA ACADÊMICA, PÓS-GRADUAÇÃO

ISBN | 978-65-992688-3-0

A.6 – Capítulo do livro "Contribuições à geologia do Rio Grande do Sul e de Santa Catarina – 2021 (disponível em: https://lume.ufrgs.br/handle/10183/221989)

Evolução termocronológica do Cinturão Dom Feliciano: implicações na geodinâmica da margem continental sul do Brasil

Andréa Ritter *Jelinek*[1]*, João Pacífico Silveira Luiz *Machado*[2], Edgar do Amaral *Santos*[2]

[1] Instituto de Geociências, Universidade Federal do Rio Grande do Sul
[2] Programa de Pós-Graduação em Geociências, Universidade Federal do Rio Grande do Sul

* *autor correspondente: andrea.jelinek@ufrgs.br*

1 Introdução

A formação da margem Atlântica Sul-Americana ocorreu no Mesozoico, em consequência da ruptura do Gondwana Ocidental e do desenvolvimento do Oceano Atlântico Sul. Essa margem passiva apresenta uma extensão de mais de 6.000 km e grande variedade de feições geológicas e topográficas, de sul a norte. Neste trabalho, será explorada a margem continental dos estados do Rio Grande do Sul (RS) e de Santa Catarina (SC) (Fig. 1). Na margem sul-rio-grandense, estão presentes uma topografia suave e exposições do Cinturão Dom Feliciano e do Terreno Taquarembó, associadas à formação do Gondwana Ocidental, durante o Neoproterozoico (Ciclo Orogênico Brasiliano/Pan-Africano). Já a margem Catarinense é dominada pelo Cinturão Dom Feliciano, representado pelos altos topográficos da Província da Mantiqueira e pelo Cráton Luís Alves.

Apesar da ampla variedade de características ao longo da costa, tanto *onshore* quanto *offshore*, a porção da margem entre os estados do RS e de SC apresenta uma mudança significativa na configuração da margem passiva sul-americana, e representa um limite entre a porção sul, de baixa topografia, e a norte, de relevo alto e acidentado. Esse limite está marcado pelo alto de Florianópolis, que, além de limitar duas porções de relevo distinto na margem continental, marca, também, o limite entre a Bacia de Pelotas, a sul, e a Bacia de Santos, a norte. A principal diferença da Bacia de Pelotas para as demais, situadas mais a norte, é a ausência de depósitos evaporíticos e de reservas de hidrocarbonetos, além de representar uma conexão entre a crosta continental e a Dorsal Mesoatlântica, através da Zona de Fratura do Rio Grande (também conhecida como Zona de Fratura de Florianópolis), uma estrutura de sentido E-W, que se propaga no fundo oceânico e que também limita a Elevação de Rio Grande e o Platô de São Paulo, dois altos batimétricos no Oceano Atlântico.

A.7 – Organização de eventos – 2022

Universidade Federal do Rio Grande do Sul
Instituto de Geociências

ANAIS
IV SEMANA ACADÊMICA DOS PÓS-GRADUANDOS DO INSTITUTO DE GEOCIÊNCIAS - SAPIGEO
Redes para Permanência
14 a 17 de março de 2022

Coordenadora

Julia Taveira Rudy (mestranda/PPGEA)

Organizadores

Alice Nardoni Marteli (doutoranda/PPGSR)
Bruna Batista Kappes (mestranda/PPGSR)
Davi Gandolphi (mestrando/PPGEA)
Éder Luís da Silva Rodrigues (doutorando/PPGEA)
Edgar do Amaral Santos (doutorando/PPGGEO)
Edvaldo José de Oliveira (doutorando/PPGGEO)
Francesco Battista (doutorando/PPGGEO)
Franciele Gonçalves Andres (doutoranda/PPGGEO)
Gabriel Barbosa Drago (mestrando/PPGGEO)
Henrique Dorneles de Castro (doutorando/PPGEA)
Igor Armindo Rockenbach (doutorando/PPGEA)
Juliana Carvalho Cardoso (doutoranda/PPGEA)
Larissa Lanes Tononi (doutoranda/PPGGEO)
Mariah Xavier Rocha (doutoranda/PPGGEO)
Pedro Luis Ammon Xavier (doutorando/PPGGEO)
Rafael Gordilho Barbosa (doutorando/PPGGEO)
Stéphanie Carvalho da Silva (doutoranda/PPGGEO)
Talita Fernandes Gonçalves (doutoranda/PPGEA)
Thamiris Barbosa dos Santos (doutoranda/PPGGEO)

Realização

Universidade Federal do Rio Grande do Sul (UFGRS)
Instituto de Geociências (IGEO/UFRGS)
Programa de Pós-Graduação em Geociências (PPGGEO/UFRGS)
Programa de Pós-Graduação em Geografia (PÓSGEA/UFRGS)
Programa de Pós-Graduação em Sensoriamento Remoto (PPGSR/UFRGS)

Apoio

Sociedade Brasileira de Geologia / Núcleo RS-SC

Porto Alegre, 2022

A.7 – Organização de eventos – 2019

UNIVERSIDADE FEDERAL DO RIO GRANDE DO SUL
INSTITUTO DE GEOCIÊNCIAS
PROGRAMA DE PÓS-GRADUAÇÃO EM GEOCIÊNCIAS (PPGGEO/UFRGS)
PROGRAMA DE PÓS-GRADUAÇÃO EM GEOGRAFIA (PÓSGEA/UFRGS)

ANAIS DA
3ª SEMANA ACADÊMICA DOS PÓS-GRADUANDOS DO INSTITUTO DE GEOCIÊNCIAS (SAPIGEO):
Ensino, Pesquisa, Extensão & Resistência

Porto Alegre de 18 a 22 de novembro de 2019

Coordenadora

Franciele Gonçalves Andres

Organizadores:

Amanda Juliano Massuda
Angela Cristine Scaramuzza dos Santos
Aurélio Fagundes Silva
Dionatan Ferri Padilha
Edgar do Amaral Santos
Edvaldo José de Oliveira
Elaine Baroni de Oliveira
Fernando Rodrigues Rios
Francesco Battista
Francyne Bochi do Amarante
Igor Armindo Rockenbach
Joseli Andrades Maia
Larissa Lanes Tononi
Laura Medeiros da Costa Pereira
Mariah Xavier Rocha
Pedro Luis Ammon Xavier
Ricardo Maahs
Talita Fernandes Gonçalves
Thamiris Barbosa dos Santos

IGEO - INSTITUTO DE GEOCIENCIAS
Porto Alegre, 2020

ANEXO I
Título da Tese:
“TERMOTECTÔNICA FANEROZOICA DA PROVÍNCIA MANTIQUEIRA E CRÁTONS ADJACENTES E SUA RELAÇÃO COM A EVOLUÇÃO DE ZONAS TRANSICIONAIS NA MARGEM CONTINENTAL BRASILEIRA”
Área de Concentração: Geoquímica
Autor: **Edgar do Amaral Santos**
Orientadora: Profa. Dra. Andrea Ritter Jelinek
Examinador: Prof. Dr. Mauricio Parra Amézquita
Data: 04/12/2023
Conceito: B
PARECER: O candidato apresentou uma tese bem estruturada composta por uma síntese muito bem escrita de dois artigos publicados em revistas de alto impacto e um terceiro submetido a um periódico de qualidade semelhante. Os dados termocronológicos foram adquiridos e trabalhados de forma exemplar. O trabalho ressalta o controle reológico entre a litosfera cratónica e orogênica nos padrões de resfriamento fanerozoicos. O candidato respondeu satisfatoriamente questionamentos sobre aspectos metodológicos e interpretativos e de concordância entre objetivos declarados do trabalho e resultados obtidos.
Assinatura: 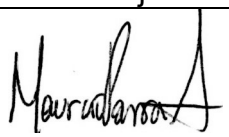 Data:04/12/2023
Ciente do Orientador: Ciente do Aluno:

ANEXO I

Título da Tese:

“TERMOTECTÔNICA FANEROZOICA DA PROVÍNCIA MANTIQUEIRA E CRÁTONS ADJACENTES E SUA RELAÇÃO COM A EVOLUÇÃO DE ZONAS TRANSICIONAIS NA MARGEM CONTINENTAL BRASILEIRA”

Área de Concentração: Geoquímica

Autor: **Edgar do Amaral Santos**

Orientadora: Profa. Dra. Andrea Ritter Jelinek

Examinadora: Profa. Dra. Ana Maria Pimentel Mizusaki

Data: 04/12/2023

Conceito: A

PARECER:

O candidato apresentou uma tese que cumpre os requisitos exigidos para um doutorado. O trabalho está muito bem apresentado, estruturado e trata de um tema inovador. Destaca-se que o candidato já tem dois artigos publicados em revista de Qualis Capes A (Tectonophysics) e um terceiro submetido e aceito na revista Gondwana Research (Qualis Capes A). A metodologia foi utilizada de forma precisa e os resultados apresentados e discutidos mostram o seu domínio sobre o tema. Os resultados são de grande importância para o aprimoramento do conhecimento sobre a evolução termocronológica da margem continental brasileira. Os questionamento feitos ao candidato foram respondidos de forma precisa. Foram sugeridas pequenas correções em relação aos processos evolutivos da margem continental descritos no volume mas que não impactam na discussão dos resultados. A apresentação oral foi muito boa mostrando domínio e segurança sobre a pesquisa efetuada. Parabenizo o doutorando e orientadora pelo excelente trabalho realizado.

Assinatura: Ana Maria Pimentel Mizusaki Data: 4/12/2023

Ciente do Orientador:

Ciente do Aluno:

ANEXO I

Título da Tese:

“TERMOTECTÔNICA FANEROZOICA DA PROVÍNCIA MANTIQUEIRA E CRÁTONS ADJACENTES E SUA RELAÇÃO COM A EVOLUÇÃO DE ZONAS TRANSICIONAIS NA MARGEM CONTINENTAL BRASILEIRA”

Área de Concentração: Geoquímica

Autor: **Edgar do Amaral Santos**

Orientadora: Profa. Dra. Andrea Ritter Jelinek

Examinador: Prof. Dr. Miguel Antonio Tupinambá Araujo Souza

Data: 4/12/2023

Conceito: A

PARECER:

O documento da tese estava bem escrito, estruturado, sem conter erros na escrita e na forma. Contém dois artigos publicados e um submetido em revistas de alto impacto. Os resultados apresentados e discutidos são de grande revelia para a termocronologia da margem atlântica da América do Sul. Foram feitos dois questionamentos ao candidato, um sobre método e outro sobre a revisão bibliográfica, aos quais respondeu adequadamente. Foi feita uma crítica e sugestão para trabalhos futuros sobre as áreas de transição da margem continental sugeridas pelo candiato.

Assinatura:  Data: 4 dez 2023

Ciente do Orientador:

Ciente do Aluno: